LONGITUDINAL DISPERSION IN NONUNIFORM, ISOTROPIC POROUS MEDIA

Thesis by

James Evan Houseworth

In Partial Fulfillment of the Requirements

for the Degree of

Doctor of Philosophy

California Institute of Technology

Pasadena, California

1984

(Submitted May 3, 1984)

ACKNOWLEDGEMENTS

This research project has enlisted the support of several people whom I would like to thank.

Norman Brooks, my advisor, has provided an excellent environment for doing research. While allowing me the freedom necessary to explore different ideas, as well as providing essential, constructive criticisms during the course of the research, he has been a constant source source of encouragement. His support is deeply appreciated.

Many thanks are due Bob Koh, who has given generous assistance and advice concerning computational and data acquisition problems encountered. Bob's computer programs were used extensively for data processing and computer graphics, and his random number generator is the basis of the one used for this work.

The assistance of Elton Daly, who has been instrumental in the design and construction of the experimental apparatus, is greatly appreciated. Consultation sessions with Elton were essential in translating concepts into actual experimental equipment.

The help of all the shop staff members is also appreciated. Rich Eastvedt gave considerable assistance in the construction and installation of experimental apparatus. Joe Fontana also provided valuable assistance, particularly in the design and construction of the conductivity probes. Leonard Montenegro helped locate and assemble

the components of the data acquisition system used for conductivity measurements.

I wish to thank Rayma Harrison and Gunilla Hastrup, who have cheerfully tracked down a large number of books and papers needed for this research.

Much appreciation is due the staff members who assisted in the production of this text. Joan Mathews and Mary Ann Gray efficiently handled the onerous task of typing the equations. The illustrations and graphics labeling were produced with great skill by Theresa Fall and Joseph Galvin.

I am ever grateful to Pat Rankin for making sure my stipends and tuition support were not overlooked in the tangle of administrative paperwork.

Finally, I thank my wife, Pat, for her assistance in putting together the text and, most of all, for her love and support through the years.

This study was supported by the Andrew W. Mellon Foundation through the Caltech Environmental Quality Laboratory.

ABSTRACT

A theoretical and experimental investigation has been made of the longitudinal dispersion of chemically and dynamically passive solutes during flow through nonuniform, isotropic porous media. Both theoretical and experimental results are limited to the high Peclet number, low Reynolds number flow regime. The goal of the theoretical investigation is to provide a quantitative method for calculating the coefficient of longitudinal dispersion using only measurable structural features of the porous medium and the characteristics of the carrying fluid and solute. A nonuniform porous medium contains variations in grain scale pore structure, but is homogeneous at the macroscopic level for quantities such as the permeability or porosity.

A random capillary tube network model of nonuniform porous media is developed which uses a pore radius distribution and pore length distribution to characterize the grain scale structure of porous media. The analysis gives the asymptotic longitudinal dispersion coefficient in terms of integrals of kinematic properties of solute particles flowing through individual, random capillary tubes. However, shear dispersion within individual capillary tubes (discussed in Appendix C) is found to have negligible impact on the overall longitudinal dispersion in porous media. The dispersion integrals are evaluated using a Monte Carlo integration technique. An analysis of the permeability in nonuniform porous media is used to establish a proper flow field for the analysis of longitudinal dispersion.

The experimental investigation of longitudinal dispersion is carried out by measuring (with conductivity probes) the development of an initially sharp miscible displacement interface. The experimentally determined longitudinal dispersion coefficients are found to be greater in nonuniform media than in uniform media when compared using Peclet numbers based on the geometric mean grain diameter. The experimental breakthrough curves also display highly asymmetrical shapes, in which the "tail" of the breakthrough is longer than would be expected from advection-diffusion theory.

Although the theoretical model does not predict the tailing behavior, it is found that the leading portion of the breakthrough curve is described by advection-diffusion theory. The theoretically determined longitudinal dispersion coefficients lie roughly within a factor of 1.35 of the measured values.

TABLE OF CONTENTS

TABLE OF CONTENTS (continued)

TABLE OF CONTENTS (continued)

TABLE OF CONTENTS (continued)

LIST OF FIGURES

LIST OF FIGURES (continued)

LIST OF FIGURES (continued)

LIST OF FIGURES (continued)

LIST OF TABLES

CHAPTER 1

INTRODUCTION

This research report presents an investigation into the relationship between microscopic structure of porous media and miscible transport phenomena during flow through porous media. This work was done to provide a more fundamental understanding of environmental problems relating to mass transport in soil and groundwater. With the generation of roughly 10 million tons of non-radioactive hazardous wastes per year, increasing 5 to 10 percent annually, it is not surprising that a disposal problem exists (Eichenberger, et al., 1978). In addition, current disposal practices put over 50 percent of these wastes into the ground (Hill, et al., 1981). Demands on the land to contain or degrade waste material poses serious design problems for environmental engineers who are asked to predict the effects of disposal in extremely complex environments. In addition to waste disposal, pesticide management and salinity control in agriculture call for an ability to predict mass transport in soil and groundwater to prevent contamination of water supplies.

From a broader perspective, the ideas and techniques developed for analyzing transport phenomena in porous media are useful in a variety of engineering problems. Applications include packed bed reactors, ion exchange, chromatography, enhanced petroleum recovery, filtration, and transport in physiological systems such as blood capillaries and the lungs.

While the details may differ in different applications, it is important to recognize the similarities of these problems. For problems involving the transport of passive solutes, the fluid and solute properties are often well known, while the the geometrical structure of the pore system is usually difficult to characterize and use in a solute transport model. The common practice is to neglect the grain scale structure of the porous medium and use macroscopic transport equations with transport coefficients that are determined empirically. By using a macroscopic approach, however, valuable insight into the relationship of pore structure and transport processes is lost.

1.1 Phenomenological Description of Flow Through Porous Media

Ever since the experiments of Henri Darcy (Darcy, 1856), the relationship between flow rate and hydraulic gradient has been recognized. For the one-dimensional system shown in Figure 1.1 and an incompressible Newtonian fluid, the relationship is given as

$$Q = KA\left(\frac{\phi_1 - \phi_2}{L}\right) \tag{1.1}$$

where

Q = volume flux through the column (L^3/T)

K = hydraulic conductivity (L/T)

A = cross-sectional area of the column (L^2)

L = column length (L)

$\phi = z + p/(\rho g)$ = piezometric head (L)

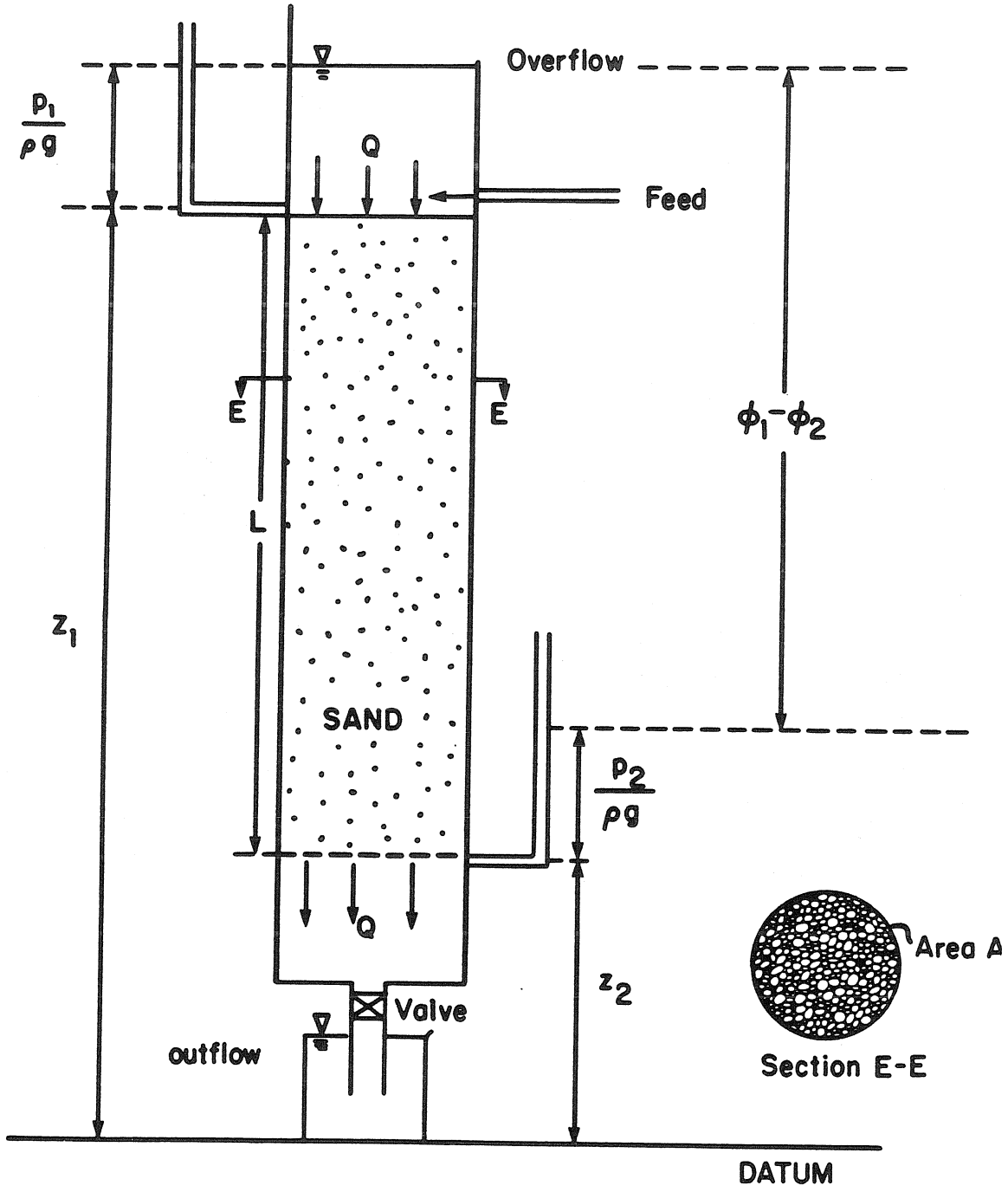

FIGURE 1.1

Flow in a One-Dimensional, Homogeneous Packed Column

ρ = fluid density (M/L^3)

g = gravitational acceleration (L/T^2)

p = fluid pressure (M/LT^2)

Dividing Q by A gives the specific discharge (or Darcy velocity), V_D. The specific discharge is a fictitious velocity, but the average linear velocity in the direction of the column axis is given by $V_s = V_D/\sigma$, where V_s is the seepage velocity (L/T) and σ is the volumetric porosity (volume of voids/total volume of medium). The seepage velocity may be visualized as the velocity of a stable, immiscible displacement front passing through the column.

A qualitative explanation of Darcy's law can be made by considering a balance between the applied piezometric head gradient and viscous stress gradient. For a uniform porous medium (which has a single grain size), the pore spaces may be scaled by a single length scale,a. The dimensional piezometric head gradient is, $\rho g \nabla \phi$, and the viscous force, F_v, is scaled by

$$F_v \sim \mu V_s a$$

where μ is the dynamic fluid viscosity (M/LT).

The viscous stress gradient, $\nabla \tau_{sh}$, is scaled by F_v/a^3, or

$$\nabla \tau_{sh} \sim \mu V_s / a^2$$

so if

$$\rho g \nabla \phi \sim \mu V_s / a^2$$

we have

$$V_s \sim \frac{a^2 g}{\nu} \nabla \phi$$

or $$V_D \sim \frac{\sigma a^2 g}{\nu} \nabla\phi \qquad (1.2)$$

where $\nu = \frac{\mu}{\rho}$ is the kinematic fluid viscosity (L^2/T).

Darcy's law, given by equation (1.1), is limited to low Reynolds number flows, where

$$Re = \frac{V_s d}{\nu}$$ is the Reynolds Number

and d is the grain size (L).

When the Reynolds number exceeds 1, nonlinear (inertial) effects become significant and Darcy's law is no longer valid.

1.2 Phenomenological Description of Dispersion in Porous Media

Solute molecules flowing through a porous medium do not all move at the same velocity, demonstrating that the mean velocity is an average of a velocity distribution. As an example, consider again one-dimensional flow in a packed column, with a solute slug introduced at the origin, spread uniformly over the cross section. As the solute moves downstream, the spatial profile of the solute concentration spreads, indicating the distribution of longitudinal speed of the solute molecules (see Figure 1.2). Under certain conditions (to be discussed in Section 1.4), this process has been found to be adequately described by a macroscopic advection-diffusion equation (Bear, 1972).

$$\frac{\partial C}{\partial t} + V_s \frac{\partial C}{\partial x} = D_L \frac{\partial^2 C}{\partial x^2} \qquad (1.3)$$

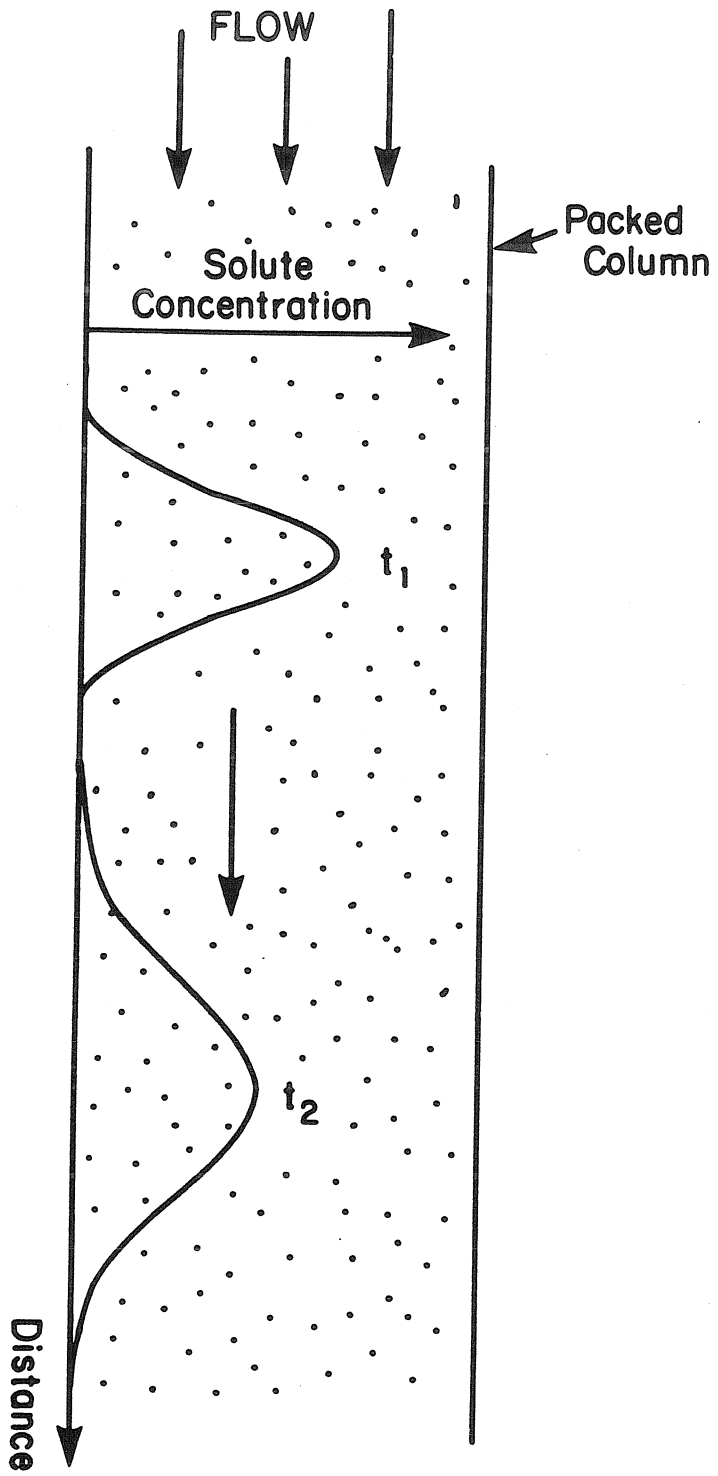

FIGURE 1.2

Development of an Instantaneous Point Source
During Flow Through a One-Dimensional, Homogeneous Packed Column

where C = solute concentration (M/L^3)

D_L = longitudinal dispersion coefficient (L^2/T)

t = time coordinate (T)

x = longitudinal coordinate (L)

The value of D_L is a function of the flow and porous medium characteristics, and is mathematically analogous to molecular diffusion. It should be recognized here, however, that D_L may be orders of magnitude greater than the coefficient of molecular diffusion.

The mathematical representation of an instantaneous point source in an unbounded domain requires the following initial and boundary conditions for a unit mass input:

$$C(x,0) = \delta(x)$$

$$C(x,t) = 0$$

where $\delta(x)$ is the delta function

$$\delta(x) = \lim_{t \to 0} \frac{1}{\sqrt{4\pi t}} \text{ EXP} \left[\frac{-x^2}{4t}\right]$$

The solution of equation (1.3) under the initial and boundary conditions given above is well known to be

$$C(x,t) = \frac{1}{\sqrt{4\pi D_L t}} \text{ EXP} \left[\frac{-(x - V_s t)^2}{4D_L t}\right] \qquad (1.4)$$

The typical experimental investigation of longitudinal dispersion does not use an instantaneous slug, but displaces the resident fluid with a solution of some constant solute concentration, C_0 (Rose, 1977). Again, assuming an infinite, one-dimensional medium, the boundary conditions are

$$\lim_{x \to -\infty} \quad C(x,t) = C_0$$

$$\lim_{x \to +\infty} \quad C(x,t) = 0$$

and the initial condition is

$$C(x,0) = C_0$$

$$C(x,0) = 0$$

The solution to equation (1.3) under these initial and boundary conditions is

$$C(x,t) = \frac{C_0}{2} \text{ erfc } \left[\frac{x - V_s t}{\sqrt{4D_L t}}\right] \tag{1.5}$$

where erfc is the complementary error function.

The complementary error function solution, shown in Figure 1.3, is commonly known as a breakthrough curve. Actually, breakthrough curves are more often measured at a fixed location over time than as a spatial profile at a fixed time. The difference between the two profiles is small under the following condition (Fischer, 1964):

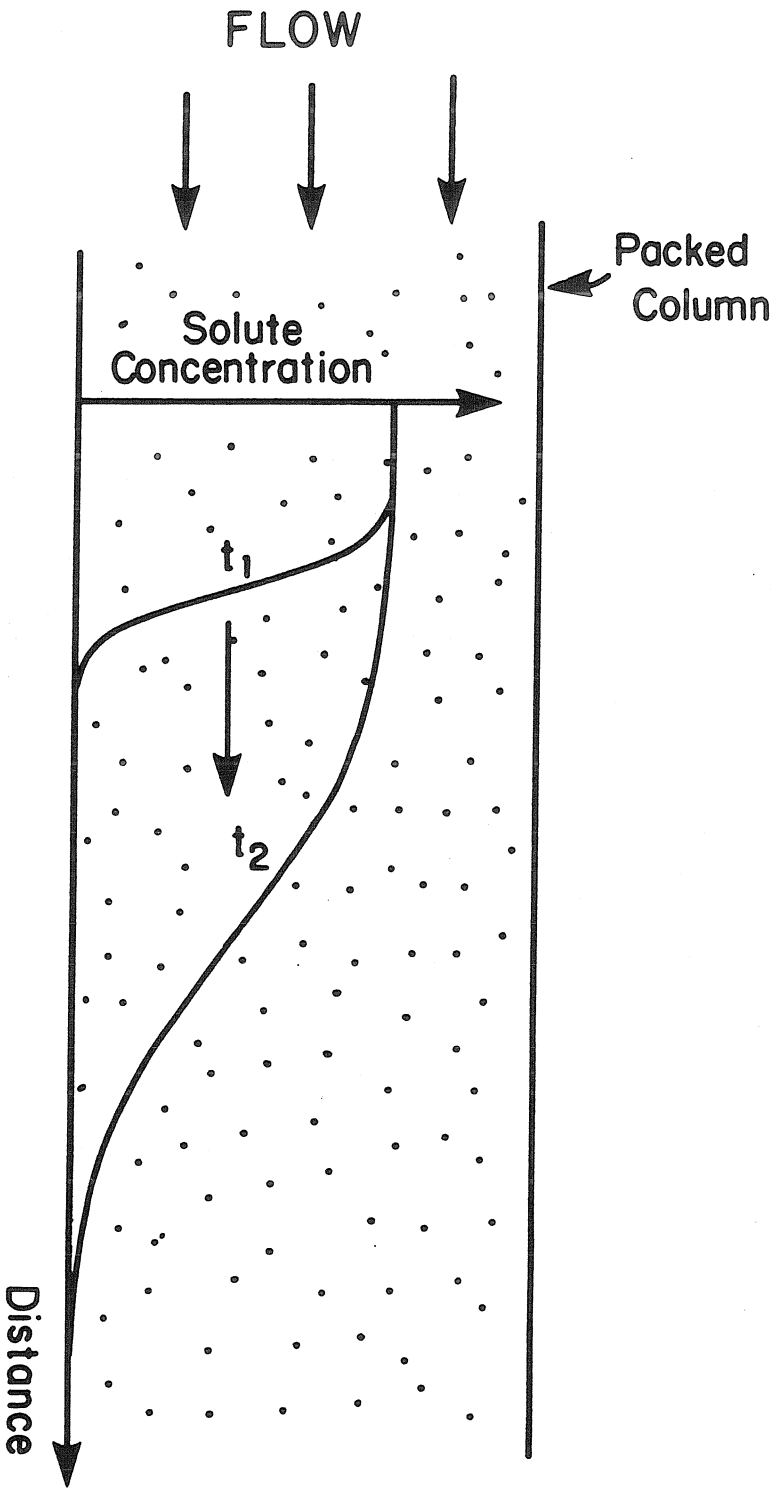

FIGURE 1.3

Miscible Displacement in a One-Dimensional, Homogeneous Packed Column

$$V_s x/D_L >> 1$$

As $V_s x/D_L$ becomes small, breakthrough curves measured at a fixed location become increasingly skew.

Despite the general acceptance of an advection-diffusion model of longitudinal mixing in packed beds, some deficiencies are evident. As brought out in the review article by Sundaresan, et al. (1980), the advection-diffusion model predicts backmixing at the source in breakthrough problems and infinite propagation speed of the initial solute appearance downstream. Backmixing was studied experimentally by Hiby (1963), and his conclusion was that no backmixing occurs. The infinite propagation speed of initial solute breakthrough is physically impossible. These artifacts of advection-diffusion theory could be significant at the "tails" of the concentration-distance profiles, where a small amount of breakthrough would be erroneously predicted using advection-diffusion theory.

Generalizing equation (1.3) to 3 dimensions, with flow along the x direction, gives

$$\frac{\partial C}{\partial t} + V_s \frac{\partial C}{\partial x} = D_L \frac{\partial^2 C}{\partial x^2} + D_T \left(\frac{\partial^2 C}{\partial y^2} + \frac{\partial^2 C}{\partial z^2} \right) \qquad (1.6)$$

where D_T is the transverse dispersion coefficient (L^2/T).

Transverse dispersion is a hydrodynamic effect of the velocity distribution transverse to the mean flow direction. The value of D_T,

like D_L, is a function of the flow and medium characteristics. Similarly, its value may be orders of magnitude greater than the coefficient of molecular diffusion. Experimental investigations of D_T have used a steady-state dispersion pattern developed from coflowing streams (List and Brooks, 1967). For steady-state dispersion in two dimensions, as in Figure 1.4, equation (1.6) reduces to

$$V_s \frac{\partial C}{\partial x} = D_L \frac{\partial^2 C}{\partial x^2} + D_T \frac{\partial^2 C}{\partial y^2}$$

The longitudinal dispersive flux is considered negligible for a continuous source when advection dominates longitudinal transport or

$$\frac{V_s x}{D_L} >> 1$$

where x is the longitudinal distance from the source. Therefore, sufficiently far from the source, the transport equation may be approximated by

$$V_s \frac{\partial C}{\partial x} = D_T \frac{\partial^2 C}{\partial y^2} \qquad (1.7)$$

and the appropriate boundary conditions are (neglecting boundary effects in Figure 1.4)

$$C(0,y) = C_0 H(y)$$

H(y) is a step function, defined by

$$H(y) = 1 \qquad y \leq 0$$

$$H(y) = 0 \qquad y > 0$$

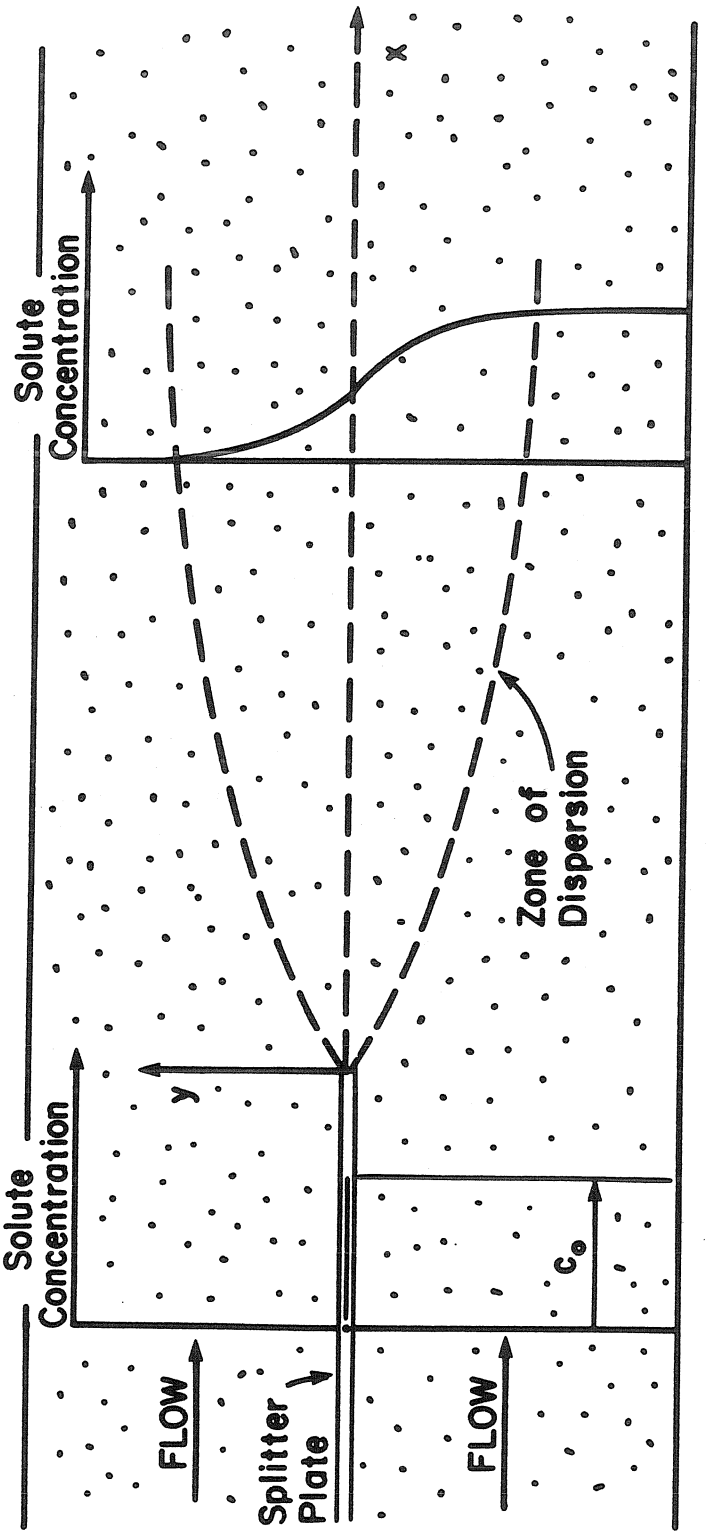

FIGURE 1.4

Transverse Dispersion with Coflowing Streams in a Homogeneous Sand Pack

The solution of equation (1.7) under these boundary conditions is

$$C(x,y) = \frac{C_0}{2} \text{Erfc} \left[\frac{y}{\sqrt{\frac{4D_T X}{V_s}}} \right] \tag{1.8}$$

The complementary error function solution is shown in Figure 1.4.

By comparing the data for longitudinal dispersion presented in Bear (1972) with the data for lateral dispersion given in List and Brooks (1967), the ratio D_L/D_T is found to be greater than or equal to one. These data are the result of dispersion measurements in isotropic media, and show that the existence of a flow direction creates anisotropy in the dispersion. Since the medium is isotropic and molecular diffusion behaves isotropically, the distinction between D_L and D_T must be a hydrodynamic effect.

1.3 Mechanisms of Dispersion

The use of the advection-diffusion equation with an enhanced dispersion coefficient to model solute transport in porous media is justified if sufficient time of motion is allowed for the solute to sample the velocity distribution. To obtain a better understanding of the phenomenon, the underlying physical mechanisms responsible for solute behavior must be determined. Many mechanisms have been given as the cause of dispersion in porous media (Greenkorn, 1981, Fried and Combarnous, 1971). For a passive tracer, three general mechanisms are proposed to explain dispersion.

1.3.1 Molecular Diffusion

In stagnant or slowly flowing fluids, molecular diffusion is the main dispersive transport mechanism. The rate of macroscopic or overall molecular diffusion in a porous medium is related to the rate of diffusion in a free fluid by (Karger, et al., 1973):

$$D_M = \sigma D/\lambda$$

where D_M = diffusion coefficient in porous medium (L^2/T)

D = diffusion coefficient in free fluid (L^2/T)

λ = tortuosity (-)

Tortuosity is defined as the ratio of the average path length followed by a solute molecule to the straight line distance between the initial and final locations. As would be expected, the reduction of free space, σ , and the increase in path length, λ , reduces the overall diffusion rate. In higher velocity flows, mechanical or hydrodynamic dispersion tends to increase in importance relative to molecular diffusion. The effect of molecular diffusion on dispersion can be enhanced by the presence of dead-end pores or pores with relatively stagnant fluid (Coats and Smith, 1964). Diffusion into and out of stagnant zones combined with advective transport can produce highly asymmetric breakthrough curves or "tailing."

1.3.2 Tortuosity

Tortuosity, as defined above, refers to the tortuous path a solute molecule must take to pass through a porous medium. Empirical studies

have found the tortuosity to be related to the formation factor, F, which is the ratio of the resistivity of the porous medium saturated with electrolyte to the resistivity of the pure electrolyte over an identical distance. The relationship found is (Bear, 1972; Winsauer, et.al., 1952):

$$\lambda = (F\sigma)^{3/5}$$

Tortuosity can cause lateral dispersion by forcing solute molecules to take random lateral steps. It affects the longitudinal dispersion by presenting a selection of paths of different lengths which may be used to travel from one point to another. In general, solute molecules traveling along different streamlines will encounter various random paths resulting in dispersion of the solute.

1.3.3 Differential Advection

Solute speed is defined as the tangential advective speed of a solute molecule along a pore. Dispersion due to differential advection is familiar from the work of G.I. Taylor (1953) on dispersion in pipe flow. Differential advection creates dispersion on two scales in a porous medium. First, speed varies within a pore due to the viscous velocity profile. Second, the speed varies between different pores due to a varying hydraulic gradient and differing pore sizes. Differential advection can be seen to cause longitudinal dispersion and, coupled with tortuosity, can increase lateral dispersion.

The relative importance of these mechanisms is a function of the molecular diffusion coefficient, the porous medium, and flow conditions. These mechanisms will be discussed quantitatively in Chapter 3 to develop a solute transport model.

1.4 Porous Medium Classification and Dispersion

A porous medium can be classified according to the character of its pore spaces. A well-defined classification system is needed to discuss the structural properties of a porous medium. Figure 1.5 outlines the terminology to be used here. Although many of the terms are in general use, there are still differences in nomenclature used in the different engineering fields which study flow through porous media.

From Figure 1.5, a porous medium is found to be either homogeneous or heterogeneous at the macroscopic level. Properties at the macroscopic level are averaged over a sufficiently large volume, called the macroscopic averaging volume, to define continuous, stable functions of spatial position (Bear, 1972). A homogeneous medium contains two subcategories at the grain-scale level (or "microscopic" level), the uniform or nonuniform medium. A porous medium is also seen to be either isotropic or anisotrpic at the macroscale. The final structural feature in Figure 1.5 is distinguished from the rest in that it does not directly relate to the porous medium's ability to conduct and disperse fluids. However, the difference between a consolidated

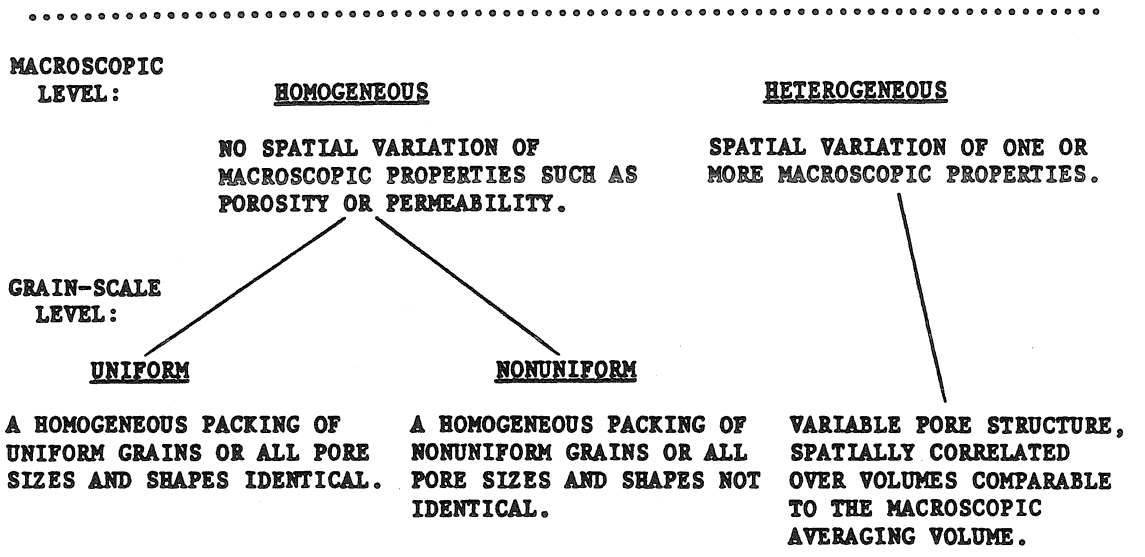

FIGURE 1.5

Structural Features of Porous Media

porous medium and an unconsolidated one is important in the determination of structure at the grain scale.

The transport and dispersion of solutes are dependent on the type of medium involved. Simple advection-diffusion (equation (1.6)) is found to be valid for homogeneous, isotropic porous media, subject to the limitations described in Section 1.2. Although the mechanisms of dispersion are the same, nonuniformity and heterogeneity provide greater variations in solute speed and tortuosity. The result of this is increased dispersion, as indicated by the data of Orlob (1958) for nonuniform material. For heterogeneous, isotropic porous media, a generalization of equation (1.6) is possible (Bear, 1972) if the spatial variations of all the macroscopic properties are known. The effects of anisotropy on miscible mass transport are not completely understood.

Heterogeneous porous media are often modeled as homogeneous media with an overall (super-macroscopic) mean flow direction and super-macroscopic dispersion coefficient, since data on the exact nature of the heterogeneities are usually not available. At this level, the heterogeneity in permeability creates significant dispersive effects. Extremely high dispersion coefficients are found when an advection-diffusion modeling approach is used at this scale (Bredehoeft and Pinder (1973)). Viewing the effects of heterogeneous permeability as a dispersive phenomenon may create a nondiffusive dispersion in which transport cannot be satisfactorily modeled using the advection-diffusion equation. Nondiffusive dispersion is expected when

heterogeneities in the medium are large compared to the scale of the problem being analyzed (Smith and Schwartz, 1978).

1.5 Scope of this Study

A random capillary tube model has been developed for analyzing miscible transport phenomena during flow through nonuniform, isotropic, unconsolidated porous media. The analysis for a uniform porous medium is a special case of the general model. The solute is assumed to be chemically inert; i.e., no adsorption or reaction and dynamically passive in that its presence does not create significant density or viscosity deviations from the pure solvent state. In addition, the flow must be saturated, and is restricted to the Darcy regime (linear, laminar flow).

A laboratory investigation of solute transport in nonuniform porous materials has been conducted. Previously, very little data existed regarding the relationship of solute transport characteristics and grain or pore size distribution data. Laboratory data characterizing pore structure are used as input to the solute transport model and results from model simulation and experiments are compared.

CHAPTER 2

LITERATURE REVIEW

Transport phenomena during flow through porous media have been an active topic of research over the past 30 years. During this time, several distinct classes of porous media models have been developed. Considering the geometrical complexity of a porous medium, a crucial element in any model is the conceptual representation of the pore spaces. The different idealizations used to model a porous medium vary widely, ranging from simple capillary models which bear little resemblance to a porous medium to statistical models in which the complex geometry is modeled through probability density functions.

The results of this effort at modeling solute transport in porous media are encouraging but far from complete. The problem in this type of modeling appears to be a reluctance to use more detailed information on the pore structure to define the medium. This reluctance is understandable for two reasons:

1. It is difficult to incorporate microscopic structural information into a solute transport model, particularly if one is interested in eventually using a macroscopic model such as the advection-diffusion equation.

2. Pore structural information is difficult to obtain and interpret.

Despite the limitations of the theoretical models reviewed here, they provide reasonably accurate predictions for mass transport in

uniform porous media and a useful conceptual framework for thinking about more complex problems. The models of Saffman (1959) and Haring and Greenkorn (1970) discussed here provide the foundation for the model developed in Chapter 3.

2.1 Permeability Models

2.1.1 Bundle of Capillary Tubes

Due to the intricate geometrical detail of a real porous medium, an exact representation of the pore spaces is impossible. One approach is to neglect all detail except that the porous medium contains uninterrupted connecting pathways of some characteristic size, and model the medium as a bundle of straight cylindrical capillary tubes (Bear, 1972). This simplistic model neglects the important effects of tortuosity and interconnectedness, but is still able to represent the basic functional behavior of the permeability. For incompressible, linear-laminar flow conditions, such models are based on Poiseuille's law for flow in cylindrical capillaries. Only Newtonian fluids of constant density will be considered. According to this law, the average velocity in a capillary tube is

$$\overline{u} = - \frac{\rho g}{\mu} \frac{a^2}{8} \frac{d\phi}{dx} \qquad (2.1)$$

where a = capillary radius (L)

$\frac{d\phi}{dx}$ = piezometric head gradient along capillary axis (-)

ρ = fluid density (M/L^3)

g = gravitational acceleration (L^2/T)

μ = dynamic viscosity (M/LT)

$\bar{u}$ = average velocity (L/T)

If we assume the seepage velocity, V_s, to be equal to u and employ Darcy's law

$$\sigma V_s = \frac{-\rho g k}{\mu} \frac{d\phi}{dx} \tag{2.2}$$

where σ = porosity (-)

k = permeability (L^2)

combining equations (2.1) and (2.2) we find

$$k = \frac{\sigma a^2}{8} \tag{2.3}$$

The relationship between the permeability and hydraulic conductivity (equation (1.1)) is given by $K = kg/\nu$. As Bear (1972) points out, the constant (1/8) is meaningless since the model is too idealized. However, the basic functional relationship $k \sim \sigma a^2$ is valid, with the constant to be determined by experiment.

2.1.2 Hydraulic Radius Model

Probably the best-known permeability model is the Carman-Kozeny theory (Carman, 1937). This permeability relationship is developed using dimensional arguments similar to those given in Chapter 1. The main difference is that the length scale is taken to be the hydraulic

radius, r_H, rather than an effective capillary radius, a. The hydraulic radius is given by $r_H = \sigma/S$, where S is the surface area of solids per unit volume of medium (L^{-1}). For a bed of uniform spheres,

$$S = \frac{6(1 - \sigma)}{d}$$

where d is the sphere diameter (L). The relation for r_H becomes

$$r_H = \frac{\sigma d}{6(1 - \sigma)}$$

Substituting r_H for a in equation (1.1) and fixing the constant of proportionality by comparison with experiments, we find

$$V_D = \frac{-\sigma^3 d^2}{180(1 - \sigma)^2} \left(\frac{g}{\nu}\right) \nabla\phi$$

The permeability is

$$k = \frac{\sigma^3 d^2}{180(1 - \sigma)^2} \tag{2.4}$$

Carman (1937) quotes experimental verification of the dependence of the permeability on porosity as given in equation (2.4).

2.1.3 Random Capillary Tube Network

Saffman (1959) used a random capillary tube network to model a porous medium. By assuming random orientation for the capillary tubes, conduction of fluid through each capillary tube to be independent of the network interconnections, and flow in each capillary tube following Poiseuille's law, a permeability for the network could be determined.

Saffman (1959) finds for the permeability, k

$$k = \frac{\sigma a^2}{24} \tag{2.5}$$

where a is the pore radius. Comparing the Saffman model (equation (2.5)) with equation (2.4) we find

$$a = \frac{\sigma d}{2.74(1 - \sigma)} \tag{2.6}$$

Experimental evidence for this relation is scant, but the data of Saffman (1959) and data given in Chapter 4 show the expression to be accurate to within 10%. A more detailed discussion of this model is given in Chapter 3 where the model is extended to nonuniform media.

2.1.4 Volume-Averaging Model

Bear (1972) presents a volume-averaging model which is based on averaging the conservation equations for mass and momentum over a representative elementary volume. No specific pore geometry is assumed, but the pore space is assumed to consist of channels which have definite directions (and axes) along which the flow is directed. The development of Bear's (1972) model requires some assumptions regarding the spatial correlation of fluid properties, medium properties, and the pressure field. A particularly significant assumption is that there is no correlation between the pressure field and the pore geometry. Bear's result for the permeability is

$$k_{ij} = \sigma\overline{BT_{ij}} \tag{2.7}$$

where B is the channel conductance (L^2) and T_{ij} (-) is the coordinate transformation from a local coordinate system oriented along the pore channels to a fixed Cartesian coordinate system. The overbar denotes a volume average. As an example, Bear (1972) shows for an isotropic medium consisting of straight cylindrical capillaries of radius a and channel conductance $B = a^2/8$

$$k = \frac{\sigma a^2}{24} \tag{2.8}$$

which is the same result as found by Saffman (1959) (equation (2.5)). Although the model is difficult to evaluate in general, it does provide a theoretical relation for anisotropic porous media.

2.1.5 Deterministic Network Model

A natural extension of the capillary tube model is a capillary tube network which accounts for the exact nature of the interconnections. This type of network model differs from the Saffman (1959) model in that a deterministic network is used. The effects of flow in one capillary tube on other capillaries in the network is taken into account. The network approach was investigated in detail by Fatt (1956), who employed various two-dimensional regular networks to represent porous media. Fatt's model also presents one of the earliest investigations of the effect of nonuniform pore structure on

permeability (and relative permeability for multi-phase flow). Fatt was able to vary both pore radius and length, although the deterministic two-dimensional network did not allow random path lengths between junctions. An interesting finding of this work is that the permeability of networks in which pore radius and length vary randomly and independently is nearly the same as for a similar network in which there is a deterministic relationship between pore radius and pore length.

2.2 Dispersion Models

2.2.1 Cell Models

As in permeability models, a crucial element of any dispersion model is the representation of the geometry of the porous medium. Previous theoretical investigations into the nature of dispersion in porous media have used a variety of geometrical models. Cell models are highly idealized representations of porous media in which the pores are considered to act as a linear series of well-mixed storage cells. The dispersion in this case is derived from the randomness of particles making a transition from one cell to the next. The mechanisms of dispersion as discussed in Chapter 1 are not specifically included. The effect of these mechanisms are lumped into the random residence time of a particle in a mixing cell. Despite these simplifications, cell models produce the correct functional relationship between the longitudinal dispersion coefficient and the velocity and length scales for flow in uniform media at high Peclet number ($V_s d/D$).

Aris and Amundson (1957) calculate the probability density for the position of a particle passing through a series of well-mixed cells. The residence time in each cell is t_r (cell volume/ flow rate), and the time of passage between cells is neglected. Their result, for the probability that a particle introduced at the origin at time t=0 is in the nth cell at time t, is

$$P_n(t) = \frac{(t/t_r)^n}{n!} e^{-t/t_r} \qquad (2.9)$$

Being a Poisson distribution, the mean and variance are equal, and tend to a Gaussian as $t/t_r \to \infty$. The Gaussian distribution

$$P(x,t) = \frac{1}{\sqrt{4\pi D_L t}} \text{ EXP } \left[\frac{-(x - V_s t)^2}{4D_L t}\right] \qquad (2.10)$$

will approximate the distribution in equation (2.1) if the dimensionless mean and variance in equation (2.10) are equated to t/t_r, the mean and variance of the Poisson distribution. D_L is the longitudinal dispersion coefficient (L^2/T). Aris and Amundson introduce γd as the length scale to nondimensionalize the mean and variance of the Gaussian distribution, where γ is called the packing factor. The dimensionless mean and variance are, respectively,

$$\varepsilon = V_s t/\gamma d$$

$$\delta^2 = 2D_L t/(\gamma d)^2$$

Aris and Amundson equate ε and δ^2 to solve for D_L.

$$D_L = (1/2)\ V_s \gamma d \qquad (2.11)$$

From experiments, they find $\gamma \sim 1$ for a random packing of grains.

Since the basic cell model does not model the internal structure of a porous medium and uses a single velocity and length scale, it is simpler to analyze the problem with dimensional analysis. The pertinent variables are

D_L = longitudinal dispersion coefficient (L^2/T)

D = molecular diffusion coefficient in a free fluid (L^2/T)

V_s = seepage velocity (L/T)

d = grain size (L)

from the Buckingham pi theorem

$$D_L/V_s d = f(V_s d/D)$$

or

$$D_L/D = f(V_s d/D)$$

where $Pe = V_s d/D$ is the Peclet number of the flow. Data for longitudinal dispersion in uniform media (Figures 2.1 and 2.2) show good correlation with these dimensionless groups. When the Peclet number is greater than 1, a good order of magnitude approximation for the longitudinal dispersion coefficient can be made with

$$D_L = V_s d$$

A similar dimensional analysis can be made for transverse dispersion.

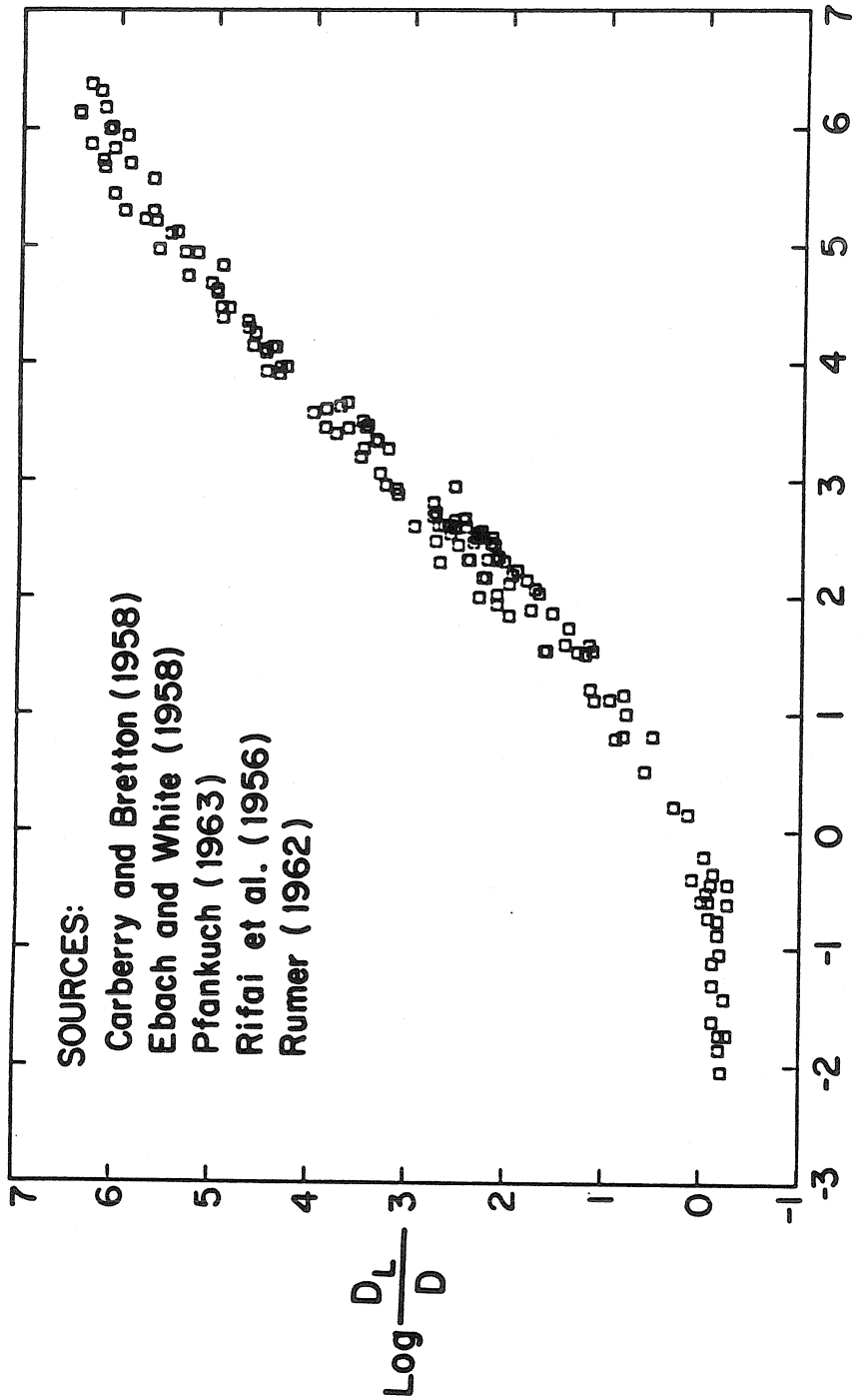

FIGURE 2.1

Longitudinal Dispersion vs. Peclet Number in Uniform Porous Media

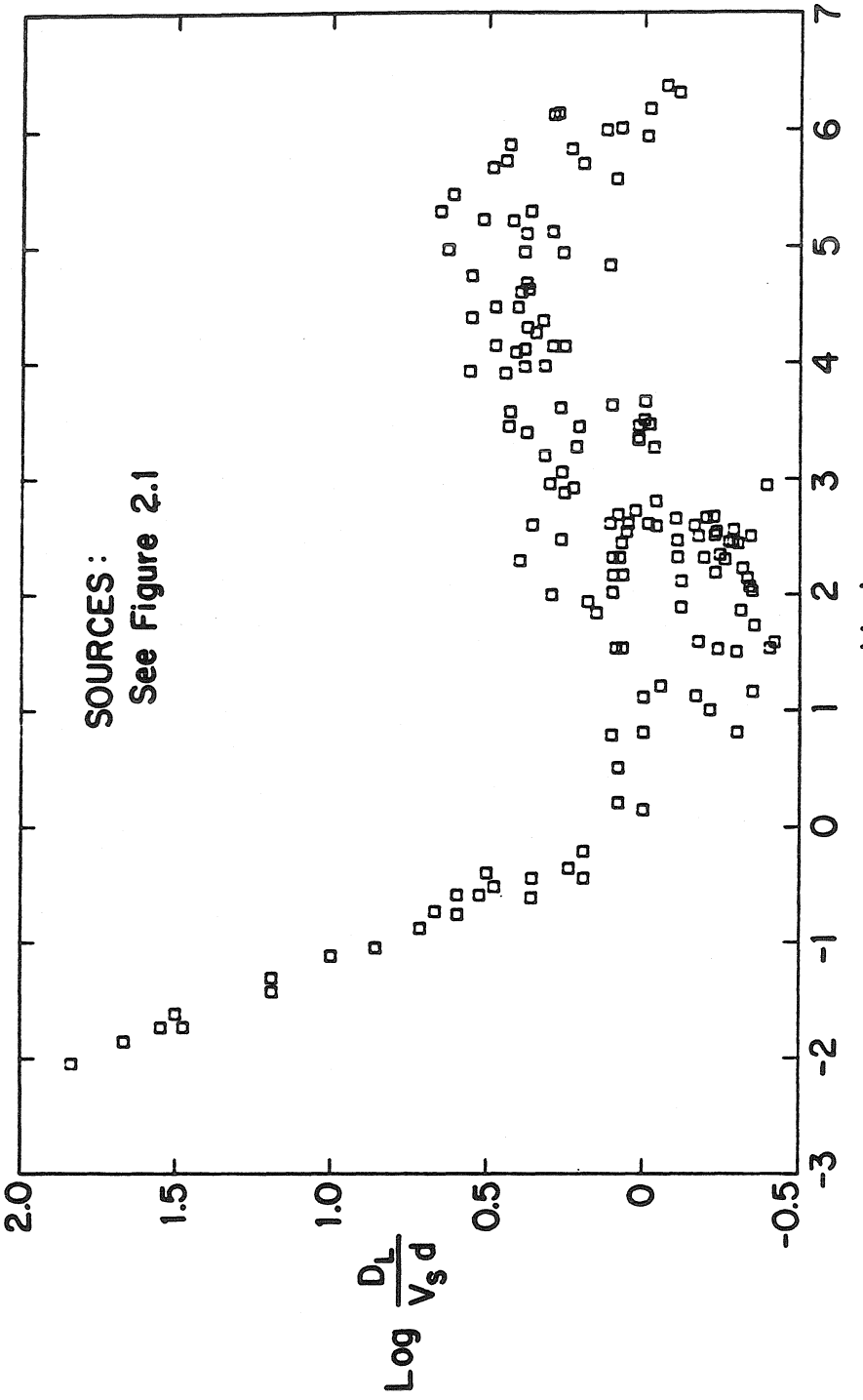

FIGURE 2.2

Inverse Dynamic Peclet Number for Longitudinal Dispersion
vs. Peclet Number in Uniform Porous Media

Figures 2.3 and 2.4 display the experimental findings in dimensionless form. The numerous experiments shown in Figures 2.1 to 2.4 have been performed on uniform unconsolidated materials. The various experiments have used different materials (glass beads, natural sands, etc.), measuring techniques, apparatus and packing methods. This partially accounts for the scatter, but strong correlations of the dimensionless groups are still present.

2.2.2 Statistical Models

The cell model is a highly idealized representation of a porous medium, with a structure that is difficult to relate to the porous medium. Statistical models assume a random pore structure which can be quantified in a statistical sense. A random or statistical character is assigned to the medium since a deterministic description of the complex geometry of a porous medium is impossible. Statistical models can use more detailed and realistic descriptions of the pore structure than is possible in deterministic models. All statistical models described here depend on the basic linearity or noninteraction of solutes. This is needed since the behavior of a cloud of particles (or solute solution) is investigated through analysis of the statistics of a single particle. If interaction occurs, such as in nonlinear adsorption phenomena, the statistics of a single-particle transport do not describe how a cloud of particles behave.

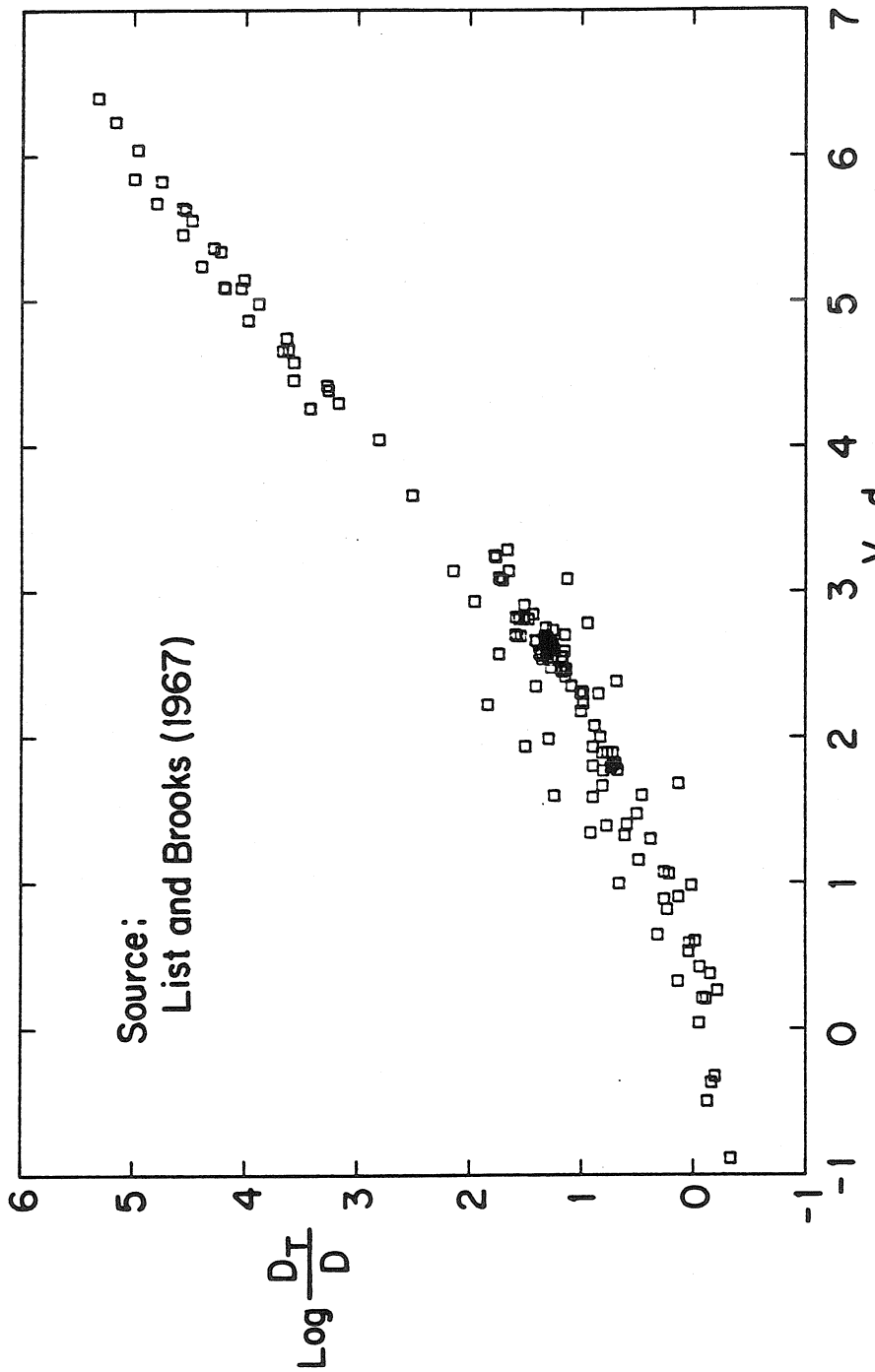

FIGURE 2.3

Transverse Dispersion vs. Peclet Number in Uniform Porous Media

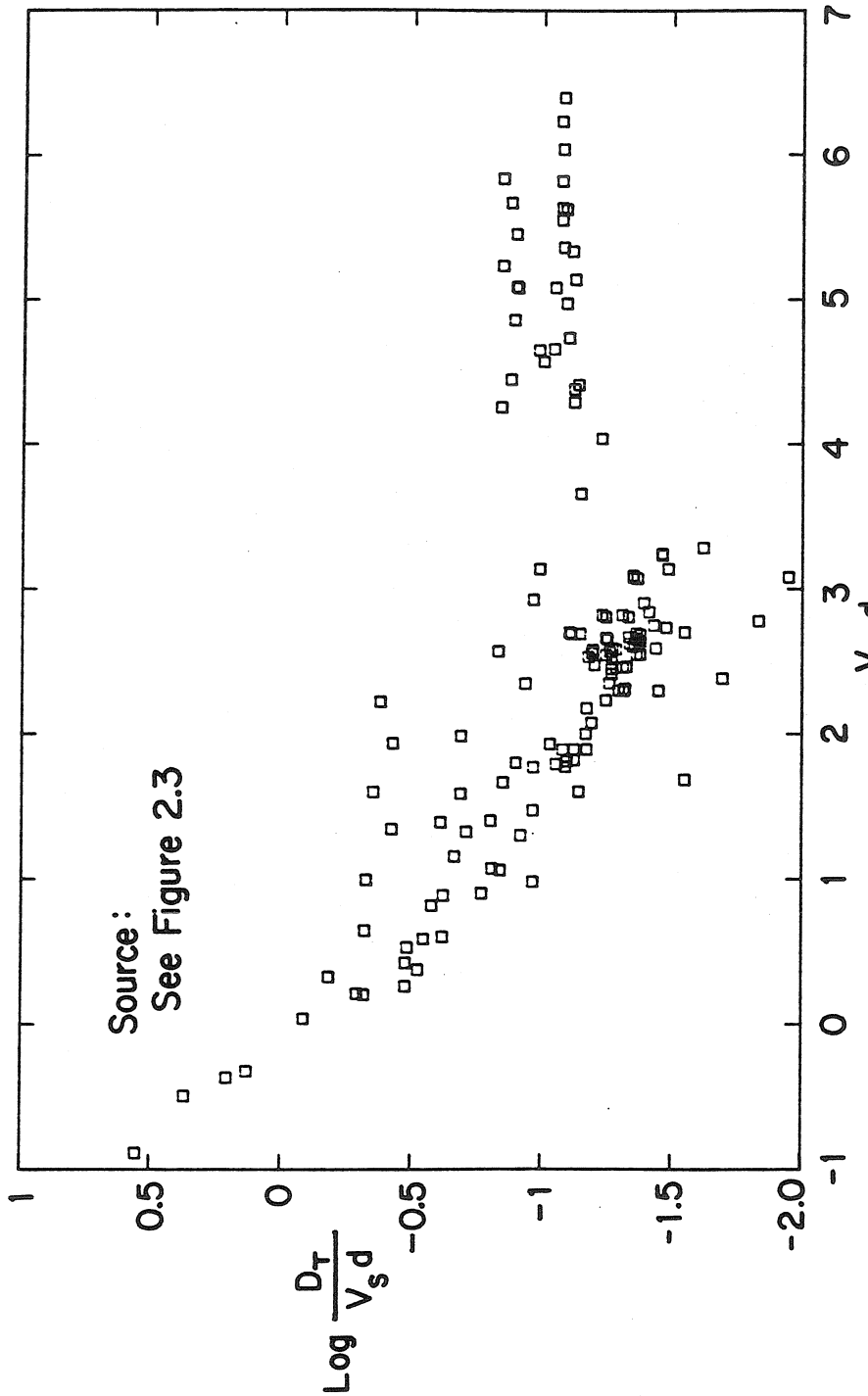

FIGURE 2.4

Inverse Dynamic Peclet Number for Transverse Dispersion
vs. Peclet Number in Uniform Porous Media

2.2.2.1 Random Capillary Tube Models

The first models of dispersion in porous media based on pore structure are those of de Josselin de Jong (1958) and Saffman (1959, 1960). The Saffman (1959) model and the de Josselin de Jong (1958) model use a similar approach, but Saffman's work is more general and includes the effects of molecular diffusion on dispersion. A separate review of the de Josselin de Jong (1958) model will not be given.

Saffman's (1959) model assumes a porous medium to consist of a random interconnected network of capillary tubes. He considers a passive tracer particle which proceeds through the capillary tube network by making a series of random, independent steps, in which the probability for making a given step is governed by the geometry of the random network and the physics of laminar flow in a tube. Each step consists of passing from one junction to another through a capillary tube. The mean and variance for the motion of a single particle is calculated and, using the ergodic hypothesis, determines the properties for a "cloud" of particles. The variance about the mean is then related to a dispersion coefficient through the Einstein relation

$$\sigma_L^2 = 2D_L t \quad ; \quad \sigma_T^2 = 2D_T t$$

where σ_L^2 = longitudinal variance of position about the mean (L^2)

σ_T^2 = transverse variance of position about the mean (L^2)

Through an analysis of the statistics of particle trajectories in the network, Saffman was able to compute the mean and variance of the

particle's position at a given time for both longitudinal and transverse motion. When the pore length to radius tends to infinity, the resulting expression for the longitudinal dispersion is (Saffman, 1959)

$$\frac{D_L}{D} = \frac{1}{2} Pe \left[\frac{1}{3} \ln\left(\frac{3}{2} Pe\right) - \frac{1}{12} \right] \tag{2.12}$$

Actually, the condition for equation (2.12) to hold is $Pe << 8\,\delta^2$, where δ is the ratio of the pore length to pore radius. The only implication in letting δ tend to infinity is that shear dispersion within individual pores will be neglected. For the near field, $V_s t/D < 0.5(Pe)$, Saffman finds that the dispersion coefficient is a logarithmic function of time. The longitudinal dispersion coefficient for the case when δ is small is also calculated. Figure 2.5 shows a comparison between equation (2.12) and the data presented in Figure 2.1.

Saffman determines the transverse dispersion to be

$$D_T/D = (3/16)Pe \tag{2.13}$$

and is independent of time or molecular diffusion. When compared to the data in Figure 2.3, D_T is seen to be about 0.4 order of magnitude high for Peclet >100 (Figure 2.6). Saffman states that the results for transverse dispersion are questionable due to an assumption of independence of the azimuthal angle in successive steps, which may not be valid. A more detailed discussion of this theory will be given in Chapter 3, where the model is extended to a nonuniform medium.

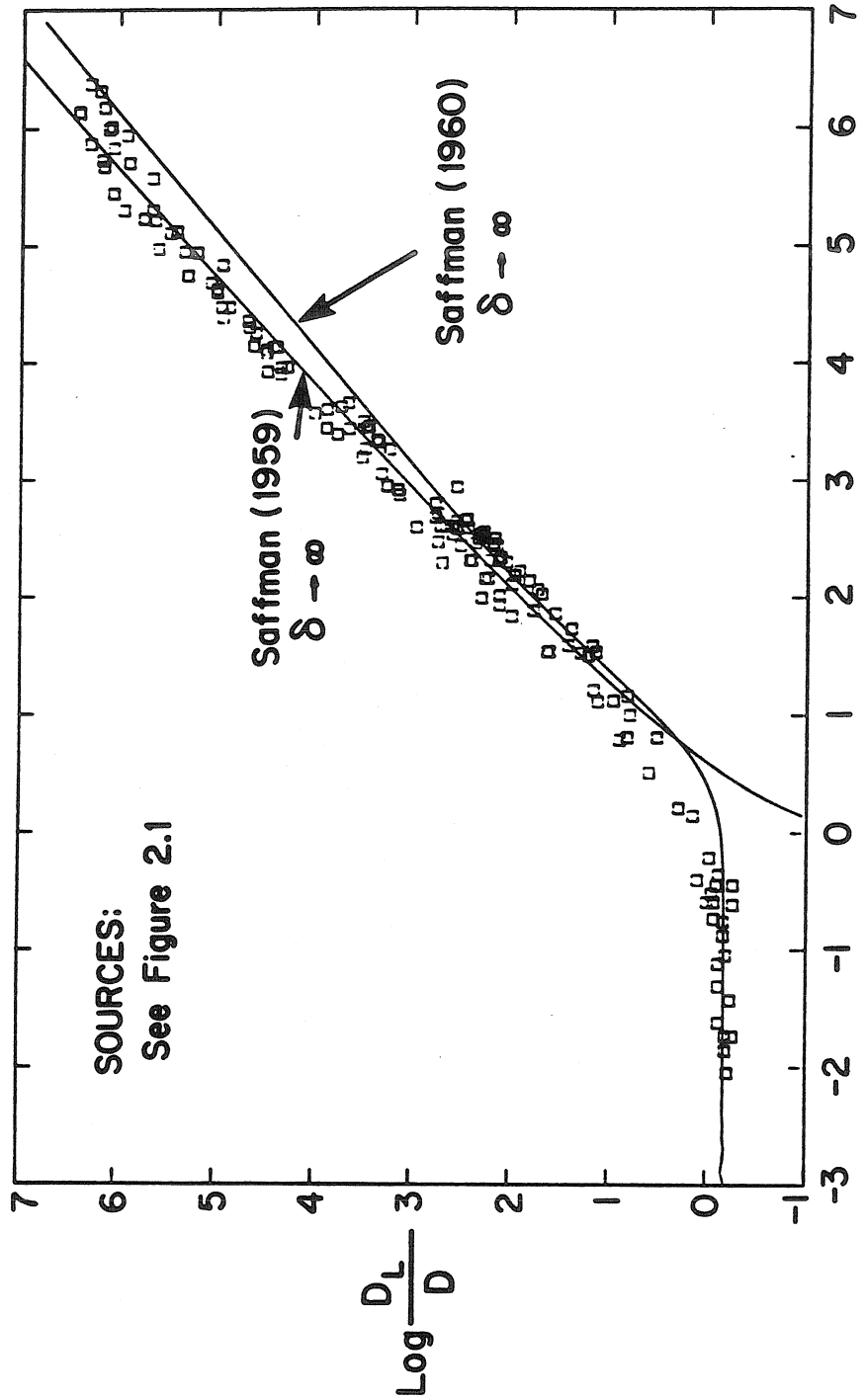

FIGURE 2.5

Random Capillary Tube Network Theories for Longitudinal Dispersion

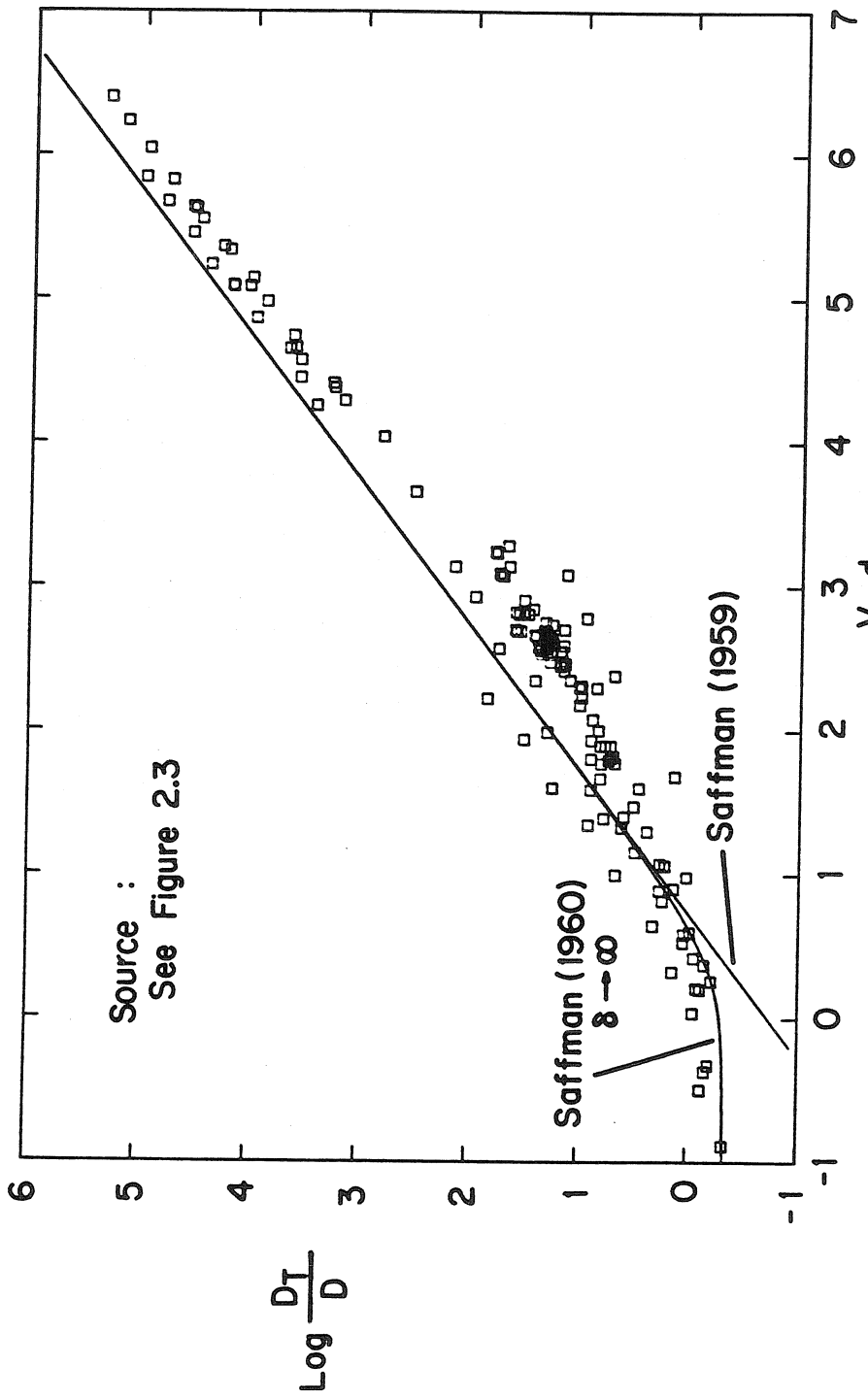

FIGURE 2.6

Random Capillary Tube Network Theories for Transverse Dispersion

In a second paper, Saffman (1960) addresses the problem of dispersion when the Peclet number is not large with respect to 1. The previous random walk approach is not valid for this case for two reasons. First, the residence time of a significant fraction of particles begins to depend on the molecular diffusion, which is only crudely accounted for in the random walk theory. Second, the basis for the selection of a pore by a particle at a junction does not follow the simple probability density function previously derived, since diffusion becomes significant in comparison to advection. Particles no longer choose streamlines in proportion to the advective velocity along the streamline. Saffman solves both problems by taking an entirely different approach which uses Taylor's (1921) classic analysis of diffusion by continuous movements. According to Taylor (1921), the variance of the positions of particles released at a point is (in 1 dimension)

$$\sigma_L^2 \sim 2t \int_0^\infty R(\hat{\tau}) d\hat{\tau}$$

where $R(\hat{\tau}) = \overline{u(t)u(t')}$ = Lagrangian correlation function (L^2/T^2)

$\hat{\tau} = |t - t'|$ (T)

$u(t)$ = longitudinal component of the particle velocity (L/T)

and bar denotes an average overall network configuration.

Saffman assumes the velocity to be low enough such that the results of Taylor (1953) may be applied to each tube in the network. Under these conditions, the dispersion of a tracer within a given capillary tube is

governed by an effective advection-diffusion equation for the mean flow through the tube, with the dispersion along the tube given by the results of Taylor's (1953) analysis. The mean velocity through a tube is given by Poiseuille's law and the projection of the macroscopic pressure gradient. The longitudinal component of the velocity along a tube (denoted by u(t)) is the sum of the longitudinal component of the mean velocity plus a random component due to the effects of Taylor dispersion. Averaging the Lagrangian correlation function over all network configurations and integrating the time difference from 0 to ∞, Saffman finds

$$\frac{D_L}{D} = \frac{1}{3} + \frac{3}{80}\,\frac{Pe^2}{\delta^2} + \frac{Pe^2}{4}\int_0^1 (3\omega^2 - 1)^2\,\frac{M\coth M - 1}{D_e M^2}\,d\omega \qquad (2.14)$$

where $\delta = d/a$ = pore length/pore radius

$\omega = \cos(\theta)$; θ = direction of motion relative to mean flow direction

$$M = (3/2)Pe \cdot \omega/D_e$$

$$D_e = 1 + (3/16)(Pe \cdot \omega/\delta)^2$$

The final integral is a function of Peclet number ($V_s d/D$) and δ. Equation (2.14) is plotted as a function of Peclet number in Figure 2.5 for $\delta \to \infty$.

Following a similar procedure, Saffman calculates the lateral dispersion coefficient

$$\frac{D_T}{D} = \frac{1}{3} + \frac{1}{80}\,\frac{Pe^2}{\delta^2} + \frac{9}{8}\,Pe^2\int_0^1 \omega^2(1 - \omega^2)\,\frac{M\coth M - 1}{D_e M^2}\,d\omega \qquad (2.15)$$

As seen in Figure 2.6, the results for transverse dispersion have roughly the correct exponential dependence on the Peclet number but are off by a constant multiple. When $Pe \rightarrow 0$, the longitudinal and transverse dispersion coefficients tend to a constant value, $D_L = D_T = (1/3)D$. Saffman (1960) found these values too low in comparison with experimental findings and suggested the value of $D_L = D_T = (2/3)D$. The constant has been adjusted to give the best fit as $Pe \rightarrow 0$ in Figures 2.5 and 2.6.

In summary, Saffman (1959, 1960) proposed two dispersion models based on flow in a random capillary tube network. The random walk model (Saffman, 1959) is valid for high Peclet number flow ($Pe \gg 1$), while the Lagrangian correlation approach (Saffman, 1960) applies when the Peclet number is limited by $Pe \ll 8\delta^2$.

2.2.2.2 Volume-Averaging Model

Bear (1972) presents a statistical theory of flow and transport in porous media that is based on building macroscopic equations from averaging microscopic quantities over a representative elementary volume. Such an averaging volume is assumed to contain enough pores to define macroscopic quantities such as porosity, permeability, and dispersivity. The development of Bear's theory contains some questionable assumptions concerning mass conservation equations. Bear derives a general expression for the dispersion tensor in an anisotropic medium, but evaluation for the general case is difficult.

Through the use of scaling arguments, Bear finds for a uniform, isotropic medium

$$\frac{D_L}{D} = Pe\left(\frac{Pe}{Pe + 2 + \delta^2}\right) + \overline{\lambda} \qquad (2.16)$$

where $\overline{\lambda}$, experimentally determined, represents the effect of the porous medium on the macroscopic molecular diffusion coefficient. Dispersion due to direct molecular diffusion is added to the hydrodynamic dispersion. Equation (2.16) is seen to be in good agreement with the experimental data (Figure 2.7). Note that the limit $\delta \to \infty$ is entirely different for Bear's theory as compared with Saffman's (1960) theory. The scaling arguments used by Bear to arrive at equation (2.16) break down for this limit. Bear does not derive a corresponding expression for transverse dispersion in uniform, isotropic media.

2.3 Transport Phenomena in Nonuniform Media

Theories discussed to this point have been directed towards dispersion in a uniform medium. While it may be hoped that nonuniform media could be handled by using an average value for the length scale in the uniform media theories, existing data do not support this. In the review by Perkins and Johnston (1963), the experiments of Raimondi, et. al. (1959) and Orlob and Radhakrishna (1958) are summarized. Perkins and Johnston (1963) show that the coefficient of dispersion increases with increasing nonuniformity. Niemann (1969) also finds that dispersion is greater when the grain size distribution becomes

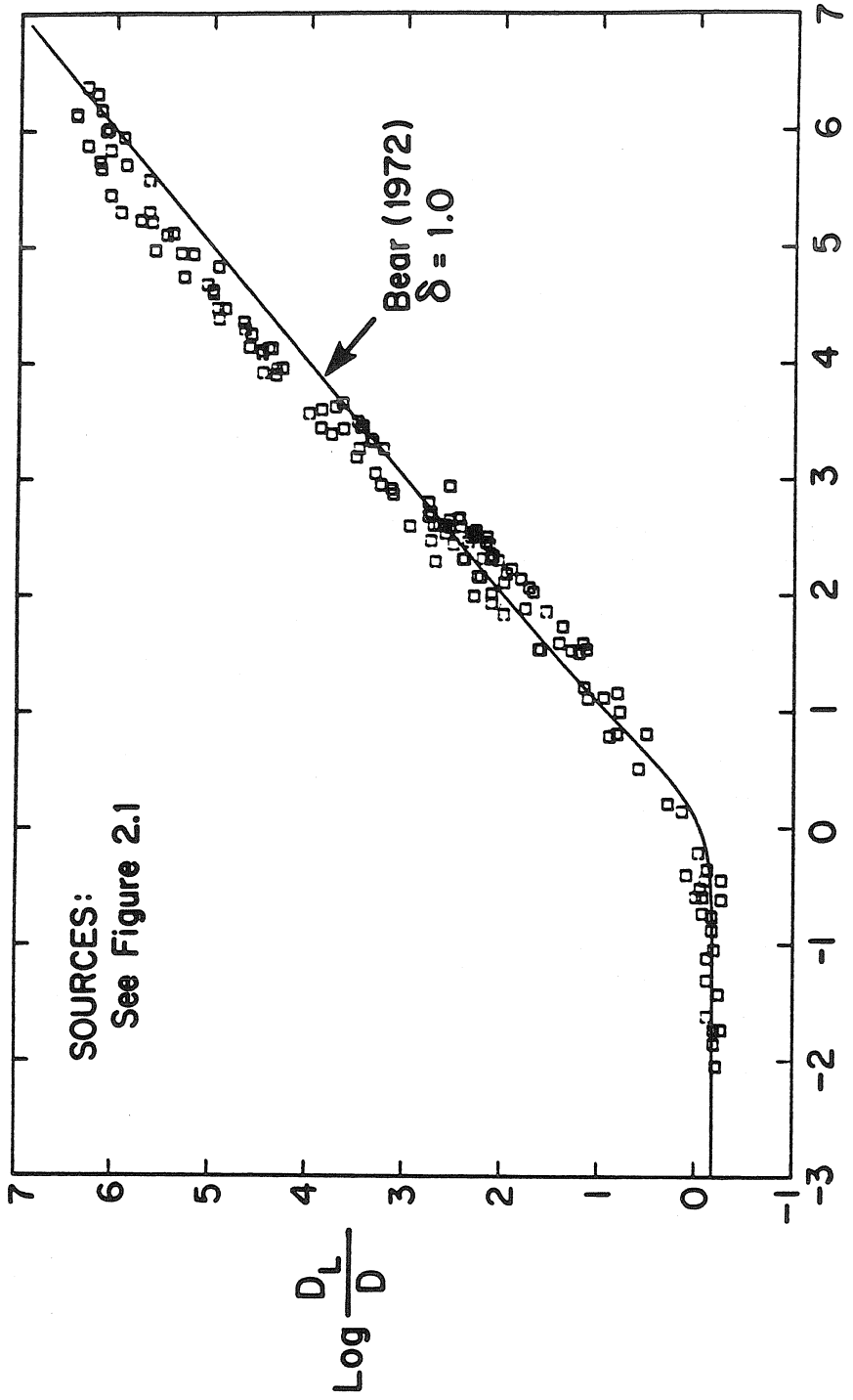

FIGURE 2.7

Volume-Averaging Theory for Longitudinal Dispersion

wider. The data are not conclusive in terms of quantitative predictions of dispersion. The recent review by Greenkorn (1981) indicates little progress has been made on dispersion in nonuniform porous media beyond the few studies mentioned here.

The first theoretical model which explicitly includes the effects of nonuniform media on dispersion is that of Haring and Greenkorn (1970). Their approach is similar to Saffman's (1959), in which the statistics of a single particle executing a random walk through a three-dimensional capillary network describe the behavior of a cloud of particles. In addition to the random orientation of pores, Haring and Greenkorn (1970) allow for distributions of pore length and radius. Their model assumes that the pore length distribution and pore radius distribution can be described by beta distributions. The beta distributions require specification of a maximum pore length and maximum pore radius. The seepage velocity is calculated by averaging the mean longitudinal velocity for each pore over a representative sample of pores of random radius and orientation. The permeability determined by combining this expression for the seepage velocity with Darcy's law. The fact that pores of larger radius will conduct larger quantities of fluid due to the larger cross-sectional area is neglected. They find for the permeability

$$k = \frac{\sigma \quad \bar{a}^2}{24} K(\tilde{\alpha}, \tilde{\beta}) \tag{2.17}$$

where $\bar{a}$ = arithmetic mean pore radius

a_m = maximum pore radius

$a_d = a/a_m$

$g(a_d)$ = probability density function for a_d

$$g(a_d) = \frac{(\tilde{\alpha} + \tilde{\beta} + 1)!}{\tilde{\alpha}!\ \tilde{\beta}!}\ (a_d)^{\tilde{\alpha}}(1 - a_d)^{\tilde{\beta}}$$

$$K(\tilde{\alpha},\tilde{\beta}) = (\tilde{\alpha} + 2)(\tilde{\alpha} + \tilde{\beta} + 2)/(\tilde{\alpha} + 1)(\tilde{\alpha} + \tilde{\beta} + 3)$$

The derivations of expressions for the longitudinal and transverse dispersion coefficients follow the analysis developed by Saffman (1959). However, molecular diffusion is not included in the model, so the longitudinal dispersion coefficient does not reach an asymptotic limit for large times. They find for the longitudinal and transverse dispersion coefficients

$$\frac{D_L}{D} = \frac{1}{12}\ \frac{K(\tilde{m},\tilde{n})}{J^2(\tilde{\alpha},\tilde{\beta})}\ Pe \cdot \ln\left[\frac{27}{2}\ \frac{I^2(\tilde{m},\tilde{n})}{J^3(\tilde{\alpha},\tilde{\beta})}\ \frac{V_s t}{\bar{\ell}}\right] \qquad (2.18)$$

$$\frac{D_T}{D} = \frac{3}{16}\ \frac{K(\tilde{m},\tilde{n})}{J(\tilde{\alpha},\tilde{\beta})}\ Pe \qquad (2.19)$$

where $\bar{\ell}$ = arithmetic mean pore length

$Pe = V_s\ \bar{\ell}\ /D$

ℓ_m = maximum pore length

$\ell_d = \ell/\ell_m$

$f(\ell_d)$ = probability density function for pore length

$$f(\ell_d) = \frac{(\tilde{m} + \tilde{n} + 1)!}{\tilde{m}!\ \tilde{n}!}\ (\ell_d)^{\tilde{m}}(1 - \ell_d)^{\tilde{n}}$$

$$J(\tilde{\alpha},\tilde{\beta}) = \frac{(\tilde{\alpha}+1)(\tilde{\alpha}+2)(\tilde{\alpha}+\tilde{\beta}+4)(\tilde{\alpha}+\tilde{\beta}+5)}{(\tilde{\alpha}+3)(\tilde{\alpha}+4)(\tilde{\alpha}+\tilde{\beta}+2)(\tilde{\alpha}+\tilde{\beta}+3)}$$

$$I(\tilde{m},\tilde{n}) = \frac{\tilde{m}+\tilde{n}+2}{\tilde{m}+1}$$

The model does provide a method of estimating pore radius distributions using capillary drainage curves but does not provide a way to estimate pore length distributions other than fitting with dispersion experiments. Pakula and Greenkorn (1971) performed dispersion experiments on a nonuniform glass bead medium. The bead sizes ranged from 0.59mm to 0.84mm. The longitudinal dispersion coefficient found for this medium was about 5 times larger than what would be expected based on an average bead diameter and the uniform media results given in Section 2.2. The results are not consistent with the dispersion experiments of Rifai, et al. (1956), whose data are shown in Figure 2.1. Rifai, et al. used sands with a particle size range of the same order as Pakula and Greenkorn, yet found values for the longitudinal dispersion coefficient in agreement with other dispersion results for uniform media. The Haring and Greenkorn (1970) model was found to predict the measured longitudinal and transverse dispersion coefficients found by Pakula and Greenkorn (1971) within about 30%. The permeability calculation was found to be within 10% of the measured value.

Wilson and Gelhar (1974) adopt a similar approach, building on the work of Saffman (1959), to evaluate permeability and dispersion in a nonuniform, partially saturated porous medium.

2.4 Summary

Several different classes of permeability and dispersion models have been reviewed and compared with published experimental data. The vast majority of experimental and theoretical work pertain to transport in uniform media. Both experimental and theoretical results for uniform media indicate that miscible mass transport may be described by the advection-diffusion equation with an enhanced dispersion coefficient. Theoretical expressions derived by Saffman (1959) and Carman (1937) are found to give accurate predictions of permeability for uniform media. Experimental evidence supports the hypothesis that the two permeability relations are equivalent. Theoretical results for longitudinal dispersion (Saffman, 1959, 1960; Bear, 1972) show acceptable agreement with experimental measurements, while for transverse dispersion, theoretical calculations (Saffman, 1959, 1960) are found to have the correct trend but do not have quantitative agreement with the experimental data. The Saffman (1959, 1960) models are particularly satisfying since the three dispersion mechanisms (given in Section 1.3) are explicitly included in the analysis of solute transport through a random capillary tube network.

Research on dispersion in nonuniform media is quite limited, but the evidence indicates an increased dispersion due to nonuniformity. Attempts to use an average grain size in uniform media dispersion theories to predict dispersion in nonuniform media have not been successful. Through an extension of the Saffman (1959) model, Haring

and Greenkorn (1970) use a nonuniform random capillary tube network to model permeability and dispersion in nonuniform media. The Haring and Greenkorn model is found to have the following deficiencies:

1) The permeability model neglects the fact that pores conduct fluid in proportion to the fourth power of the pore radius.

2) Neglect of molecular diffusion leads to an unbounded longitudinal dispersion coefficient for large times.

3) Pore radius distributions and pore length distributions must follow beta distributions.

4) No technique is developed to estimate pore length distributions from measurable structural features of porous media.

5) Experimental support for the model is very limited.

CHAPTER 3

A THEORETICAL MODEL FOR PERMEABILITY AND LONGITUDINAL DISPERSION IN NONUNIFORM POROUS MEDIA

In this chapter, a theoretical method is developed for computing permeability and longitudinal dispersion in isotropic, nonuniform porous media based on structural features of the medium. As discussed in Chapter 2, the spectrum of length scales present in a nonuniform medium is important in determining the transport behavior of miscible solutes. Because of additional variables describing the distribution of length scales, there are more dimensionless groups to correlate through experimentation. Since the range of parameters is large, it would be helpful to have reliable models. Of the models presented in Chapter 2, the network model, statistical capillary tube model, and the volume-averaging model are capable of being extended to nonuniform media. The model to be developed here is an extension of the random capillary tube model proposed by Saffman (1959). No extensions were attempted with the network model or the volume-averaging model.

As for the original model for uniform media (Saffman, 1959), the extended model is also limited to high Peclet number flows. The model follows the original Saffman (1959) model closely, and is similar in some respects to the nonuniform media model proposed by Haring and Greenkorn (1970); however, there are some important differences:

1. Molecular diffusion is included as in the Saffman (1959) model such that an asymptotic longitudinal dispersion coefficient may be obtained, in contrast to the Haring and Greenkorn (1970) model.

2. Permeability is found to be sensitive to "network" effects in the medium which tend to equalize volume flux rates through different sized pores. A pressure fluctuation function is introduced to take account of this effect.

3. Actual pore radius and grain size distributions are included in the model. It is not necessary to fit these distributions to any predetermined frequency distributions.

4. A method for estimating pore length distributions from measured grain size distributions is proposed.

3.1 Permeability in a Random Capillary Tube Network

The random capillary tube network is an approximate geometrical representation of the pore space in a porous medium. This type of network is a three-dimensional, interconnected network of straight capillary tubes, where the capillary tubes join at node points. The nature of the network interconnections is not prescribed by the model, which only describes the statistical behavior of the orientation and size of each capillary tube element. The orientation of the capillary tube is given by the distribution of two angles for the capillary tube axis (Figure 3.1). The azimuthal angle, ϕ_a, is not needed to describe the longitudinal motion of a miscible solute because this angle has no effect on the flow speed through a capillary tube, nor any effect on the longitudinal component of the particle motion. Since we are only considering longitudinal transport phenomena here, the orientation of a

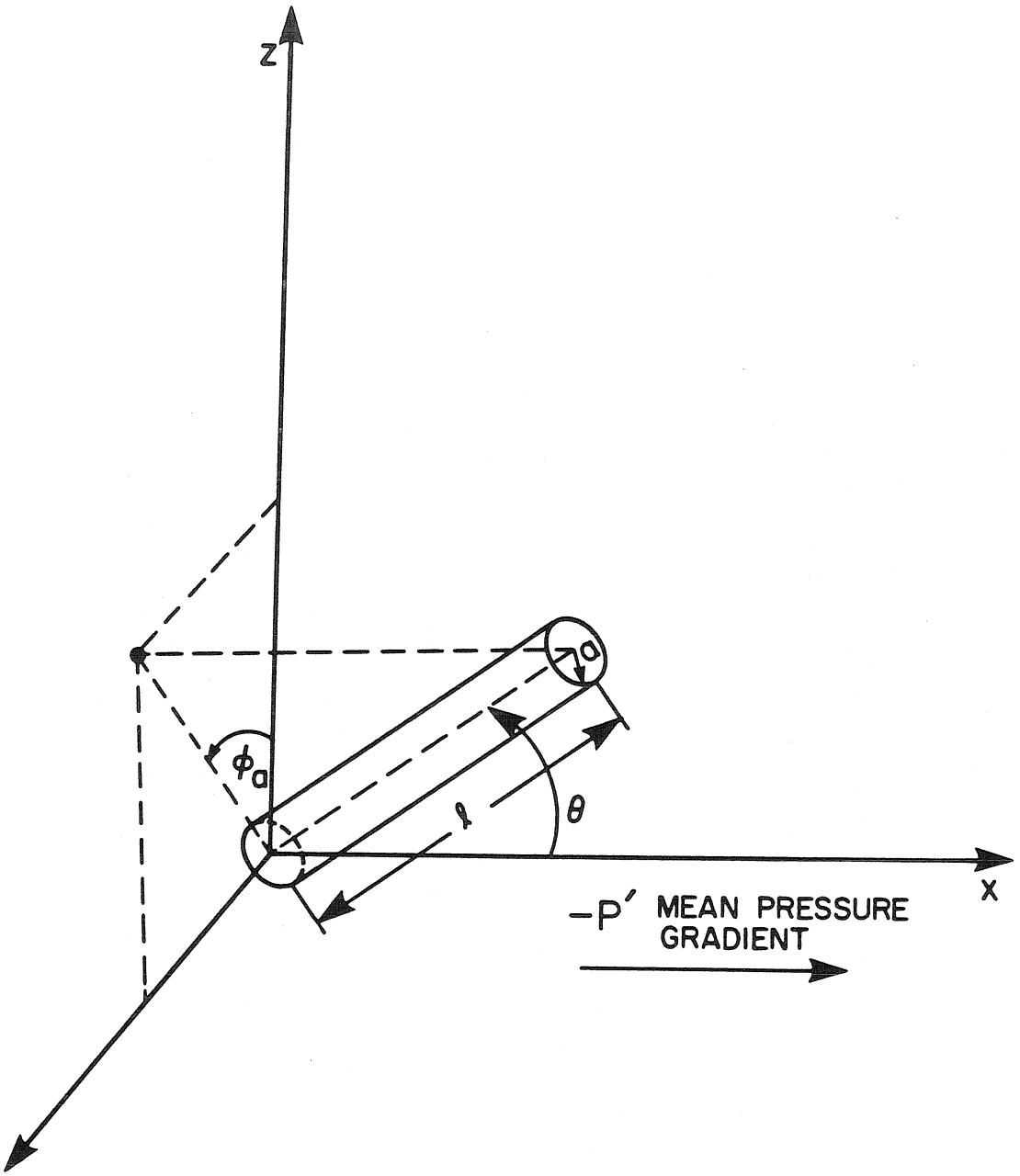

FIGURE 3.1

Definition Sketch for the Random Capillary Tube

given capillary tube will be specified with the angle θ relative to the mean flow direction. The azimuthal angle, ϕ_a, will not be used further. The size of a capillary tube is specified by a pore radius, a, and a pore length, ℓ. The assumption to be used here is that the pore radius and pore length vary independently and randomly according to their respective frequency distributions.

The basic unit of the random capillary tube model is the straight capillary tube as shown in Figure 3.1. A fundamental assumption of the model is that the pressure gradient along a pore is simply the projection of the mean pressure gradient. Assuming steady, laminar flow in each tube, the flux of fluid through a given tube may be computed using Poiseuille's law with the orientation and radius of the tube. This assumption "decouples" the network in that each capillary tube conducts fluid independently of the network. For an isotropic medium, the capillary tube is randomly oriented in space (as well as having the length and radius vary independently of the orientation). The probability of a given angle, θ, of the capillary tube axis relative to the mean flow direction within a range $d\theta$ is given by the proportion of area (or amount of solid angle) on a unit sphere swept out by the pore axis, $\sin\theta d\theta$. It is now possible to derive a simple permeability relationship for the network.

Consider a cross section through the capillary tube network, perpendicular to the flow direction. The flux through each pore is given by Poiseuille's law

$$Q = \frac{-\pi a^4 P' \cos\theta}{8\mu} \tag{3.1}$$

where $P'\cos\theta$ is the projection of the mean pressure gradient along the pore axis. The frequency that the a cross sectional plane (perpendicular to the x-axis) will intersect a capillary tube of length ℓ and orientation θ is proportional to $\ell\cos\theta$. The probability for intersecting a given pore within the differential range ℓ to $(\ell+d\ell)$, θ to $(\theta+d\theta)$, a to (a+da) is

$$dS = 2\ell\cos\theta\sin\theta g(a)f(\ell)d\ell da d\theta$$

where g(a) is the probability density for pore radius and $f(\ell)$ is the probability density for pore length. The 2 normalizes the probability density function. The variables ℓ and a range from 0 to ∞ and θ ranges from 0 to $\pi/2$. Assuming a given cross section is a representative sample of pores, the total flux through the cross section is equal to the average flux through a pore multiplied by the total number of pores in the cross section, N. The total flux, Q, passing through the cross section is N times the probability-weighted average of equation (3.1)

$$Q_T = 2N \int_0^{\infty}\int_0^{\infty}\int_0^{\pi/2} \frac{-\pi a^4 P' \cos^2\theta}{8\mu} \sin\theta g(a)\ell f(\ell) d\ell da d\theta \tag{3.2}$$

where the triple integral represents the arithmetic average flux through a pore. The seepage velocity through the porous medium is given by Q/A_p, where A_p is the total area of pores in the cross

section. A_p may also be found by taking the average pore area exposed by the cross section and multiplying by N. The area of a given pore exposed in the cross sectional plane is $\frac{\pi a^2}{\cos\theta}$. The total area is then

$$A_p = 2N\int_0^{\infty}\int_0^{\infty}\int_0^{\pi/2}\left(\frac{\pi a^2}{\cos\theta}\right)\cos\theta\sin\theta g(a)\ell f(\ell)d\ell da d\theta \tag{3.3}$$

For the seepage velocity, V_s, we divide equation (3.2) by (3.3) to give

$$V_s = \frac{-P'}{24\mu}\frac{\int_0^{\infty} a^4 g(a)da}{\int_0^{\infty} a^2 g(a)da} \tag{3.4}$$

and from Darcy's law

$$V_s = \frac{-k}{\sigma\mu}P' \tag{3.5}$$

Combining equations (3.4) and (3.5) we find

$$k = \frac{\sigma}{24}\frac{\int_0^{\infty} a^4 g(a)da}{\int_0^{\infty} a^2 g(a)da}$$

which can be written as

$$k = \frac{\sigma}{24}\frac{\overline{a^4}}{\overline{a^2}} \tag{3.6}$$

The Haring and Greenkorn (1970) permeability model can be written as

$$k = \frac{\sigma \overline{a^2}}{24} \tag{3.7}$$

which results from averaging the x-component of velocity through each pore rather than using the average flux divided by the average area. In general, $\overline{a^2} \neq \overline{a^4}/\overline{a^2}$. As pointed out by Wilson and Gelhar (1974), the Haring and Greenkorn permeability derivation is inconsistent under the assumptions of the model.

To investigate equation (3.6) further, we let g(a) take a specific functional form. A commonly used form for representing the distribution of lengths is the log-normal distribution

$$g(a) = \frac{1}{a\sqrt{2\pi(\ln\sigma_a)^2}} \; \text{EXP}\left[\frac{-(\ln a - \ln\mu_a)^2}{2(\ln\sigma_a)^2}\right] \tag{3.8}$$

where μ_a is the geometric mean radius and σ_a is the geometric standard deviation. The general relation for moments of g(a) is

$$\int_o^\infty a^N g(a)da = \mu_a^N \, \sigma_a^{\frac{N^2}{2}\ln\sigma_a} \tag{3.9}$$

so, for the permeability, we find using equations (3.6), (3.8), and (3.9)

$$k = \frac{\sigma\mu_a^2}{24} \, \sigma_a^{6\ln\sigma_a} \tag{3.10}$$

This relationship consists of two parts. The factor $\frac{\sigma\mu_a^2}{24}$ is analogous to the Saffman (1959) permeability relationship for a uniform medium (equation (2.5)), with the pore radius for a uniform medium being replaced by the geometric mean pore radius of the nonuniform medium. The second factor represents the effect of pore radius variance on the permeability. As an example, let $\sigma_a = 2$. The geometric standard deviation is equal to the square root of the ratio of the 84.1-percentile radius to the 15.9-percentile radius for a log-normal distribution. Therefore

$$\sigma_a^{6\ln\sigma_a} \approx 18$$

The permeability formula (equation 3.10) is much too sensitive to pore radius variance when compared with measured permeabilities. Experimental results (to be presented in Chapters 4 and 5) suggest the permeability may be given by

$$k = \frac{\sigma\mu_{a^2}^2}{24} \tag{3.11}$$

where μ_{a2} is the geometric mean pore <u>area</u> divided by π, i.e., the square of the geometric mean pore radius as determined from the capillary drainage curve (see Chapter 4). Note that equation (3.11) is independent of the pore radius variance.

One hypothesis to explain why the permeability is insensitive to the pore radius variance is that "network" effects tend to even out flux rates through the various sized pores. For example, consider a

large pore which is connected to smaller pores in the network. It is quite likely that the smaller pores will not be capable of supplying a sufficient quantity of fluid to the large pore (note that flux is proportional to the fourth power of the radius) such that the large pore can conduct fluid according to Poiseuille's law and the projection of the mean pressure gradient. Mass balance would then require a reduced pressure gradient over the large pore and increased pressure gradients over the smaller pores. This is equivalent to saying that the pressure gradient in a nonuniform medium is not necessarily uniform down to the grain scale, and would expect spatial fluctuations in the pressure gradient to occur on the grain scale. By definition, however, the macroscopic pressure gradient must be constant on the macroscale for a homogeneous medium.

The nature of the random capillary tube model makes it difficult to describe quantitatively network effects on the pressure gradient. To include this effect in an *ad hoc* manner, consider the "unit cell" shown in Figure 3.2. A hypothetical "cell" of capillary tubes replaces each original capillary tube in the network, but only for the purpose of calculating a pressure gradient over the original tube. The capillary tubes in each cell have radii which vary randomly according to the measured distribution for pore radii (g(a)), but their lengths are constant. All pores in each cell are oriented in the same direction (parallel to the original tube) and the number of pores leading to and from a junction are equal. The pressure gradient over the entire cell (between locations 1 and 2 in Figure 3.2) is assumed to

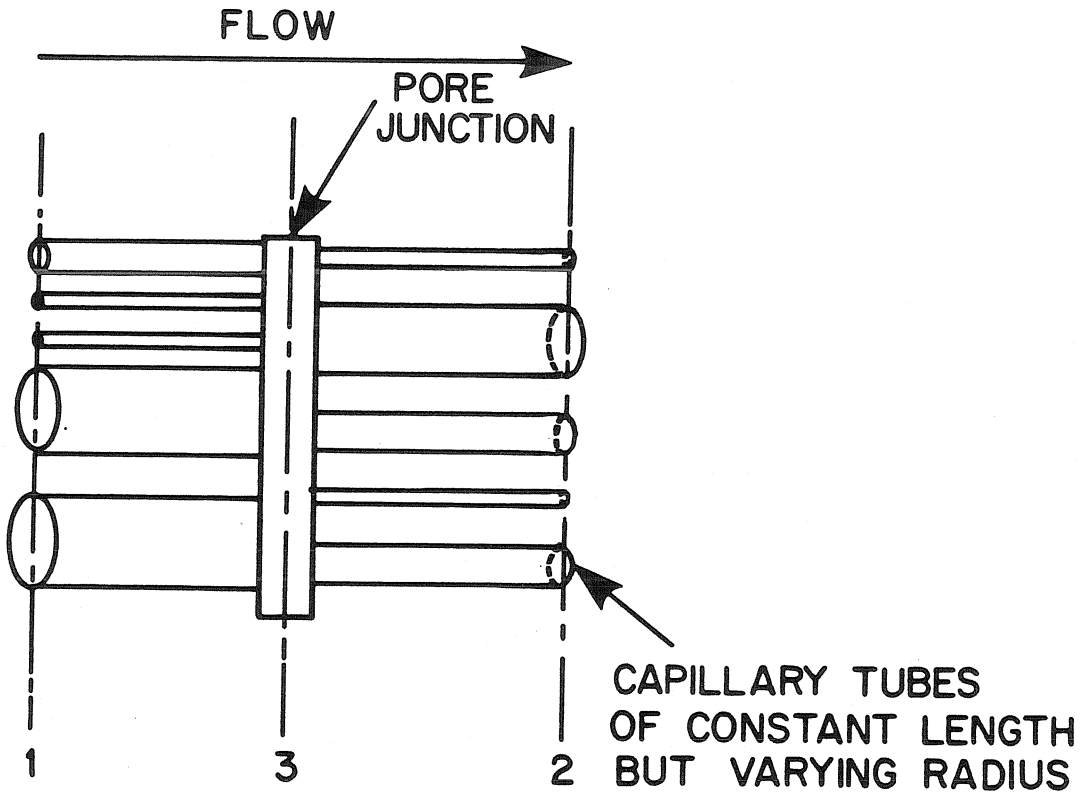

FIGURE 3.2

Definition Sketch for the Unit Cell

be equal to the projection of the macroscopic pressure gradient. The pressure at the junction, however, is allowed to fluctuate according to the requirements of a mass balance for the unit cell. The pressure gradient computed for the outflow pores for the unit cell is used in combination with the a_C (outflow) pore radius. The only requirement here is that an outflow pore radius from the unit cell be used with the computed outflow pressure gradient. The selection of a_C is arbitrary. Alternatively, we could use an inflow pore radius in conjunction with the inflow pressure gradient for the cell; the results are statistically identical.

The pressure gradient over the inflow and outflow pores may be computed using the following simple mass balance. Let i = (1, IF) denote the inflow pores and C = 2(IF) be the total number of pores connected to the junction. C will be called the connectivity of the medium. The pressure gradient over the cell is assumed to be

$$P' = \frac{P_2 - P_1}{2\ell_j} \tag{3.12}$$

where ℓ_j is the constant pore length. Note that the junction is assumed to have negligible volume. The mass balance over the unit cell requires

$$\frac{P_1 - P_j}{\ell_j} \left\{ \sum_{i=1}^{IF} a_i^4 \right\} + \frac{P_2 - P_j}{\ell_j} \left\{ \sum_{i=IF+1}^{C} a_i^4 \right\} = 0 \tag{3.13}$$

Substituting (3.12) into (3.13) and rearranging, we find

$$\Delta(a_1,\ldots,a_C) = \frac{\frac{P_2 - P_j}{\ell_j}}{P'} = \frac{2\sum_{i=1}^{IF} a_i^4}{\sum_{i=1}^{C} a_i^4} \qquad (3.14)$$

The pressure gradient over the outflow pores is $\Delta P'$, where Δ is a function of $a_1,\ldots, a_C$. If

$$\sum_{i=1}^{C} a_i^4 >> 2\sum_{i=1}^{IF} a_i^4$$

then $\Delta \to 0$ since nearly all the pressure loss occurs over the inflow pores. If

$$\sum_{i=1}^{C} a_i^4 \to \sum_{i=1}^{IF} a_i^4$$

then $\Delta \to 2$ since nearly all of the pressure loss occurs over the outflow pores. Thus Δ is seen to vary between 0 and 2, with $\Delta = 1$ giving no fluctuation in the pressure gradient.

Now, if we assume that all pores are replaced by the hypothetical unit cells, it is possible to compute the permeability for a given junction connectivity, C. The radius of the pore a_C is arbitrarily selected as the actual, physical radius for each tube, but the pressure gradient is determined by $\Delta(a_1,\ldots,a_C)P'\cos\theta$ for each capillary tube. The capillary tubes $a_1,\ldots,a_{C-1}$ are used only for the computation of the pressure gradient and are not considered "true" members of the capillary tube network. Including equation (3.14) for the pressure gradient the permeability is now given by

$$k = \frac{\sigma}{24} \frac{\int_0^\infty \cdots \int_0^\infty a_c^4 \Delta(a_1,\ldots,a_c) g(a_1)\ldots g(a_c) da_1 \ldots da_c}{\int_0^\infty a^2 g(a) da} \tag{3.15}$$

where the flux must now be averaged with respect to all components of the unit cell.

3.2 Longitudinal Dispersion in a Random Capillary Tube Network

The longitudinal (and transverse) dispersion coefficients for isotropic, uniform porous media were determined by doing a statistical analysis of particle trajectories through the medium. The first assumption needed is that particle paths through the pores are random. When a particle leaves one capillary tube, the next tube is selected on a basis that is independent of the previous motion. Therefore, particle trajectories represent a random walk, subject to specified rules governing the selection of a pore and transport through a pore.

Due to the approximate nature of the capillary network model of a porous medium, the velocity profile within a pore will be neglected. All streamlines within a given pore will be assumed to flow at the mean velocity of the pore. Appendix C gives details on the effects of shear dispersion within a capillary tube, but these effects are neglected for the purposes of the porous medium model. It is possible to include the effects of shear dispersion within pores as was done by Saffman (1959). The results for a uniform medium (Figure 2.5), however, show good

agreement when these effects are neglected. Since a random capillary tube network is only a rough approximation to a real porous medium, details such as the velocity profile within pores cannot be modeled with confidence.

As shown by Saffman (1959), the probability density for the selection of a given pore is proportional to the flux into the pore times the probability density for orientation of the pore axis. From the analysis of permeability presented in Section 3.1, we know the probability of a given flux rate through a pore within the differential range $(a_1+da_1),\ldots,(a_C+da_C),(\theta+d\theta)$ is proportional to

$$a_C^4 \Delta(a_1,..,a_C)\cos\theta g(a_1)\ldots g(a_C)da_1\ldots da_C d\theta \qquad (3.16)$$

We also know that the probability for the orientation of pores relative to the mean flow direction within a differential range $\theta+d\theta$ is

$$\sin\theta d\theta \qquad (3.17)$$

For a nonuniform medium, we also need to include the probability density for pore lengths. The probability of a pore length within the range $\ell+d\ell$ is

$$f(\ell)d\ell \qquad (3.18)$$

where $f(\ell)$ is the probability density for pore length. Combining the

independent factors in expressions (3.16), (3.17), and (3.18), the probability for a given step, dF, within the differential range $(a_1+da_1),\ldots,(a_C+da_C),(\theta+d\theta),(\ell+d\ell)$ is

$$dF = 2a_C^4 \Delta(a_1,\ldots,a_C)\cos\theta\sin\theta\tilde{g}(a_1)\ldots\tilde{g}(a_C)f(\ell)da_1..da_C d\ell d\theta \qquad (3.19)$$

Note that $\tilde{g}(a_i)$ is normalized such that the integrals over $a_1,\ldots,a_C$ are one.

Assuming the probability of selection of a given pore to be proportional to the flux through the pore is equivalent to assuming that all particles that enter a given pore will finish the transit through the pore, i.e., that the particles will enter one end of the pore and exit the other end. This is not necessarily true when the diffusion time scale for mass transport is on the same order or smaller than the advective time scale, since diffusion will allow some particles to enter and exit a pore through the same end. The Peclet number represents the ratio of the diffusive to advective time scales, so for low Peclet numbers the random walk approach is not valid. The Saffman (1959) model as originally derived and as extended here is limited to high Peclet number flows (Pe >> 1).

Once the pore is selected, the residence time in the pore is needed to determine the kinematics of the particle motion. Since the concentration of a solute may be thought of as the probability density for position and time of a single particle, the advection-diffusion equation for solute concentration also describes the probabilistic

motion of a single particle. Hence the residence time for a particle in a capillary tube (without shear) is governed by the following equation

$$\frac{\partial c}{\partial t_s} + \bar{u} \frac{\partial c}{\partial s} = D \frac{\partial^2 c}{\partial s^2} \tag{3.20}$$

where $\bar{u}$ is the mean velocity in the pore and s is the local axial coordinate. The boundary conditions imposed on equation (3.20) reflect the definition of residence time to be used. For example, if we consider an infinite domain with a point source at s = 0 we know the solution is

$$c(s,t_s) = \frac{1}{\sqrt{4\pi D t_s}} \text{ EXP} \left[\frac{-(s - \bar{u}t_s)^2}{4Dt_s} \right]$$

For an observation point, s_1, the residence time distribution is $c(s_1,t_s)$, where residence time means the duration between $t_s = 0$ and the first time the particle has a position $s > s_1$ for all subsequent times. Alternatively, we could have the boundary conditions

$$\lim_{s \to -\infty} c(s,t_s) = 0$$

$$c(s_1,t_s) = 0 \qquad s_1 > s_o$$

with the initial condition $c(s,0) = \delta(s-s_o)$. The residence time in this case implies the duration between $t_s = 0$ and the first time the particle encounters the position $s = s_1$. It is not clear as to what definition of residence time is appropriate for the porous medium model considered here. Initiating the source on the inlet boundary of a capillary tube makes interpretation of upstream diffusion difficult.

Due to the complexity of the problem and to the fact that the model is already limited to high Peclet number flows, the following simple rules developed by Saffman (1959) will be used for the residence time. Let t_s denote the residence time, t_A denote the advective time scale and t_D the diffusive time scale. Then we have

$$t_A = \ell/\bar{u}$$

$$t_D = \ell^2/(2D)$$

When a pore is flowing under high Peclet number conditions (based on u and the pore length, ℓ), the residence time for a particle to pass through a pore is approximately given by t_A. However, if the pore is flowing so slowly such that $t_A < t_D$, then the residence time will be approximated by t_D. The following summarizes the rules for calculating the residence time:

$$t_s = t_A \qquad \text{if } t_A < t_D \tag{3.21}$$

$$t_s = t_D \qquad \text{otherwise} \tag{3.22}$$

The rules for the residence time neglect the effect of diffusion except in pores where the velocity is so low that $t_A > t_D$. Under these conditions, it is necessary to invoke diffusion to prevent unrealistic residence times. For high Peclet number flows, most pores will be advection dominated, while some pores (usually at large angles with respect to the mean flow direction) will be diffusion dominated.

3.3 Asymptotic Behavior of the Longitudinal Dispersion

At this point we have sufficient information to simulate the motion of particles in a random, nonuniform capillary tube network. A comparison of the permeability model with experiments is required to fix the connectivity of the unit cell and measurements of the porosity, pore-radius distribution and pore-length distribution are needed. A simulation of mass transport from an instantaneous point source was carried out to investigate the near-field behavior of mass transport during flow through a uniform medium. The analysis performed by Saffman (1959) shows that an asymptotic (constant) dispersion coefficient is not obtained until

$$n >> \frac{Pe^2}{4 \ln\left(\frac{3}{2} Pe\right)} \tag{3.23}$$

where n is the average number of steps taken by a particle during a given time. Saffman (1959) also derives relations for the longitudinal dispersion coefficient for the near field, which is shown to be a logarithmic function of time, but there is no guarantee that the dispersive transport process in the near field is Fickian. Using the simulation, it is possible to check the development of an instantaneous point source to see if a symmetric or skew profile develops downstream. The simulation was carried out by generating particle trajectories through the random capillary tube network based on the the probability for choosing a given step (equation (3.18)) and the rules for the residence time for each step (equations (3.20) and (3.21)). Figure 3.3

shows a histogram of 10000 particle locations after a time $t^* = V_s t/d_g$ = 100, with Peclet = 10000. The number of steps required before the asymptotic dispersion coefficient applies is 2.6×10^6, while n = 150 for Figure 3.3. The dispersion coefficient at this point is only 54% of its asymptotic value, but the coefficient of determination between the histogram and the standard Gaussian profile is 0.965. Thus, no exaggerated skewness of the tracer profile is expected from this theory, even in the extreme near field.

The change in the dispersion coefficient during the initial stages of longitudinal transport has not been observed experimentally and is apparently not significant over the length scales important in laboratory measurements (Haring and Greenkorn, 1970). Figure 2.5 shows that the experimentally determined longitudinal dispersion coefficients match the asymptotic theory fairly well (within 50%) even under extremely high Peclet number conditions when the column lengths were clearly not long enough to reach the asymptotic limit. The simulation is computationally time-consuming for calculation of the asymptotic longitudinal dispersion coefficient since the particle trajectories must be carried out for a sufficient distance downstream. At high Peclet numbers this downstream distance becomes too large for practical calculations. The analysis of the random walk as given by Saffman (1959) for the asymptotic longitudinal dispersion coefficient provides a direct method for calculating the asymptotic dispersion coefficient and requires only trivial modification to be used for a nonuniform medium.

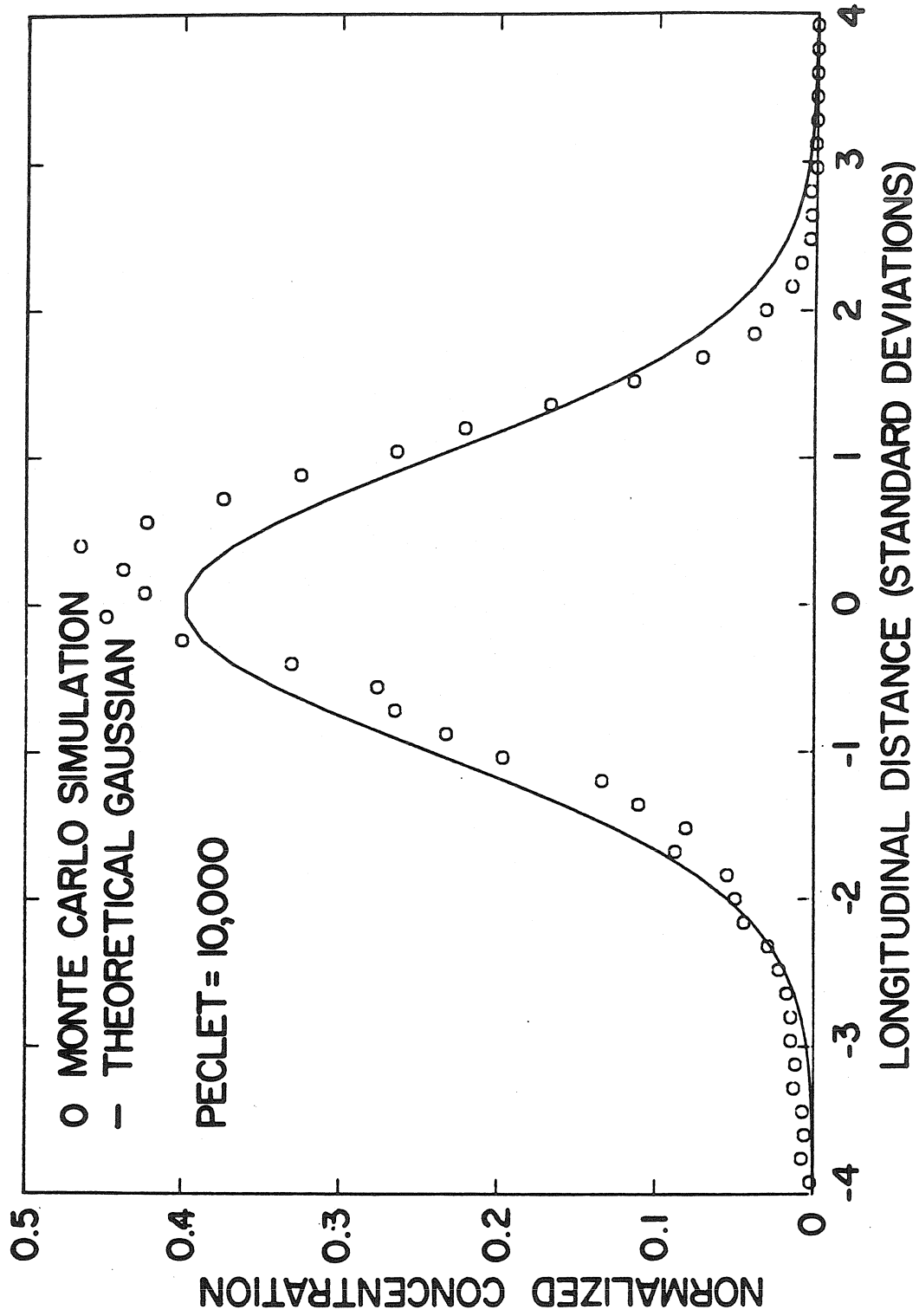

FIGURE 3.3

Longitudinal Profile, Developed from an Instantaneous Point Source
$V_s t/d_g$ = 100 (10,000 particles)

Following Saffman (1959), we define normalized variables for the position and time of motion of a given particle after n steps

$$\chi_n = \frac{x_n^* - \overline{x_n^*}}{n^{\frac{1}{2}}} \tag{3.24}$$

$$\tau_n = \frac{t_n^* - \overline{t_n^*}}{n^{\frac{1}{2}}} \tag{3.25}$$

where

$$x_n^* = \frac{x_n}{d_g} = \sum_{i=1}^{N} x_{si}/d_g$$

$$t_n^* = \frac{V_s t_n}{d_g} = \frac{V_s \sum_{i=1}^{n} t_{si}}{d_g}$$

x_n is the total longitudinal displacement of a particle after n steps, $\overline{x}_n$ is the (ensemble) mean position of a particle after n steps, t_n is the total time of motion after n steps, and $\overline{t}_n$ is the ensemble mean time of motion after n steps. The values x_{si} and t_{si} represent the longitudinal step length and residence time for the i^{th} step, respectively. Ensemble mean averages denoted by the overbar represent integral averages using the probability density function given in equation (3.19). V_s is the seepage velocity and d_g, the geometric mean grain size, is a length scale used to nondimensionalize χ_n and τ_n. From the central limit theorem, we know that for $n \to \infty$

$$\overline{\chi_n} = 0 \qquad \overline{\tau_n} = 0$$

$$\overline{\chi_n^2} = \overline{(x_s^* - \overline{x_s^*})^2} = \sigma_{x_s^*}^2$$

$$\overline{\tau_n^2} = \overline{(t_s^* - \overline{t_s^*})^2} = \sigma_{t_s^*}^2$$

where $$x_s^* = x_s/d_g = (\ell\cos\theta)/d_g$$
$$t_s^* = V_s t_s/d_g$$

The dimensionless variances, $\sigma^2_{x_s^*}$ and $\sigma^2_{t_s^*}$, are for a single step. Both $\sigma^2_{x_s^*}$ and $\sigma^2_{t_s^*}$ are defined in terms of known integrals

$$\sigma^2_{x_s^*} = \int_F (x_s^* - \overline{x_s^*})^2 dF \tag{3.26}$$

$$\sigma^2_{t_s^*} = \int_F (t_s^* - \overline{t_s^*})^2 \, dF \tag{3.27}$$

The differential probability density, dF, is given in equation (3.19) and t_s is given by equations (3.21) and (3.22).

For $\sigma^2_{x_s^*}$ we may calculate

$$\sigma^2_{x_s^*} = \int_F (\ell^*\cos\theta - \overline{\ell^*\cos\theta})^2 dF$$

where $\ell^* = \ell/dg$ and

$$\overline{\ell^*\cos\theta} = \int_F \ell^*\cos\theta dF = \frac{2}{3}\,\overline{\ell^*}$$

so

$$\sigma^2_{x_s^*} = \frac{\overline{\ell^{*2}}}{2} - \frac{4}{9}\,\overline{\ell^*}^2$$

Therefore, $\sigma^2_{x_s^*}$ is finite for a pore length distribution with finite variance. From the central limit theorem, we find χ_n to be asymptotically normal as $n \to \infty$.

Since the residence time is bounded by a diffusion time scale, the variance of the residence time distribution, $\sigma^2_{t_s^*}$, may be expected to be unbounded as $Pe \to \infty$. The analysis to follow requires the asymptotic behavior of the residence time distribution to be Gaussian with a finite variance. An estimate of when τ_n will be normally distributed is given by (Saffman, 1959)

$$\overline{\tau_n^3} \ll 1$$

now

$$\overline{(t_n^* - \overline{t_n^*})^3} = n\overline{(t_s^* - \overline{t_s^*})^3}$$

so

$$\overline{\tau_n^3} = \frac{1}{n^{\frac{1}{2}}} \overline{(t_s^* - \overline{t_s^*})^3}$$

The restriction on n such that τ_n is Gaussian is

$$n^{\frac{1}{2}} \gg \overline{(t_s^* - \overline{t_s^*})^3} \tag{3.28}$$

Evaluation of this integral for a nonuniform medium requires numerical calculations.

For the analysis of the dispersion coefficient, we want the variance of the longitudinal displacement at a fixed time (rather than a fixed number of steps). Let x denote the random longitudinal position of particles after a given time t, and χ the dimensionless coordinate

$$\chi = \frac{x^* - n\overline{x_s^*}}{n^{\frac{1}{2}}} \tag{3.29}$$

Rearranging equation (3.29) we find

$$x^* = n^{\frac{1}{2}}\chi + n\overline{x_s^*} \tag{3.30}$$

Further analysis requires the determination of the distribution of n, the number of steps, for a fixed time t. To do this, we will use the dimensionless time, τ, defined by

$$\tau = \frac{t^* - n\overline{t_s^*}}{n^{\frac{1}{2}}} \tag{3.31}$$

At this point, it is convenient to address the asymptotic ($n \to \infty$) relationship between χ_n and χ, and τ_n and τ. For a fixed number of steps, n

$$\overline{t_n^*} = n\overline{t_s^*}$$

$$\overline{(t_n^* - \overline{t_n^*})^2} = \sigma_{t_n^*}^2 = n\overline{(t_s^* - \overline{t_s^*})^2} = n\sigma_{t_s^*}^2$$

therefore

$$\frac{\sigma_{t_n^*}}{\overline{t_n^*}} = \frac{\sigma_{t_s^*}}{\sqrt{n}\,\overline{t^*}} \to 0 \quad \text{as} \quad n \to \infty$$

As $n \to \infty$, a unique time $\overline{t_n^*}$ corresponds to each χ_n. So for a given time $t^* \to \infty$, $\overline{n} = \overline{t_n^*}/\overline{t_s^*}$ and $\chi = \chi_{\overline{n}}$. This implies

$$\overline{\chi} = \overline{\chi_{\overline{n}}} = 0$$

$$\overline{\chi^2} = \overline{\chi_{\overline{n}}^2} = \sigma_{x_s^*}^2$$

and χ is Gaussian as $\overline{n} \to \infty$. For τ_n, we know,

$$\tau_n = \frac{t_n^* - n\overline{t_s^*}}{n^{\frac{1}{2}}}$$

and as $n \to \infty$, $\overline{\tau_n} = 0$, $\overline{\tau_n^2} = \sigma^2_{t_s^*}$, and τ_n is Gaussian. Therefore τ_n becomes independent of n as $n \to \infty$. So $\tau = \tau_{\bar{n}}$ as $\bar{n} \to \infty$,

$$\overline{\tau} = \overline{\tau_{\bar{n}}} = 0$$

$$\overline{\tau^2} = \overline{\tau_{\bar{n}}^2} = \sigma^2_{t_s^*}$$

and τ is Gaussian as $\bar{n} \to \infty$.

Using $\tau = \tau_{\bar{n}}$ and $\chi = \chi_{\bar{n}}$ for large times, equations (3.30) and (3.31) become

$$x^* = n^{\frac{1}{2}}\chi_{\bar{n}} + n\overline{x_s^*} \tag{3.32}$$

$$\tau_{\bar{n}} = \frac{t^* - n\overline{t_s^*}}{n^{\frac{1}{2}}} \tag{3.33}$$

Using equation (3.33) to solve for n we find

$$n = \frac{t^*}{\overline{t_s^*}} + \frac{1}{2}\left(\frac{\tau_{\bar{n}}}{\overline{t^*}}\right)^2 - \frac{\tau_{\bar{n}}}{\overline{t^*}}\sqrt{\frac{t^*}{\overline{t_s^*}}}\sqrt{1 + \frac{\tau_{\bar{n}}^2}{4\overline{t_s^*}t^*}} \tag{3.34}$$

where n goes from 0 to ∞ as $\tau_{\bar{n}}$ goes from $-\infty$ to $+\infty$. Since $\tau_{\bar{n}}/t^*$ is small as $\bar{n} \to \infty$, we can approximate equation (3.34) by

$$n \approx \frac{t^*}{\overline{t_s^*}} - \frac{\tau_{\bar{n}}}{\overline{t_s^*}}\sqrt{\frac{t^*}{\overline{t_s^*}}} + \frac{1}{2}\left(\frac{\tau_{\bar{n}}}{\overline{t_s^*}}\right)^2 - \frac{1}{8}\left(\frac{\tau_{\bar{n}}}{\overline{t_s^*}}\right)^2 \frac{\tau_{\bar{n}}}{\sqrt{\overline{t_s^*}t^*}} \tag{3.35}$$

Since $t^*/\overline{t_s^*} \to \infty$ as $\bar{n} \to \infty$ and $\tau_{\bar{n}}/\overline{t_s^*}$ is independent of n

$$n \approx \frac{t^*}{\overline{t_s^*}} - \frac{\tau_{\overline{n}}}{\overline{t_s^*}} \sqrt{\frac{t^*}{\overline{t_s^*}}} \tag{3.36}$$

To the same order of approximation, we find $n^{1/2}$ is

$$n^{\frac{1}{2}} \approx \sqrt{\frac{t^*}{\overline{t_s^*}}} - \frac{1}{2} \frac{\tau_{\overline{n}}}{\overline{t_s^*}} \tag{3.37}$$

Substituting equations (3.36) and (3.37) into equation (3.32), we find

$$x^* = \left(\frac{t^*}{\overline{t_s^*}} \right) \overline{x_s^*} + \sqrt{\frac{t^*}{\overline{t_s^*}}} \left\{ \chi_{\overline{n}} - \left(\frac{\overline{x_s^*}}{\overline{t_s^*}} \right) \tau_{\overline{n}} \right\} - \frac{1}{2} \frac{\tau_{\overline{n}} \chi_{\overline{n}}}{\overline{t_s^*}} \tag{3.38}$$

Again, since $t^*/\overline{t_s^*} \to \infty$ as $\overline{n} \to \infty$, equation (3.38) becomes for large $\overline{n}$

$$x^* = \left(\frac{t^*}{\overline{t_s^*}} \right) \overline{x_s^*} + \sqrt{\frac{t^*}{\overline{t_s^*}}} \left\{ \chi_{\overline{n}} - \left(\frac{\overline{x_s^*}}{\overline{t_s^*}} \right) \tau_{\overline{n}} \right\} \tag{3.39}$$

Taking the average of equation (3.39) gives

$$\overline{x^*} = \frac{t^*}{\overline{t_s^*}} \overline{x_s^*} \tag{3.40}$$

Since the mean position is defined to move with the seepage velocity, we find

$$\frac{\overline{x_s^*}}{\overline{t_s^*}} = 1 \tag{3.41}$$

Rearranging equation (3.39) and using equation (3.41), we find

$$x^* - \overline{x^*} = \sqrt{\frac{t^*}{t_s^*}} \left\{ \chi_{\overline{n}} - \tau_{\overline{n}} \right\} \tag{3.42}$$

A longitudinal dispersion coefficient may be defined by

$$D_L^* = D_L/(V_s d_g) = \frac{\overline{(x^* - \overline{x^*})^2}}{2t^*} \tag{3.43}$$

therefore

$$D_L^* = \frac{1}{2t_s^*} \left\{ \overline{\chi_{\overline{n}}^2} + \overline{\tau_{\overline{n}}^2} - 2\overline{\chi_{\overline{n}} \tau_{\overline{n}}} \right\} \tag{3.44}$$

where $\overline{\chi_{\overline{n}}^2} = \sigma_{x_s^*}^2$; $\overline{\tau_{\overline{n}}^2} = \sigma_{t_s^*}^2$

$$\overline{\chi_{\overline{n}} \tau_{\overline{n}}} = \overline{(x_s^* - \overline{x_s^*})(t_s^* - \overline{t_s^*})}$$

In summary, the analysis of Section 3.3 provides a method of calculating the asymptotic ($\bar{n} \to \infty$) longitudinal dispersion coefficient of a cloud of passive tracer particles in terms of the statistical properties of the transport of tracer particles for a single step. In Section 3.4, methods used to obtain the distributions of pore radii (g(a)) and pore length (f(ℓ)) are presented, and Section 3.5 will discuss the numerical technique used to evaluate equations (3.15) and (3.44).

3.4 Determining the Pore Radius and Pore Length Distributions

The theoretical model gives the permeability and longitudinal dispersion coefficient in terms of integrals (equations (3.15) and

(3.44)) involving the pore size distribution, pore length distribution, and porosity which characterize the structure of the porous medium. The utility of the model is dependent on a means of determining these properties. Measurements of the porosity follow standard methods which are described in Chapter 4.

The pore radius distribution as determined by capillary drainage or mercury porosimetry experiments gives the "effective" pore size as a function of the pore volume of the sample. For a given pore radius, we can measure what fraction of the pore volume is "controlled" by pores with effective radii less than or equal to the given pore radius. This type of pore radius distribution is a volume-weighted distribution, while the theoretical model requires a pore radius distribution according to the frequency of occurrence of a given pore radius. The necessary change is made as follows.

Following Haring and Greenkorn (1970), we can relate the measured pore radius distribution to the random capillary tube network model. Let N be the total number of pores contained in the medium. Assuming the pore length to vary independently of the pore radius, the fraction of pore volume contained in an infinitesimal range $d\eta$ of pore radius η is given by

$$N\bar{\ell}\pi\eta^2 g(\eta)d\eta \tag{3.45}$$

where $\bar{\ell}$ is the mean pore length. The cumulative volume of pore space in the medium with pore radius between 0 and a is given by integrating

equation (3.45) from 0 to a

$$V(a) = N\bar{\ell}\pi \int_0^a \eta^2 g(\eta) d\eta \tag{3.46}$$

The total volume of pores in the medium is given by

$$V_T = N\bar{\ell}\pi \int_0^\infty \eta^2 g(\eta) d\eta \tag{3.47}$$

The cumulative probability of radius a, according to volume is given by the ratio of equations (3.46) and (3.47).

$$P_a(a) = \frac{V(a)}{V_T} = \frac{\int_0^a \eta^2 g(\eta) d\eta}{\int_0^\infty \eta^2 g(\eta) d\eta}$$

or

$$P_a(a) \sim \int_0^a \eta^2 g(\eta) d\eta \tag{3.48}$$

Differentiating equation (3.48) gives

$$g(a)da \sim \frac{1}{a^2} dP_a(a)$$

therefore

$$G(a) = \int_0^a g(\eta) d\eta \sim \int_0^a \frac{1}{\eta^2} dP_a(\eta) \tag{3.49}$$

This expression gives the frequency distribution G(a) in terms of the measured cumulative distribution for pore radius by volume, $P_a(a)$. The distribution G(a) is normalized such that $G(\infty) = 1$. In practice, the "infinite" radius is the largest radius measured. In this way, we obtain from measurements the appropriate pore radius distribution for the theoretical model. The details of implementing this technique for specific cases is given in Chapter 4.

The pore length distribution is also required for the calculation of longitudinal dispersion. Very little work has been published regarding pore length distributions in porous media, and there are no standard techniques for its measurement. The results for dispersion in uniform media (Saffman, 1959; 1960) have shown that the pore length is roughly equal to the grain diameter. To extend this idea for a nonuniform medium, we will relate the pore length distribution to the grain size distribution. The grain size distribution for medium and coarse sand materials is typically measured using mechanical sieving (to be described in Chapter 4). Sieving gives the cumulative size distribution of diameters by mass. Assuming that all the grains have the same density and similar shapes, we can write an expression relating the frequency distribution for a given grain size, h(d), to the measured cumulative distribution by mass, $P_d(d)$,

$$P_d(d) = \frac{W(d)}{W_T} = \frac{\rho_g \int_0^d \alpha \zeta^3 h(\zeta) d\zeta}{\rho_g \int_0^\infty \alpha \zeta^3 h(\zeta) d\zeta} \qquad (3.50)$$

where ρ_g is the grain density

α is the constant ratio of particle volume to the cube of the effective grain diameter

$W(d)$ is the cumulative mass of sand of grain size between 0 and d

W_T is the total sample mass.

Therefore

$$P_d(d) \sim \int_o^d \zeta^3 h(\zeta) d\zeta \tag{3.51}$$

Consider a grain packed in a nonuniform medium. Since we assume the association of the grains to be random, it is expected that large grains will have more grain contacts than smaller grains, in proportion to the surface area of the grain. If we assume that pores are created through grain contacts, then the number of pores associated with a given grain is proportional to the surface area of the grain. Therefore, the cumulative distribution as weighted by surface area would seem more appropriate when concerned with the relation between grain size and pore length. Manipulating equation (3.51), we find

$$\zeta^2 h(\zeta) d\zeta \sim \frac{1}{\zeta} dP_d(\zeta)$$

so

$$J(d) = \frac{A(d)}{A_T} \sim \int_o^d \frac{1}{\zeta} dP_d(\zeta) \tag{3.52}$$

This expression gives the cumulative grain size distribution, J(d), weighted by area, where

A(d) is the cumulative area of sand between grain size 0 and d

A_T is the total area of the sample.

The distribution is normalized such that $A(\infty) = A_T$. As with the pore radius distribution, the "infinite" grain diameter is taken to be the largest measured value when analyzing actual data.

To relate the grain size to pore length, the following simple packing model is used. As shown in Figure 3.4, three grains pack to form a pore space. When the grains are all the same diameter, we expect the pore length to be about equal to the grain diameter. For grains of unequal size, we would intuitively expect the pore length to be related to the interparticle grain spacing. Since the exact definition of pore length is not clear in terms of the geometry of packed spheres, we scale the pore length as the cube root of the interparticle "volume" defined by the three interparticle distances shown in Figure 3.4.

$$\ell = (\beta_1 \beta_2 \beta_3)^{1/3}$$

where β_i , i = 1, 3, represents the three interparticle distances

$$\beta_1 = \frac{d_2+d_3}{2} \quad ; \quad \beta_2 = \frac{d_1+d_3}{2} \quad ; \quad \beta_3 = \frac{d_2+d_3}{2}$$

Integrals involving the distribution of pore lengths, $f(\ell)$, as required

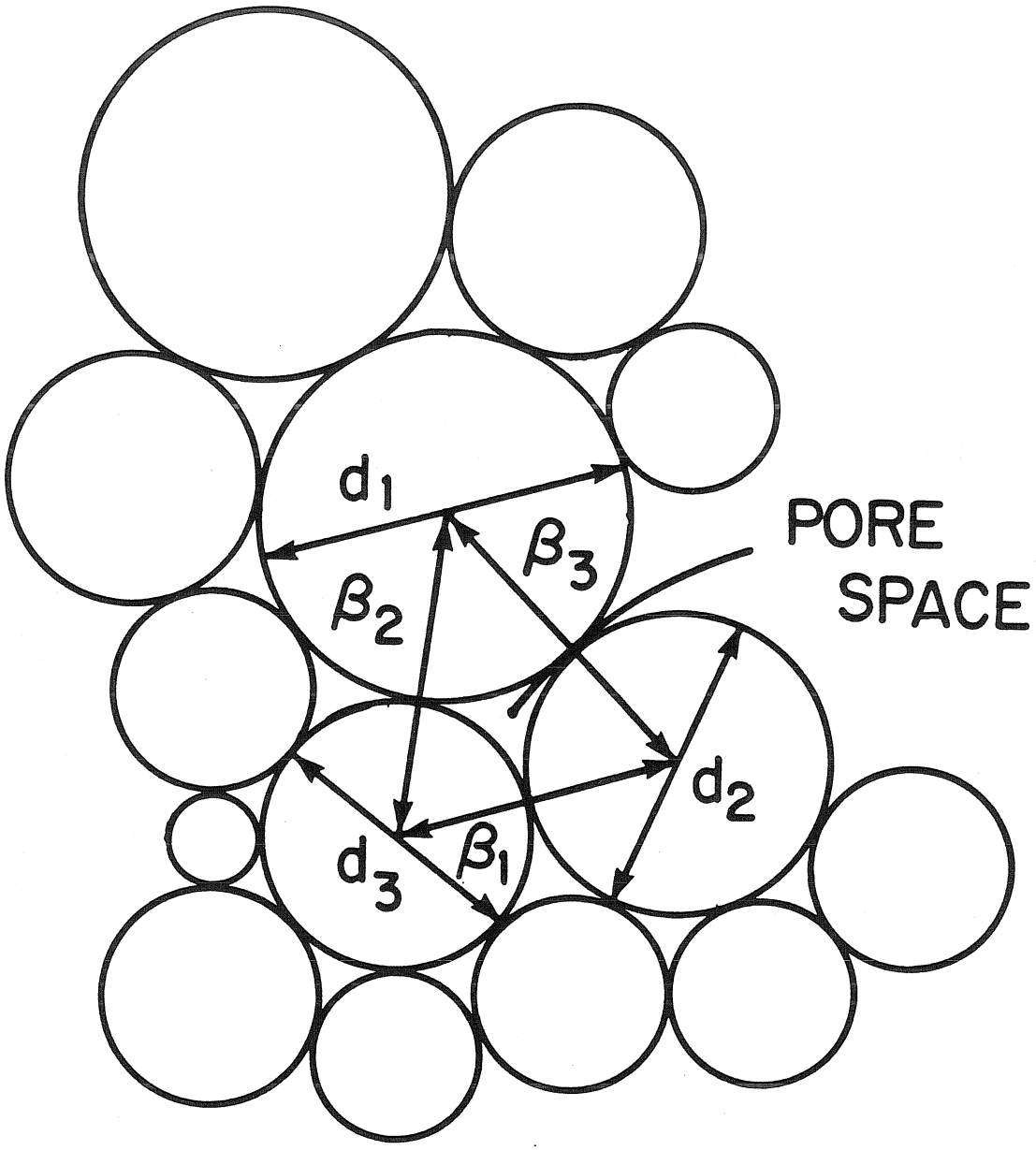

FIGURE 3.4

Packing Model for a Nonuniform Porous Medium

in equation (3.44) may be represented by the following:

$$\int_0^\infty w(\ell)f(\ell)d\ell = \int_0^\infty\int_0^\infty\int_0^\infty w\left(\frac{1}{2}\left\{(\zeta_1+\zeta_2)\cdot(\zeta_2+\zeta_3)\cdot(\zeta_1+\zeta_3)\right\}^{1/3}\right) \tag{3.53}$$
$$j(\zeta_1)j(\zeta_2)j(\zeta_3)d\zeta_1 d\zeta_2 d\zeta_3$$

where $w(\ell)$ is any function of ℓ and $j(\zeta_i) = \zeta_i^2 h(\zeta_i)$

3.5 Monte Carlo Integration for the Permeability and Dispersion

Calculations for permeability and dispersion are carried out by numerically integrating the expressions given in equations (3.15) and (3.44). The required integrals are summarized in Tables 3.1 and 3.2. These integrals include experimentally determined distributions for pore radius, $g(a^*)$, and grain diameter $j(d^*)$. Note that the probability density functions in the above integrals may be written in terms of the corresponding cumulative distributions:

$$g(a_i^*)da_i^* = dG_i^*$$

$$j(\zeta_i^*)d\zeta_i^* = dJ_i^*$$

$$\sin\theta\, d\theta = -d(\cos\theta)$$

where the limits of integration for all the independent variables are from 0 to 1. Integrals of this type may be calculated using a Monte Carlo numerical integration technique, which has the advantage of simple implementation when applied to multidimensional integrals with complex integrands. The basis of the technique is to generate uniform

TABLE 3.1

Summary of the Theoretical Relationship for Permeability in Nonuniform Porous Media

PERMEABILITY

$$k^* = \frac{\sigma}{24} \frac{\int_0^\infty \cdots \int_0^\infty a_C^{*4} \Delta(a_1^*, \ldots, a_C^*) g(a_1^*) \ldots g(a_C^*) da_1^* \ldots da_C^*}{\int_0^\infty a_C^{*2} g(a_C^*) da_C^*} \tag{3.15}$$

where $k^* = k/dg^2$ $\qquad$ $a_i^* = a_i/dg$

$$\Delta(a_1^*, \ldots, a_C^*) = \frac{2 \sum_{i=1}^{IF} a_i^{*4}}{\sum_{i=1}^{C} a_i^{*4}} \quad ; \quad IF = C/2 \tag{3.14}$$

MONTE CARLO INTEGRATION

$$k^* = \frac{\sigma}{24} \frac{\int_0^1 \int_0^1 a_C^{*4} \Delta(a_1^*, \ldots, a_C^*) dG_1^* \ldots dG_C^*}{\int_0^1 a_C^{*2} dG_C^*}$$

where dG_i^* is a differential element of the cumulative distribution, G_i^*.

$$k^* = \frac{\sigma}{24} \left\{ \frac{\sum_{i=1}^{N} a_{Ci}^{*4} \Delta(a_{1i}^*, \ldots, a_{Ci}^*)}{\sum_{i=1}^{N} a_{Ci}^{*2}} \right\}$$

where N is the number of integration points.

TABLE 3.2

Summary of the Theoretical Relationship for Longitudinal Dispersion in Nonuniform Porous Media

LONGITUDINAL DISPERSION

$$D_L^* = \frac{1}{2t^*}\left\{\sigma_{x^*}^2 + \sigma_{t^*}^2 - 2\sigma_{x^*t^*}\right\} \tag{3.44}$$

$$D_L^* = D_L/V_s d_g \qquad t^* = V_s t/d_g \qquad x^* = x/d_g$$

$$x = \ell\cos\theta \;; \quad t = \ell/\bar{u} \quad \text{IF} \quad \ell/\bar{u} < \ell^2/2D$$

$$t = \ell^2/2D \text{ OTHERWISE}$$

$$\bar{u} = \frac{-a_C^2 P'\cos\theta}{8\mu}$$

since $\overline{x^*} = \overline{t^*}$, $\sigma_{x^*}^2 + \sigma_{t^*}^2 - 2\sigma_{x^*t^*} = \overline{x^{*2}} + \overline{t^{*2}} - 2\overline{x^*t^*}$

MONTE CARLO INTEGRATION FOR A GENERAL FUNCTION, w

$$\bar{w} = \int_F w\,dF = 2\int_0^\infty \cdots \int_0^\infty\int_0^{\pi/2} w a_C^{*4}\Delta\cos\theta\sin\theta g(a_1^*)\ldots g(a_C^*)j(\zeta_1^*)j(\zeta_2^*)j(\zeta_3^*)$$

$$da_1^*\ldots da_C^* d\zeta_1^* d\zeta_2^* d\zeta_3^* d\theta$$

$$= 2\int_0^1 \cdots \int_0^1 w a_C^{*4}\Delta\cos\theta\, dG_1^*\ldots dG_C^* dJ_1^* dJ_2^* dJ_3^* d(\cos\theta)$$

$$= 2\cdot\frac{1}{N}\sum_{i=1}^{N} w_i a_{C_i}^{*4}\Delta(a_{1_i}^*,\ldots,a_{C_i}^*)(\cos\theta)_i$$

random numbers for each of the independent variables ($\cos\theta$, G_1^*, ... , G_C^*, J_1^*, J_2^*, J_3^*) and compute the integrand, $I(a_1^*,\ldots,a_C^*,\zeta_1^*,\zeta_2^*,\zeta_3^*,\cos\theta)$, for the selected values of the independent variables. Since any given value of the integrand computed in this way is equally likely, the value of the integrand, $\bar{I}$, may be estimated from the average of N values of the integrand with a weighting of 1/N for each, i.e.,

$$\bar{I}_E = \frac{2}{N}\sum_{i=1}^{N} I(a_{1_i}^*, \ldots, a_{C_i}^*, \zeta_{1_i}^*, \zeta_{2_i}^*, \zeta_{3_i}^*, (\cos\theta)_i) a_{C_i}^{*4} \Delta(a_{1_i}^*,\ldots,a_{C_i}^*)(\cos\theta)_i$$

From the central limit theorem, it is possible to show that the estimate, $\bar{I}_E$, converges to the true value, $\bar{I}$, like $1/\sqrt{N}$ (Hammersley and Handscomb, 1979). The method used to generate uniform random numbers is discussed in Appendix A. Values of $a_1^*,\ldots,a_C^*$ and $\zeta_1^*,\zeta_2^*,\zeta_3^*$ are generated from random values of $G_1^*,\ldots,G_C^*$, and J_1^*, J_2^*, J_3^*, respectively, using a table of values based on the measured cumulative distributions.

The results of an experimental study on permeability and longitudinal dispersion in two different porous media are given in Chapter 4. Pore radius and pore length distributions are determined for the two media. Calculations of permeability and longitudinal dispersion using the theoretical models developed in this Chapter are made for the two porous media investigated experimentally. Results of these calculations plus a comparison of the experimental and theoretical results are given in Chapter 5.

CHAPTER 4

AN EXPERIMENTAL INVESTIGATION OF PERMEABILITY AND LONGITUDINAL DISPERSION IN NONUNIFORM POROUS MEDIA

To test the theory developed in Chapter 3, a laboratory investigation was undertaken to measure permeability and longitudinal dispersion on two carefully selected granular media. The porosity, pore size distribution, and grain size distribution, which are needed to make predictions of a porous medium's permeability and longitudinal dispersion for a given flow, were also determined. No known experimental study of permeability and longitudinal dispersion have provided the latter measurements to characterize the porous medium. The experiments are carried out for two spatially homogeneous (in the macroscopic sense), unconsolidated sand media. These two porous materials will be referred to as a uniform porous medium and a nonuniform porous medium, although the uniform medium does have some variations in the pore and grain sizes.

Measurements of pore and grain size distributions were done on representative samples of the porous media. For the pore size distribution measurement, a saturated sample is placed in contact with a porous disc containing fine pore sizes, acting as a semipermeable membrane. Suction head is applied on the saturated sample through the disc in order to drain water from the sample. A capillary drainage curve is determined by varying the magnitude of the suction and measuring the volume of water drained. The pore size distribution is related to the capillary drainage curve through the capillary rise

equation. The total void volume of the sample is obtained from the total volume of water drained and the residual saturation which is determined by weight loss during oven drying. The total void volume is used to calculate the total porosity. A separate sample of the porous medium is used to determine the grain size distribution. This measurement is made using a standard sieve analysis technique.

The dispersion experiments are carried out in a packed column, in which a one-dimensional flow proceeds from top to bottom (Figure 4.1). The dispersion experiments consist of displacing a resident solution of homogeneous salinity from the column by a solution of different salinity. As the displacing solution penetrates the column, the initially sharp interface between the two solutions mixes and produces a zone of intermediate salinity. The mixed zone continuously increases in longitudinal extent as it is displaced downstream. Conductivity probes in the column measure the change in salinity over time during the passage of the mixed zone. These measurements comprise a breakthrough curve (Figure 4.2), from which a dispersion coefficient is obtained. Permeability is calculated for the packed column from measurements of the flow rate and gradient of piezometric head. Standard piezometer tubes are used to measure the piezometric head along the column. Conductivity measurements are also used to estimate the seepage velocity (the velocity of an immiscible displacement front). The ratio of the Darcy velocity (flow rate/gross cross-sectional area) to the seepage velocity is the effective porosity between the top of the column and the conductivity probe.

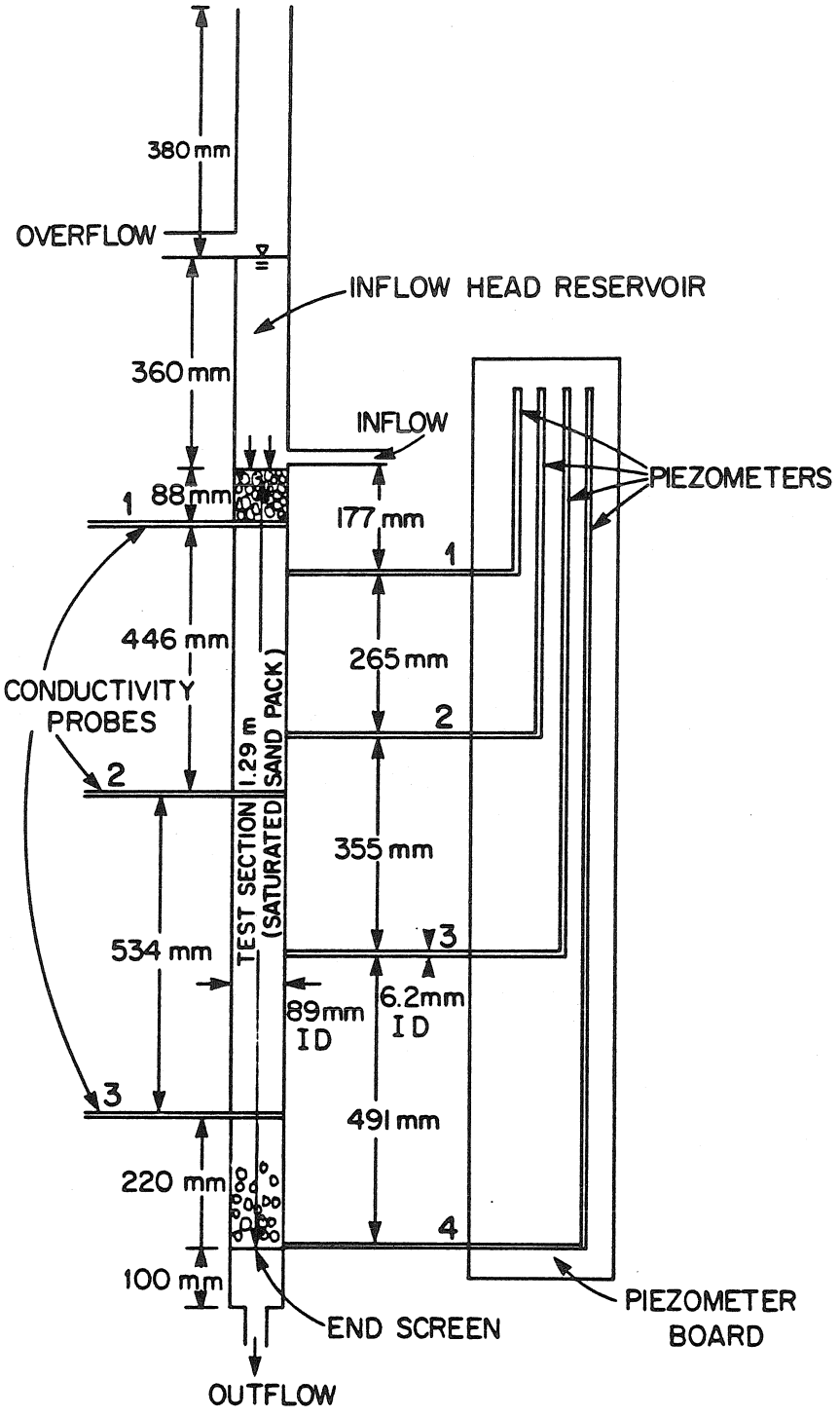

FIGURE 4.1

Packed Column for Miscible Displacement Experiments
Showing Conductivity Probes and Piezometers

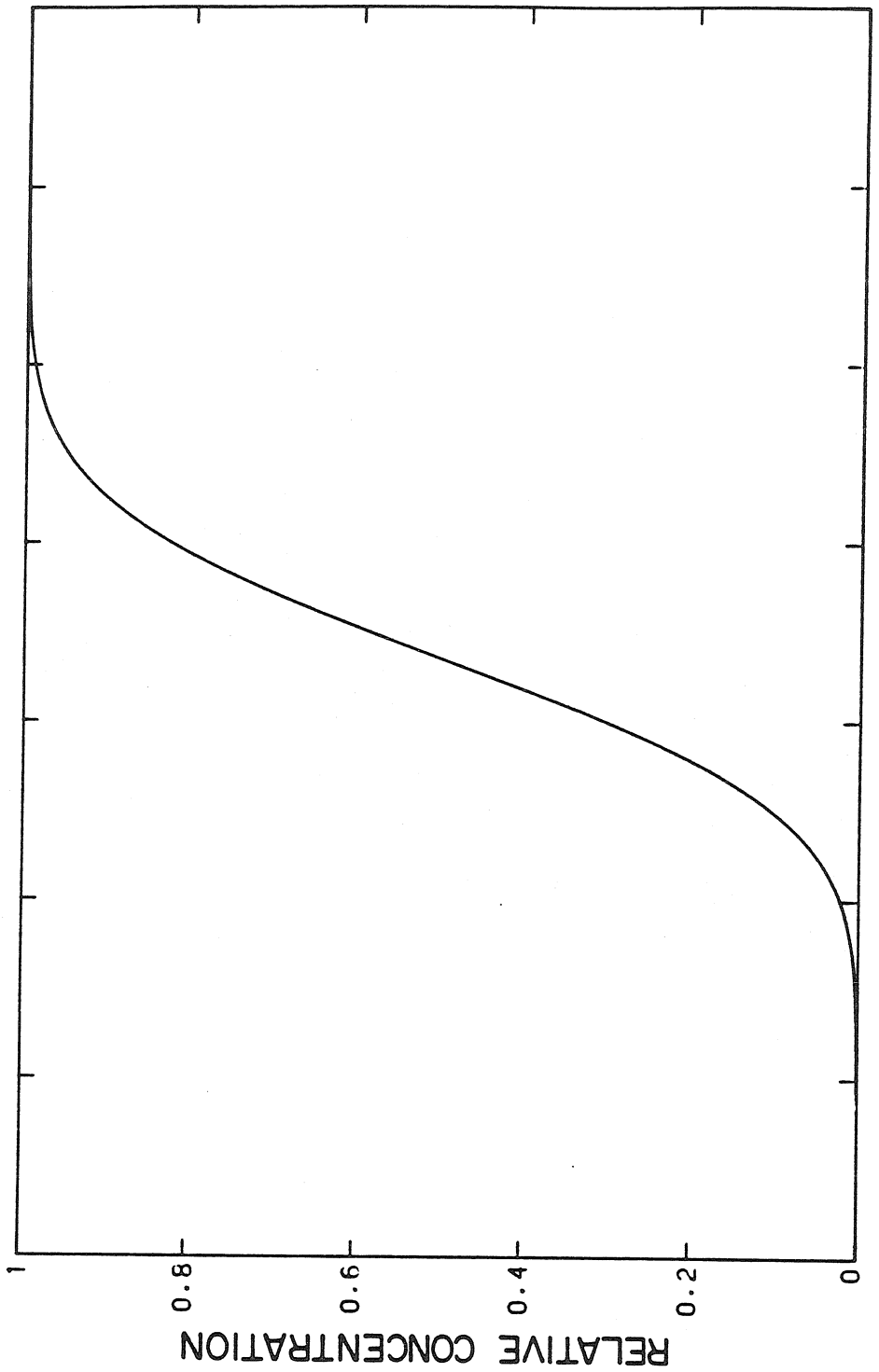

FIGURE 4.2

Characteristic Breakthrough Curve Measured at a Fixed Location

The dispersion experiments cover Peclet number from 50 to 700 for the uniform medium and from 50 to 2600 for the nonuniform medium. As seen in Chapter 3, the theoretical model is only valid when Pe >> 1, due to assumptions on the role of molecular diffusion in the transport process. By a comparison of theory and experiments for uniform media (Figure 2.5), this restriction is seen to be Pe > 10. Although the theory holds for all Pe > 10, flow conditions are limited to the linear laminar regime (Darcy's law regime) for which the Reynolds number, $Re = v_s d_g/\nu$, must be less than 10 (Bear, 1972). Taking the ratio of Pe to Re we find

$$Pe/Re = \nu/D = Sc = \text{Schmidt number}$$

and for the experiments done here, $Sc \sim 10^3$. Thus $Pe < 10^4$ is needed to maintain linear-laminar flow in these experiments. From these considerations, an approximate restriction on Pe for the theoretical model is

$$10 < Pe < 10^4$$

for the solute-solvent system used in these experiments.

An attempt was made to measure transverse dispersion using a different experimental arrangement. For this measurement, a long narrow box with a rectangular cross section was used. The overall dimensions of the box are roughly 2.44m by 0.305m by 0.100m. Due to the bulk of the apparatus, the box was set up for horizontal flow. The packing of the box proved to be a difficult task. The box was vibrated

to pack the saturated sand to its maximum packing density. When the flow was turned on, however, the fluid pressure on the inflow end would cause the box to bulge, resulting in a subsequent separation of the sand pack from the lid of the box. This separation caused serious short circuiting of the flow. Problems were also encountered in the detection of transverse dispersion. Probes packed into the medium were built to slide up and down through the medium in order to detect the transverse dispersion pattern. The tight packing of sand around the probes created so much frictional resistance, however, that sliding the probes was nearly impossible without damaging them. Due to the technical problems encountered with this apparatus, the vertically packed column shown in Figure 4.1 was used instead. The experiments carried out in the packed column were limited to longitudinal dispersion (miscible displacements).

4.1 Apparatus and Materials

The two porous materials used for these experiments are a relatively uniform natural sand and a highly nonuniform natural sand. The uniform sand is a medium grained sand which has been further sorted to produce a relatively uniform grain size distribution. The nonuniform sand is a natural gravelly sand obtained from a local (Eaton Canyon) stream terrace. Due to the steep slopes and highly variable discharge, the local mountain streams tend to deposit well-graded sediments during the recession of flood flows. These naturally mixed deposits provide a convenient source of homogeneous, nonuniform porous

media. More quantitative descriptions of the sand media will be given following the descriptions of the measurement techniques.

The experimental set-up for the permeability and dispersion experiments is diagrammed in Figure (4.1). This arrangement is similar to one used by Rumer (1962). The column is a clear lucite tube with an inside diameter of 89mm. The sand occupies a 1.29m long section of the tube. Piezometer tubes are connected along the column at four locations and are mounted on a vertically scaled piezometer board. The piezometric head levels can be read to within 0.5mm. The piezometer tubes are made of Poly-Flo tubing with an inside diameter of 6.2mm. A small amount of cloth is loaded into the fitting which connects the piezometer tube to the column to prevent sand from being pushed up into the tube. It should be noted that the cloth makes the piezometers slow to equilibrate after changing the flow rate through the column, so this technique is not appropriate for transient flow measurements. Valves are placed in all of the piezometer lines so that the column may be made air tight for vacuum saturation procedures and since air will enter the column through the piezometers when running at high flow rates.

Water is supplied to the column through two separate supply systems for fresh and saline (tracer) water (Figure 4.3). Water is pumped from a reservoir to a head tank mounted above the column. Water from the head tank flows into the inlet chamber just above the top of

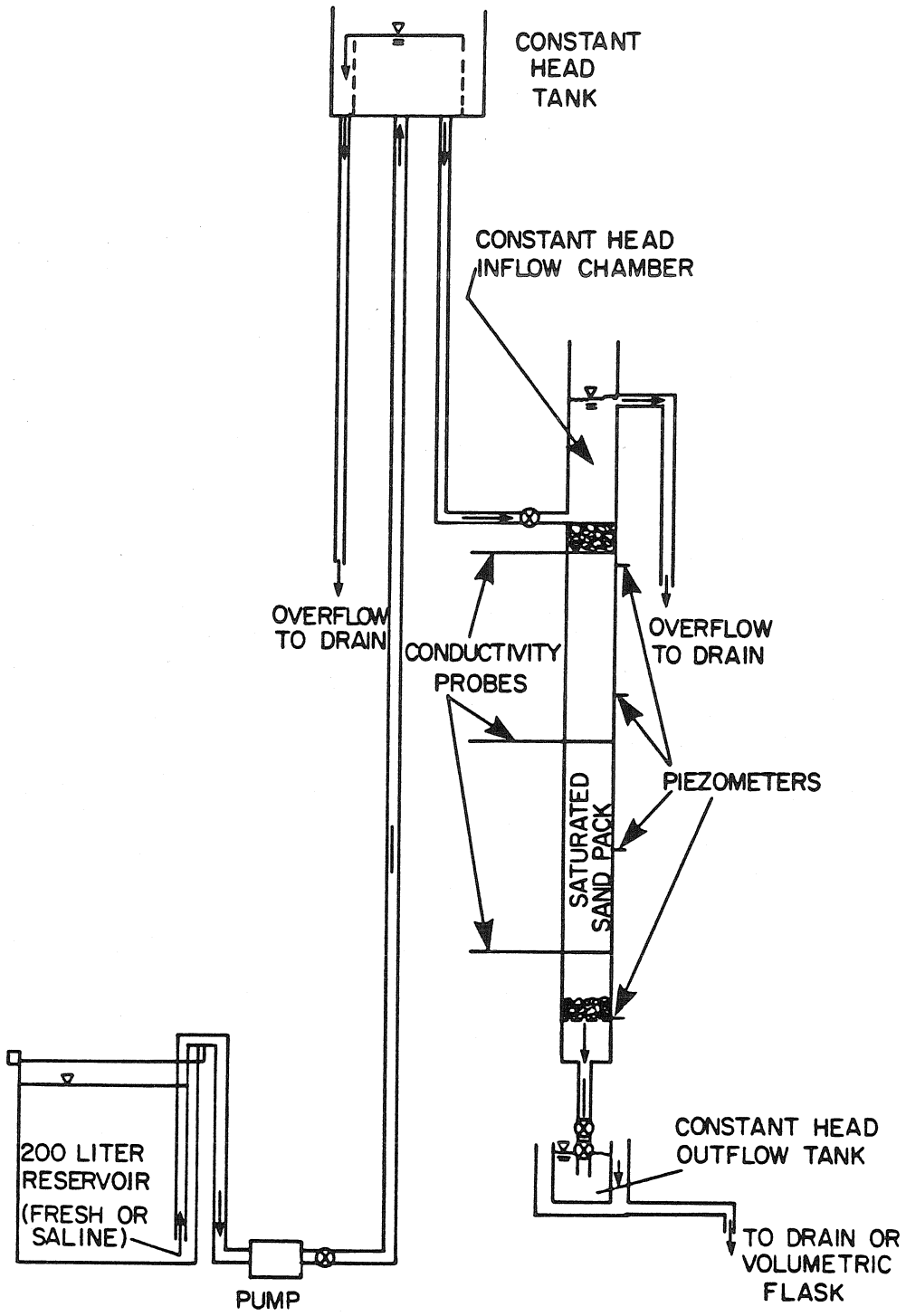

FIGURE 4.3

Packed Column Apparatus Showing Flow System

the sand pack. Constant head is maintained in the inlet chamber through an overflow weir. When the valve at the outflow end of the column is open, water percolates through the sand into the end chamber of the column and drains into a constant head receiving reservoir which overflows to drain. The flow rate is controlled by a ball valve at the outflow end of the column. Flow rate is measured by directing the outflow from the column into a volumetric flask and measuring its time to fill.

Changes in salinity within the column are measured by a conductivity probe-recording system. A block diagram of the system is given in Figure 4.4. Conductivity probes are placed at three locations along the column, with the probe plates lying close to the column axis. The probes are held in Swagelock fittings attached to the column and the probe rod penetrates the entire diameter of the column. The probes (Figure 4.5), constructed in the Keck lab machine shop, are made of 6.4mm (outside diameter) lucite tubing. The tubing is cut and grooved such that two stainless steel rings slide onto each grooved end with their outer surface flush with the tubing outside diameter. To join the pieces, the tubing ends are bored and grooved such that one end will slide into the other. A lucite spacer ring separates the stainless steel rings and provides additional strength to the joint. A fine conducting wire is soldered to each stainless steel ring and drawn through the lucite tube to connect the probe with the external circuitry. The pieces are assembled and glued together to produce the finished probe.

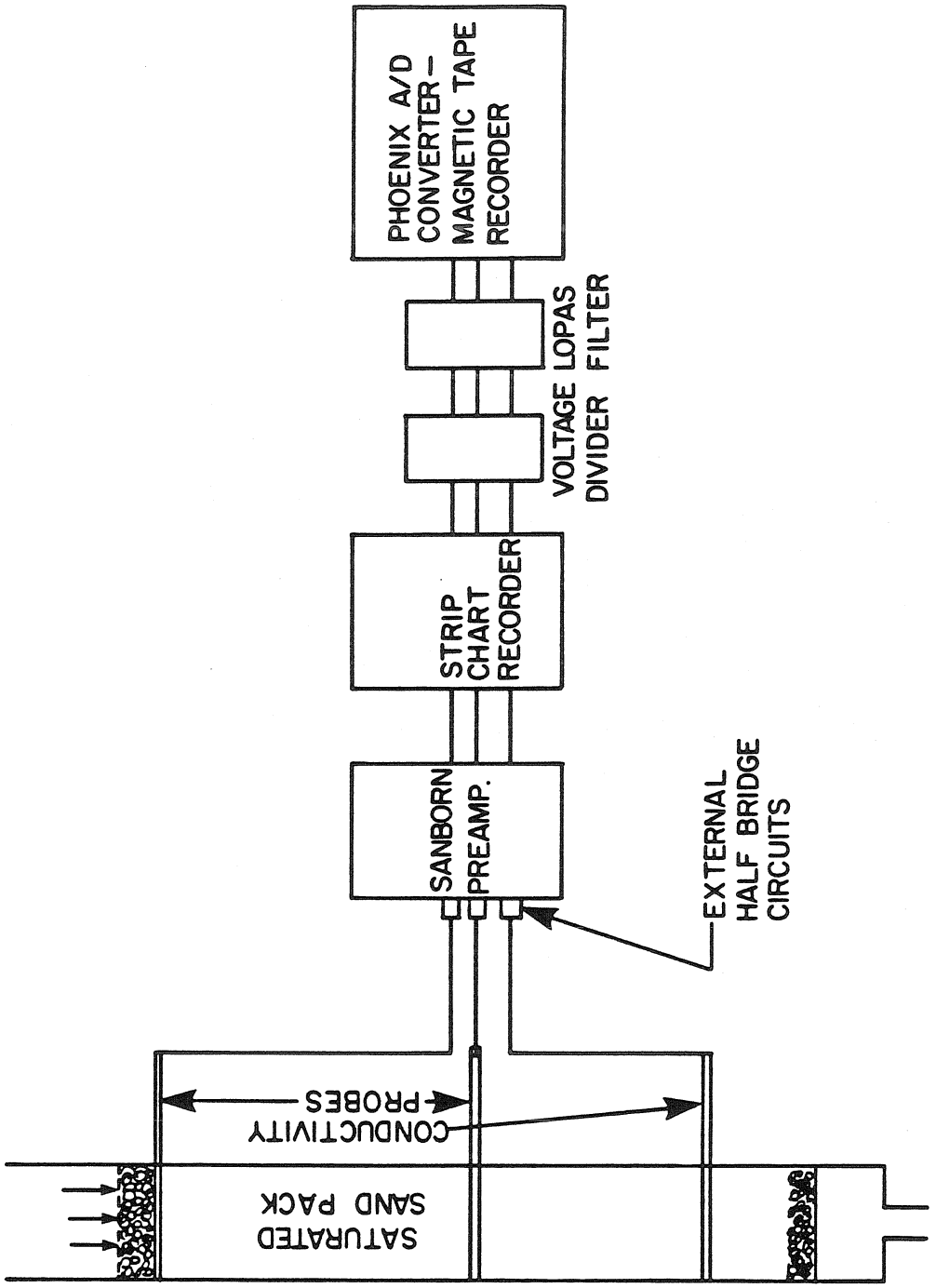

FIGURE 4.4

Packed Column Apparatus Showing Conductivity Data Acquisition System

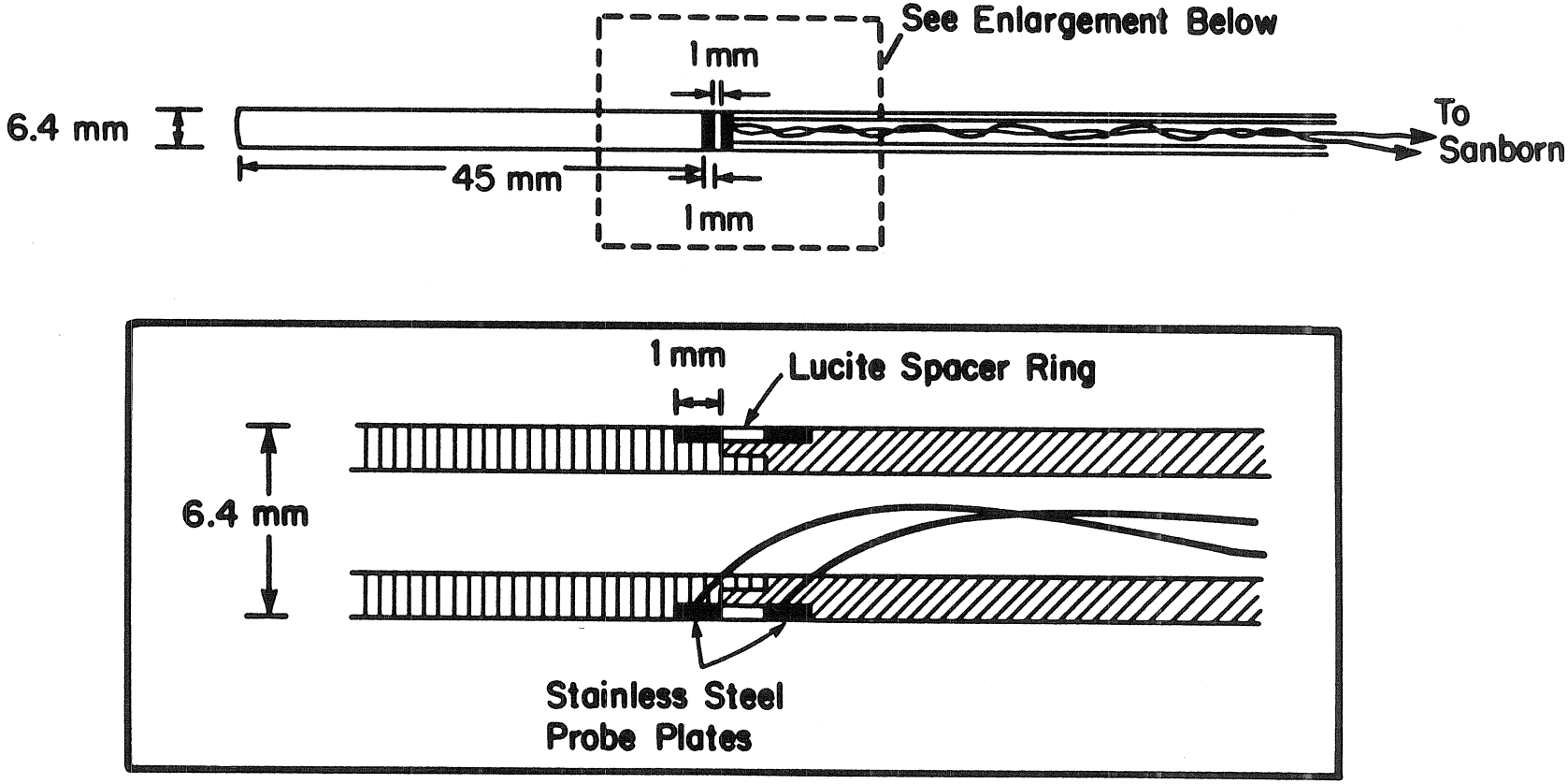

FIGURE 4.5

Cross-Sectional Sketch of Conductivity Probe
with Detail of Probe Plates

The probes are driven by a Sanborn carrier preamplifier model 150-1100AS, which has an excitation frequency of 2400cps and a frequency response of 0 to 100cps. The probe is part of an external half-bridge circuit (Figure 4.6) which connects to the preamplifier. Salinity changes detected by the probe are displayed on a Sanborn model 154-100B strip chart recorder. The voltage output (which drives the recorder stylus) is sent through a voltage divider and low pass filter (Figure 4.7) and is recorded digitally by a Digital Data model ADC 1370 analogue-to-digital system. The voltage divider is necessary since the 150 volt output of the Sanborn preamplifier exceeds the ±10 volt input allowed by the A/D system. The low pass filter removes the carrier frequency from the output voltage (which is mechanically filtered by the strip chart stylus). The A/D converter has a digitizing resolution of one part in 2047 and a maximum sampling rate of 1600 samples/second. The sampling window has an aperture of 0.17μsec, which is independent of the sampling rate. The sampler voltage is converted from binary to binary coded decimal and written on a magnetic tape. Further information on the Digital Data A/D system is available in Okoye and Raichlen (1969).

The hanging water column method is employed for measuring capillary drainage curves. The experimental arrangement is shown in Figure 4.8. The heart of the system is the fritted glass porous disc in the Buchner funnel. The disc enables suction head (tensile stress) to be applied to the porous medium sample without allowing air to enter the water column and disrupt the tensile stress being applied. By lowering the burette, greater suction is applied to the porous medium

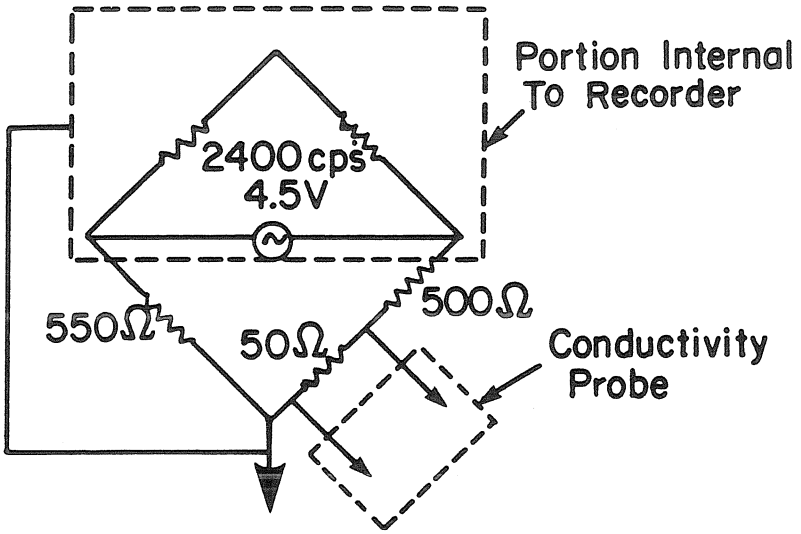

FIGURE 4.6

External Half-Bridge Circuit

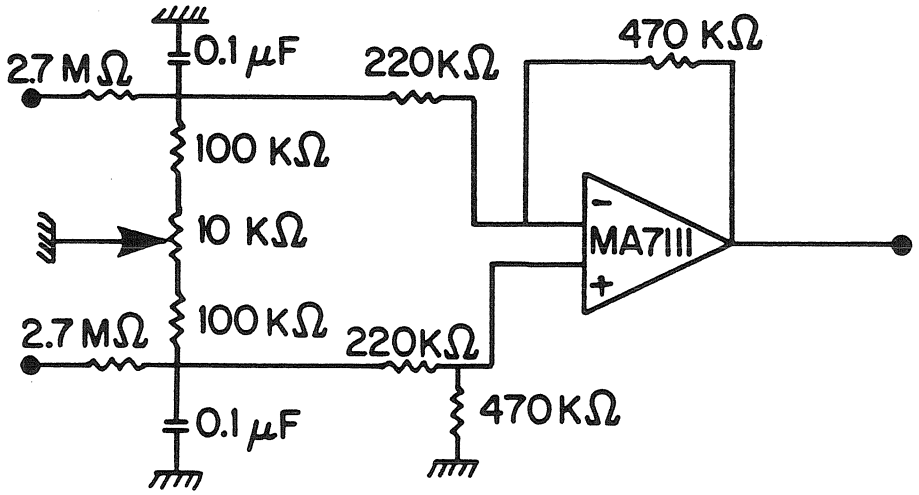

FIGURE 4.7

Voltage Divider and Low Pass Filter
for Sanborn Output
(after Lepelletier, 1980)

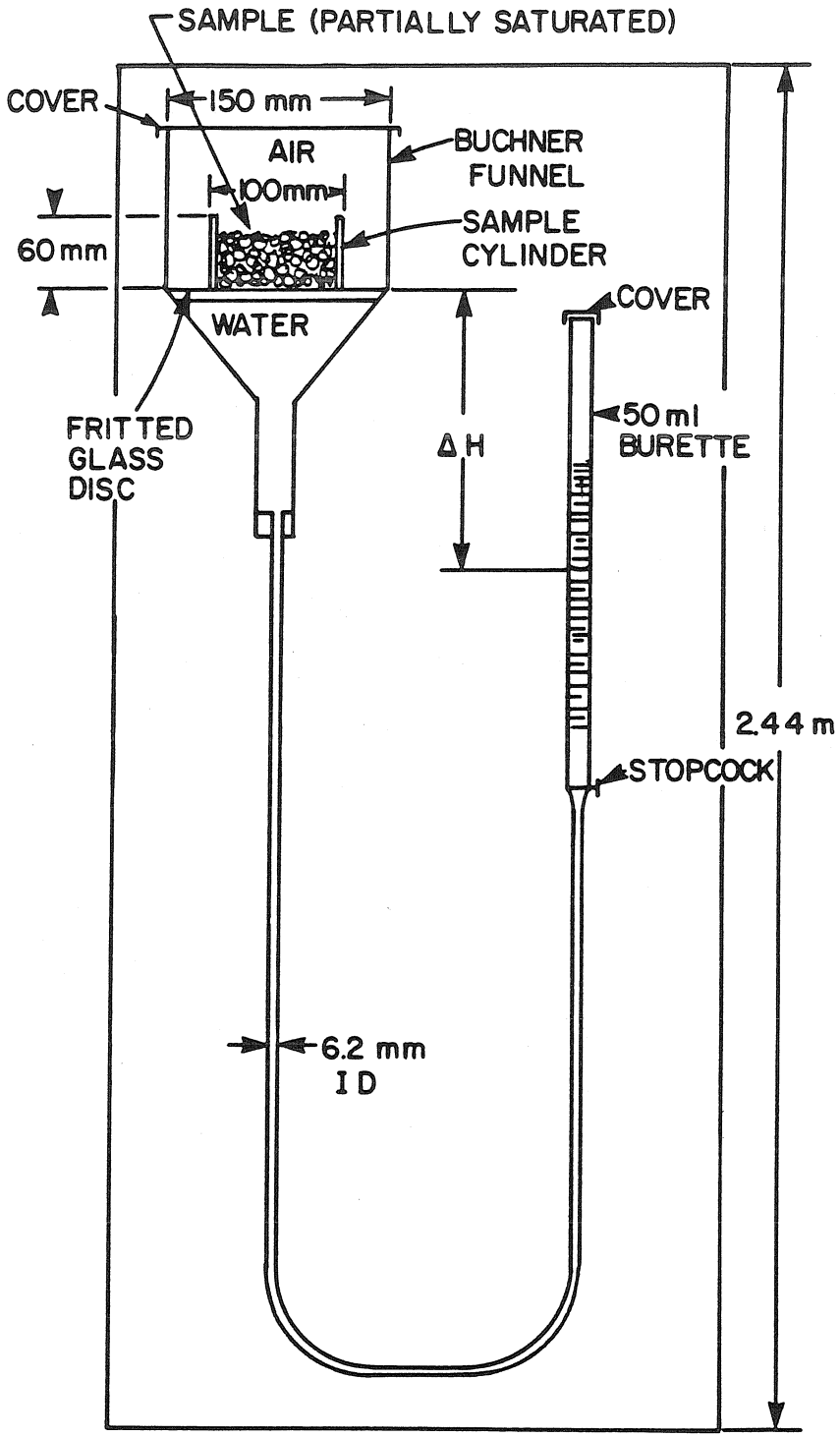

FIGURE 4.8

Apparatus for the Capillary Drainage Measurements

and more water drains out of the sample. The suction head is determined by the difference in elevation between the porous plate and the water surface level in the burette. The maximum suction which may be applied before drawing air through the fritted glass disc is determined from the capillary equation and the maximum pore size in the disc. The maximum pore size in the disc is 8μm, which corresponds to 1.9m of suction head. The inner cylinder which holds the porous medium is sealed to the fritted glass disc with silicone sealant. A loose cover is placed over the Buchner funnel to reduce evaporation from the sample.

Precision screens manufactured by the W.S. Tyler Co. are used for the sieve analysis of grain size distributions. The stack of successively finer screens ($\sqrt[4]{2}$ series) is shaken by a mechanical sieve shaker. The screenings are weighed on a mechanical beam balance which is accurate to 0.001g.

4.2 Characterization of the Porous Media

A large sample of several kilograms is taken and split down to a sample size large enough to be representative but not so large such that significant blocking of smaller grains by larger grains occurs. For the uniform medium, samples on the order of 40g are used while a sample of about 175g is used for the nonuniform medium. Being a natural sand, the nonuniform medium contains a good deal of silt and clay which is removed by washing the sand in a $(NaPO_3)_6$ and $(Na_2CO_3)_2$ solution. Due to the uniform grain sizes in the uniform medium, only 6

screens are needed to characterize the grain size distribution. A series of 25 screens are needed to characterize the nonuniform grain size distribution. The sieves are stacked and placed in the mechanical shaker for 10 minutes. The sand retained on each screen is weighed to give the fraction by weight of grains which are nominally larger than the opening size of the given screen but less than the opening size of the screen immediately above. The results are generally given as a cumulative distribution of grain size by weight and often follow a log-normal distribution (Vanoni, 1975). If we let d_{84}, d_{50}, and d_{16} represent the 84^{th}, 50^{th}, and 16^{th} percentile grain size on the cumulative distribution, respectively, then the geometric mean grain size, d_g, and the geometric standard deviation, σ_g, are given by d_{50} and $(d_{84}/d_{16})^{1/2}$, respectively, for a log-normal distribution.

Figure 4.9 shows the grain size distributions for the two porous media. Both distributions are reasonably log-normal, the nonuniform grain size distribution having a much greater geometric standard deviation ($\sigma_g = 2.93$) than the uniform medium ($\sigma_g = 1.15$). The nonuniform medium also has a much greater mean grain size, $d_g = 1.26$mm, compared to $d_g = 0.382$mm for the uniform medium.

As discussed in Chapter 3, the grain size distribution is a volume-weighted distribution (equation (3.51))

$$P_d(d) \sim \int_o^d \zeta^3 h(\zeta) d\zeta$$

where h(d) is the probability density for the grain diameter according to the frequency of occurrence of a given grain. $P_d(d)$ is the

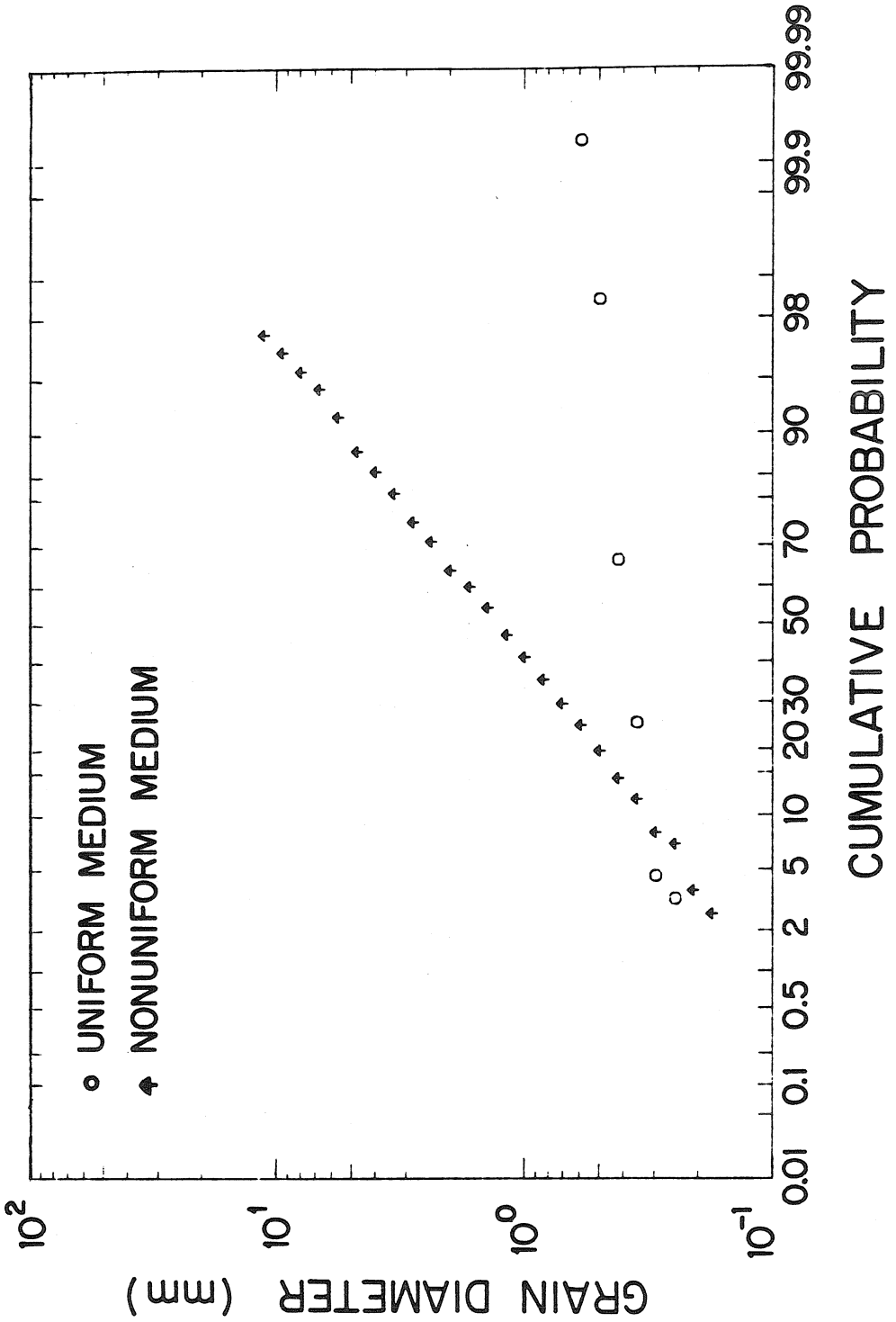

FIGURE 4.9

Volume-Weighted Grain Size Distributions, $P_d(d)$

cumulative probability distribution shown in Figure 4.9. The influence of each grain on the pore length distribution is expected to follow the cumulative grain size distribution weighted by the area of a given particle

$$J(d) \sim \int_o^d \zeta^2 h(\zeta) d\zeta$$

To produce J(d) from $P_d(d)$, we first interpolate the experimental data to 1000 equally spaced probabilities on the cumulative distribution. For probabilities beyond the range of the experimentally determined values, the length is set to the maximum or minimum grain size. The distribution is given by equation (3.52)

$$J(d) \sim \int_o^d \frac{1}{\zeta} dP_d(\zeta)$$

where the values of J(d) are normalized such that the integral over the entire domain is one. This integration is performed numerically (trapezoidal integration). Figure 4.10 shows the final grain size distribution from this calculation. The d_{50} values for the uniform and nonuniform media are 0.380mm and 0.453mm, respectively, for the area-weighted distributions shown in Figure 4.10. The nominal geometric standard deviations $((d_{84}/d_{16})^{1/2})$ for the uniform and nonuniform media (Figure 4.10) are 1.16 and 2.42, respectively. Table 4.1 presents a summary of the information on the grain size distributions.

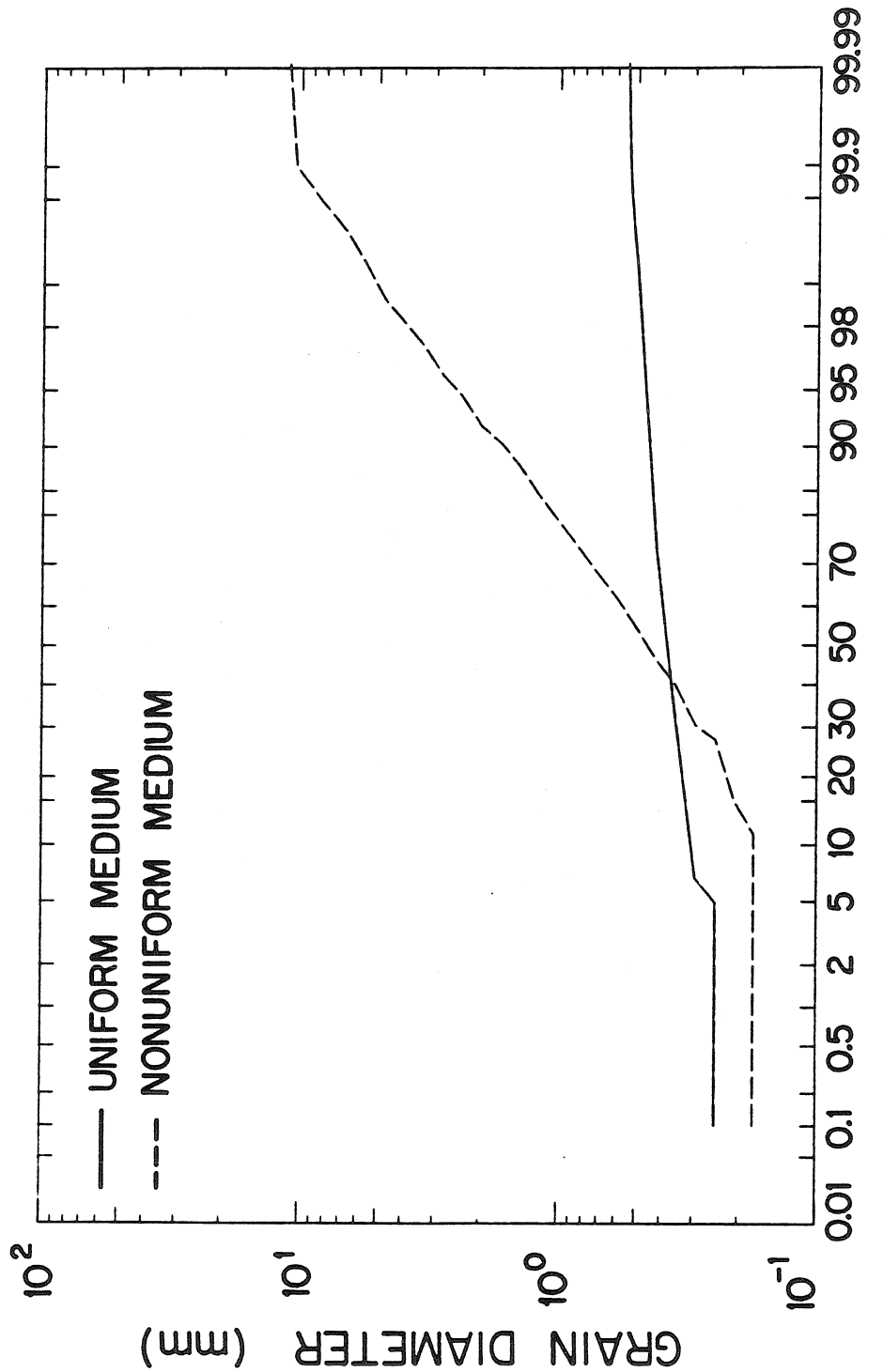

FIGURE 4.10

Area-Weighted Grain Size Distribution, J(d)

Table 4.1
Grain Diameter Distribution Data

UNIFORM MEDIUM

Volume-Weighted Distribution[a]		Area-Weighted Distribution[b]	
Grain Diameter(mm)	Cumulative Probability(%)	Grain Diameter(mm)	Cumulative Probability(%)
0.246	3.29	0.246	0.100
0.294	4.57	0.251	5.0
0.351	25.4	0.307	10.0
0.417	66.6	0.320	15.0
0.495	98.5	0.331	20.0
0.589	99.9	0.341	25.0
		0.350	30.0
		0.358	35.0
		0.365	40.0
		0.373	45.0
		0.380	50.0
		0.388	55.0
		0.396	60.0
		0.405	65.0
		0.414	70.0
		0.421	75.0
		0.428	80.0
		0.437	85.0
		0.448	90.0
		0.464	95.0
		0.549	99.9

(a) $d_g = 0.382$ mm $\sigma_g = 1.15$

(b) $d_g = 0.380$ mm $\sigma_g = 1.16$

Table 4.1 (continued)
Grain Diameter Distribution Data

NONUNIFORM MEDIUM

Volume-Weighted Distribution[a]		Area-Weighted Distribution[b]	
Grain Diameter(mm)	Cumulative Probability(%)	Grain Diameter(mm)	Cumulative Probability(%)
0.175	2.60	0.175	0.100
0.208	3.70	0.175	5.00
0.246	7.00	0.175	10.0
0.295	8.10	0.203	15.0
0.351	12.0	0.223	20.0
0.417	15.0	0.240	25.0
0.495	19.7	0.290	30.0
0.589	24.8	0.322	35.0
0.701	29.6	0.352	40.0
0.833	35.4	0.406	45.0
0.991	41.2	0.454	50.0
1.17	47.1	0.506	55.0
1.40	54.4	0.568	60.0
1.65	59.9	0.652	65.0
1.98	64.1	0.754	70.0
2.36	71.1	0.879	75.0
2.79	75.4	1.05	80.0
3.33	81.0	1.27	85.0
3.96	84.7	1.64	90.0
4.70	87.7	2.52	95.0
5.61	91.8	11.2	99.9
6.68	94.3		
7.93	95.5		
9.42	96.6		
11.2	97.4		

(a) d_g = 1.26 mm σ_g = 2.93

(b) d_g = 0.453 mm σ_g = 2.42

Water in the column experiments and the capillary drainage measurements comes under tensile stress. To minimize the formation of bubbles in the fluid, all water used in these experiments is de-aerated under vacuum for about 30 minutes. Since several hundred liters of water are needed for the column experiments, a battery of 11, 19-liter glass jugs are connected in series to a vacuum line for de-aeration. The de-aerated water is siphoned from the jugs into the supply reservoirs to minimize air entrainment while transferring the water.

Procedures for the capillary drainage measurements follow those given by Vomocil (1965). The Buchner funnel's porous disc is saturated by submerging the funnel in de-aerated water overnight and then drawing water through the funnel and tubing by using a vacuum pump. The saturated Buchner funnel, tubing, and burette assembly are mounted vertically as shown in Figure 4.8. Before putting sand into the sample cylinder, the system is calibrated for any plate drainage or tubing collapse by running through the entire series of suction heads and noting the drainage into the burette. A 600-700g sample of the porous medium is stirred into the de-aerated water to completely saturate the sand. The sand and water mixture is then poured into the sample cylinder in the Buchner funnel. The saturated sample is compacted by a hand-held vibrator until the packing is at equilibrium. Excess water is poured of the funnel while holding the sample in place. By lowering the burette, a tension is applied to the sample and water drains into the burette until equilibrium is reached. Due to the water draining into the burette, the burette must be lowered as it fills to maintain a

constant tension. Equilibrium measurements of the volume drained for a series of successively greater tensions determine the capillary drainage curve.

Pore radii are related to the tension head, ΔH, through the capillary equation for circular cylindrical capillaries

$$a = 2\gamma \cos \beta/\rho g \Delta H \qquad (4.1)$$

where γ is the surface tension of water, ρ the density, g the gravitational acceleration, and β the contact angle between the air-water interface and the solid-water interface. Since equation (4.1) is used for a drainage capillary curve, the contact angle is generally assumed to be zero (Vomocil, 1965). As indicated by Vomocil (1965) and others, the capillary drainage method is a crude, semi-quantitative technique for measuring pore sizes. Blockage of larger pores by smaller pores during drainage, pore geometries which are not circular cylindrical capillaries, and variation of the contact angle are some of the problems neglected by this method. Unfortunately, there is no practical alternative technique, although direct microscopic examination has been proposed (Dullien, 1979). Due to the approximate nature of the measurement, it is sufficient to take $\gamma = 72.8 g/sec^2$ $\rho = 0.998 \times 10^{-3} g/mm^3$, $g = 9800. mm/sec^2$, so that equation (4.1) becomes

$$a = 0.149/\Delta H \qquad (4.2)$$

where a and ΔH are in millimeters. An important distinction between the pore radius distribution and the grain size distribution is that the pore radius distribution corresponds to lengths scaling the void

space in the medium, while the grain size distribution is a measure of the lengths scaling the solid space in the medium.

The capillary drainage curve for most porous media display a residual saturation which cannot be removed by increasing the tension head (Bear, 1972). This residual saturation is apparently due to water trapped in pendular rings, nonconducting pores, and other situations which isolate water from conducting pathways. Interpretation of this problem for pore size distributions is difficult and for this study the residual saturation will be ignored for the purposes of determining the pore size distributions. The residual saturation will be taken into account, however, for the determination of total porosity.

The results of the pore size distribution measurements are shown in Figure 4.11. As discussed in Chapter 3, the pore size distribution corresponds to (equation (3.48))

$$P_a(a) \sim \int_0^a \eta^2 g(\eta) d\eta$$

where $g(\eta)$ is the frequency distribution (by number) for the occurrence of pores of a given size a. While the pore sizes for a uniform medium change rapidly near the extremes of the distribution, the distribution is relatively flat between the 5 and 95 percentile. The nonuniform medium pore size distribution has a 50 percentile size close to that of the uniform medium, but shows a less peaked, more log-normal distribution of pore sizes. The 5 to 95 percentile range in pore sizes is 5.6 times greater than the corresponding range of pore sizes in the uniform medium. Nominal values for the geometric mean and standard

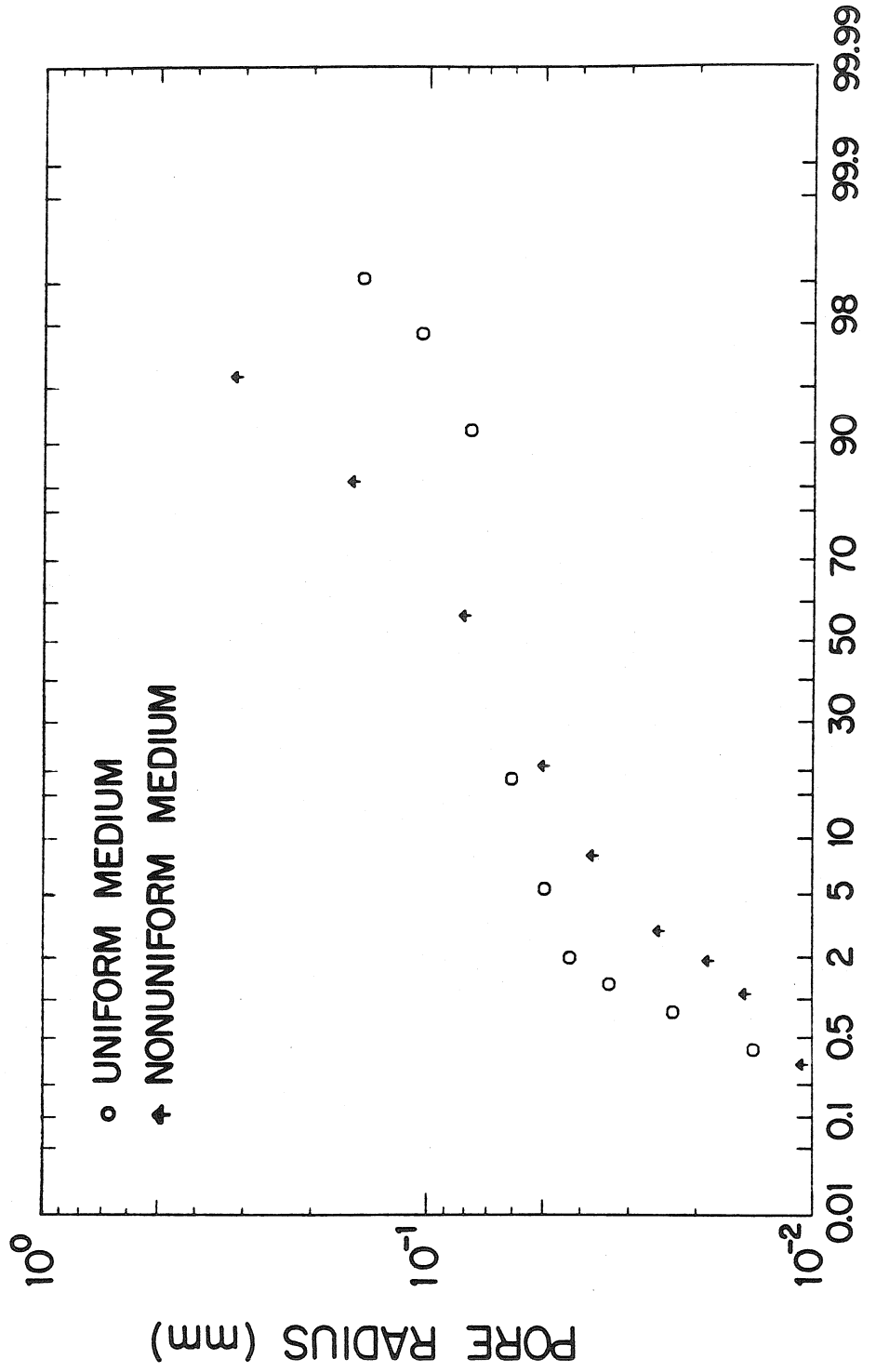

FIGURE 4.11

Volume-Weighted Pore Radius Distribution, $P_a(a)$

deviations for these distributions may be assigned (as discussed for the grain size distributions). The values of a_{50} for the uniform and nonuniform media are 0.0679mm and 0.0745mm, respectively. The nominal geometric standard deviations for the uniform and nonuniform media are 1.14 and 1.85, respectively.

When the sample has been drained to its residual saturation, it is transferred from the Buchner funnel to a beaker. The sample is then weighed and placed in an oven to dry the sample completely. After drying, the sample is weighed. The weight loss during drying determines the volume of water, V_w, contained in the sample at residual saturation. The residual saturation for both porous media is found to be about 10% of the total saturation volume. The dry weight of the sample gives the volume of sand, V_s, by assuming the sand density to be 2.65g/cc. The total porosity, $\sigma = V_w/(V_s + V_w)$, is found to be 0.313 for the uniform medium and 0.291 for the nonuniform medium.

To compute the cumulative probability distribution for pore sizes according to the frequency of occurrence, we follow a procedure similar to the analysis of the grain size distribution. The measured distribution is interpolated to provide the pore radii at 1000 equally spaced values in the cumulative distribution. For probabilities beyond the range of the experimentally determined values, the radius is set to the maximum or minimum pore size measured. The cumulative distribution for the occurrence of pore sizes according to frequency is derived by noting that (see equation (3.49))

$$G(a) \sim \int_{o}^{a} \frac{1}{\eta^2} \, dP_a(\eta)$$

The cumulative probability distribution according to frequency, G(a), is calculated from the above integral using numerical trapezoidal integration. Figure 4.12 shows the distribution resulting from these calculations. The a_{50} values for the uniform and nonuniform media are 0.0635mm and 0.0383mm, respectively, for the distributions shown in Figure 4.12. Values of the nominal geometric standard deviation for the uniform and nonuniform media (Figure 4.12) are 1.27 and 2.17, respectively. Table 4.2 presents a summary of the information on the pore radius distributions.

4.3 Column Experiments for Porosity and Permeability

Dry sand is loaded into the vertical column by continuous pouring through the opening at the top of the column. The conductivity probes are in place in the column before the sand is loaded. When the test section is filled, the sand is compacted by tapping on the column until an apparent equilibrium is reached. Vibration compaction was not used due to the possibility of radial segregation of grain sizes when compacting nonuniform sand (Ripple, et al., 1974). During compaction, the sand level drops and additional sand is added to fill the test section. The process is continued until the sand level is stable at the proper level. All ports and openings are sealed and air is evacuated through a port on the bottom of the column with a vacuum

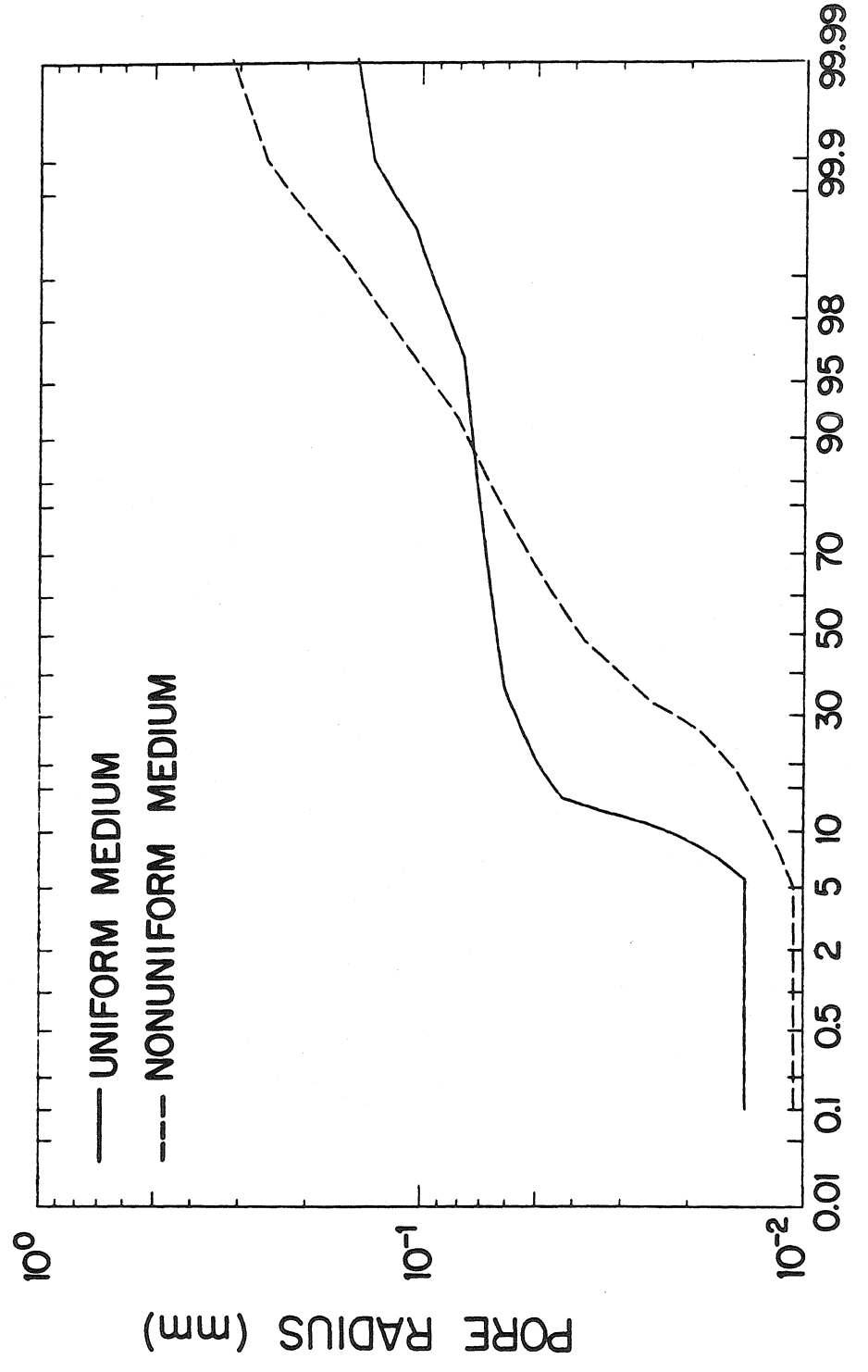

FIGURE 4.12

Pore Radius Frequency Distribution, G(a)

Table 4.2
Pore Radius Distribution Data

UNIFORM MEDIUM

Volume-Weighted Distribution[a]		Number Frequency Distribution[b]	
Pore Radius(mm)	Cumulative Probability(%)	Pore Radius(mm)	Cumulative Probability(%)
0.0142	0.400	0.0142	0.100
0.0230	0.800	0.0142	5.00
0.0337	1.30	0.0227	10.0
0.0426	2.00	0.0435	15.0
0.0496	5.40	0.0493	20.0
0.0604	18.6	0.0531	25.0
0.0776	91.4	0.0565	30.0
0.104	97.7	0.0596	35.0
0.148	99.1	0.0613	40.0
		0.0624	45.0
		0.0635	50.0
		0.0645	55.0
		0.0656	60.0
		0.0666	65.0
		0.0677	70.0
		0.0689	75.0
		0.0703	80.0
		0.0718	85.0
		0.0738	90.0
		0.0765	95.0
		0.148	99.9

(a) $\mu_a = 0.0679$ mm $\sigma_a = 1.14$

(b) $\mu_a = 0.0635$ mm $\sigma_a = 1.27$

Table 4.2 (continued)
Pore Radius Distribution Data

NONUNIFORM MEDIUM

Volume-Weighted Distribution[a]		Number Frequency Distribution[b]	
Pore Radius(mm)	Cumulative Probability(%)	Pore Radius(mm)	Cumulative Probability(%)
0.0106	0.300	0.0106	0.100
0.0149	1.10	0.0107	5.00
0.0186	1.90	0.0123	10.0
0.0250	3.00	0.0139	15.0
0.0372	8.20	0.0156	20.0
0.0499	20.9	0.0179	25.0
0.0801	56.6	0.0218	30.0
0.156	85.0	0.0264	35.0
0.315	95.7	0.0301	40.0
		0.0343	45.0
		0.0384	50.0
		0.0416	55.0
		0.0449	60.0
		0.0485	65.0
		0.0524	70.0
		0.0567	75.0
		0.0617	80.0
		0.0679	85.0
		0.0760	90.0
		0.0942	95.0
		0.315	99.9

(a) μ_a = 0.0745 mm σ_a = 1.85

(b) μ_a = 0.0383 mm σ_a = 2.17

pump. De-aerated water is then allowed to enter through the inlet. After roughly 25% of the medium is saturated, atmospheric pressure is allowed into the space above the water surface. This increases the driving head to saturate the column and causes the water to move quickly through the column with a sharp saturation front. The vacuum pump is turned off after the entire porous medium has been saturated. The packing of the sand was not visibly affected by the saturation process; no further settling of the sand pack was observed.

All water used in the column is de-aerated, as described in Section 4.2. The saline tracer water is prepared by adding 0.03% NaCl by weight to each de-aeration jug. This low concentration minimizes density differences ($\Delta\rho \sim 0.0002$g/ml) and viscosity differences, which can produce unstable flow conditions (Bear, 1972).

Probe calibration is carried out by flushing known concentrations of saline solution through the column and recording the probe voltage output. Figure 4.13 shows that all probes give a linear relationship between relative concentration and voltage. This simplifies data reduction and allows one to perform experiments without having to calibrate for each experiment, which is quite time-consuming. Only one of the probes is used at a given time as a simple way to prevent signal cross talk between probes. A breakthrough experiment is performed by draining the inlet chamber and refilling it with fresh or salt water (depending on what currently saturates the porous medium), and then opening the outlet valve to begin the flow. One experiment consists of measuring a complete displacement of the resident water by the

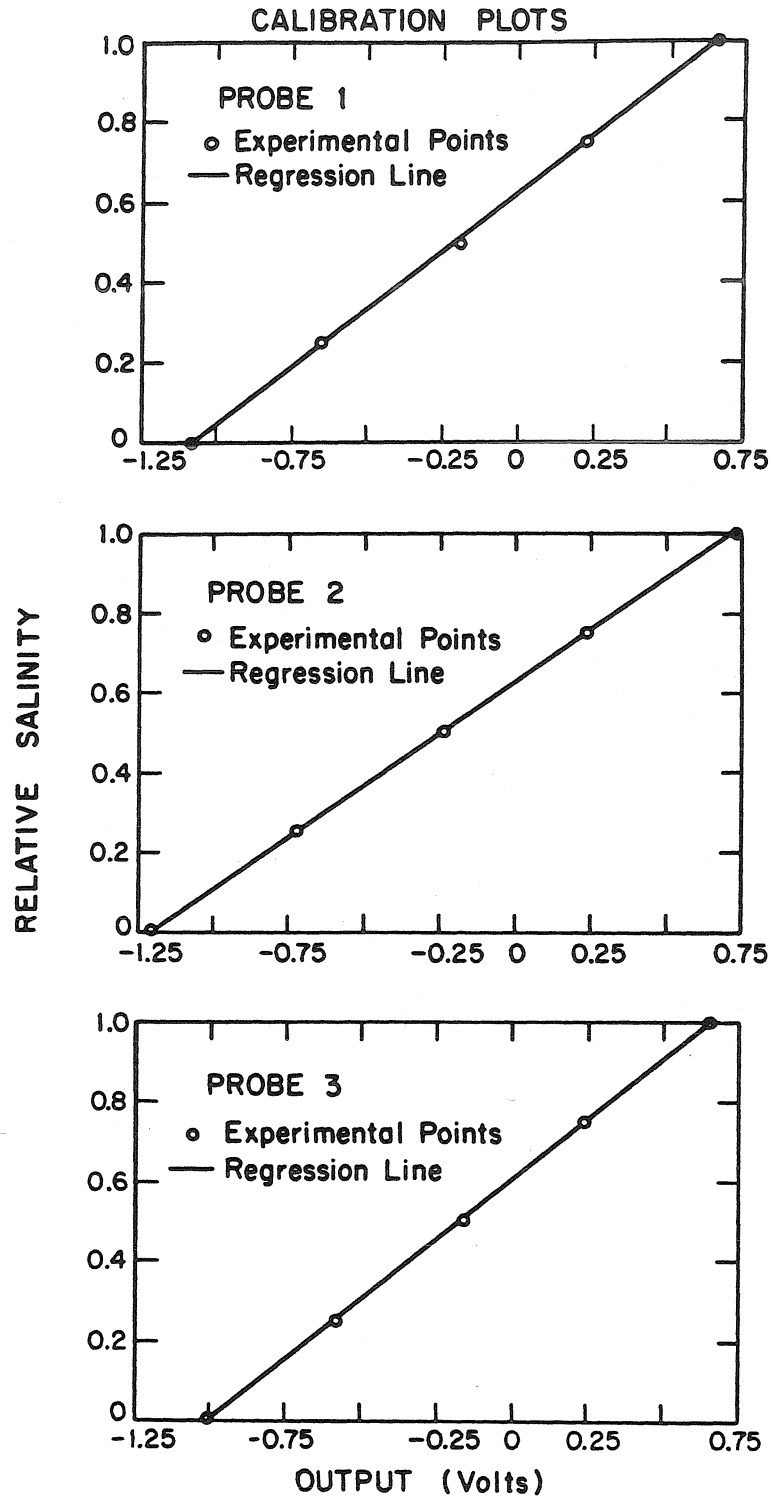

FIGURE 4.13

Conductivity Probe Calibration Curves

displacing water. Three experiments are required to measure the breakthrough at all three probes. No distinctions were observed between salt water displacing fresh water, versus fresh water displacing salt water.

The Darcy velocity, V_D, is obtained for each experiment by measuring the flow rate and dividing this by the cross-sectional area of the column. The flow rate is determined by measuring the time required for the outflow from the column to fill a 1 liter volumetric flask. The piezometric head gradient, $\nabla\phi$, (which should be uniform in a homogeneous sand pack) is obtained by taking the difference in piezometric head at successive piezometers along the column and dividing by the difference in distance between the piezometers. Since the column has four piezometers, three independent measurements of the piezometric head gradient may be made. Darcy's law states ,

$$V_D = -K\nabla\phi$$

where K is the hydraulic conductivity. Dimensional analysis shows that $K = kg/\nu$, where k, the permeability, has dimensions of area and is a property of the porous medium. The quantities ν and g are the kinematic viscosity of water and gravitational acceleration. Combining Darcy's law with the expression for K gives,

$$k = V_D\nu/\nabla\phi g.$$

Since $\nabla\phi$ is measured over three different sections of the column and V_D

is constant by continuity, we have a measure of the permeability variation along the column.

Table 4.3 shows the permeability variations and overall permeability for both porous media. The estimate experimental error for the permeability measurement is ±1%. The average permeability of the nonuniform medium is seen to be slightly larger than that of the uniform medium. This is consistent with the results found for the pore size distributions. The 50% pore size for the two distributions are quite close although the spread and shape of the two pore size distributions are distinct. Permeability variations within the porous media are seen to be relatively small, with both permeabilities showing a minimum in the middle section. This may be expected since packing constraints at the top of the column and at the bottom may not allow maximum packing density. The overall variation figures given in Table 4.3 are the maximum permeability differences found in the column divided by the respective overall permeability between piezometers 1 and 4. This gives a quantitative estimate of the packing homogeneity.

Wall effects during flow through packed columns are difficult to estimate quantitatively. Theoretical and experimental work presented by Cohen and Metzner (1981) for uniform media suggest for uniform media that a column diameter to grain diameter ratio greater than 30 is necessary to avoid significant wall effects. For the uniform medium, the column to geometric mean grain diameter ratio is 233, while for the nonuniform medium the ratio is 71.

Table 4.3
Permeability Data

Piezometers: (see Figure 4.1)	1 to 2	2 to 3	3 to 4	1 to 4	Overall Variation
Uniform Medium Permeability(10^{-5} mm^2): (±1%)	5.83	5.53	5.72	5.56	6%
Nonuniform Medium Permeability(10^{-5} mm^2): (±1%)	6.34	5.69	5.95	5.95	11%

Table 4.4
Porosity Data

Probes: (see Figure 4.1)	Effective Porosity			Total Porosity
	1	2	3	
Uniform Medium Porosity: (±1%)	0.337	0.318	0.322	0.313
Nonuniform Medium Porosity: (±1%)	0.337	0.278	0.290	0.291

When one fluid displaces another immiscibly, the interface velocity (or seepage velocity, V_s) is greater than the Darcy velocity. This is caused by a portion of the cross section's being occupied by grains which reduces the available cross-sectional area for flow. The average areal porosity is known to be equal to the volumetric porosity (Bear, 1972), but flow takes place only in pores which interconnect. Thus an effective porosity may be defined by,

$$\sigma_e = V_D/V_s \tag{4.3}$$

The difference in effective porosity to total porosity gives an estimate of the amount of fluid which is stagnant. If the miscible displacement process follows advection-diffusion theory, the seepage velocity is equal to the velocity of the 50% concentration point (assuming adsorption is not significant). Using the conductivity measurements, the velocity of the 50% concentration point is easily found. Table 4.4 shows the variation in average effective porosity between the top of the sand pack and each probe for both porous materials. Experimental error for the effective porosity and total porosity measurements is ±1%. The effective porosity at the first probe, which measures over the top 7% of the column, is seen to be higher than subsequent porosities further down the column. This effect is most noticeable in the nonuniform medium, where the smaller grains tend to filter down, leaving the top portion of the column with larger, more uniform grain sizes. Porosities measured at the other two probes show more uniformity, as expected, since these measurements average over a much greater portion of the column. Comparison of the average

effective porosity for each medium (the effective porosity measured at the third probe) with the total porosity (Table 4.4) shows no significant differences. This indicates little or no stagnant water in either column.

4.4 Column Experiments for Longitudinal Dispersion

For each dispersion experiment, the concentration of the saline tracer vs. time is recorded at just one of the three probe locations. Most theoretical descriptions of longitudinal dispersion in porous media are based on the advection-diffusion equation, as discussed in Chapter 2. The dispersion experiments consist of one-dimensional miscible displacements which produce breakthrough curves for the variation of concentration versus time measured at a conductivity probe (see Section 1.2). Several different forms of boundary conditions have become popular since the exact physical circumstances which the boundary conditions represent are not well understood. For example, given the physical circumstances associated with these experiments, it is difficult to say whether the proper inlet boundary condition for a miscible displacement is

$$C(0,t) = C_o \qquad t > 0$$

which is a constant concentration condition, or

$$V_s C(0^+,t) - D_L \frac{\partial C}{\partial x}(0^+,t) = V_s C_o \qquad t > 0$$

which is a mass balance condition. The problem in deciding on the

proper boundary condition arises since the inlet chamber is a distinct physical system which should be considered for a complete solution. Mass transport in the inlet chamber is not well understood, however, such that a complete model is not possible. Appendix B discusses the behavior of the solutions of equation (1.3) for miscible displacements according to various boundary conditions. The important conclusion from Appendix B is that all of the solutions using the various boundary conditions are convergent to the same solution only a short distance downstream ($V_s x/D_L > 24$). Therefore, to analyze the experimental data we will use the simpler solution for an infinite medium with the initial condition

$$C(x,0) = C_0 \qquad x < 0$$

$$C(x,0) = 0 \qquad x > 0$$

In nondimensional form, this solution is (see Appendix B)

$$C/C_o = \frac{1}{2}\,\mathrm{erfc}\left(\frac{X - T}{2\sqrt{T}}\right) \tag{4.4}$$

where $X = V_s x/D_L$, $T = (V_s)^2 t/D_L$ and erfc is the complementary error function. Equation (4.4) may be used more conveniently in the following form

$$C/C_o = \frac{1}{2}\,\mathrm{erfc}\left[\sqrt{Pe_D}\left(\frac{x^*-t^*}{2\sqrt{t^*}}\right)\right] \tag{4.5}$$

where d_g is the geometric mean grain size and

$$x^* = x/d_g \qquad t^* = v_s t/d_g \qquad Pe_D = V_s d_g/D_L$$

Written in this way, we see that the experimental value of Pe_D may be obtained by a linear regression of $erfc^{-1}(2C/C_0)$ and $(x^*-t^*)/(2\sqrt{t^*})$. The dynamic Peclet number, Pe_D, is used to obtain D_L/D through the relationship

$$D_L/D = Pe/Pe_D$$

which puts the dispersion data into a form common to other experimental results (see Figure 2.1).

Figures 4.14a and 4.15a show typical experimental breakthrough curves for high Peclet flow in the uniform and nonuniform media, respectively. These profiles show the entire breakthrough (i.e., $C/C_0 \rightarrow 1$), while Figures 4.14b and 4.15b show an expanded view of the central portions of Figures 4.14a and 4.15a. The solid line in these figures is a best fit of equation (4.5) to the experimental data. The procedure for producing the best fit is discussed below. Figures 4.14c and 4.15c are additional views of the same breakthrough curves, but plotted such that equation (4.5) is a straight line. The P^{-1} function used in Figures 4.14c and 4.15c (also seen in Figures 4.16 - 4.21) is the inverse of the cumulative Gaussian probability integral, which is proportional to $erfc^{-1}$. A significant feature of these curves is that the experimental breakthrough curves start deviating from the theoretical solution in the vicinity of $C/C_0 = 0.8$. The exact point of this deviation depends on the Peclet number, probe position and porous

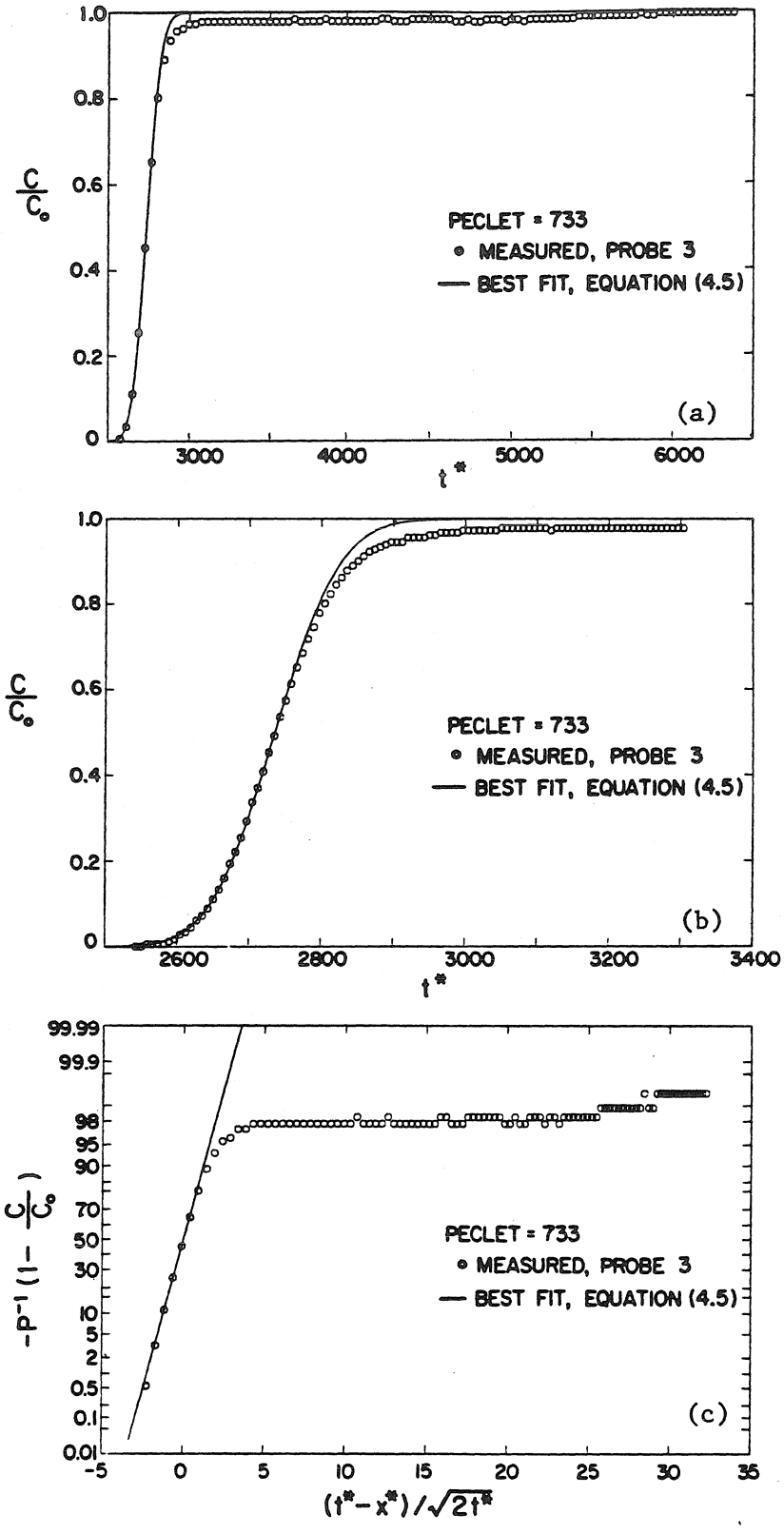

FIGURE 4.14

Breakthrough Curve, Uniform Medium
(Pe = 733, Probe 3)

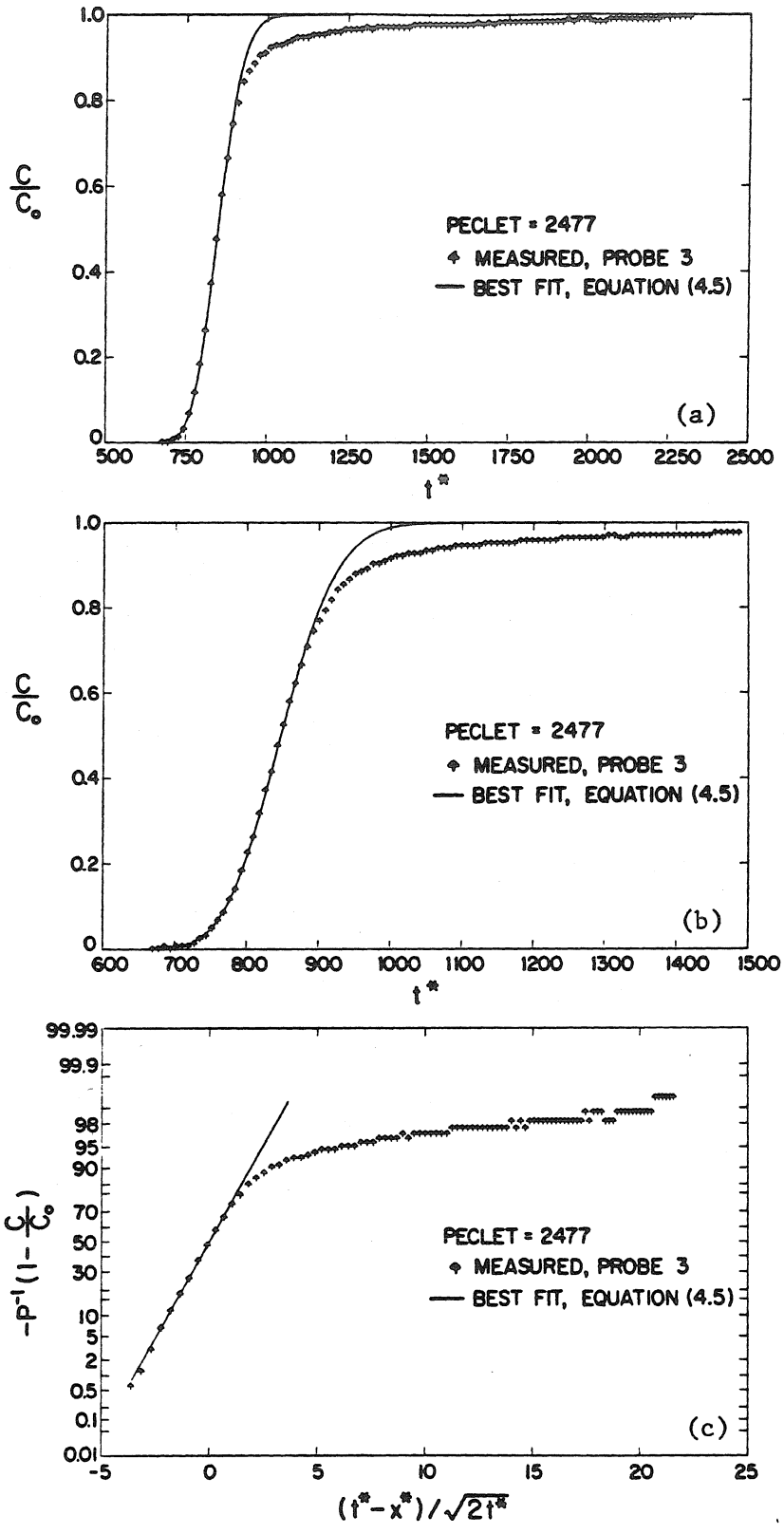

FIGURE 4.15

Breakthrough Curve, Nonuniform Medium
(Pe = 2477, Probe 3)

medium type. This deviation of the experimental breakthrough curve from the theoretical curve is called "tailing", since the "tail" of the breakthrough curve requires more time to complete breakthrough (C/C_0 = 1) than would be expected theoretically. One hypothesis, to be discussed in Chapter 5, is that the tailing behavior is a result of heterogeneous features in the sand packs.

Since the experimental breakthrough curves tend to deviate from the theoretical curve at high values of C/C_0, the only way we may use equation (4.5) to calculate dispersion coefficients is to match the theory to the leading portion of the experimental breakthrough curves. As a consistent and practical technique for analyzing the breakthrough curves, we will use C/C_0 between 1% and 80% to evaluate D_L. The theoretical curves are seen in Figures 4.14 and 4.15 to fit within 5% the leading portion of the breakthrough curves (up to $C/C_0 = 0.8$).

Figures 4.16 through 4.21 show breakthrough curves in the uniform and nonuniform medium for various Peclet numbers and probe positions. Note that the fit is slightly improved in the tail when the Peclet number is lower. Comparing Figure 4.15 with Figures 4.20 and 4.21, we see more pronounced tailing as the breakthrough curve is displaced further along the column. Further discussion of the tailing phenomenon and its interpretation are given in Chapter 5.

The variation of D_L/D with the molecular Peclet number for both uniform and nonuniform media is shown in Figure 4.22 and Table 4.5. The separation of the two data sets on Figure 4.22 is dependent on the

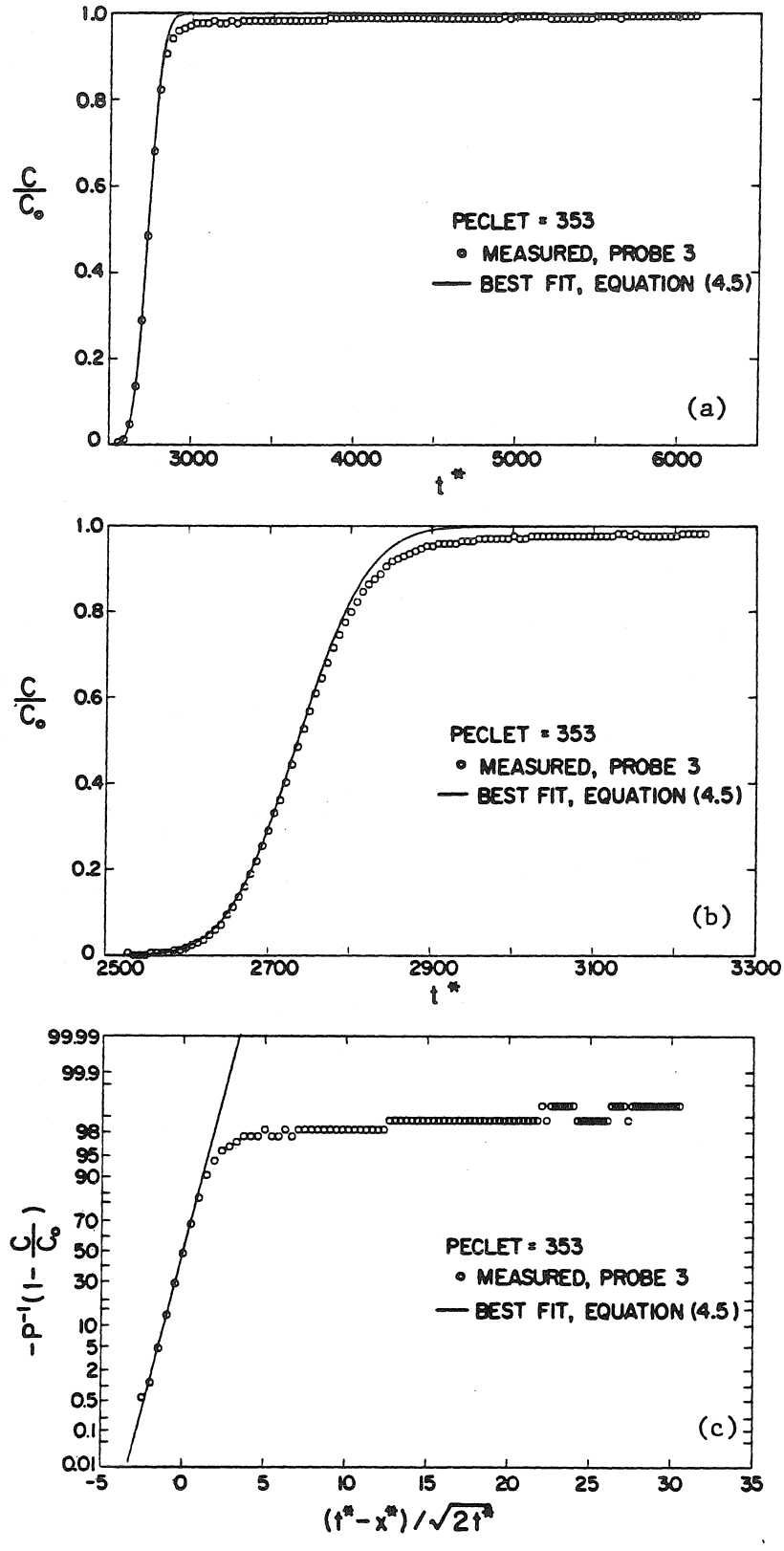

FIGURE 4.16

Breakthrough Curve, Uniform Medium
(Pe = 353, Probe 3)

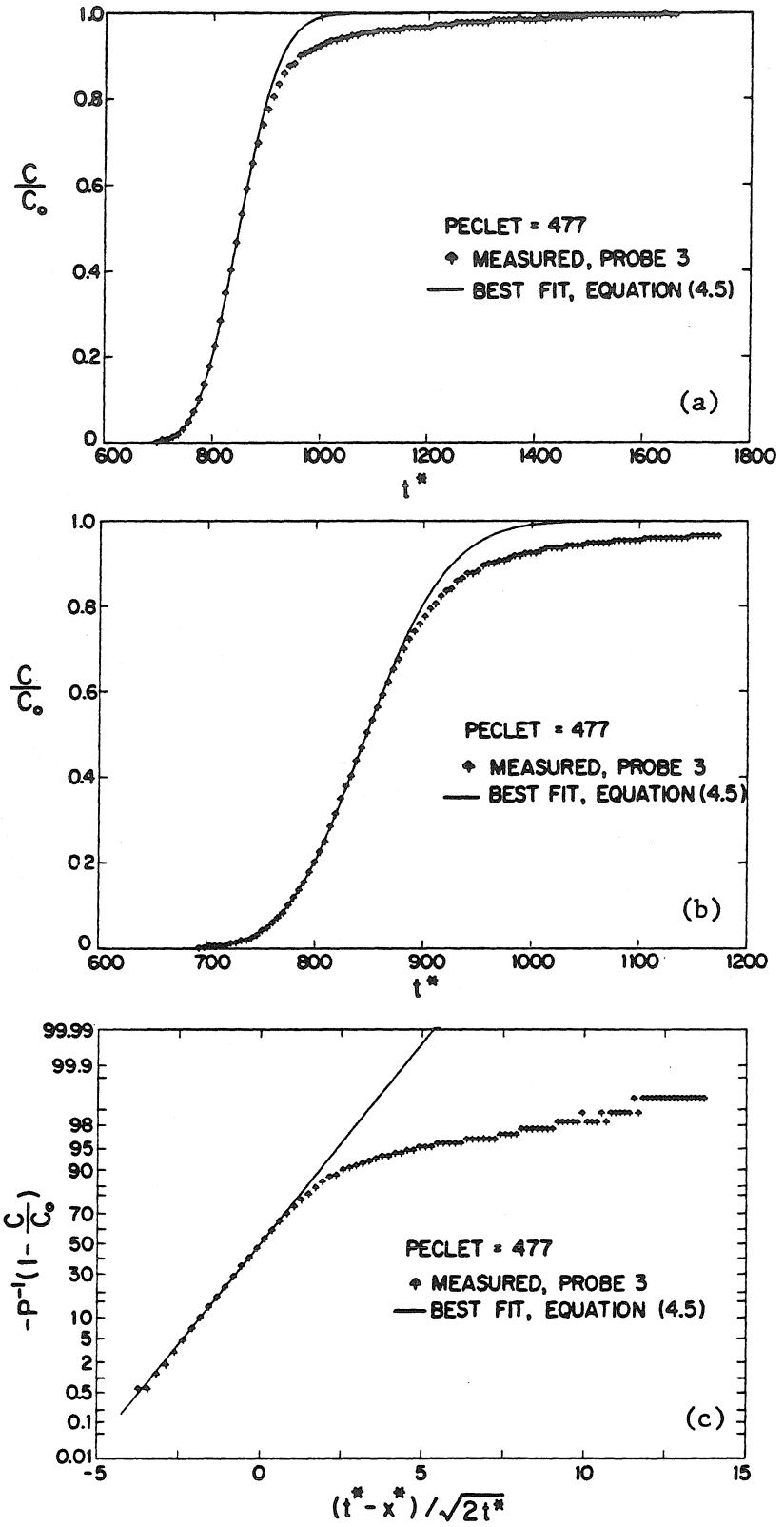

FIGURE 4.17

Breakthrough Curve, Nonuniform Medium
(Pe = 477, Probe 3)

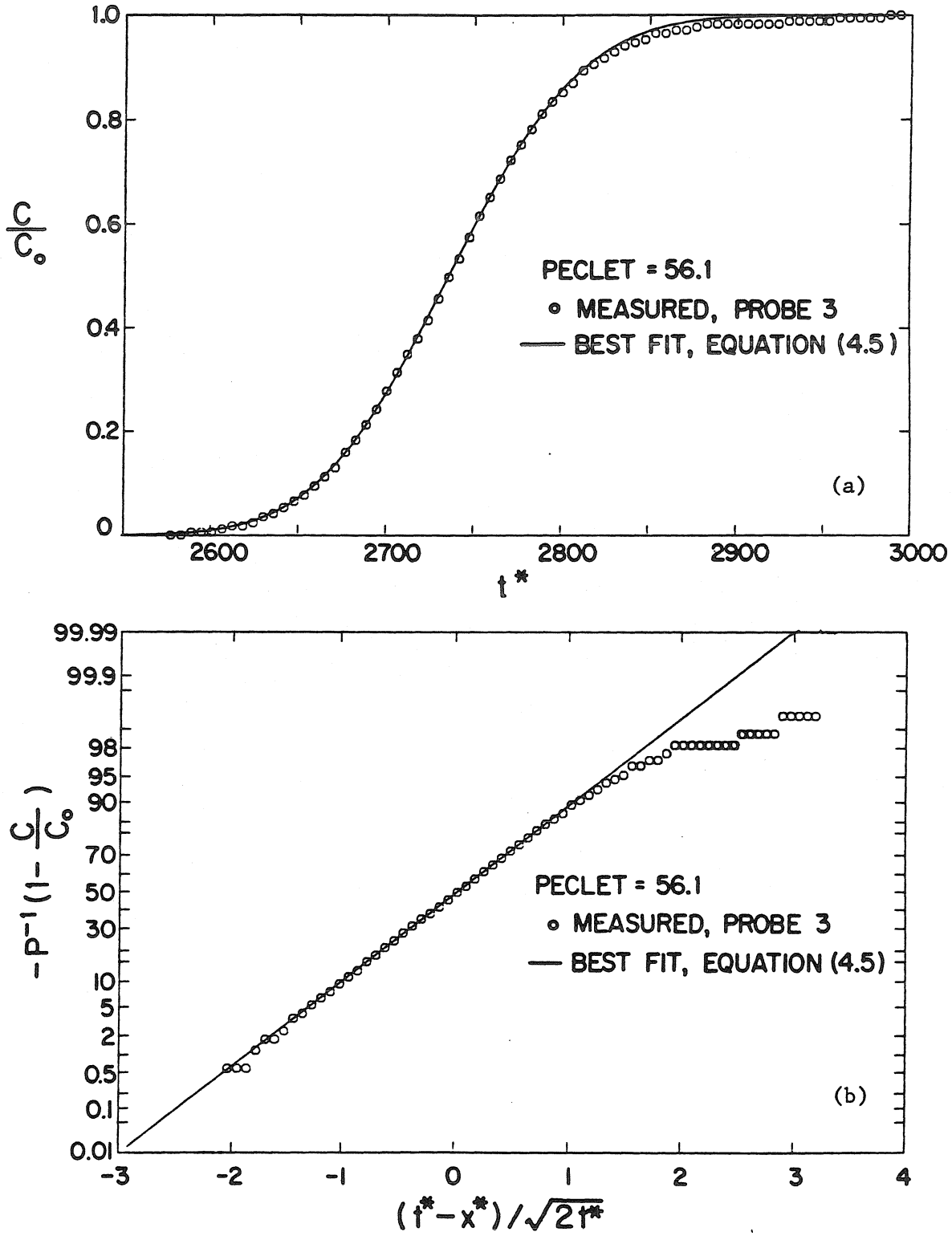

FIGURE 4.18

Breakthrough Curve, Uniform Medium
(Pe = 56.1, Probe 3)

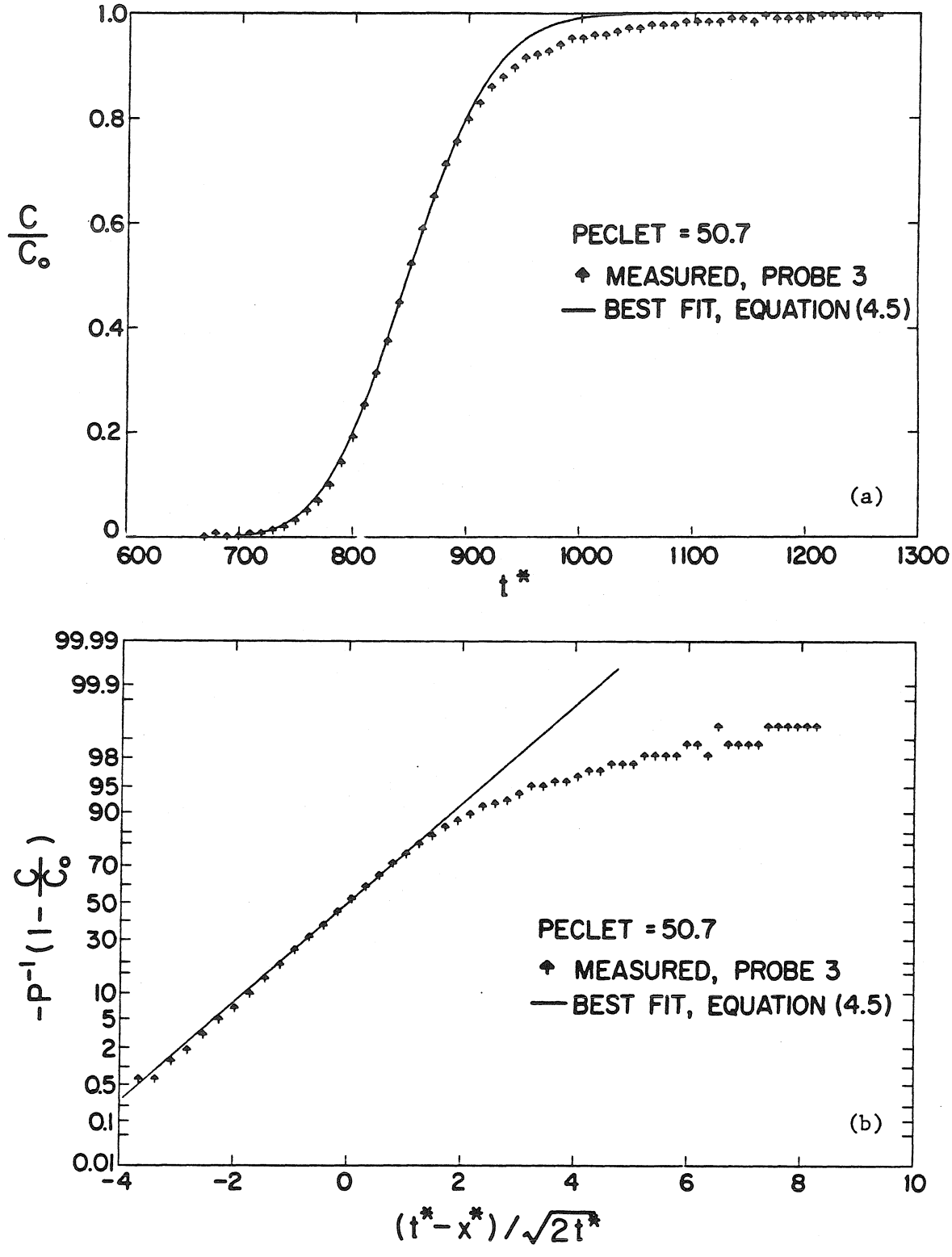

FIGURE 4.19

Breakthrough Curve, Nonuniform Medium
(Pe = 50.7, Probe 3)

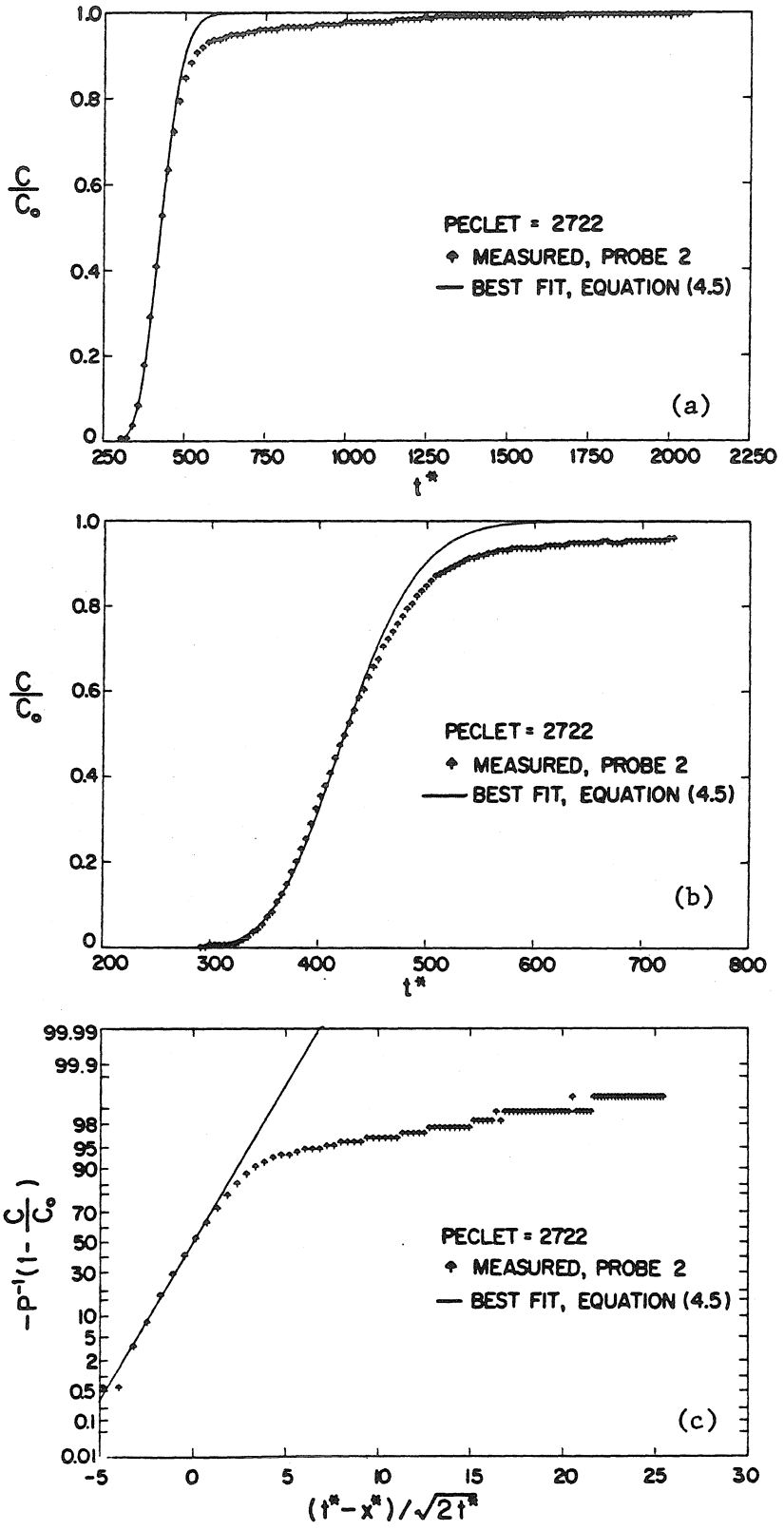

FIGURE 4.20

Breakthrough Curve, Nonuniform Medium
(Pe = 2722, Probe 2)

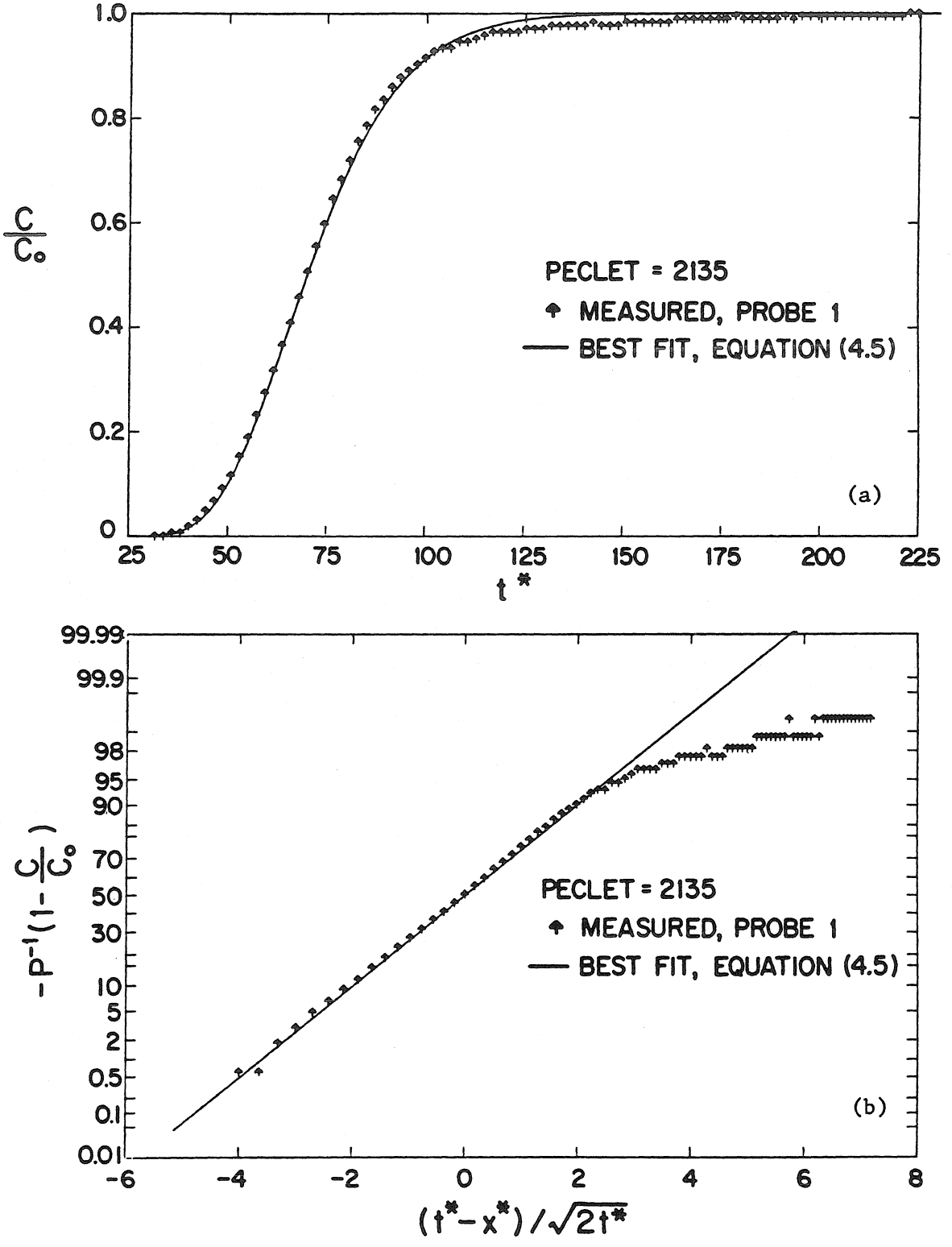

FIGURE 4.21

Breakthrough Curve, Nonuniform Medium
(Pe = 2135, Probe 1)

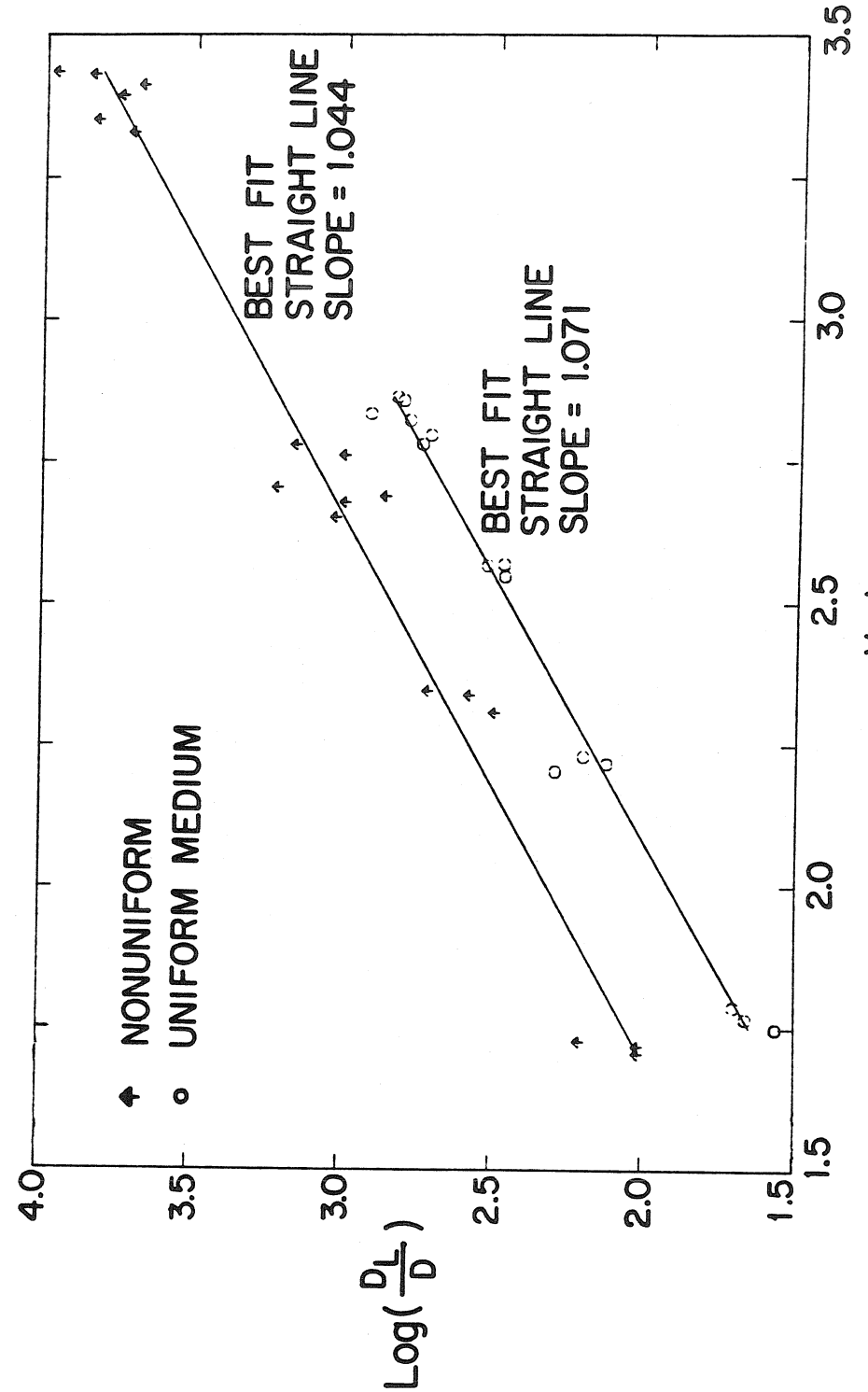

FIGURE 4.22
Measured Longitudinal Dispersion
Coefficients Versus Peclet Number

Table 4.5
Longitudinal Dispersion Data

Uniform Medium			Nonuniform Medium		
Peclet Number ($V_s d_g/D$)	Longitudinal Dispersion (D_L/D)	Probe #	Peclet Number ($V_s d_g/D$)	Longitudinal Dispersion (D_L/D)	Probe #
56.1	36.3	3	50.7	103.	3
58.4	45.6	2	52.3	103.	1
61.3	50.1	1	53.3	161.	2
160.	197.	1	203.	313.	1
165.	133.	3	218.	379.	3
170.	159.	2	222.	519.	2
353.	293.	3	449.	1060.	1
369.	334.	2	477.	988.	3
371.	295.	1	489.	727.	2
604.	553.	1	507.	1660.	2
627.	519.	1	578.	993.	3
667.	609.	3	603.	1440.	2
685.	821.	2	2135.	5090.	1
723.	639.	2	2249.	6690.	1
733.	671.	3	2477.	5550.	3
			2583.	4750.	3
			2697.	6910.	2
			2722.	9170.	2

$D = 1.545 \times 10^{-3}$ mm^2/sec

$\nu = 1.010$ mm^2/sec

length scale chosen for calculating the Peclet number. The geometric mean grain size is chosen here because it is a commonly used length scale for describing sand. If we use d_{80} (the 80^{th} percentile grain size on Figure 4.9) as the length scale, the nonuniform medium dispersion data will fall onto the uniform medium curve in Figure 4.22. However, d_{80} is not necessarily a "similarity" length scale which will cause longitudinal dispersion data for any porous medium to collapse onto the same line. For example, consider two porous media with the same value of d_{80}. If the two grain size distributions have different slopes or entirely different shapes, the dispersion coefficients may be different. In general, the longitudinal dispersion is dependent on the variance and higher moments of the grain size distribution as well as the pore size distribution.

The dispersion coefficient is quite sensitive to changes in the shape of the breakthrough curve. As seen in equation (4.5), the dispersion coefficient is proportional to the square of the slope of the linear regression line. This doubles the effects of errors in the slope on the dispersion coefficient. The presence of the breakthrough curve tail is another source of error for estimating a "pure" advection-diffusion dispersion coefficient from the experimental data. An additional source of error is longitudinal variations in the packing. While the media used here are ideally homogeneous in the macroscopic sense, the results for permeability do show some macroscopic variations along the column. These problems are the most likely sources of the scatter in Figure 4.22.

CHAPTER 5

A COMPARISON OF MODEL CALCULATIONS AND EXPERIMENTAL RESULTS

As discussed in Chapter 3, the random capillary tube network model cannot predict the permeability of a nonuniform porous medium based on measurable structural features of the medium. The hypothesis suggested in Chapter 3 is that "network" effects on the pressure gradient tend to even out flux rates through pores of different sizes. Although the model is not suitable to predict permeability, it is still valuable as a dispersion model. The permeability model can be used to set the connectivity of the unit cell (see Chapter 3) by comparison with experimental data for the permeability. Alternatively, some other permeability model could be used which is able to predict permeability from structural features. The limited experimental data given in Chapter 4 support equation (3.11) as a permeability formula, although there is no theoretical support for this relation. The approach used here is to match the experimental results for permeability with the permeability model by adjusting the junction connectivity. Once the junction connectivity is set, the dispersion model is capable of predicting the coefficient of longitudinal dispersion based on structural features of the medium.

5.1 Permeability Calculations; Determining Junction Connectivity

Permeability calculations using equation (3.15) were carried out with various junction connectivities in an attempt to match the measured permeabilities. These calculations were carried out using the

Monte Carlo integration technique described in Section 3.5. The pore size distribution used for the calculations is shown in Figure 4.12. Although the same number of pores leading to and from a junction are required for a given unit cell (see Figure 3.2), it is possible to have a continuous range of junction connectivity for the network. This is accomplished by using the two nearest even connectivities, say C1 and C2, in proportion α, such that the connectivity for the network, C, is,

$$C = \alpha C1 + (1-\alpha)C2$$

Table 5.1 shows the computed and measured permeabilities using the "best fit" junction connectivity, C = 16. This parameter was set primarily to adjust the calculated permeability of the nonuniform medium, since the uniform medium was fairly insensitive to the junction connectivity parameter. Table 5.1 also shows the permeability calculations when network effects are ignored ($C \to \infty$). As expected, the permeability of the nonuniform medium is significantly higher when the network effects are not taken into account. Convergence of the Monte Carlo integration scheme for the nonuniform medium is slower than for the uniform medium, as shown in Figures 5.1 and 5.2. The nonuniform medium required 400,000 iterations (unit cells), while the uniform medium permeability was calculated using 100,000 iterations to get within $\pm$1% of the final asymptotic value. Permeability as computed from equation (3.11) is seen in Table 5.1 to do reasonably well (within 15%) for both the uniform and nonuniform medium. The Haring and

Table 5.1

Measured and Calculated Permeabilities

	Uniform Medium [a] (10^{-5} mm^2)	Nonuniform Medium [b] (10^{-5} mm^2)
Measured	5.55	5.94
Calculated (C = 16) (equation (3.15))	5.94	5.64
Calculated (C $\rightarrow \infty$) (equation (3.15))	6.29	16.0
Calculated (equation (3.11))	6.18	6.71
Calculated (equation (3.7))	5.02	3.31

(a) d_g = 0.382 mm σ_g = 1.15 (see Table 4.1)

(b) d_g = 1.26 mm σ_g = 2.93 (see Table 4.1)

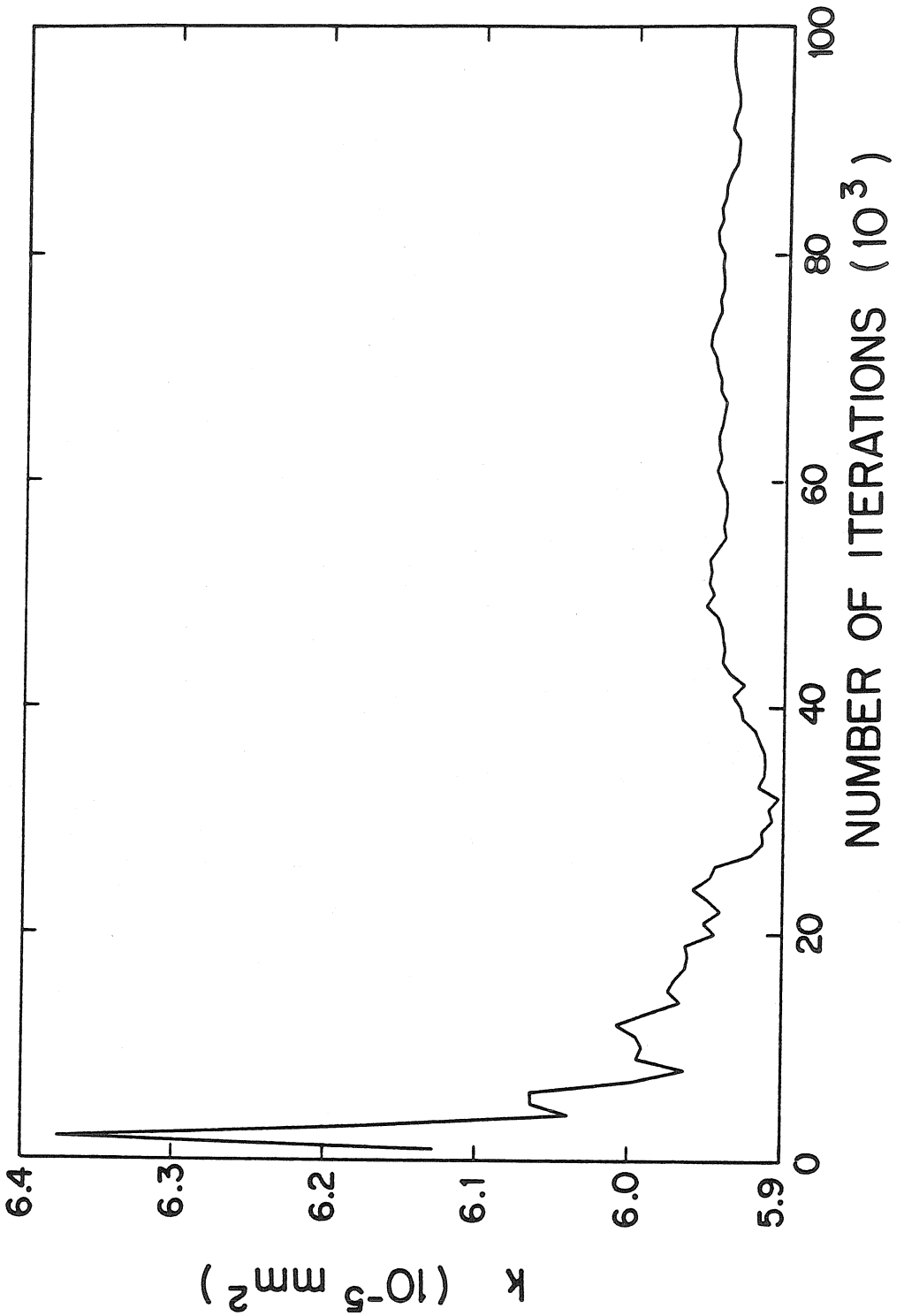

FIGURE 5.1

Monte Carlo Convergence for the Calculation of Permeability in the Uniform Medium (Equation (3.15))

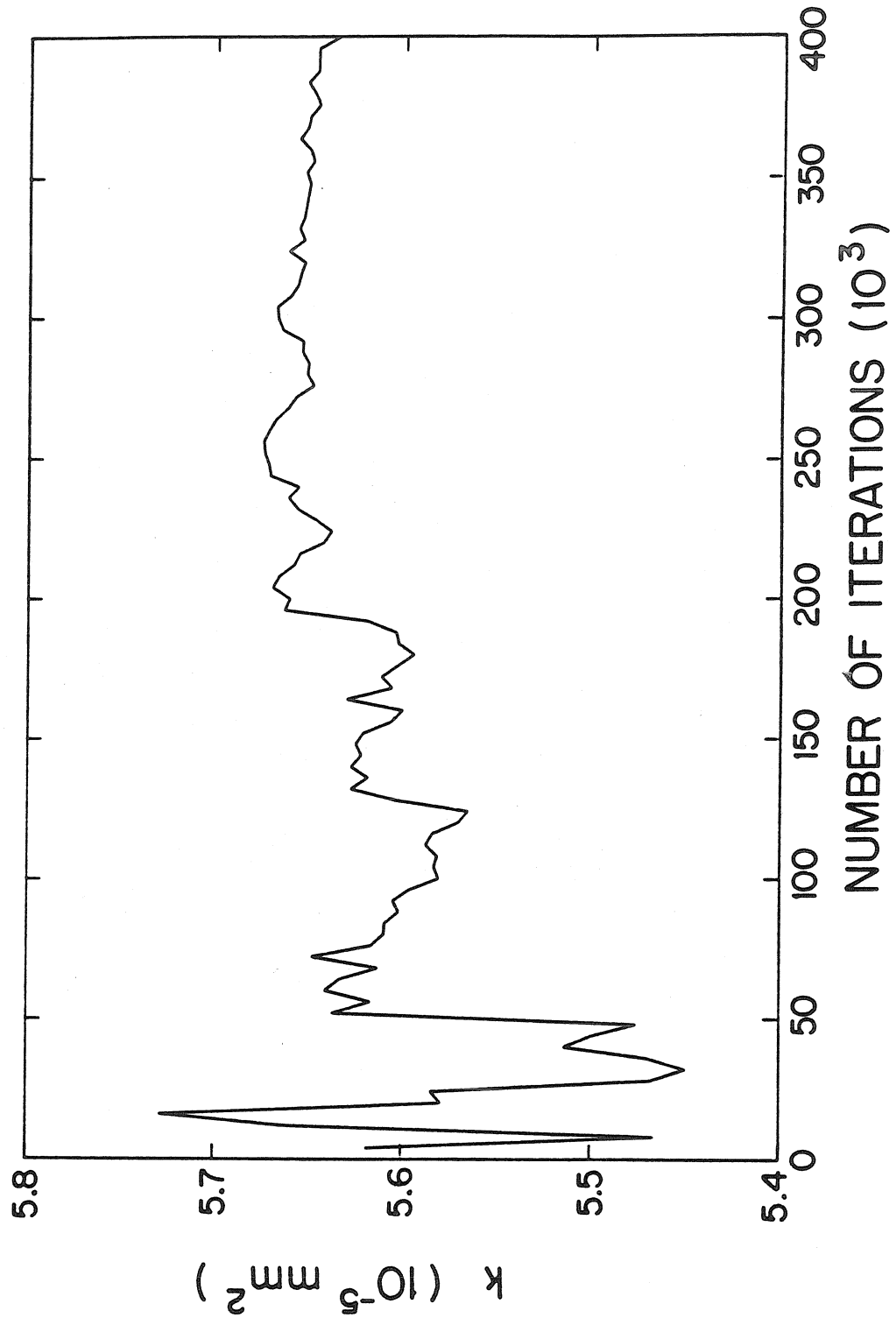

FIGURE 5.2

Monte Carlo Convergence for the Calculation of Permeability in the Nonuniform Medium (Equation (3.15))

Greenkorn (1970) permeability model, generalized for an arbitrary pore radius distribution in equation (3.7), is found to do well for the uniform medium, but is significantly low (44%) compared to the measured value for the nonuniform medium.

5.2 Calculation of the Longitudinal Dispersion Coefficient

With the junction connectivity set (equal to 16 for both cases), it is possible to make dispersion calculations to compare with measured results. Table 5.2 summarizes the computed variances which contribute to the longitudinal dispersion (see equation (3.44) and Table 3.2). If longitudinal dispersion were purely hydrodynamic, we would expect the longitudinal dispersion coefficient to go like $D_L \sim V_s d_g$. Thus any variations in the dimensionless group $D_L/V_s d_g$ with Peclet number indicates the effect of molecular diffusion on the dispersion process. Table 5.2 shows that variations in $D_L/V_s d_g$ versus Peclet number are largely due to differences in the mean-square residence time for a single step. The table also shows that the main difference between dispersion in uniform and nonuniform media is the effect on the mean-square residence time, which is due to the different pore length and pore radius distributions of the two media. The theory presented in Section 3.3 requires that $\overline{x^*}_s = \overline{t^*}_s$; $\overline{x^*_s}$ and $\overline{t^*_s}$ are shown in Table 5.2. This requirement is met with two place accuracy for all runs except the low Peclet calculation for the nonuniform medium. The deviation of $\overline{t^*_s}$ from $\overline{x^*_s}$ indicates that molecular diffusion is playing a more significant role in the theoretical calculations.

Table 5.2
Computed Results from the Dispersion Model

UNIFORM MEDIUM

Peclet #	$D_L/V_s d_g$	$\overline{x_s^{*2}}$	$\overline{t_s^{*2}}$	$\overline{x_s^* t_s^*}$	$\overline{x_s^*}$	$\overline{t_s^*}$
58.0	0.788	0.470	1.17	0.315	0.644	0.641
165.	1.00	0.470	1.45	0.315	0.644	0.644
365.	1.17	0.470	1.67	0.315	0.644	0.645
670.	1.30	0.470	1.84	0.315	0.644	0.646

NONUNIFORM MEDIUM

Peclet #	$D_L/V_s d_g$	$\overline{x_s^{*2}}$	$\overline{t_s^{*2}}$	$\overline{x_s^* t_s^*}$	$\overline{x_s^*}$	$\overline{t_s^*}$
52.0	1.30	0.225	1.01	0.150	0.373	0.358
215.	2.14	0.225	1.66	0.151	0.373	0.370
525.	2.80	0.225	2.16	0.151	0.373	0.373
2450.	3.99	0.225	3.07	0.152	0.373	0.375

UNIFORM MEDIUM

Peclet #	$\dfrac{\overline{x_s^{*2}} - 2\overline{x_s^* t_s^*}}{2\overline{t_s^*}}$	$\dfrac{\overline{t_s^{*2}}}{2\overline{t_s^*}}$
58.0	-0.125	0.913
165.	-0.124	1.13
365.	-0.124	1.30
670.	-0.124	1.42

NONUNIFORM MEDIUM

Peclet #	$\dfrac{\overline{x_s^{*2}} - 2\overline{x_s^* t_s^*}}{2\overline{t_s^*}}$	$\dfrac{\overline{t_s^{*2}}}{2\overline{t_s^*}}$
52.0	-0.105	1.41
215.	-0.104	2.24
525.	-0.103	2.90
2450.	-0.105	4.09

Definitions:

$$x^* = x_s/d_g \qquad t_s^* = V_s t_s/d_g \qquad D_L/V_s d_g = (\overline{x_s^{*2}} + \overline{t_s^{*2}} - 2\overline{x_s^* t_s^*})/2\overline{t_s^*}$$

Figure 5.3 shows the calculated longitudinal dispersion coefficients as compared to the measured values. Agreement is acceptable (within 35%) for the uniform medium, as expected since Saffman's (1959) original analysis for a uniform medium is seen (Figure 2.5) to predict the longitudinal dispersion coefficient within 50% when Pe > 10. The agreement between calculations and experiments for the nonuniform medium is not as good, having about 70% discrepancy with measured results at the high and low Peclet number extremes. As previously noted, the low Peclet number result for the nonuniform medium shows a 3% deviation of $\overline{t_s^*}$ from $\overline{x_s^*}$, while the other cases show differences less than 1%. This deviation indicates that a significant fraction of pores are diffusion limited, which are treated only approximately in the theory. When molecular diffusion becomes important, we expect the theoretical calculations to fall below the measured values (as the original theoretical predictions do when Pe < 10 in Figure 2.5).

Table 5.3 shows results of the calculations for longitudinal dispersion and the estimate of the required number of steps such that the asymptotic dispersion coefficient should apply (equation (3.28)). Note that this condition should be considered sufficient, but not necessary, for the asymptotic dispersion coefficient to apply. The average number of steps to each probe for both the uniform and nonuniform medium are given in Table 5.4. These are calculated by dividing the total (nondimensional) distance to each probe by the average longitudinal step length, $\overline{x_s^*}$, given in Table 5.2. Comparison

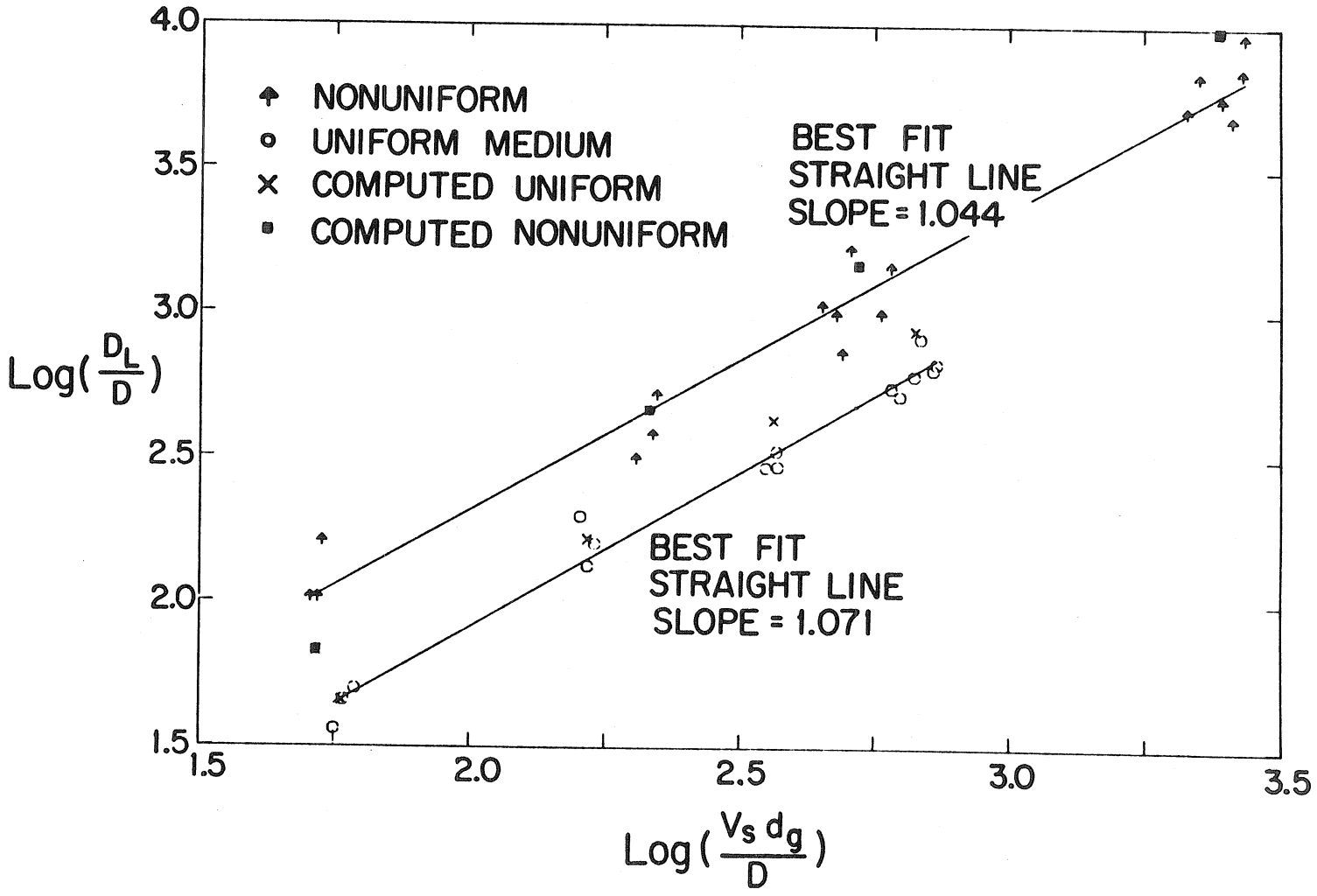

FIGURE 5.3

Longitudinal Dispersion Versus Peclet Number;
Measured and Computed Values
(- Best Fit of Measurements)

Table 5.3
Computed Results for the Average Number of Steps
Required before the Asymptotic Theory is Valid

UNIFORM MEDIUM

Peclet #	D_L/D	n
58.0	45.5	80
165.	165.	902
365.	427.	4880
670.	873.	17300

NONUNIFORM MEDIUM

Peclet #	D_L/D	n
52.0	67.6	688
215.	460.	25400
525.	1470.	187000
2450.	9770.	2660000

Table 5.4
Average Number of Steps to Each Probe

UNIFORM MEDIUM

Probe	n
1	350
2	2100
3	4200

NONUNIFORM MEDIUM

Probe	n
1	170
2	1000
3	2100

of the required number of steps for the asymptotic dispersion coefficient to apply to the actual average number of steps downstream to each of the probes indicates that the experimental measurements have not been made sufficiently far downstream to reach this criterion for the asymptotic condition, particularly for the higher Peclet number experiments. This fact may explain the increase in the calculated dispersion coefficient compared to measured values at the higher Peclet numbers. It is difficult, however, to determine the necessary downstream distance for the longitudinal dispersion coefficient to approach the asymptotic value. This difficulty centers on the inability to say what difference is expected between the asymptotic dispersion coefficient and measured dispersion coefficient when the asymptotic distance requirement is not met. In the Saffman (1959) model for uniform media, the relation derived for the "near-field" longitudinal dispersion coefficient shows a logarithmic growth in time. This type of slow variation in the dispersion coefficient would suggest that the measured dispersion coefficients will be close to the asymptotic value long before the asymptotic distance is reached.

The discrepancy found at the higher Peclet numbers in Figure 5.3 was not expected, based on the experimental results and theoretical predictions shown in Figure 2.5. In this figure, the asymptotic dispersion coefficient compares well over a range of Peclet numbers from 10 to 10^6, although the typical experiment (using water) will lie outside Darcy's regime when $Pe > 10^4$. Based on equation (3.23), the required number of steps at Peclet = 10^3 is $n > 3.4 \times 10^4$ or a distance

of 23m for a 1mm grain diameter. At a Peclet number of 10^4, the downstream distance required for the asymptotic limit to apply is 1.7km, when the grain size is 1mm. It is quite obvious that the experiments at the higher Peclet numbers do not satisfy the asymptotic distance requirement.

Typical plots of the Monte Carlo convergence for the dispersion integral are shown in Figures 5.4 and 5.5. As with the permeability, a greater number of iterations were required for the nonuniform medium to attain acceptable convergence. The same number of iterations for both media were used as for the permeability calculations. Convergence also was slower for the high Peclet number calculations. This is probably due to the greater spread in residence times under high Peclet conditions, which results in a larger Monte Carlo integration error (Hammersley and Handscomb, 1979).

5.3 Tailing in the Breakthrough Curves

As mentioned in Chapter 4, the experimental breakthrough curves show highly asymmetrical shapes over the last 10 to 20 percent of the breakthrough (i.e., C/C_0 = 0.8 to 1.0). Figures 4.14 - 4.21 demonstrate that the "tail" is much more pronounced for high Peclet number flows and tends to disappear at lower Peclet number flows. This phenomenon is not a result of the "near field" in the sense that the downstream distance is insufficient to apply the asymptotic theory presented in Chapter 3. Proof of this statement is based on the observations that "tailing" at the first probe is always much less than at the second or

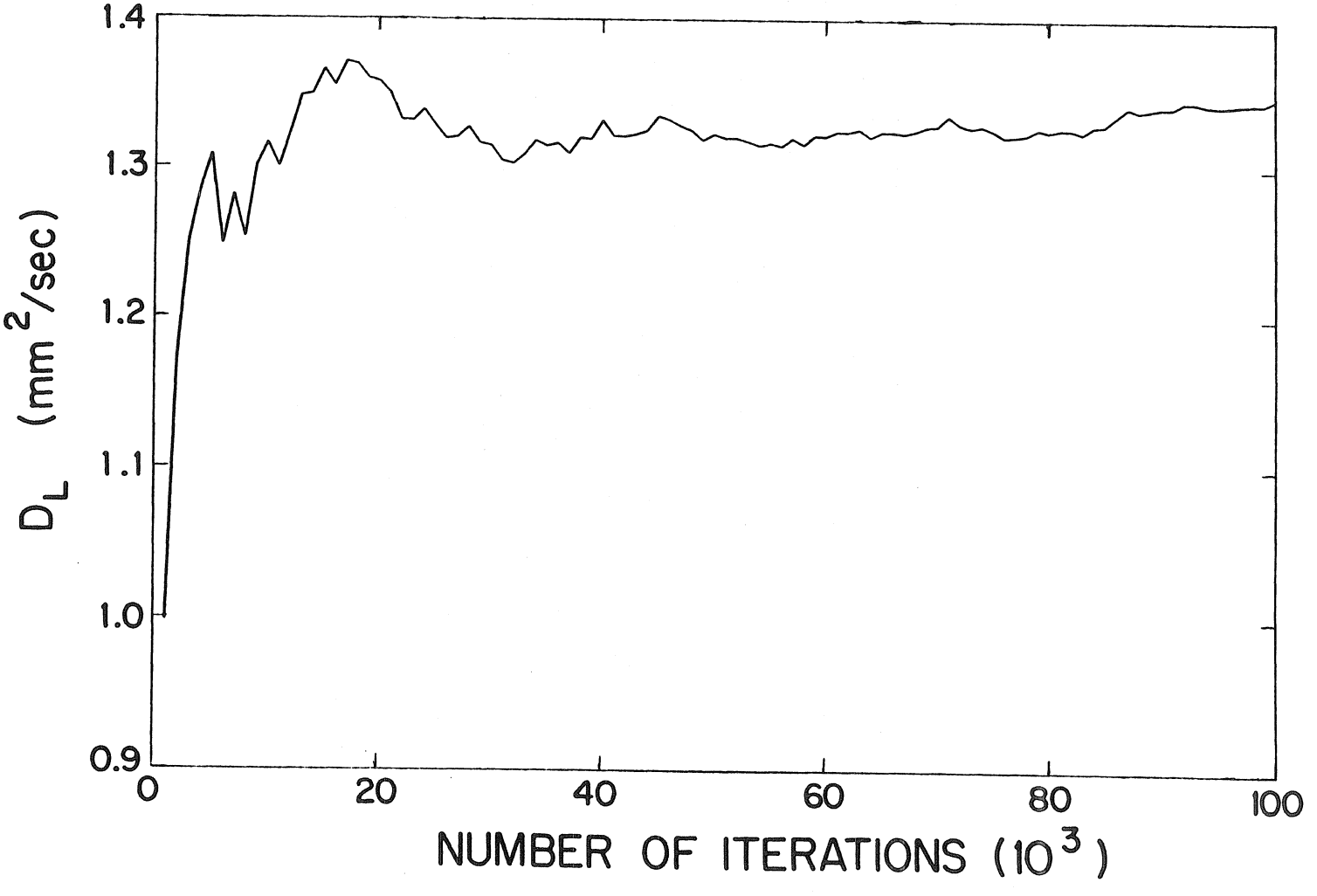

FIGURE 5.4

Monte Carlo Convergence for the Calculation of the Longitudinal Dispersion Coefficient in the Uniform Medium; Peclet = 670
(Equation (3.44))

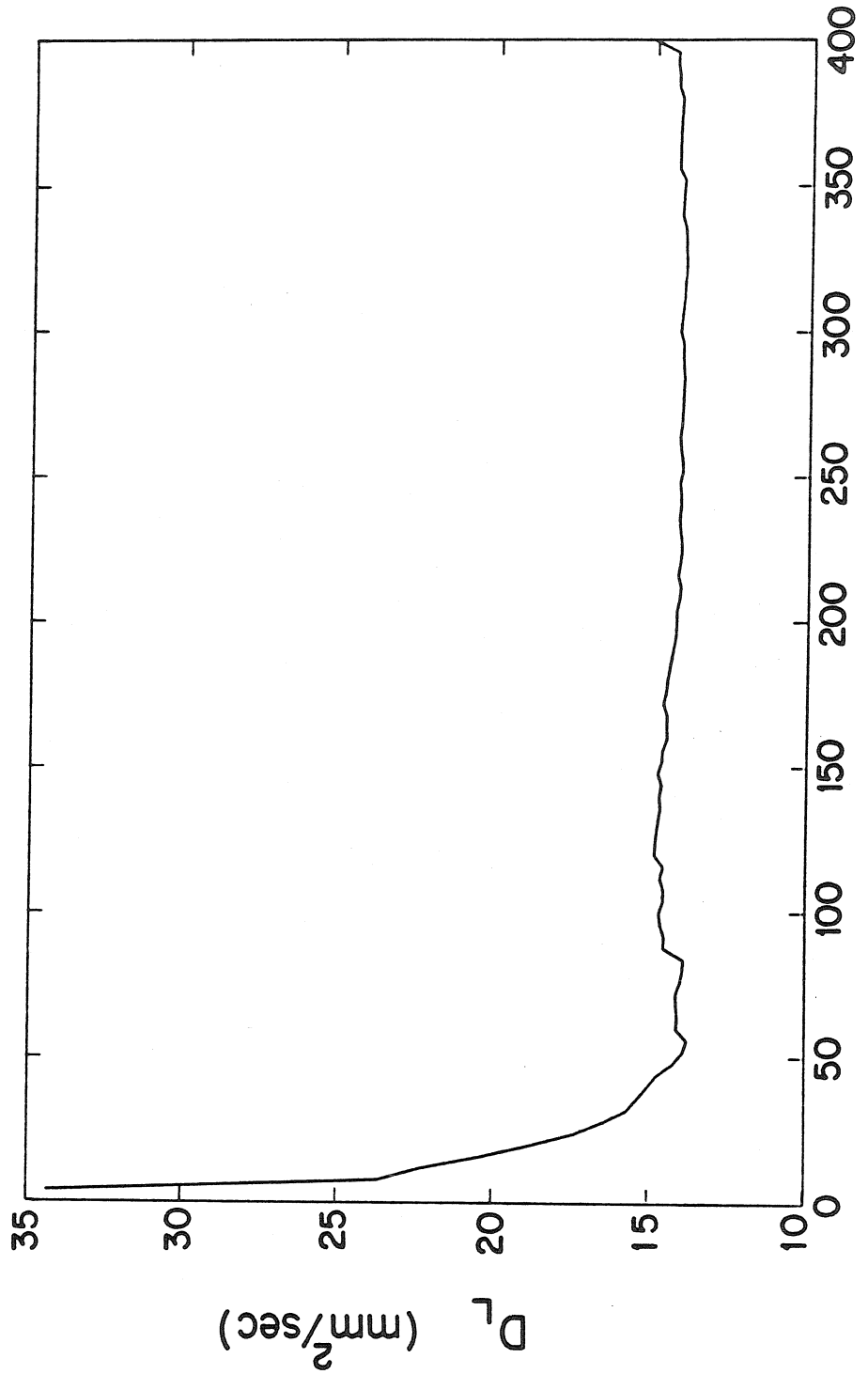

FIGURE 5.5

Monte Carlo Convergence for the Calculation of the Longitudinal Dispersion Coefficient in the Nonuniform Medium; Peclet = 2450 (Equation (3.44))

third probes and the simulations discussed in Section 3.3 did not demonstrate any tail in the near field.

A possible qualitative explanation of the tailing phenomenon can be made in terms of diffusion-limited mass transfer (in macroscale). Consider a packing of nonuniform grains which is nonideal in the sense that segregation of particle sizes occurs over sufficiently large length scales such that the medium is nonhomogeneous. Some spatial variations in permeability, porosity, etc. are expected. Regions of very fine material may form which have extremely low permeability. These low permeability regions may have substantial (molecular) diffusional mass transfer during a breakthrough experiment. Thus, even during conditions which are high Peclet flows based on <u>average</u> length and velocity scales, there may be regions in which the mass transfer occurs under local low Peclet conditions.

Taking this to the extreme, we might consider the medium to consist of separate advective dominated and diffusion dominated (microporous) regions which are allowed to exchange solutes through molecular diffusion. A model of such a system was proposed by Passioura (1971), in which he determines the effects of a bidisperse pore system on overall longitudinal mass transfer. The results of this analysis show that, after sufficient time, the longitudinal mass transfer may be described by advective-diffusion theory, where the longitudinal dispersion coefficient is given by (Passioura, 1971)

$$K_L = D_L + \frac{\sigma_m}{\sigma_T} \frac{V_s^2 \ell_m^2}{15 D_m}$$

where σ_T = total porosity

σ_m = porosity of micropore regions

ℓ_m = length scale for the microporous regions

D_m = overall coefficient of molecular diffusion in the micropore regions

D_L = longitudinal dispersion coefficient in the porous medium without microporous regions

K_L = longitudinal dispersion coefficient for macropore/micropore system

The dispersion coefficient is the sum of direct molecular diffusion, hydrodynamic effects, and the diffusional exchange between flowing and stagnant regions in the bidisperse pore system. If the time of motion is not sufficient, the mass transfer process is not described by advection-diffusion theory. The required time is estimated by (Passioura, 1971)

$$t >> 0.1 \frac{\sigma_T}{\sigma_m} \frac{\ell_m^2}{D_m}$$

Systems which display the tailing phenomenon are also known to show an early initial breakthrough, in which the 50% relative concentration point penetrates the column before the entire resident fluid has been displaced from the column. Early breakthrough is a result of the advecting pore regions in the column being displaced from the column before the diffusion-dominated regions have enough time to undergo any significant mass transfer. This may be detected through the difference in the total and effective porosities. Early

There is no page 152 in this manuscript

breakthrough will give a lower effective porosity as compared to the total porosity. As shown in Table 4.4, no significant differences are detected between the two porosity measurements. A possible explanation for the absence of an early breakthrough may be that the amount of diffusion-limited pore space in the column is small compared to the total pore space in the column.

Now if the slope of D_L/D versus Peclet number is one to one on the log-log plot (Figure 5.3), then the dimensionless group $D_L/V_s d_g$ is constant, i.e., independent of the Peclet number. From the slopes quoted in Figure 5.3, we see that the longitudinal dispersion coefficient is practically independent of the value of the molecular diffusion coefficient (i.e., $D_L \propto D^{-0.044}$ for the nonuniform medium). Consider the advective diffusion equation nondimensionalized by

$$t^* = V_s t/d_g \qquad x^* = x/d_g$$

$$\frac{\partial C}{\partial t^*} + \frac{\partial C}{\partial x^*} = K \frac{\partial^2 C}{\partial x^{*2}}$$

where K is a constant. In this case, we would expect all breakthrough curves at a given location to lie on top of one another, regardless of the Peclet number. Figure 5.6 shows breakthrough curves at the third (last) probe in the nonuniform medium at three Peclet numbers. The majority of the breakthrough for the three curves does lie close to a single line, but the tail shows significantly different behavior as a function of the Peclet number. The tail is longer for higher Peclet

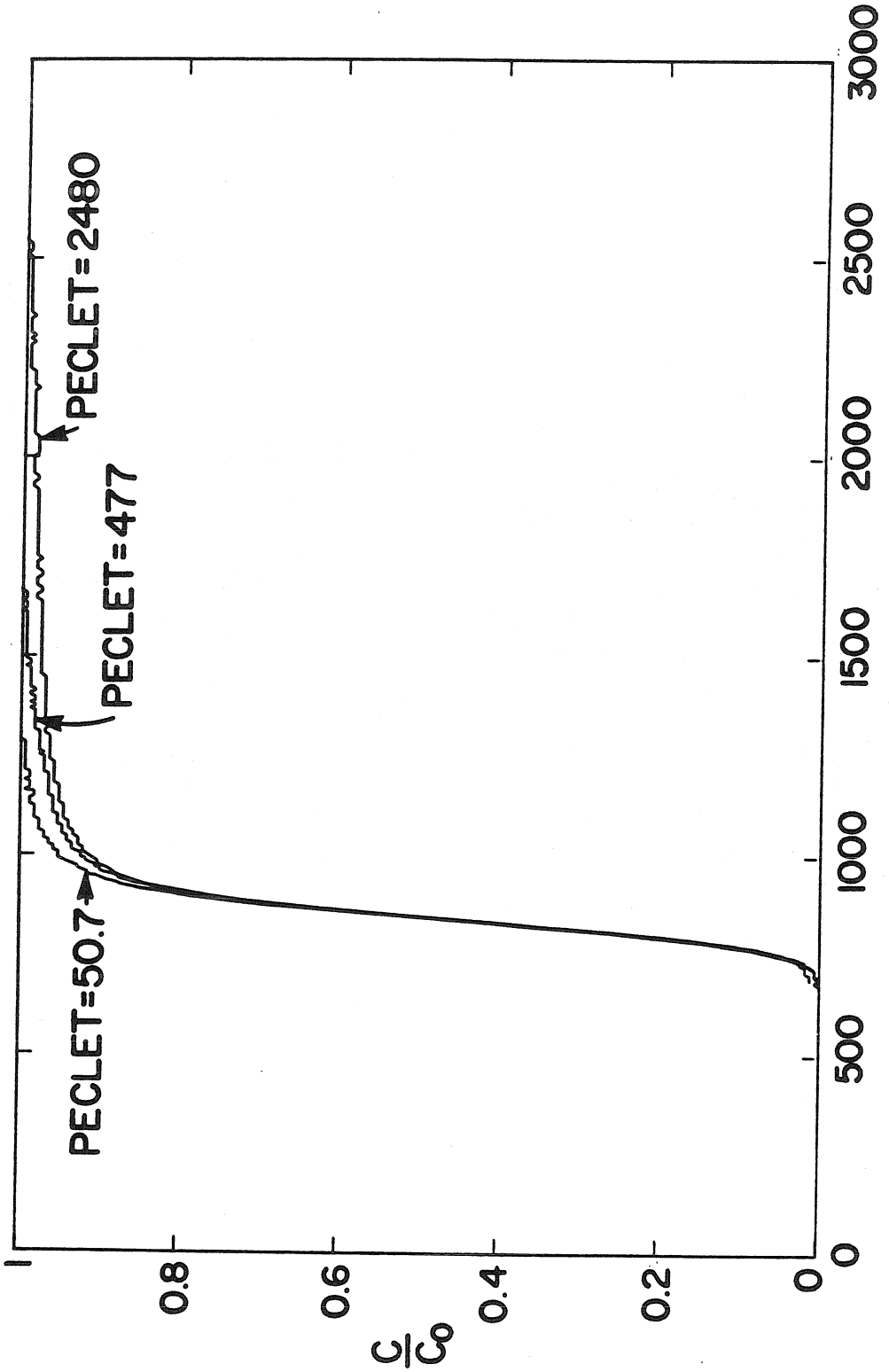

FIGURE 5.6
Dependence of the Tail of Normalized Breakthrough Curve on Peclet Number for Nonuniform Media (Probe 3)

number flows since the advection time scale for mass transfer becomes shorter while the diffusion time scale remains constant.

The conclusions are summarized in the next chapter, and suggestions for future work are presented.

CHAPTER 6

SUMMARY AND CONCLUSIONS; SUGGESTIONS FOR FUTURE RESEARCH

Longitudinal dispersion in flow through nonuniform porous media has been studied theoretically and experimentally. An analysis to include the effect of nonuniform grain size was developed from Saffman's (1959) random capillary tube model for passive solutes flowing through homogeneous, isotropic, unconsolidated porous materials. Miscible displacement experiments were carried out on two sands in order to test the theoretical model. The experiments also demonstrated asymmetrical breakthrough curves which could not be described by advection-diffusion theory.

6.1 Summary and Conclusions for the Investigation of Longitudinal Dispersion

The theoretical model of longitudinal dispersion developed here may be used to predict the asymptotic longitudinal dispersion coefficient based on the measured permeability, pore radius distribution, grain size distribution, and Peclet number of the flow ($V_s d_g/D$). No free parameters are used to fit the calculated longitudinal dispersion coefficients with the measured values. Therefore, this dispersion theory is based on measurable structural features and the permeability. The permeability is required to fix a parameter; the junction connectivity, to obtain a proper flow distribution through the various sized pores. The following features have been added to the Saffman (1959) model:

1. Measured grain size distributions and pore radius distributions are used directly in the theoretical model.

2. The area-weighted grain size distribution is proposed to describe the frequency of interaction of grains with pores in nonuniform porous media. A simple packing model is used to define the pore length as the cube root of the three interparticle distances between grains forming the pore.

3. Shear dispersion within individual capillary tubes is not included in the model. Comparison of previous theoretical work with experimental measurements (see Figure 2.5) and using the analysis carried out in Appendix C in the capillary tube network model indicate that this mechanism is generally negligible.

4. A Monte Carlo integration technique is introduced to allow greater flexibility in modeling the physical system.

Miscible displacement experiments were carried out on two nonuniform porous media for the purpose of determining the permeability and longitudinal dispersion coefficient. One of the materials is a medium grade sand with a narrow grain size distribution (geometric mean d_g = 0.382mm , geometric standard deviation σ_g = 1.15) and the other is a gravelly sand with a wide grain size distribution (d_g = 1.26mm, σ_g = 2.93). The following conclusions may be made concerning the theoretical model and experimental results:

1. Longitudinal dispersion in nonuniform media is found to be roughly 0.4 order of magnitude greater than in uniform media when compared using a Peclet number based on the geometric mean grain diameter. For the experiments done here, a Peclet number based on the d_{80} grain diameter will cause the longitudinal dispersion data (see Figure 4.22) for the uniform and nonuniform media to collapse to a single curve.

2. Comparison of theoretical predictions and measurements for the longitudinal dispersion coefficient show agreement within a factor of 1.35 for the "uniform" medium ($\sigma_g = 1.15$) and within a factor of 1.7 for the highly nonuniform medium ($\sigma_g = 2.93$). The larger discrepancies for the nonuniform medium occur at the Peclet number extremes of the experiments. The discrepancy at high Peclet numbers is thought to be due to the fact that the experimentally determined dispersion coefficients were measured in the "near-field" before the asymptotic dispersion theory is considered fully valid. The discrepancy at low Peclet numbers is a result of the limitation of the theoretical model to high Peclet number flows. The decision as to when the flow may be considered high Peclet number must be made on an individual basis from a comparison of $\overline{x_s^*}$ and $\overline{t_s^*}$ in the theoretical calculations. When $\overline{x_s^*}$ deviates from $\overline{t_s^*}$ by more than 1%, the flow should not be considered a high Peclet number flow. At intermediate Peclet numbers, theoretical predictions lie within a factor of 1.35 of the measured results.

3. The mean-square residence time for a solute particle to pass through a pore is the critical component in the dispersion integral, containing the true Peclet number dependence of the asymptotic

longitudinal dispersion coefficient. The mean-square residence time is the principal component which causes greater dispersion in the nonuniform medium as compared to the uniform medium.

4. Observations of breakthrough curves in both materials studied indicate that highly asymmetric tails are a common feature of the miscible displacement process in natural materials. The tails are thought to be a result of local heterogeneities in the packing which produce low-permeability, diffusion-limited regions. Greater tailing is observed in the highly nonuniform medium, presumably due to greater packing heterogeneities. One hypothesis for the tailing mechanism is that material in diffusion-limited regions slowly diffuses into advection dominated regions, causing the breakthrough curve tail to be extended. The Peclet number dependence of the shape of the breakthrough tail is demonstrated in Figure 5.6, where time is nondimensionalized by an advection time scale. This finding adds support to the hypothesis that the tailing is a result of diffusion-limited mass transfer.

6.2 Summary of the Permeability Investigation

The permeability relationship (equation (3.15)) derived for a nonuniform medium incorporates a "unit cell" or manifold to represent each pore for the calculation of the pressure gradient over each pore in the network. The inclusion of this feature in the model was necessary to take into account network effects on the pressure gradient. The artificial nature of the unit-cell concept, however,

makes it impossible to calculate the permeability based on measurable structural features alone. The permeability model contains a free parameter, the junction connectivity, which is established empirically. Thus the permeability model trades one parameter (the permeability) for another (the junction connectivity). The following conclusions on permeability modeling can be made based on the theoretical development and experimental results:

1. Network effects in flow through porous media are important for determining the permeability. Theoretical models which use the pore radius distribution but do not take network effects into account are likely to overpredict the permeability.

2. Due to the network effects, the variance in the pore radius distribution does not have a strong impact on the permeability. The geometric mean pore size, as measured using the capillary drainage technique, may act as an equivalent uniform pore size for predicting permeability.

6.3 Suggestions for Future Research

There are a variety of important areas in need of further research related to transport phenomena in flow through porous media. Some of these topics are suggested by the results given above and some have not been touched upon in this study.

1. While advection-diffusion theory is valid for homogeneous porous materials, the results of this study indicate that perfectly

homogeneous packing is not to be expected in general. The highly extended breakthrough tails found experimentally are thought to be a result of nonideal packing. A quantitative model of this process is needed, since in some cases the residual concentrations in the tail are important. Methods for determining the effective length and volume scales of the diffusion limited regions are needed. Further experiments are needed to test sands having different values of σ_g.

2. Many problems concerning transport phenomena in the natural environment must deal with large-scale, radical heterogeneity in the permeability as well as adsorption and chemical reactions. For regional scale problems, spatial heterogeneity in the permeability dominates the macroscopic dispersion of contaminants. Although there has been a large amount of work on this subject over the past 15 years, there is still no consensus on the best way to deal with the problem. The effects of adsorption, chemical reaction, and biodegradation can also be extremely important.

3. A permeability model is needed for the purposes of understanding transport phenomena based on the grain scale characteristics of the medium. The results of this research indicate a deterministic network model may be appropriate. On the other hand, empirical observations may show equation (3.11) is satisfactory. A theoretical basis for the permeability in terms of a capillary tube network model would provide a better understanding of the flow distribution in nonuniform porous media.

4. Experimental and theoretical work on lateral dispersion is needed. Data on lateral dispersion in nonuniform porous media are extremely limited. Lateral dispersion may be important in determining the longitudinal dispersion rate through layered media. Also, viscous fingering during immiscible displacement may be sensitive to lateral dispersion.

5. The use of network models (deterministic and random) should be considered for modeling deep bed filtration processes. Most of the work to date has concentrated on single "unit collector" models which ignore the network as a whole.

6. The effects of density stratification and viscosity differences on mixing are not well understood. Leachate plumes from landfills and gasoline contamination are two common problems strongly influenced by density differences.

REFERENCES

Aris, R. and N. R. Amundson, "Some Remarks on Longitudinal Mixing or Diffusion in Fixed Beds," AIChE Journal, Vol. 3, No. 2, June 1957, pp. 280-282.

Bear, J., Dynamics of Fluids in Porous Media, American Elsevier, New York, New York, 1972, 764 pp.

Bredehoeft, J. D. and G. F. Pinder, "Mass Transport in Flowing Groundwater," Water Resources Research, Vol. 9, No. 1, February, 1973, pp. 194-210.

Carberry, J. J. and R. H. Bretton, "Axial Dispersion of Mass in Flow Through Fixed Beds," AIChE Journal, Vol. 4, No. 3, September 1958, pp. 367-375.

Carman, P. C., "Fluid Flow Through Granular Beds," Transactions, Institution of Chemical Engineers, Vol. 15, 1937, pp. 150-166.

Coats, K. H. and B. D. Smith, "Dead End Pore Volume and Dispersion in Porous Media," Society of Petroleum Engineers Journal, Vol. 4, No. 1, March 1964, pp. 73-84.

Cohen, Y. and A. B. Metzner, "Wall effects in Laminar Flow of Fluids through Packed Beds," AIChE Journal, Vol. 27, No. 5 September 1981, pp. 705-715.

Darcy, H., "Les Fontaines Publiques de la Ville de Dijon," Dalmont, Paris, 1856

de Josselin de Jong, G., "Longitudinal and Transverse Diffusion in Granular Deposits," Transactions, American Geophysical Union, Vol. 39, No. 1, February 1958, pp. 67-74.

Dullien F. A. L., Transport Phenomena in Porous Media and Pore Structure, Academic Press, New York, New York, 1979, 396 pp.

Ebach, A. and R. R. White, "Mixing of Fluids Flowing Through Beds of Packed Solids," AIChE Journal, Vol. 4, No. 2, June 1958, pp. 161-169.

Eichenberger, J. R., J. R. Edwards, K. Y. Chen, and R. D. Stephens, "A Case Study of Hazardous Wastes in Class I Landfills," EPA-600/2-78-064, Municipal Environmental Research Laboratory, Office of Research and Development, U.S. Environmental Protection Agency, Cincinnati, Ohio, June 1978, 106 pp.

Fatt, I., "The Network Model of Porous Media, I, II, and III," Petroleum Transactions, AIME, Vol. 207, 1956, pp.144-181.

Fischer, H. B., "Determination of Dispersion Coefficients by the Change of Moment Method," Technical Memorandum 64-6, W. M. Keck Laboratory of Hydraulics and Water Resources, California Institute of Technology, Pasadena, California, June 1964, 22 pp.

Fried, J. J. and M. A. Combarnous, "Dispersion in Porous Media," Advances in Hydroscience, Vol. 7, 1971, pp. 169-282.

Greenkorn, R. A., "Steady Flow Through Porous Media," AIChE Journal, Vol. 27, No. 4, July 1981, pp. 529-545.

Hammersley, J. M. and D. C. Handscomb, Monte Carlo Methods, Chapman and Hall, London, 1979, 178 pp.

Haring, R. E. and R. A. Greenkorn, "A Statistical Model of a Porous Medium with Nonuniform Pores," AIChE Journal, Vol. 16, No. 3, May 1970, pp. 477-483.

Hiby, J. W., "Longitudinal and Transverse Mixing During Single-Phase Flow Through Granular Beds," Interaction Between Fluids and Particles, Institute of Chemical Engineers, London, England, 1963, p. 312.

Hill, R. D., N. B. Shoemaker, R. E. Landreth and C. C. Wiles, "Four Options for Hazardous Waste Disposal," Civil Engineering, American Society of Civil Engineers, Vol. 51, No. 9, September 1981, pp. 82-85

Karger, B. L., L. R. Snyder, and C. Horvath, An Introduction to Separation Science, Wiley Interscience, New York, New York, 1973, 586 pp.

Lepelletier, T. G., "Harbor Oscillations Induced by Nonlinear Transient Long Waves," Ph.D. Thesis, W. M. Keck Laboratory of Hydraulics and Water Resources, California Institute of Technology, Pasadena, California, 1980.

List, E. J. and N. H. Brooks, "Lateral Dispersion in Saturated Porous Media," Journal of Geophysical Research, Vol. 72, No. 10, May 15, 1967, pp. 2531-2541.

Niemann, E. H., "Dispersion During Flow in Non-uniform, Heterogenous Porous Media," M. S. Thesis, Purdue University, June 1969, 91 pp.

Okoye, J. and F. Raichlen, "Description and Operation of Analogue-to-Digital Data Acquisition System," Technical Memorandum 69-9, W. M. Keck Laboratory of Hydraulics and Water Resources, California Institute of Technology, Pasadena, California, 1969, 21 pp.

Orlob, G. T. and G. N. Radhakrishna, "The Effects of Entrapped Gases on the Hydraulic Characteristics of Porous Media," Transactions, American Geophysical Union, Vol. 39, No. 4, August 1958, pp.648-659.

Pakula, R. J. and R. A. Greenkorn, "An Experimental Investigation of a Porous Medium Model with Nonuniform Pores," AIChE Journal, Vol. 17, No. 5, September 1971, pp.1265-1268.

Passioura, J. B., "Hydrodynamic Dispersion in Aggregated Media," Soil Science, Vol. 111, No. 6, June 1971, pp. 339-344.

Perkins, T. K. and O. C. Johnston, "A Review of Diffusion and Dispersion in Porous Media," Society of Petroleum Engineers Journal, Vol. 3, No. 1, March 1963, pp. 70-84.

Pfankuch, H. O., "Contribution a l'Etude des Deplacements de Fluides Miscibles dans un Milieu Poreux," Rev. Inst. Fr. Petrol., Vol. 18, No. 2, 1963, pp. 215-270.

Raimondi, P., G. H. F. Gardner, and C. B. Petrick, "Effect of Pore Structure and Molecular Diffusion on the Mixing of Miscible Liquids Flowing in Porous Media," Preprint 43, Presented at the AIChE- SPE Joint Symposium, San Francisco, California, December 6-9, 1959.

Rifai, M. N. E., W. J. Kaufman, and D. K. Todd, Progress Report No. 2, Sanitary Engineering Research Laboratory, Division of Civil Engineering, University of California, Berkeley, July 1956, 157 pp.

Ripple, C. D., R. V. James, and J. Rubin, "Packing-Induced Radial Particle-Size Segregation: Influence on Hydrodynamic Dispersion and Water Transfer Measurements," Soil Science Society of America, Proceedings, Vol. 38, No. 2, March-April 1974, pp. 219-222.

Rose, P. A., "Hydrodynamic Dispersion in Porous Materials," Soil Science, Vol. 123, No. 5, May 1977, pp. 277-283.

Rumer, R. R., "Longitudinal Dispersion in Steady and Unsteady Flow," Proceedings of the American Society of Civil Engineers, Hydraulics Division, Vol. 80, HY 4, July 1962, pp.147-172.

Saffman, P. G., "A Theory of Dispersion in a Porous Medium," Journal of Fluid Mechanics, Vol. 6, Part 3, October 1959, pp. 321-349.

Saffman, P. G., "Dispersion Due to Molecular Diffusion and Macroscopic Mixing in Flow Through a Network of Capillaries," Journal of Fluid Mechanics, Vol. 7, Part 2, February 1960, pp. 194-208.

Smith, L. and F. W. Schwartz, "Mass Transport I. A Stochastic Analysis of Macroscopic Dispersion," Water Resources Research, Vol. 16, No. 2, April 1978, pp. 303-313.

Sundaresan, S., N. R. Amundson and R. Aris, "Observations on Fixed-Bed Dispersion Models: The Role of the Interstitial Fluid," AIChE Journal, Vol. 26, No. 4, July 1980, pp. 529-536.

Taylor, G. I., "Diffusion by Continuous Movements," Proceedings of the London Mathematical Society, Vol. 20, 1921, pp.196-212.

Taylor, G. I., "Dispersion of Soluble Matter in Solvent Flowing Slowly Through a Tube," Proceedings of the Royal Society of London, Series A, Vol. 219, August 1953, pp. 186-203.

Vanoni, V. A.(editor), Sedimentation Engineering, American Society of Civil Engineers, Manuals and Reports on Engineering Practice No. 64, New York, New York, 1975, 745 pp.

Vomocil, J. A., "Porosity," from Methods of Soil Analysis, Part I: Physical and Mineralogical Properties, Including Statistics of Measurement and Sampling (C. A. Black, editor), Agronomy No. 9, American Society of Agronomy, Inc., Madison, Wisconsin, 1965, pp. 299-314.

Wilson, J. L. and L. W. Gelhar, "Dispersive Mixing in a Partially Saturated Porous Medium," Report Number 191, Ralph M. Parsons Laboratory for Water Resources and Hydrodynamics, Massachusetts Institute of Technology, Cambridge, Massachusetts, September 1974, 353 pp.

Winsauer, W. O., H. M. Shearin, Jr., P. H. Masson, M. Williams, "Resistivity of Brine Saturated Sands in Relation to Pore Geometry," Bulletin of the American Association of Petroleum Geologists, Vol. 36, No. 2, February 1952, pp.253-277.

NOTATION

A = cross-sectional area (L^2)

A_p = cross-sectional area of pores (L^2)

A_T = total area of sample (L^2)

$A(d)$ = cumulative area of grains up to size d (L^2)

a = pore radius (L)

$a^* = a/d_g$ = dimensionless pore radius (-)

$a_d = a/a_m$ = dimensionless pore radius (-)

a_g = geometric mean pore radius (L)

a_i = i^{th} percentile pore radius (L)

B = channel conductance (L^2)

C = solute concentration (M/L^3)

C_0 = source solute concentration (M/L^3)

D = molecular diffusion coefficient in free fluid (L^2/T)

$D_e = 1 + (3/16)(Pe \cdot \omega/\delta)^2$

D_L = longitudinal hydrodymamic dispersion coefficient (L^2/T)

D_m = molecular diffusion coefficient in porous medium (L^2/T)

D_T = transverse hydrodymamic dispersion coefficient (L^2/T)

$D_L^* = D_L/V_s d_g$ (-)

d = effective grain diameter (L)

$d^* = d/d_g$ = dimensionless grain diameter (-)

d_g = geometric mean grain diameter (L)

d_i = i^{th} percentile grain diameter (L)

F = formation factor (-)

F_v = viscous force (ML/T^2)

$f(\ell)$ = probability density for pore length by frequency (L^{-1})

$G(a)$ = cumulative probability for pore radius by frequency (-)

g = gravitational acceleration (L/T^2)

$g(a)$ = probability density for pore radius by frequency (L^{-1})

$h(d)$ = probability density for grain diameter by frequency (L^{-1})

$J(d)$ = area-weighted cumulative probability for grain diameter (-)

$j(d)$ = area-weighted probability density for grain diameter (L^{-1})

K = hydraulic conductivity (L/T)

K_L = longitudinal dispersion coefficient in a bidisperse porous medium (L^2/T)

k = permeability (L^2)

k_{ij} = permeability tensor (L^2)

L = column length (L)

ℓ = pore length (L)

$\ell^* = \ell/d_g$ = dimensionless pore length (-)

$\ell_d = \ell/\ell_m$ = dimensionless pore length (-)

ℓ_m = maximum pore length (L)

ℓ_j = pore length in the unit cell (L)

ℓ_{mp} = length scale of microporous regions (L)

$M = 3Pe \cdot \omega/2D_e$ (-)

$\tilde{m}$ = parameter in beta distribution for pore length (-)

N = number of pores (-)

n = number of steps taken (-)

$\tilde{n}$ = parameter in beta distribution for pore length (-)

P' = pressure gradient (M/L^2T^2)

$Pe = V_s d_g/D$ = Peclet number (-)

$P_a(a)$ = volume-weighted cumulative probability for pore radius (-)

$P_d(d)$ = volume-weighted cumulative probability for grain diameter (-)

$P_n(t)$ = probability for the location n at time t (-)

$Pe_D = V_s d_g / D_L$ = dynamic Peclet number (-)

p = fluid pressure (M/LT^2)

Q = volume flux (L^3/T)

$Re = V_s d_g / \nu$ = Reynolds number (-)

$R(\hat{\tau})$ = Lagrangian correlation function (L^2/T^2)

r_H = hydraulic radius (L)

r_m = maximum pore radius (L)

S = specific surface area (L^{-1})

s = local axial coordinate along capillary tube (L)

$T = V_s^2 t / D_L$ = dimensionless time (-)

T_{ij} = transformation tensor from local to fixed coordinate system (-)

t = time (T)

t_A = advective time scale (T)

t_D = diffusive time scale (T)

t_r = residence time in a mixing cell (T)

t_s = residence time in a capillary tube (T)

$t^* = V_s t / d_g$ = dimensionless time (-)

t_s^* = dimensionless residence time in a capillary tube (-)

$\bar{u}$ = average velocity in a capillary tube (L/T)

V_D = specific discharge (L/T)

V_s = seepage velocity (L/T)

V_T = total volume drained (L^3)

$V(a)$ = cumulative volume drained up to pore radius a (L^3)

W_T = total sample mass (M)

$W(d)$ = cumulative sample mass up to grain diameter d (M)

$X = V_s x/D_L$ = dimensionless longitudinal coordinate (-)

x = longitudinal coordinate (L)

x_n = longitudinal distance after n steps (L)

$x^* = x/d_g$ = dimensionless longitudinal coordinate (-)

$x_n^* = x_n/d_g$ = dimensionless longitudinal coordinate after n steps (-)

x_s = longitudinal distance for a single step (L)

$x_s^* = x_s/d_g$ = dimensionless longitudinal distance for a single step (-)

y = transverse coordinate (L)

z = transverse coordinate (L)

α = ratio of particle volume to cube of effective grain diameter (-)

$\tilde{\alpha}$ = parameter in beta distribution for pore radius (-)

β = interparticle distance (L)

$\tilde{\beta}$ = parameter in beta distribution for pore radius (-)

γ = surface tension (M/T^2)

$\Delta(a_1,\ldots,a_C)$ = dimensionless pressure fluctuation function (-)

$\delta = \ell/a$ = ratio of pore length to pore radius (-)

ζ = effective grain diameter (L)

$\zeta^* = \zeta/d_g$ = dimensionless grain diameter (-)

η = effective pore radius (L)

θ = direction of motion relative to mean flow (-)

λ = tortuosity (-)

μ = dynamic fluid viscosity (M/LT)

μ_a = geometric mean pore radius (L)

ν = kinematic fluid viscosity (L^2/T)

ρ = fluid density (M/L^3)

ρ_g = particle density (M/L^3)

σ = volumetric porosity (-)

σ_a = geometric standard deviation for pore radius (-)

σ_g = geometric standard deviation for grain diameter (-)

σ_L^2 = longitudinal variance (L^2)

σ_T^2 = transverse variance (L^2)

σ_m = porosity of microporous regions (-)

$\sigma_{x_s^*}^2$ = dimensionless longitudinal variance for a single step (-)

$\sigma_{t_s^*}^2$ = dimensionless residence time for a single step (-)

$\tau = (t^*-\bar{t}^*)/n^{1/2}$ = dimensionless time (-)

$\hat{\tau}$ = time lag in Lagrangian correlation function (T)

$\tau_n = (t_n^*-\bar{t}_n^*)/n^{1/2}$ = dimensionless time for n steps (-)

τ_{sh} = shear stress (M/LT^2)

ϕ = piezometric head (L)

ϕ_a = azimuthal angle (-)

$\chi = (x^*-\bar{x}^*)/n^{1/2}$ dimensionless longitudinal distance (-)

$\chi_n = (x_n^*-\bar{x}_n^*)/n^{1/2}$ = dimensionless longitudinal distance after n steps (-)

$\omega = \cos(\theta)$ (-)

APPENDIX A

GENERATION OF UNIFORM RANDOM NUMBERS

Numerical evaluation of the multidimensional integrals derived in chapter 3 are performed using a Monte Carlo integration technique. This technique requires the use of a large number of real random numbers uniformly distributed between 0 and 1. Truly random numbers are difficult to obtain and not necessarily the most desirable, so computer generated pseudo-random number sequences are used for most Monte Carlo calculations. A pseudo-random number sequence contains no apparent patterns, but is deterministic in the sense that the same sequence is always generated when started under the same initial conditions. It is useful to use the same sequence of random numbers for testing and comparing calculations so that differences observed in the calculations will not be due to the random number sequence. This appendix describes the pseudo-random number generator used for the Monte Carlo calculations presented in chapter 5. For convenience, the descriptor "pseudo" will be dropped, but is implied throughout the remainder of the appendix. Most of the discussion to follow is covered in Knuth (1969).

The most common method for generating uniform random numbers is the linear congruential method. The basis of this method is to compute a new value of the sequence from the previous value using a linear equation, i.e.,

$$I_{N+1} = AI_N + B \qquad (A.1)$$

where $I_N = N^{th}$ integer in the sequence

A = fixed constant

B = fixed constant

The randomness occurs due to integer overflow upon calculation of the new value, I_{N+1}. Integer overflow results in a loss of the most significant bits, leaving I_{N+1} defined by the least significant bits. The random number generator (equation (A.1)) gives a sequence of random integers. To convert this to a sequence of real random numbers between 0 and 1, the sequence is divided by the largest integer in the sequence.

There are two important characteristics that a random number sequence should satisfy. These are sufficient randomness in the sequence and a sequence length equal to the maximum integer which can be represented on the computer. It is fairly easy to obtain the maximum sequence length and it is easy to check. For an N bit processor, the maximum sequence length which can be obtained with equation (A.1) is $2^{(N-1)}$. Rules for selecting A and B for equation (A.1) have been developed (Knuth, 1969) such that the maximum sequence length is obtained. The computer used for the Monte Carlo calculations in chapter 5 is a PDP 11/60, which has a 16 bit processor. This means the maximum sequence length which can be obtained by using equation (A.1) is 32,768. This sequence length has not been found to be satisfactory since some of the Monte Carlo calculations need many

times this number. It is possible to increase the sequence length dramatically at the expense of using two linear congruential sequences simultaneously, which approximately doubles the computation time spent on generating random numbers. If the two generators have sequence lengths which are prime relative to each other (no common factors), the sequence length of the combined generators can be made to produce a sequence length equal to the product of the two original sequence lengths. The algorithm shown below was first proposed by MacLaren and Marsaglia, and is discussed in Knuth (1969).

Algorithm:

$$I_{N+1} = A_1 I_N + B_1 \qquad (A.2)$$

$$J_{N+1} = A_2 I_N + B_2 \qquad (A.3)$$

Generate 100 values from, say, the J sequence and store in an array called L(k). Use the I sequence to generate a random integer value of k, i.e.,

$$k = 100(I_{N+1}/I_{max})$$

where I_{max} is the maximum integer that can be represented on the computer. The real random number, R, is

$$R = L(k)/J_{max}$$

where J_{max} would typically be equal to I_{max}.
Use the J sequence to replace the value used, i.e.,

$$L(k) = J_{N+1}$$

It turns out that a sequence length of 32,768 factors into 2^{15} and 32,767 factors into 7,31,151 which has no common factors. The I sequence is shortened by 1 by throwing out a predetermined value (in this case 0). Thus the sequence length for the combined generators is 32,767x32,768 = 1,073,709,056.

To determine if a sequence is sufficiently random is a more difficult question than the sequence length. A number of empirical and theoretical tests have been developed to detect nonrandom behavior. Unfortunately, there is no single test which may be considered both necessary and sufficient to declare a given random number generator satisfactory for all applications (Knuth, 1969). One commonly used test for a continuous random number sequence is the Kolmogorov-Smirnov test. The basis of the test is to compare the cumulative distribution of sample observations from the random number generator with the theoretical cumulative distribution for the population. The following description of the test follows Knuth (1969).

Kolmogorov-Smirnov Test

1. Generate N random numbers.
2. Order the numbers to compute the cumulative distribution for the sample.
3. Compute $K^+ = N^{1/2} \max(j/N - F(X_j))$
   $K^- = N^{1/2} \max(F(X_j) - (j-1)/N)$

For a uniform distribution, $F(X_j) = X_j$. If the generated numbers are random, then the values of K^+ and K^- are randomly distributed according

to a known distribution function. The values may be compared to tabulated values of K^+ (or K^-) which give the probability of the computed K^+ (or K^-). Table A.1 shows 30 independent samples of N = 1000 using the random number generator given by equations (A.2) and (A.3). The values of K^+ (or K^-) which correspond to the given place in the cumulative distribution when N = 1000 are shown at the bottom of Table A.1. By comparing the sample with the theoretical values, we see that no extraordinary behavior is detected. Table A.2 shows a similar calculation for a single linear congruential random number generator (equation (A.1)). Again, acceptable random behavior is found. The Kolmogorov-Smirnov test may be applied to the sets of K^+ and K^- values displayed in Tables A.1 and A.2. This is useful in detecting global nonrandom behavior in the original sequences. Global nonrandom behavior refers to deviation from expected random behavior over the entire sequence of random numbers (which is 30000 random numbers in this case). The theoretical cumulative distribution for the Kolmogorov-Smirnov coefficients (K^+ and K^-) is approximated by

$$F(x) = 1 - \exp(-2x^2).$$

Table A.3 shows the global test as applied to the values in Tables A.1 and A.2. We find that both generators display acceptable bahavior at the global scale (30000 random numbers). Table A.4 presents a summary of the constants and seed numbers used in the random number generators tested.

Table A.1

Kolmogorov-Smirnov Test of the Dual Linear Congruential Method

N	K^+	K^-
1 - 1000	0.7254	0.5695
1001 - 2000	0.1279	0.4951
2001 - 3000	0.8831	0.2571
3001 - 4000	0.6881	0.5165
4001 - 5000	0.8464	0.1472
5001 - 6000	0.6498	0.9749
6001 - 7000	0.5952	0.8585
7001 - 8000	0.4781	0.9395
8001 - 9000	0.6586	0.1215
9001 - 10000	0.4222	0.9876
10001 - 11000	0.3533	0.6019
11001 - 12000	0.7830	0.2979
12001 - 13000	0.1789	0.9061
13001 - 14000	0.7827	0.1527
14001 - 15000	0.4602	1.1114
15001 - 16000	0.8752	0.4569
16001 - 17000	0.5086	0.7681
17001 - 18000	0.6731	0.5046
18001 - 19000	0.2417	0.8539
19001 - 20000	0.6249	0.6061
20001 - 21000	1.0093	0.4433
21001 - 22000	0.3779	0.7720
22001 - 23000	1.1243	0.3525
23001 - 24000	0.4456	0.4906
24001 - 25000	0.9829	0.5472
25001 - 26000	0.3859	0.6732
26001 - 27000	0.4626	0.6303
27001 - 28000	0.1594	1.1121
28001 - 29000	1.2748	0.1341
29001 - 30000	0.0506	1.3684

Theoretical Cumulative Distribution:

Cumulative Probability	99%	95%	75%	50%	25%	5%	1%
Value (K)	0.0661	0.1557	0.3746	0.5840	0.8275	1.2185	1.5111

Table A.2

Kolmogorov-Smirnov Test of the Linear Congruential Method

N	K^+	K^-
1 - 1000	0.5549	0.6587
1001 - 2000	1.0379	0.4043
2001 - 3000	0.8436	0.7181
3001 - 4000	1.1094	0.2984
4001 - 5000	0.4815	1.0630
5001 - 6000	0.4404	0.8116
6001 - 7000	0.4668	0.5469
7001 - 8000	0.2685	0.6848
8001 - 9000	0.7827	0.3320
9001 - 10000	0.5234	1.0798
10001 - 11000	0.1162	1.3399
11001 - 12000	0.6983	0.8313
12001 - 13000	0.9578	0.0446
13001 - 14000	0.9058	0.1592
14001 - 15000	0.8462	0.4796
15001 - 16000	1.2432	0.1472
16001 - 17000	0.4831	0.5006
17001 - 18000	0.5867	0.9533
18001 - 19000	0.5601	0.7326
19001 - 20000	0.1924	1.2429
20001 - 21000	0.5801	0.4387
21001 - 22000	0.5574	0.6648
22001 - 23000	0.4351	0.7326
23001 - 24000	0.2879	0.9061
24001 - 25000	0.9993	0.1662
25001 - 26000	0.5867	0.9750
26001 - 27000	0.3050	0.9714
27001 - 28000	0.8617	0.5788
28001 - 29000	0.5719	0.6234
29001 - 30000	0.0374	1.0122

Theoretical Cumulative Distribution:

Cumulative Probability	99%	95%	75%	50%	25%	5%	1%
Value (K)	0.0661	0.1557	0.3746	0.5840	0.8275	1.2185	1.5111

Table A.3

Global Kolmogorov-Smirnov Test

Dual Linear Congruential Generator:

Sequence	K^+	K^-
K^+	0.4205	0.2973
K^-	0.4807	0.5022

Single Linear Congruential Generator:

Sequence	K^+	K^-
K^+	0.7429	0.6311
K^-	0.4358	0.8042

Theoretical Cumulative Distribution:

Cumulative Probability	99%	95%	75%	50%	25%	5%	1%
Value (K)	0.0435	0.1351	0.3509	0.5605	0.8306	1.1916	1.4801

Table A.4

Parameters for the Random Number Generators

For Equation (A.1): A = 405 B = 6925 Seed = I_1 = 15735

For Equation (A.2): A_1 = 405 B_1 = 6925 Seed = I_1 = 17375

For Equation (A.3): A_2 = 405 B_2 = 6923 Seed = J_1 = 29841

REFERENCE

Knuth, Donald E. 1969 *Seminumerical Algorithms - The Art of Computer Programming*, Vol. 2, Addison-Wesley.

APPENDIX B

A COMPARISON OF SOLUTIONS FOR THE BREAKTHROUGH PROBLEM IN POROUS COLUMNS

The transport of a nonreactive, conservative solute through a porous medium for one-dimensional flow is often described by the advective diffusion equation for the solute, c

$$\frac{\partial c}{\partial t} + v \frac{\partial c}{\partial x} = D_L \frac{\partial^2 c}{\partial x^2} \qquad (B.1)$$

(Bear, 1972; Greenkorn, 1981), where v is the seepage velocity, defined to be the volume flux of solution, Q, divided by the average cross-sectional area of pores, A_p. The total cross-sectional area, A_T, can be related to A_p through the relationship $A_p = \theta A_T$ (Bear, 1972), where θ is the volumetric porosity. A great deal of effort has been spent in studying D_L, the longitudinal dispersion coefficient. For a uniform porous medium (one composed of grains of a uniform size), dimensional analysis with experimental research has resulted in a quantitative relationship for D_L/D as a function of the molecular Peclet number, $Pe = vd/D$, where D is the molecular diffusivity and d is the grain size (Bear, 1972). In addition, theoretical work has been successful in describing the main features of the dispersion coefficient (Saffman, 1959; 1960). The dispersion model, although generally successful, does predict some physically unrealistic behavior, which includes dispersive mixing upstream from a source (which is not observed experimentally) and the instantaneous effect of

a change in source strength over an entire domain, implying an infinite speed of signal propagation (Sundaresan, et al., 1980).

B.1 The Breakthrough Problem

A common experimental method for studying longitudinal dispersion is to displace a resident solution from a porous column by continually injecting a solution of different solute concentration at the inlet of the column (Rose and Passioura, 1971). The well-known breakthrough curve results when the change in concentration with time is measured at a particular longitudinal position along the column. Theoretical solutions to this problem have employed equation (B.1) along with appropriate initial and boundary conditions. While the initial condition poses no difficulty, a significant body of literature is devoted to the interpretation of the boundary conditions (Pearson, 1959; Werner and Wilhelm, 1956; Gershon and Nir, 1969; Choi and Perlmutter, 1976; Kreft and Zuber, 1978). The three physical domains to be investigated here are an infinite medium ($-\infty < x < +\infty$), a semi-infinite medium ($0 < x < +\infty$), and a finite medium ($0 < x < L$). The boundary conditions for the infinite medium are

$$\lim_{x \to -\infty} c(x,t) = c_0 \qquad t > 0$$

$$\lim_{x \to \infty} c(x,t) = c_r \qquad t > 0 \tag{B.2}$$

and initial condition

$$c(x,0) = c_0 \qquad x < 0$$

$$c(x,0) = c_r \qquad x > 0 \tag{B.3}$$

where, c_0 is the feed solute concentration and c_r is the resident fluid solute concentration. For convenience in the arguments to be presented, let $c_r = 0$, since concentrations are only significant in a relative sense. Let X an T be nondimensional variables defined by

$$X = vx/D_L$$

$$T = v^2t/D_L \tag{B.4}$$

In terms of the nondimensional variables in equation (B.4), equation (B.1) takes the form

$$\frac{\partial c}{\partial T} + \frac{\partial c}{\partial X} = \frac{\partial^2 c}{\partial X^2} \tag{B.5}$$

The solution to equation (B.5) with equations (B.2) and (B.3) is (Bear, 1972):

$$\frac{c}{c_o} = \frac{1}{2}\,\mathrm{erfc}\left[\frac{X-T}{2\sqrt{T}}\right] \tag{B.6}$$

where erfc(z) is the complementary error function defined by

$$\mathrm{erfc}(z) = \frac{2}{\sqrt{\pi}} \int_z^\infty e^{-t^2}\,dt$$

A more controversial situation exists in establishing boundary conditions for a semi-infinite medium and finite medium. For the semi-infinite medium, the inlet boundary condition (at $x = 0$) has been represented as (Ogata and Banks, 1961)

$$c(0^+,t) = c_0 \qquad t > 0 \qquad (B.7)$$

which we call the source boundary condition. Let 0^+ and 0^- refer to the interface position as approached from $x > 0$ and $x < 0$, respectively. Dankwerts (1953) proposed a flux boundary condition at the inlet, in which the flux of solute on each side of the inlet is equal.

$$vc(0^+,t) - D_L \frac{\partial c}{\partial x}(0^+,t) = vc_0 \qquad t > 0 \qquad (B.8)$$

Diffusion in the free fluid ($x < 0$) is considered infinite, and being an effectively infinite reservoir, can maintain a constant concentration at $x = 0^-$. Conditions (B.7) and (B.8) are identical if the dispersive flux at $x = 0^+$ is negligible. The boundary conditions for $x \to \infty$ are

$$\lim_{x \to \infty} c(x,t) = 0 \qquad t > 0 \qquad (B.9)$$

and the initial condition is

$$c(x,0) = 0 \qquad x > 0 \qquad (B.10)$$

The solution to equation (B.5) with conditions (B.7), (B.9) and (B.10) is (Ogata and Banks, 1961)

$$\frac{c}{c_o} = \frac{1}{2}\left[\operatorname{erfc}\left(\frac{X-T}{2\sqrt{T}}\right) + \exp(X)\operatorname{erfc}\left(\frac{X+T}{2\sqrt{T}}\right)\right] \tag{B.11}$$

and for equation (B.5) with conditions (B.8), (B.9) and (B.10) is (Brenner, 1962; Coats and Smith, 1964)

$$\frac{c}{c_o} = \frac{1}{2}\left[\operatorname{erfc}\left(\frac{X-T}{2\sqrt{T}}\right) - (1+X+T)\exp(X)\operatorname{erfc}\left(\frac{X+T}{2\sqrt{T}}\right)\right] + \left(\frac{T}{\pi}\right)^{\frac{1}{2}} \exp\left[-\frac{(X-T)^2}{4T}\right] \tag{B.12}$$

Neither the source boundary condition nor the flux boundary condition is precisely correct for the typical physical situation. The flux boundary condition takes into account dispersive flux on the downstream side of the interface, but there is no guarantee that the hydrodynamic dispersion coefficient applies so close to a boundary. The flux condition also neglects dispersive flux on the upstream side of the interface. The source boundary condition makes no statement on the flux through the interface, but the system must maintain a constant concentration at the interface, which is an approximation to the physical system. It is not clear which boundary condition is a better approximation for modeling the miscible displacement experiments described in Chapter 4.

For a finite medium of length L, an appropriate boundary condition for the exit of the porous medium must be developed. Dankwerts (1953) again used a flux boundary condition

$$vc(L^-,t) - D_L \frac{\partial c}{\partial x}(L^-,t) = vc_e \qquad t > 0$$

where c_e is the exit concentration, and L^- refers to the exit interface ($x = L$) as approached from $x < L$. Dankwerts (1953) argued, however, that $c(L^-,t)$ must equal c_e, or the solute concentration within the bed would have to pass through a maximum or minimum. The exit boundary condition is then,

$$\frac{\partial c}{\partial x}(L,t) = 0 \qquad t > 0 \qquad \text{(B.13)}$$

Brenner (1962) gives the solution to equation (B.5) with equations (B.8), (B.14) and the initial condition

$$c(x,0) = 0 \qquad 0 < x < L$$

to be

$$\frac{c}{c_o} = 2\exp\left[\frac{1}{4}(2X - T)\right] x \qquad \text{(B.14)}$$

$$x \sum_{k=1}^{\infty} \frac{P\lambda_k}{(\lambda^2_k + P^2 + P)(\lambda^2_k + P^2)} \left[\lambda_k \cos\left(\frac{\lambda_k X}{2P}\right) + P\sin\left(\frac{\lambda_k X}{2P}\right)\right]$$

$$x \exp\left(-\lambda^2_k T/4P^2\right)$$

where $P = vL/4D_L$ and λ_k are the positive roots in order of increasing magnitude of

$$\tan(2\lambda) = \frac{2\lambda P}{\lambda^2 - P^2}$$

Note that an additional dimensionless parameter, P, has appeared due to the additional length scale, L. If we only consider the exit concentration (x = L), then we can write X = 4P and the solution may be expressed in terms of X and T only.

$$\frac{c}{c_o} = 1 - \exp\left[\frac{1}{4}(2X-T)\right] \sum_{k=1}^{\infty} \frac{16\lambda_k \sin(2\lambda_k)}{(16\lambda_k^2 + X^2 + 4X)} \exp\left(\frac{-4\lambda_k^2 T}{X^2}\right) \qquad (B.15)$$

Table B.1 summarizes the solutions according to the type of boundary condition employed.

B.2 Comparison of Solutions

Figures B.1-B.5 present a comparison of the solutions for a range of X from 0.8 to 80.0 as calculated from equations (B.6), (B.11), (B.12), and (B.15). The values plotted for a finite medium are taken from tabulated values given by Brenner (1962). As the value of X increases, the different solutions tend to the same curve. For X = 24., (Figure B.4), both solutions for a semi-infinite medium and the solution for an infinite medium have less than 1% maximum error among them. Maximum error is defined as the maximum difference in concentration among the breakthrough curves being considered, expressed as a per cent (i.e., a maximum concentration difference of .03 is a 3%

TABLE B.1

Solutions to the Breakthrough Problem

BOUNDARY CONDITIONS $t > 0$	SOLUTIONS $X = vx/D_L \quad T = v^2t/D_L$
$\lim_{x \to -\infty} c(x,t) = c_0$ $\lim_{x \to \infty} c(x,t) = 0$	$c/c_0 = \frac{1}{2} \operatorname{erfc}\left[\frac{X-T}{2\sqrt{T}}\right]$
$c(0^+,t) = c_0$ $\lim_{x \to \infty} c(x,t) = 0$	$c/c_0 = \frac{1}{2}\left[\operatorname{erfc}\left(\frac{X-T}{2\sqrt{T}}\right) + \exp(X)\operatorname{erfc}\left(\frac{X+T}{2\sqrt{T}}\right)\right]$
$vc(0^+,t) - D_L \frac{\partial c}{\partial x}(0^+,t) = vc_0$ $\lim_{x \to \infty} c(x,t) = 0$	$c/c_0 = \frac{1}{2}\left[\operatorname{erfc}\left(\frac{X-T}{2\sqrt{T}}\right) - (1+X+T)\exp(X)\operatorname{erfc}\left(\frac{X+T}{2\sqrt{T}}\right)\right]$ $+ \left(\frac{T}{\pi}\right)^{\frac{1}{2}} \exp\left[-\frac{(X-T)^2}{4T}\right]$
$vc(0^+,t) - D_L \frac{\partial c}{\partial x}(0^+,t) = vc_0$ $\frac{\partial c}{\partial x}(L,t) = 0$	$c/c_0 = 1 - \exp\left[\frac{1}{4}(2X-T)\right] \sum_{k=1}^{\infty} \frac{16\lambda_k \sin(2\lambda_k)}{(16\lambda_k^2 + X^2 + 4X)} \exp\left(\frac{-4\lambda_k^2 T}{X^2}\right)$ EXIT CONCENTRATION, $X = vL/D_L$

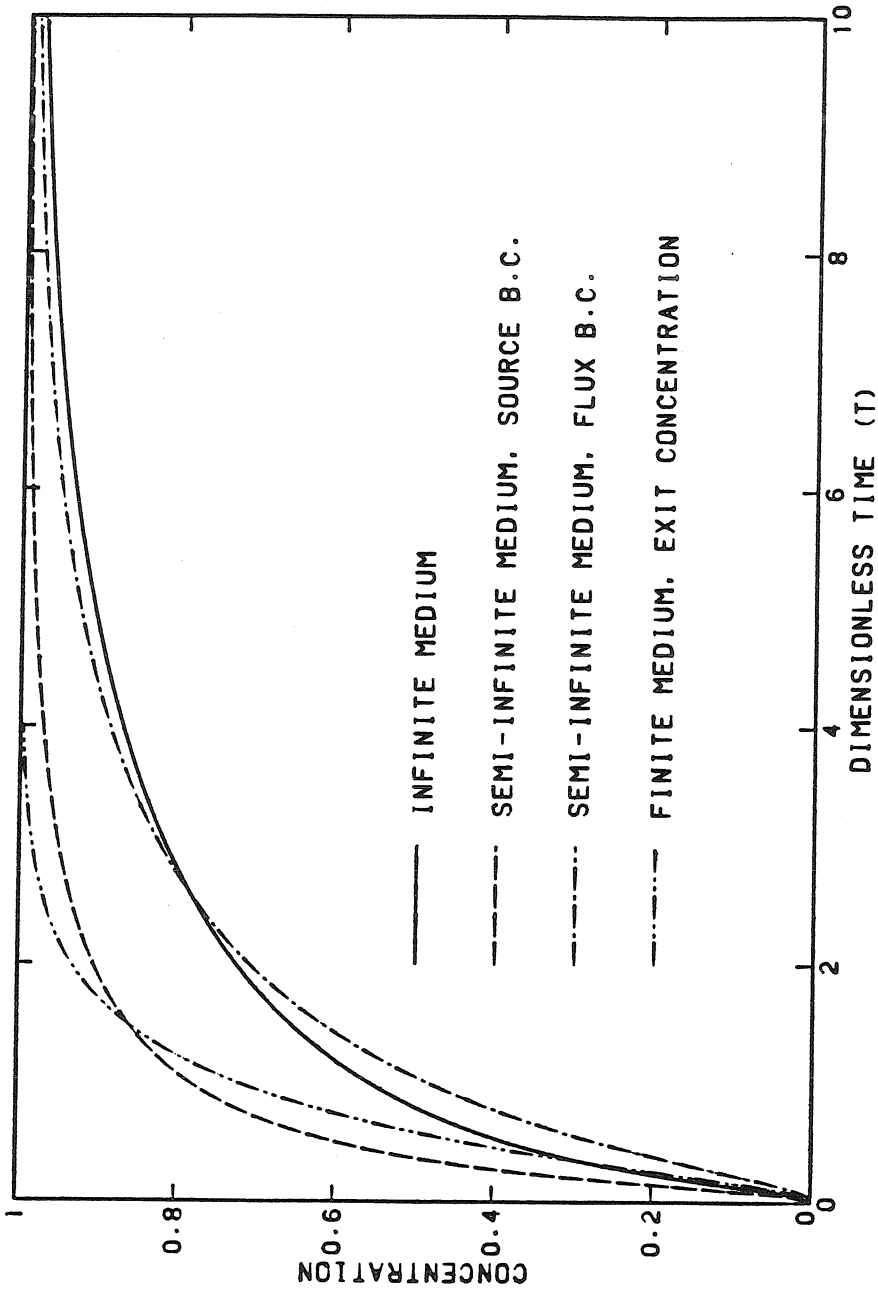

FIGURE B.1
Breakthrough Theories, X=0.8

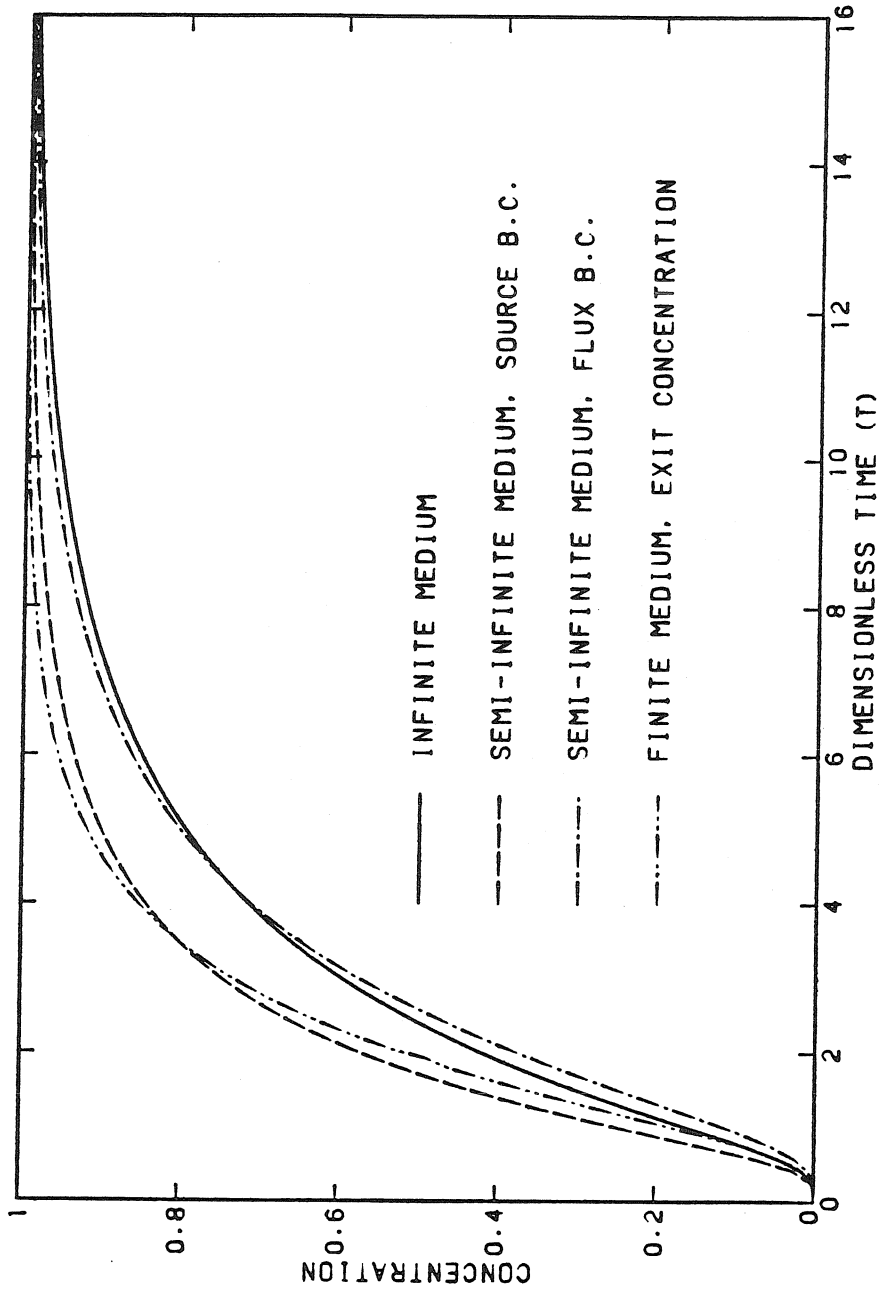

FIGURE B.2

Breakthrough Theories, X=2.4

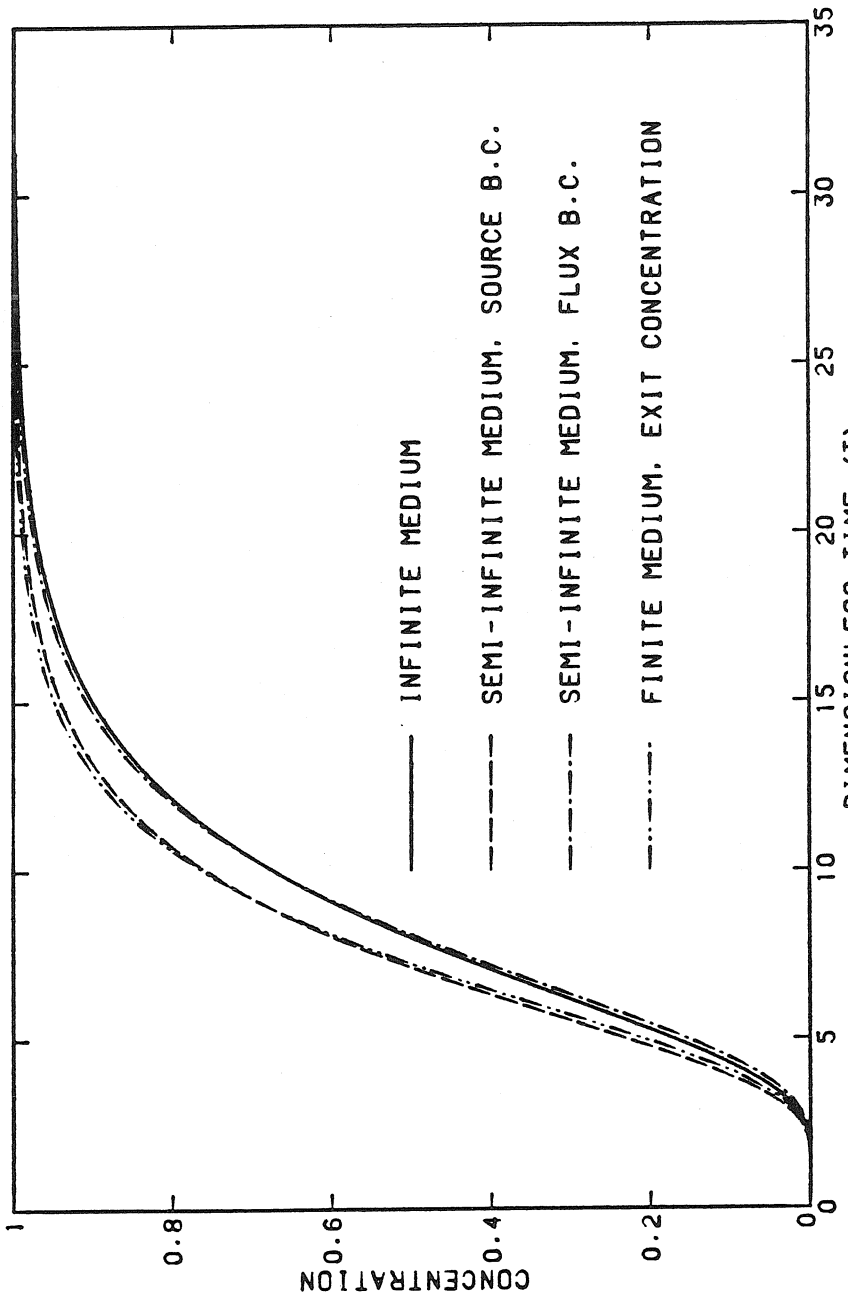

FIGURE B.3

Breakthrough Theories, X=8.0

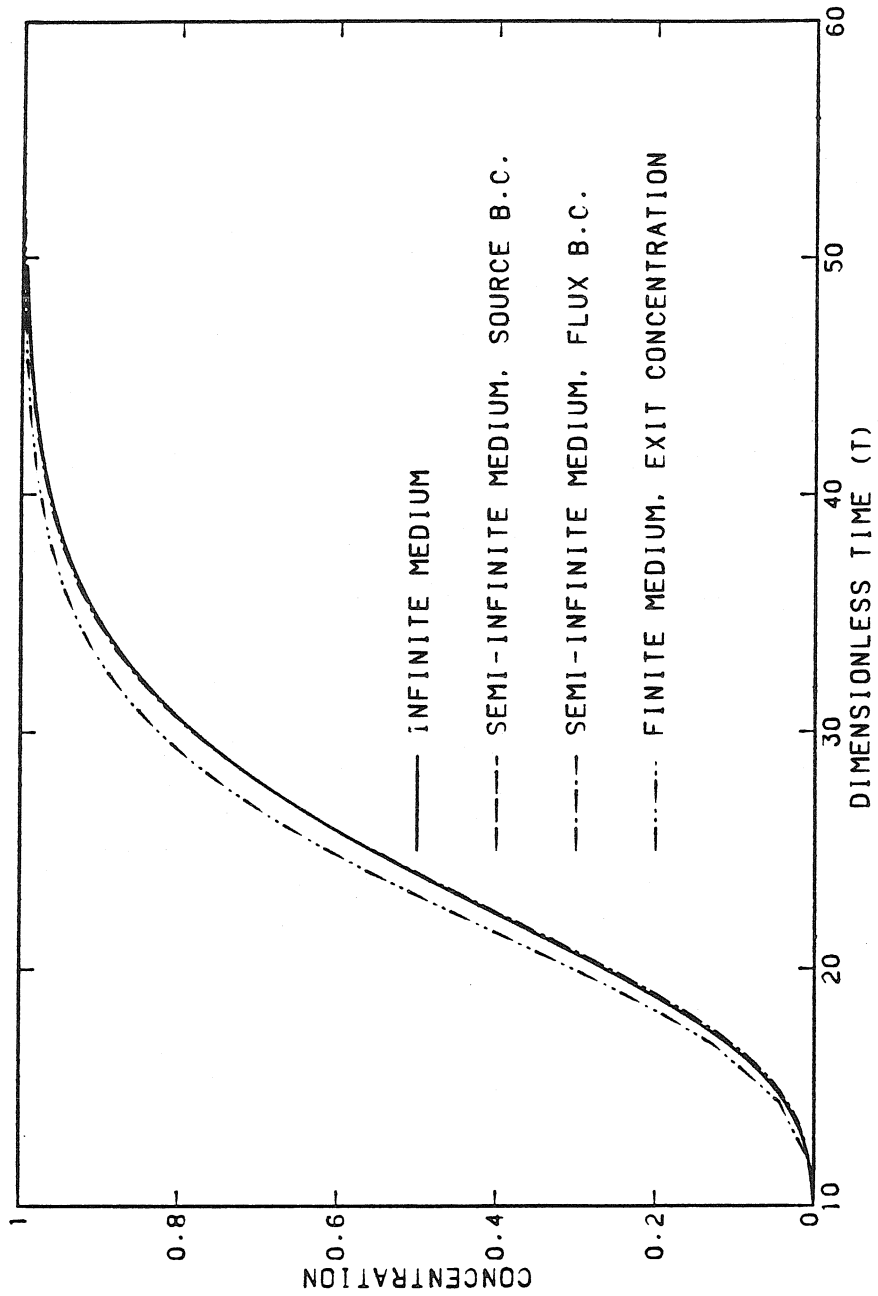

FIGURE B.4
Breakthrough Theories, X=24.0

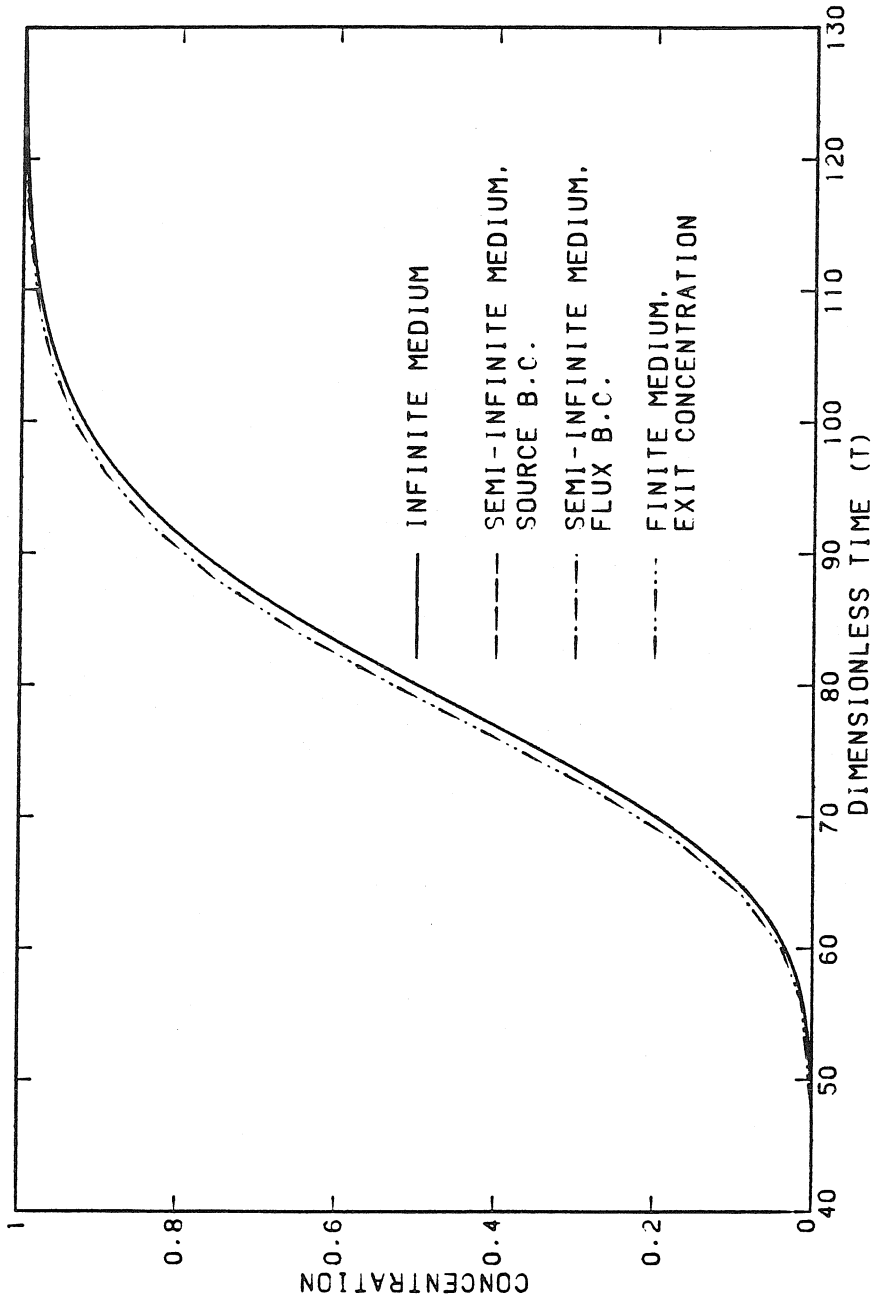

FIGURE B.5

Breakthrough Theories, X=80.0

maximum error). The breakthrough curve for the exit concentration from a finite medium has a maximum error of about 4% relative to the other solutions when X = 80. The solution for a semi-infinite medium with a flux boundary condition is approximated to within 2% for X = 8.0 (Figure B.3) by the solution for an infinite medium.

For high Peclet flows (Pe > 1.0), we can write for the dispersion coefficient in a uniform medium

$$D_L > vd/2$$

Using this in the expression for X we find,

$$X < 2x/d$$

which says that X is less than two times the number of grain diameters downstream. Thus, for Pe > 1.0, equation (B.6) approximates equation (B.12) within 2% maximum error for X = 8.0, which is less than 16 grain diameters downstream. This is probably well within the accuracy requirements for most situations. By 48 grain diameters downstream, equations (B.6), (B.11), and (B.12) have less than 1% maximum error. For low Peclet number flows (Pe < 1.0), D_L tends to a constant, which means $X \to 0$ as $v \to 0$ for a given x. Under these conditions, the different solutions according to the different boundary conditions may remain distinct far enough downstream to be significant.

B.3 Summary

Solutions for the miscible displacement of a resident fluid in infinite, semi-infinite and finite uniform porous media have been compared for downstream distances ranging from $0.8 < X < 80.$, where $X = vx/D_L$. For a finite medium, the exit concentration is calculated with $X = vL/D_L$, where L is the length of the porous medium. Under conditions of high Peclet number flow, $Pe = vd/D_L > 1$, the solution for an infinite medium is found to approximate the solution for a semi-infinite medium with a flux boundary condition at the inlet within 2% maximum error for $X = 8$. The error is found to decrease with increasing values of X. By $X = 24$, both solutions for the semi-infinite medium are approximated within 1% maximum error by the infinite medium solution. All solutions discussed are seen to lie within 4% maximum error of each other when $X = 80$.

REFERENCES

Bear, J., Dynamics of Fliuds in Porous Media, American Elsevier, New York, New York, 1972, 764 pp.

Brenner, H., "The Diffusion Model of Longitudinal Mixing in Beds of Finite Length. Numerical Values," Chemical Engineering Science, Vol. 17, No. 4, April 1962, pp. 229-243.

Choi, Cha Y. and D. D. Perlmutter, "A Unified Treatment of the Inlet Boundary Condition for Dispersive Flow Models," Chemical Engineering Science, Vol. 31, No. 3, February 1976, pp. 250-252.

Coats, K. H. and B. D. Smith, "Dead End Pore Volume and Dispersion in Porous Media," Society of Petroleum Engineers Journal, Vol. 4, No. 1, March 1964, pp. 73-84.

Dankwerts, P. V., "Continuous Flow Systems," Chemical Engineering Science, Vol. 2, No. 1, February 1953, pp. 1-13.

Gershon, N. and A. Nir, "Effects of Boundary Conditions of Models on Tracer Distribution in Flow Through Porous Media," Water Resources Research, Vol. 5, No. 4, August 1969, pp. 830-839.

Greenkorn, R. A., "Steady Flow Through Porous Media," AIChE Journal, Vol. 27, No. 4, July 1981, pp. 529-545.

Kreft, A. and A. Zuber, "On the Physical Meaning of the Dispersion Equation and its Solution for Different Initial and Boundary Conditions," Chemical Engineering Science, Vol. 33, No. 11, November 1978, pp. 1471-1480.

Ogata, Akio and R. B. Banks, "A Solution of the Differential Equation of Longitudinal Dispersion in Porous Media," United States Geological Survey Professional Paper 411-A, 1961, 7 pp.

Pearson, J. R. A., "A Note on the 'Dankwerts' Boundary Condition for Continuous Flow Reactors," Chemical Engineering Science, Vol. 10, No. 4, 1959, pp. 281-284.

Rose P. A. and J. B. Passioura, "The Analysis of Experiments on Hydrodynamic Dispersion," Soil Science, Vol. 111, No. 4, April 1971, pp. 252-257.

Saffman, P. G., "A Theory of Dispersion in a Porous Medium," Journal of Fluid Mechanics, Vol. 6, Part 3, October 1959, pp. 321-349.

Saffman, P. G., "Dispersion Due to Molecular Diffusion and Macroscopic Mixing in Flow Through a Network of Capillaries," Journal of Fluid Mechanics, Vol. 7, Part 2, February 1960, pp. 194-208.

Sundaresan, S., N. R. Amundson, and R. Aris, "Observations on Fixed-Bed Dispersion Models: The Role of the Interstitial Fluid," AIChE Journal, Vol. 26, No. 4, July 1980, pp. 529-536.

Werner, J. F. and R. H. Wilhelm, "Boundary Conditions of Flow Reactor," Chemical Engineering Science, Vol. 6, No. 2, 1956, pp. 89-93.

APPENDIX C

SHEAR DISPERSION AND RESIDENCE TIME FOR LAMINAR FLOW IN CAPILLARY TUBES

(To appear in the Journal of Fluid Mechanics
Vol. 142, May 1984, pp. 289-308.)

The behavior of passive tracer particles in capillary Poiseuille flow is investigated with regard to the residence time in short axial sections of length z, in which $z/a < Va/D$, where a is the capillary radius, V is the mean velocity, and D the coefficient of molecular diffusion. While methods exist for calculating moments of the cross-sectionally averaged axial concentration distribution as a function of time (e.g. Smith 1982b), much less is known about the distribution of residence time as a function of axial distance. An approximate theoretical solution for point sources in high Peclet number flows reveals that the mean residence time $< t(z) >$, which is asymptotic to z/V_0 near the source, will then rise faster than z/V_0 before converging to z/V for large z, provided the source is not at the capillary wall. V_0 is the advective velocity at the point of release. The variance $< t^2(z) >$ is found to initially increase in proportion to z^3 provided the source is not at the capillary wall or on the axis. A Monte Carlo method based on the solution to the diffusion equation in the capillary tube cross-section is developed to compute particle trajectories which are used to analyze both axial and residence time distributions. The residence time distribution is found to display significant changes in character as a function of axial position, for both point sources and a uniform flux of particles along the tube.

C.1 Introduction

When passive tracer particles are introduced into Poiseuille flow, random lateral excursions caused by molecular diffusion coupled with the velocity profile cause an enhanced longitudinal dispersion. This phenomenon was first analyzed by Taylor (1953), who provided a complete description of the asymptotic, cross-sectionally averaged axial concentration distribution. Since that time, Taylor's analysis has been applied to a wide variety of fluid flow circumstances (Taylor 1954; Elder 1959; Saffman 1962; Fischer 1967). Taylor's (1953) analysis requires a certain initialization time, $t > a^2/D$, where a is the tube radius and D the molecular diffusivity, before his results may be applied. In some cases, for example blood flow in arteries, there is interest in what happens for $t << a^2/D$ (Chatwin 1976). Most analytical and numerical work for the near field problem has analyzed the behavior of the spatial concentration distribution as a function of time. In this paper, we will consider the variation in concentration over time as a function of axial position. We will limit our attention to small distances from the source, $z/a < Va/D$, where V is the mean velocity.

The results to be presented are principally devoted to cases where longitudinal molecular diffusion may be neglected. It is well known that when the Peclet number, $Pe = Va/D$, is large relative to 1, the longitudinal molecular diffusion is usually negligible. Chatwin (1976) shows for a source on the axis that if

$$Dt/a^2 >> Pe^{-2/3} \tag{C.1}$$

longitudinal molecular diffusion is negligible. This relationship is developed through scaling arguments which compare the amount of longitudinal spreading due to molecular diffusion versus differential advection. This reasoning may be extended for off-axis sources as follows. For a point source far from the axis and capillary wall, such that $(Dt)^{1/2} << a-r_0$ and $(Dt)^{1/2} << r_0$, the velocity differential developed due to radial diffusion over distances of the order $(Dt)^{1/2}$ is

$$\Delta V \sim V(r_0/a)(Dt)^{1/2}/a \tag{C.2}$$

where r_0 is the radial location of the source. This leads to longitudinal spreading of the order ΔVt, while the longitudinal spreading due to molecular diffusion is of the order $(Dt)^{1/2}$. For $\Delta Vt >> (Dt)^{1/2}$ we find

$$Dt/a^2 >> (\eta_o\, Pe)^{-1} \tag{C.3}$$

where $\eta_o = r_0/a$. Relation (C.3) also happens to be valid for a source at the wall, $r_0 = a$. For sources far from the capillary wall, $(Dt)^{1/2} << a-r_0$, we may scale t by z/V_0, where V_0 is the advective velocity at the source. For Poiseuille flow, V_0 is of the order $V(1-\eta_o^2)$. Substituting into relation (C.1) for t we find

$$z/a >> Pe^{1/3} \quad \text{if} \quad \eta_o = 0 \tag{C.4}$$

For a source on the capillary wall, it is not possible to scale t by

z/V_0 since $V_0 = 0$. For this case we scale t by $z/\Delta V$, where ΔV is given in expression (C.2) using $r_0 = a$. Using this in expression (C.3) we find

$$z/a \gg Pe^{-1/2} \qquad \text{if} \quad \eta_o = 1 \tag{C.5}$$

For intermediate values of η_o, the requirement on z may be constructed from expression (C.3), scaling t by z/V_0 to give

$$z/a \gg (1- \eta_o^2)/\eta_o \tag{C.6}$$

which is valid if $(1 - \eta_o)^2 \eta_o^3 \gg Pe^{-1}$. Expressions (C.4) through (C.6) show when longitudinal molecular diffusion is negligible at a given distance z downstream of the source.

Consider a point source which instantaneously injects a small volume of tracer into high Peclet flow in a capillary tube. At an observation point downstream of the source, we are able to detect the cross-sectionally averaged concentration of tracer, $\bar{P}(z_{ob},t)$, where z_{ob} is the axial distance of the observation station from the source and t is the time since source injection. Assume z_{ob}/a to be sufficiently large such that longitudinal molecular diffusion may be neglected. The concentration distribution, $\bar{P}(z_{ob},t)$, defines the probability density that a tracer particle will be at z_{ob} at time t. In addition, $\bar{P}(z_{ob},t)$ is the probability density for a tracer particle to spend a time t in residence with $z \leq z_{ob}$. Suppose, for example, a radioactive substance is injected to irradiate a given length of the capillary tube. The residence time distribution, $\bar{P}(z_{ob},t)$, would be needed to calculate the

radiation dosage for a given distance downstream. Another example may be a chemical reaction which is desired to occur within a certain distance downstream of the source. In this case, a comparison of the residence time distribution with the reaction kinetics would be necessary.

A difficulty arises when longitudinal molecular diffusion is not negligible. Although $\overline{P}(z_{ob},t)$ is still defined, it is not the residence time distribution. Through molecular diffusion, it is possible for a particle to move upstream. A particle which has passed the observation point, z_{ob}, may diffuse upstream to $z < z_{ob}$ and again contribute to $\overline{P}(z_{ob},t)$. The time t for this particle has not been spent entirely in the region $z \leq z_{ob}$, so $\overline{P}(z_{ob},t)$ may not be considered a residence time distribution in the sense given above. The difference in interpretation of $\overline{P}(z_{ob},t)$ takes on more significance when one considers a continuous or intermittent source rather than an instantaneous source. If $\overline{P}(z_{ob},t)$ may be considered a residence time distribution, it is the same regardless of whether the source is instantaneous, intermittent, or continuous. This is not true when $\overline{P}(z_{ob},t)$ is considered the tracer concentration.

Little work has been done to develop techniques for analyzing $\overline{P}(z,t)$ as a residence time distribution when $z/a \ll Pe$. Tsai and Holley (1978) derive temporal moment equations in a manner analogous to the moment method developed by Aris (1956). Through a numerical solution of the moment equations, they compare spatial and temporal moments for a tracer concentration distribution in open

channel flow. In this paper we derive approximate analytical expressions for

$$\langle t(z)\rangle = \int_0^\infty t\bar{P}(z,t)dt$$

$$\langle t^2(z)\rangle = \int_0^\infty t^2\bar{P}(z,t)dt - (\langle t(z)\rangle)^2$$

which are derived under the condition that interaction between the tracer and the capillary wall is negligible. A Monte Carlo simulation of particle trajectories is developed to calculate moments of the residence time distribution and the full distribution $\bar{P}(z,t)$.

C.2 Governing Equations

The governing equation for the probability density of a particle's position in Poiseuille flow is the advection diffusion equation, which in standard cylindrical coordinates is:

$$\frac{\partial P}{\partial t} + u(r)\frac{\partial P}{\partial z} = D\left(\frac{\partial^2 P}{\partial z^2} + \frac{\partial^2 P}{\partial r^2} + \frac{1}{r}\frac{\partial P}{\partial r} + \frac{1}{r^2}\frac{\partial^2 P}{\partial \theta^2}\right) \qquad (C.7)$$

The velocity profile is $u(r) = 2V(1-r^2/a^2)$, a is the tube radius, V is the mean velocity, and D is the molecular diffusivity. Nondimensionalizing equation (C.1), we find

$$\frac{\partial P}{\partial \hat{t}} + 2(1-\eta^2)\frac{\partial P}{\partial \hat{z}} = \frac{1}{(Pe)^2}\frac{\partial^2 P}{\partial \hat{z}^2} + \frac{\partial^2 P}{\partial \eta^2} + \frac{1}{\eta}\frac{\partial P}{\partial \eta} + \frac{1}{\eta^2}\frac{\partial^2 P}{\partial \theta^2} \qquad (C.8)$$

where $\hat{z} = \frac{Dz}{Va^2}$ $\hat{t} = \frac{Dt}{a^2}$ $\eta = \frac{r}{a}$

and Pe = Va/D is the Peclet number.

When concerned only with the axial distribution of the cross-sectionally averaged probability, equation (C.8) may be averaged over θ. In addition, we will limit the analysis to flows with high Peclet numbers, so longitudinal molecular diffusion may be ignored. Equation (C.8) becomes:

$$\frac{\partial P^*}{\partial \hat{t}} + 2(1-\eta^2)\frac{\partial P^*}{\partial \hat{z}} = \frac{\partial^2 P^*}{\partial \eta^2} + \frac{1}{\eta}\frac{\partial P^*}{\partial \eta} \qquad (C.9)$$

where $P^* = \frac{1}{2\pi}\int_0^{2\pi} P\,d\theta$

Equation (C.9) shows that the cross-sectionally averaged probability density is a function of $\hat{z}$ and $\hat{t}$ and the initial conditions.

When advection dominates longitudinal transport, the main effect of random molecular motion on the axial position of particles is through the coupling of lateral diffusion with the velocity profile. Taylor (1953) successfully investigated the asymptotic (far-field) behavior of a passive tracer's cross-sectionally averaged axial concentration distribution by focusing on the interaction between lateral diffusion and the velocity profile. Transforming to a coordinate system moving with the mean flow, Taylor (1953) shows that the axial mass transport is proportional to the axial concentration

gradient, which leads to an effective advective diffusion equation for the mean flow. No such simple transport equation exists for near-field advective diffusion, though attempts have been made to derive one (Smith 1982a). Numerical calculations for the near field (Gill and Ananthakrishnan 1967; Jayaraj and Subramanian 1978) have shown complex behavior for the cross-sectionally averaged axial concentration distribution, which indicates that a numerical solution may be necessary to calculate the entire distribution. It is possible, though, to derive exact expressions for the mean and variance of the axial distribution which are valid for all distances from the source. These may be derived by taking moments of equation (C.8) (Aris 1956; Barton 1983), or by expanding the solution of equation (C.8) with orthogonal Hermite polynomials (Smith 1982b). Perhaps the most direct method is to use a technique due to Saffman (1960), which has been applied in the present context by Chatwin (1977), who derived approximate expressions for the axial mean and variance when $\hat{t} \ll 1$.

C.3 Analysis of Averaged Quantities

Let $\gamma(r,t;r_0)$ be the probability density for the radial position of a particle released at $r = r_0$, $t = 0$. Then the mean position may be calculated from (Saffman 1960; Chatwin 1977):

$$< V(\tau) > = \int_o^a u(r)\ \gamma(r,\tau;r_o) r dr \qquad (C.10)$$

$$< z(t) > = \int_o^t < V(\tau) > d\tau \qquad (C.11)$$

and the variance with respect to the mean (neglecting longitudinal molecular diffusion),

$$\langle V(\tau)\, V(\tau')\rangle = \int_0^a \int_0^a u(r)u(r')\gamma(r,\tau-\tau';r')\gamma(r',\tau';r_o)rr'drdr' \qquad (C.12)$$

$$\langle z^2(t)\rangle = 2\int_0^t \int_0^\tau \langle V(\tau)\, V(\tau')\rangle\, d\tau' d\tau - (\langle z(t)\rangle)^2 \qquad (C.13)$$

Now, $\gamma(r,t;r_0)$ is the solution of the diffusion equation in a circle with an initial 'ring' source, i.e.,

$$\frac{\partial\gamma}{\partial t} = D\left(\frac{\partial^2\gamma}{\partial r^2} + \frac{1}{r}\frac{\partial\gamma}{\partial r}\right) \qquad (C.14)$$

with boundary and initial conditions,

$$\frac{\partial\gamma}{\partial r} = 0 \quad \text{on} \quad r = a$$

$$\gamma(r,0;r_o) = \frac{1}{r_o}\,\delta(r - r_o)$$

where $\delta(r-r_0)$ is the Dirac delta function.

The solution for any initial axially symmetric distribution is well known (Crank 1956) and in this case gives,

$$\gamma(r,t;r_o) = \frac{2}{a^2}\left\{1 + \sum_{N=1}^{\infty} \mathrm{EXP}(-\alpha_N^2\, Dt)\ \frac{J_o(r\alpha_N)J_o(r_o\alpha_N)}{J_o^2(a\alpha_N)}\right\} \qquad (C.15)$$

where α_N is defined by $J_1(a\,\alpha_N)=0$, and J_0 and J_1 are Bessel functions of order 0 and 1. Using equation (C.15) and performing the integrals in

equations (C.10) through (C.13), the mean and variance may be found to be (in dimensionless form),

$$< \hat{z}(\hat{t}) > = \hat{t} - 8 \sum_{N=1}^{\infty} \left[1 - \mathrm{EXP}(-\beta_N^2 \hat{t}) \right] \frac{J_o(\eta_o \beta_N)}{\beta_N^4 J_o(\beta_N)} \qquad \text{(C.16)}$$

$$< \hat{z}^2 (\hat{t}) > = 128 \sum_{N=1}^{\infty} \beta_N^{-8} \left\{ \hat{t}\beta_N^2 - 1 + \mathrm{EXP}(-\beta_N^2 \hat{t}) \right\} \qquad \text{(C.17)}$$

$$- \frac{16}{3} \sum_{N=1}^{\infty} \left\{ 1 - (1+\beta_N^2 \hat{t})\ \mathrm{EXP}(-\beta_N^2 \hat{t}) \right\} \frac{J_o(\eta_o \beta_N)}{\beta_N^6 J_o(\beta_N)}$$

$$+ 128 \sum_{N=1}^{\infty} \sum_{m \neq N} \frac{(\beta_m^2 + \beta_N^2) J_o(\eta_o \beta_N)}{(\beta_m^2 - \beta_N^2)\beta_N^2 \beta_m^4 J_o(\beta_N)}$$

$$\cdot \left[1 - \frac{\beta_m^2 \mathrm{EXP}(-\beta_N^2 \hat{t}) - \beta_N^2 \mathrm{EXP}(-\beta_m^2 \hat{t})}{\beta_m^2 - \beta_N^2} \right]$$

$$-64 \left\{ \sum_{N=1}^{\infty} \left[1 - \mathrm{EXP}(-\beta_N^2 \hat{t}) \right] \frac{J_o(\eta_o \beta_N)}{\beta_N^4 J_o(\beta_N)} \right\}^2$$

where $\beta_N = a\alpha_N$. Both (C.16) and (C.17) are given in Smith (1982b).

At first thought, one may reason that the average residence time in a section of length z_s may be found by inverting expression (C.16) to solve for t, with $< z(t) > = z_s$. However, this does not give the mean residence time, but the time for the mean position to move a distance z_s. The mean and variance of the residence time distribution are,

$$< t(z) > = \int_0^\infty t\overline{P}(z,t)dt \tag{C.18}$$

$$< t^2(z) > = \int_0^\infty t^2\overline{P}(z,t)dt - (<t(z)>)^2 \tag{C.19}$$

where

$$\overline{P} = \frac{2}{a^2}\int_o^a P^*(z,r,t)rdr$$

$\overline{P}$ is the cross-sectionally averaged probability density function for an instantaneous point source. $\overline{P}$ is normalized such that

$$\int_o^\infty \overline{P}(z,t)dt = 1 \tag{C.20}$$

For $\hat{t} > 1$, we know Taylor's (1953) solution for $\overline{P}(\hat{z},\hat{t})$ applies (Chatwin, 1970). Scaling t by z/V we see that $\hat{z} > 1$ is needed for the asymptotic solution to be valid. Taylor's solution is

$$\overline{P}(\hat{z},\hat{t}) = \frac{1}{\sqrt{\frac{\pi}{12}\hat{t}}} \text{ EXP}\left[\frac{-(\hat{z}-\hat{t})^2}{\hat{t}/12}\right] \tag{C.21}$$

Substituting equation (C.21) into (C.18) and (C.19) gives for the mean and variance

$$< \hat{t}(\hat{z}) > = \hat{z} + 1/24 \tag{C.22}$$

$$< \hat{t}^2(\hat{z}) > = \hat{z}/24 + 1/288 \tag{C.23}$$

As previously stated, an exact solution for $\overline{P}(\hat{z},\hat{t})$ is not available when $\hat{z} << 1$, but an approximate solution for small times due to Chatwin (1976) may be used to investigate the initial behavior of the residence time distribution. Chatwin's solution for a point source located at $r = r_0$ does not take into account interaction between the tracer and the capillary wall, and is limited to $\hat{t} << (1-\eta_o)^2$. For Pe >> 1 and $\hat{t} << (1-\eta_o)^2$, we scale t by z/V_0, which is of the order $(z/V)(1-\eta_o^2)^{-1}$. Substituting, we find the restriction on $\hat{z}$ for Chatwin's solution to be

$$\hat{z} << (1 - \eta_o^2)(1 - \eta_o)^2 \tag{C.24}$$

Chatwin's (1976) approximate solution is:

$$\overline{P}(z,t) = \frac{A}{\pi a^2} \frac{EXP[-(z - V_o t)^2/4Dt]}{2\sqrt{\pi Dt}} \tag{C.25}$$

$$x \left[1 - \frac{4Va}{D} \left(\frac{Dt}{a^2}\right)^{3/2} \frac{(z-V_o t)}{2\sqrt{Dt}} + \frac{8}{3}\left(\frac{V}{D}\right)^2 r_o^2 \left(\frac{Dt}{a^2}\right)^2 \left\{ \frac{(z-V_o t)^2}{2Dt} - 1 \right\}\right]$$

A is determined through normalization (equation (C.20)). Performing the integral in equation (C.18), and nondimensionalizing the solution in terms of $\hat{z}$, η_o, V/V_0, and Pe, we find

$$<\hat{t}(\hat{z})> = \left(\frac{V}{V_o}\right) \hat{z} \cdot \left[1 + 12\left(\frac{V}{V_o}\right)^2 \hat{z} + 64\eta_o^2 \left(\frac{V}{V_o}\right)^3 \hat{z} + 96 \left(\frac{V}{V_o}\right)^3 \frac{1}{(Pe)^2} + 640\eta_o^2 \left(\frac{V}{V_o}\right)^4 \frac{1}{(Pe)^2}\right.$$

$$+ 2\left(\frac{V}{V_o}\right)\frac{1}{\hat{z}}\frac{1}{(Pe)^2} + 240\left(\frac{V}{V_o}\right)^4\frac{1}{\hat{z}}\frac{1}{(Pe)^4} + 1920\eta_o^2\left(\frac{V}{V_o}\right)^5\frac{1}{\hat{z}}\frac{1}{(Pe)^4}\Bigg]$$

$$\times\left[1 + 8\left(\frac{V}{V_o}\right)^2\hat{z} + 32\eta_o^2\left(\frac{V}{V_o}\right)^3\hat{z} + 24\left(\frac{V}{V_o}\right)^3\frac{1}{(Pe)^2} + 128\eta_o^2\left(\frac{V}{V_o}\right)^4\frac{1}{(Pe)^2}\right]^{-1}$$

Now, considering the case where Pe $\to \infty$, we find

$$\langle\hat{t}(\hat{z})\rangle = \left(\frac{V}{V_o}\right)\hat{z}\left\{\frac{1 + \left[12\left(\frac{V}{V_o}\right)^2 + 64\eta_o^2\left(\frac{V}{V_o}\right)^3\right]\hat{z}}{1 + \left[8\left(\frac{V}{V_o}\right)^2 + 32\eta_o^2\left(\frac{V}{V_o}\right)^3\right]\hat{z}}\right\} \qquad (C.26)$$

To neglect longitudinal diffusion for large but finite Peclet number, we have an additional restriction on $\hat{z}$ which is derived from expressions (C.4) or (C.6), depending on the source position. These give restrictions on the downstream distance required such that longitudinal molecular diffusion is negligible. The complete set of restrictions on $\hat{z}$ for use of equation (C.26) are

$$\hat{z} \ll (1 - \eta_o^2)(1 - \eta_o)^2$$

$$\hat{z} \gg Pe^{-2/3} \qquad \text{if} \qquad \eta_o = 0 \qquad (C.27)$$

$$\hat{z} \gg \frac{1 - \eta_o^2}{\eta_o Pe} \qquad \text{if} \qquad (1 - \eta_o)^2\eta_o^3 \gg Pe^{-1}$$

A more convenient nondimensional representation of the mean residence time is $\langle \overline{t}(\hat{z}) \rangle = \langle Vt(z)/z \rangle = \langle \hat{t}(\hat{z}) \rangle/\hat{z}$, since this removes the bias that a longer section will have a larger residence time. A

particle which moves with the mean velocity, V, will have a mean residence time $< \bar{t}(\hat{z}) > = 1$ for any distance downstream. Using this scaling we have,

$$<\bar{t}(\hat{z})> = \frac{V}{V_o}\left\{\frac{1 + \left[12\left(\frac{V}{V_o}\right)^2 + 64\eta_o^2\left(\frac{V}{V_o}\right)^3\right]\hat{z}}{1 + \left[8\left(\frac{V}{V_o}\right)^2 + 32\eta_o^2\left(\frac{V}{V_o}\right)^3\right]\hat{z}}\right\} \qquad (C.28)$$

when $\hat{z} << (1 - \eta_o^2)(1 - \eta_o)^2$ and $Pe \to \infty$

Through a comparison with numerical results (Section C.6), we find for roughly 10% accuracy in $< \bar{t}(\hat{z}) >$

$$\hat{z} \leq 0.1(1 - \eta_o^2)(1 - \eta_o)^2$$

Plots of $< \bar{t}(\hat{z}) >$ vs. $\hat{z}$ are shown in Figure (C.8). The initial behavior of $< \bar{t}(\hat{z}) >$ is to increase with increasing $\hat{z}$, regardless of the position of the source (provided the source is not at the wall). As an example, consider a source located at $\eta_o = 0.8$ so that $V/V_0 = 1.39$. As $\hat{z} \to 0$, we see that $< \bar{t}(\hat{z}) > \to V/V_0 = 1.39$. For $\hat{z} \to \infty$, we know $< \bar{t}(\hat{z}) > \to 1$. Equation (C.28) predicts that $< \bar{t}(\hat{z}) >$ will initially increase beyond 1.39 as $\hat{z}$ increases before eventually decreasing to 1 as $\hat{z} \to \infty$. Further comments on the behavior of the mean residence time will be given in Section C.6 when Monte Carlo simulation results are compared with equation (C.28).

Integrating equation (C.25) for the variance and nondimensionalising as before gives

$$<\hat{t}^2(\hat{z})> = \left(\frac{V}{V_o}\right)^2 \hat{z}^2\left[1 + 16\left(\frac{V}{V_o}\right)^2 \hat{z} + \frac{320}{3}\eta_o^2\left(\frac{V}{V_o}\right)^3\hat{z}\right.$$

$$+ 240\left(\frac{V}{V_o}\right)^3\frac{1}{(Pe)^2} + 1920\eta_o^2\left(\frac{V}{V_o}\right)^4\frac{1}{(Pe)^2} + 6\left(\frac{V}{V_o}\right)\frac{1}{\hat{z}}\frac{1}{(Pe)^2}$$

$$+ 1440\left(\frac{V}{V_o}\right)^4\frac{1}{\hat{z}}\frac{1}{(Pe)^4} + 13440\eta_o^2\left(\frac{V}{V_o}\right)^5\frac{1}{\hat{z}}\frac{1}{(Pe)^4} + 12\left(\frac{V}{V_o}\right)^2\frac{1}{\hat{z}^2}\frac{1}{(Pe)^4}$$

$$+ 3360\left(\frac{V}{V_o}\right)^5\frac{1}{\hat{z}^2}\frac{1}{(Pe)^6} + 35840\left(\frac{V}{V_o}\right)^6\frac{1}{\hat{z}^2}\frac{1}{(Pe)^6}\Bigg] x$$

$$\left[1 + 8\left(\frac{V}{V_o}\right)^2\hat{z} + 32\eta_o^2\left(\frac{V}{V_o}\right)^3\hat{z} + 24\left(\frac{V}{V_o}\right)^3\frac{1}{(Pe)^2} + 128\eta_o^2\left(\frac{V}{V_o}\right)^4\frac{1}{(Pe)^2}\right]^{-1}$$

$$- \left(<\hat{t}(\hat{z})>\right)^2$$

Taking the limit Pe → ∞, we find

$$<\hat{t}^2(\hat{z})> = \frac{\frac{32}{3}\eta_o^2\left(\frac{V}{V_c}\right)^5\hat{z}^3}{1+\left[16\left(\frac{V}{V_o}\right)^2 + 64\eta_o^2\left(\frac{V}{V_o}\right)^3\right]\hat{z}} \qquad (C.29)$$

Note that at this level of approximation, the first-order correction to the variance for a source on the axis ($\eta_o = 0$) does not appear. Equation (C.29) is restricted to the range of $\hat{z}$ given in expression (C.27). In the following sections a Monte Carlo method is derived which numerically solves equation (C.9). The method is used to calculate both axial distributions and residence time distributions.

C.4 A Monte Carlo Method for Axial Dispersion in Poiseuille Flow

An approximate method for modelling the longitudinal motion of a particle in Poiseuille flow is to allow the particle to make a series

of longitudinal steps for a fixed time step Δt. Neglecting axial molecular diffusion, the length of the ith longitudinal step is

$$\Delta z_i = u(r_i)\Delta t \tag{C.30}$$

The key is to select r_i from the appropriate distribution for a given time step Δt, and previous radial coordinate r_{i-1}. This selection is governed by equation (C.15), which in this case is (in dimensionless form),

$$\gamma(\eta_i, \Delta\hat{t}; \eta_{i-1}) = \frac{2}{a^2}\left\{1 + \sum_{N=1}^{\infty} \mathrm{EXP}(-\beta_N^2\,\Delta\hat{t})\ \frac{J_o(\eta_i\beta_N)J_o(\eta_{i-1}\beta_N)}{J_o^2(\beta_N)}\right\} \tag{C.31}$$

Integrating equation (C.31) over the cross section from 0 to η_i gives

$$S(\eta_i, \Delta\hat{t}; \eta_{i-1}) = \eta_i^2 + 2\eta_i \sum_{N=1}^{\infty} \frac{\mathrm{EXP}(-\beta_N^2\,\Delta\hat{t})}{\beta_N}\ \frac{J_1(\eta_i\beta_N)J_o(\eta_{i-1}\beta_N)}{J_o^2(\beta_N)} \tag{C.32}$$

where S is the cumulative probability distribution. For a fixed time step we invert equation (C.32) to give

$$\eta_i = g(S, \eta_{i-1}) \tag{C.33}$$

Since S is the cumulative probability distribution, it represents the probability that the new radial position of the particle will be less than or equal to η_i, given that the initial radial position is η_{i-1}. For a fixed η_{i-1}, S varies monotonically with η_i between S(0) = 0 and S(1) = 1. The probability that S will lie between any two values, say S_2 and S_1 is $|S_2 - S_1|$. Since the probability that S lies within any

interval is equal to the size of the interval, S is uniformly distributed between 0 and 1.

The algorithm for each step is to generate a uniform random number for S and using η_{i-1} solve for η_i. Equation (C.30) may then be used to calculate the amount of axial motion for each time step. As to the selection of the time step, it is not possible to say *a priori* how large a step may be used, but the results can always be checked by the exact analytical results given by equations (C.16) and (C.17). Restrictions on the time step are based upon accuracy requirements since the solution is stable for any time step. We have found the time step $\Delta\hat{t} = 0.001$ to be sufficiently small for the calculations done here. Generating random values of η_i from equation (C.33) turns out to be too slow for practical calculations, so a large table of values have been computed, from which η_i could be accurately estimated by four-point interpolation. A grid of g(201,51) is used to approximate equation (C.33), the finer divisions in S being necessary since g changes rapidly near S = 0 and S = 1. Uniform random numbers are generated by combining two linear congruential random number generators to produce a third "ultra" random sequence. This technique, attributed to MacLaren and Marsaglia, is discussed in Knuth (1969). Axial and residence time distributions are produced by computing simple histograms of the particle positions or times and filtering the resulting distribution with a numerical lopas filter, which removes high frequency Monte Carlo "noise" from the distribution.

The calculation procedure presented here may be extended to include longitudinal molecular diffusion. To do this, a stochastic longitudinal step, Δz_{Di}, is chosen from a Gaussian distribution with a mean of 0 and a variance $\sigma_z^2 = 2D\Delta t$. Equation (C.30) becomes

$$\Delta z_i = u(r_i)\Delta t + \Delta z_{Di}$$

As stated in section 1, when longitudinal molecular diffusion is important at the observation point, z_{ob}, $\overline{P}(z_{ob},t)$ fails to qualify as a residence time distribution. With the Monte Carlo technique, it is possible to calculate a residence time distribution based on a definition suitable to the application. For example, if the distribution in time when particles first pass z_{ob} is desired, it is very easy to set up the Monte Carlo routine to do this.

In general, the Monte Carlo method described here is attractive when an analytical solution to the diffusion equation in the cross section is available. Except for this restriction, the method is very flexible and can easily accommodate any velocity field or time-dependent phenomena. For example, it is possible to have an oscillating flow or flow through a converging-diverging tube, provided the cross section maintains a constant shape. The velocity field, which must be known for all positions and times, is always superimposed on the random motion. Turbulent flow may be modeled as well, if the

assumption of a constant transverse turbulent diffusivity is used. Calculations for turbulent flow in tubes of circular cross section may be done by changing from the laminar velocity profile to the mean turbulent velocity profile. Everything else carries through as before, including the "diffusion table," $g(S, \eta_{i-1})$. The calculations which produced $g(S, \eta_{i-1})$ are independent of the specific value of the diffusion coefficient (molecular or turbulent), due to the dimensionless nature of equation (C.32).

The Monte Carlo method has been previously used in studies of turbulent diffusion (Kraichnan 1970), for longitudinal dispersion in turbulent open channel flow (Sullivan 1971), and for longitudinal dispersion in laminar flows (Dewey and Sullivan 1982). The technique as presented here is somewhat different in that exact analytical results are used to model the random motions. It is essentially a numerical technique for solving equation (C.9). It is of some interest to see how well this technique can perform when no assumptions are involved and exact calculations are available for comparison. In addition, the Monte Carlo method has some advantages over standard numerical solution techniques. It contains no numerical dispersion, is absolutely stable, can exactly simulate delta function sources in space and time, and is extremely simple to implement on a computer.

C.5 Results of Calculations: Axial Profiles at a Given Time

Axial profiles provide an opportunity to check the calculations against the theoretical results given by equations (C.16) and (C.17) and

with other numerical results. Table C.1 summarizes the calculations for axial mean and variance, and is seen to be within 1% for the mean and 2% for the variance in most cases. Previous published work (Chatwin 1970; Gill and Ananthakrishnan 1967) have used an instantaneous spike source uniformly distributed over the cross section as a characteristic example. To produce this type of initial distribution most easily, we would like to introduce particles uniformly over the cross section in a random fashion (the AREA source in Table C.1). The probability for a particle to enter the tube at a given radius η within a differential range $d\eta$ is in proportion to the differential area $\eta d\eta$. Since the problem has axial symmetry, the initial angular position in the cross section is not important. The cumulative distribution is:

$$S(\eta_o) = 2\int_o^{\eta_o} \eta d\eta = \eta_o^2$$

To select initial coordinates, η_o , from the appropriate distribution, η_o is chosen randomly as the square root of a uniformly distributed random number. Figure C.1 shows the Monte Carlo calculations for a short time ($\hat{t} = 0.01$) after release of the tracer particles. Plotted along with this is the solution for pure advection, which in terms of the dimensionless variables $\hat{z}$ and $\hat{t}$ is (Chatwin 1970),

$$\overline{P}(\hat{z},\hat{t}) = \frac{1}{2\hat{t}}\, f(\sqrt{1 - \hat{z}/2\hat{t}}) \qquad 0 \leq \hat{z} \leq 2\hat{t} \tag{C.34}$$

$$\overline{P}(\hat{z},\hat{t}) = 0 \qquad \text{OTHERWISE}$$

Table C.1

Axial Distribution Data

Source Location	Dimensionless Time $\hat{t}$	Monte Carlo Average $\langle\hat{z}(\hat{t})\rangle$	Theoretical Average $\langle\hat{z}(\hat{t})\rangle$	Monte Carlo Variance $\langle\hat{z}^2(\hat{t})\rangle$	Theoretical Variance $\langle\hat{z}^2(\hat{t})\rangle$
0.0	0.01	0.01969	0.01960	0.9410 (-7)	0.1069 (-6)
0.0	0.05	0.09006	0.09031	0.6475 (-4)	0.6410 (-4)
0.0	0.10	0.1623	0.1622	0.7016 (-3)	0.7041 (-3)
0.0	0.20	0.2780	0.2784	0.003963	0.003949
0.0	0.30	0.3812	0.3822	0.008099	0.008079
0.0	0.50	0.5817	0.5833	0.01652	0.01648
0.67	0.01	0.01073	0.01072	0.4717 (-5)	0.4745 (-5)
0.67	0.05	0.05008	0.04997	0.3354 (-3)	0.3361 (-3)
0.67	0.10	0.09873	0.09849	0.001447	0.001443
0.67	0.20	0.1968	0.1973	0.004917	0.004845
0.67	0.30	0.2958	0.2970	0.008895	0.008816
0.67	0.50	0.4950	0.4969	0.01717	0.01709
1.0	0.01	0.002699	0.002714	0.2118 (-5)	0.2119 (-5)
1.0	0.05	0.02644	0.02643	0.1629 (-3)	0.1654 (-3)
1.0	0.10	0.06700	0.06691	0.8809 (-3)	0.8823 (-3)
1.0	0.20	0.1596	0.1603	0.003736	0.003711
1.0	0.30	0.2574	0.2588	0.007463	0.007458
1.0	0.50	0.4562	0.4584	0.01550	0.01564
AREA*	0.01	0.01005	0.01000	0.3108 (-4)	0.3177 (-4)
AREA	0.05	0.05023	0.05000	0.6146 (-3)	0.6295 (-3)
AREA	0.10	0.1003	0.1000	0.001975	0.002024
AREA	0.20	0.1994	0.2000	0.005627	0.005702
AREA	0.30	0.2986	0.3000	0.009614	0.009756
AREA	0.50	0.4979	0.5000	0.01779	0.01806

*Equivalent to an instantaneous source uniformly distributed over the cross section

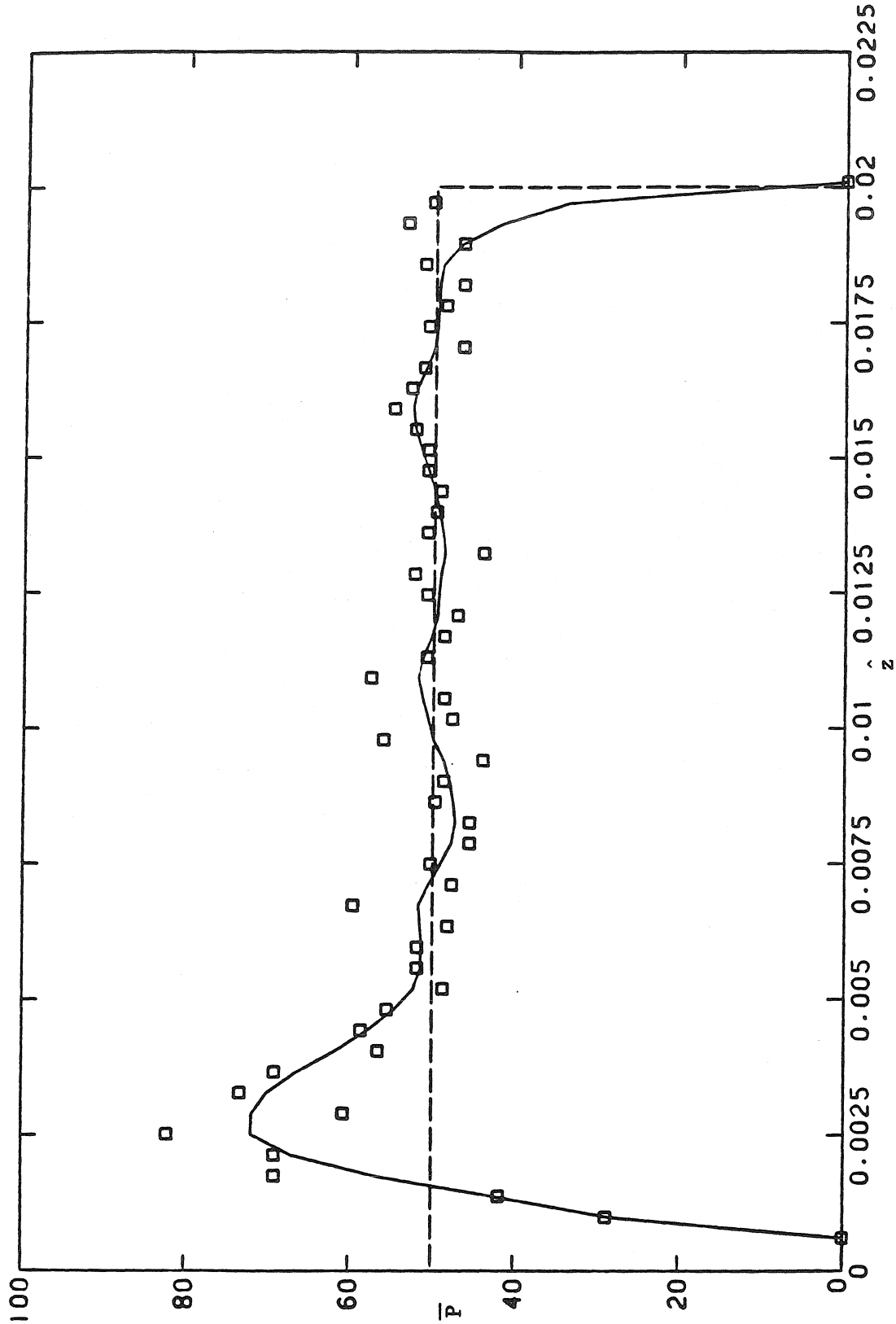

FIGURE C.1

Axial distribution, area source: probability density, $\bar{P}$, vs. axial distance, $\hat{z}$. □, Monte Carlo (unfiltered) 5000 particles; ———, Monte Carlo (filtered), – – – –, equation (C.35), $\hat{t} = 0.01$.

where $f(\eta)$ is the initial radial distribution of tracer at $\hat{t} = 0$ and $\hat{z} = 0$, subject to the condition

$$2\int_0^1 f(\eta)\eta d\eta = 1$$

For the present case $f(\eta) = 1$, and the pure advection solution is

$$\bar{P}(\hat{z},\hat{t}) = \frac{1}{2\hat{t}} \qquad 0 \leq \hat{z} \leq 2\hat{t}$$

$$\bar{P}(\hat{z},\hat{t}) = 0 \qquad \text{OTHERWISE} \tag{C.35}$$

The peak lagging the mean in Figure C.1 is in agreement with intuitive arguments put forward by Chatwin (1970) regarding the effects of preferential, radially inward diffusion of particles initiated near the capillary wall. Figure C.2a compares the finite difference calculations of Gill and Ananthakrishnan (1967) with the current Monte Carlo calculations. The two calculations compare very closely, with the finite difference solution showing slightly lower peak values with greater spreading at the tails of the distribution. These differences may be the result of inclusion of longitudinal molecular diffusion in the finite difference calculations. As is evident from Figures C.1 and C.2, the unfiltered Monte Carlo histogram contains a great deal of high frequency noise which results from the estimation of a probability density function from a finite set of discrete samples. Figure C.2b shows the effect of doubling the number of particles and

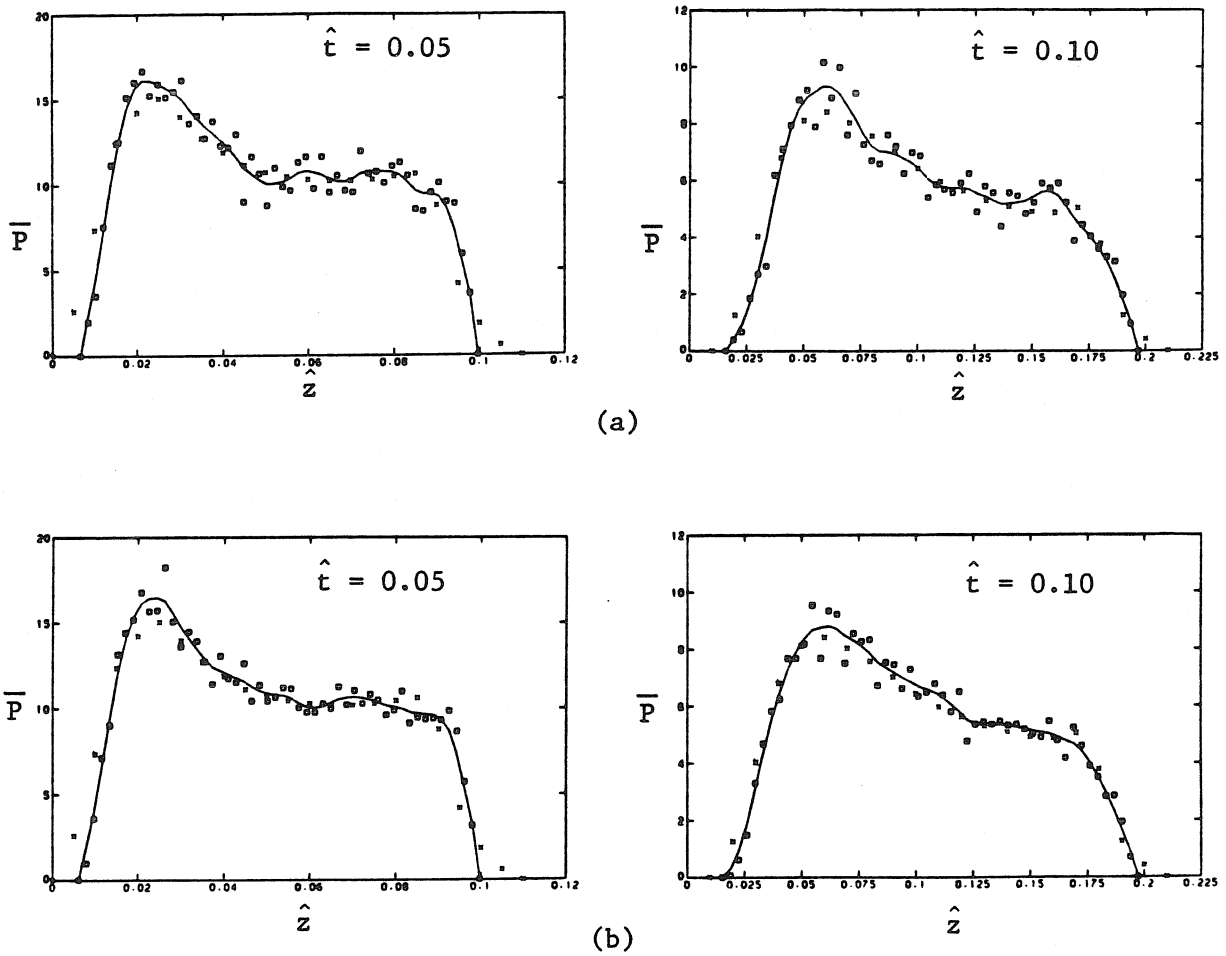

FIGURE C.2

Axial distributions, area source: probability density, $\overline{P}$, vs. axial distance, $\hat{z}$. □ , Monte Carlo (unfiltered), (a) 5000 particles, (b) 10000 particles, ———, Monte Carlo (filtered); x, finite difference Gill and Ananthakrishnan (1967)

indicates that the Monte Carlo solution is less reliable for high frequency information. The various small "bumps" in the filtered Monte Carlo solution should be considered residual noise which is passed through the lopas numerical filter. Figure C.3 shows a sequence of distributions from $\hat{t} = 0.01$ to $\hat{t} = 0.5$. Taylor's (1953) asymptotic Gaussian solution (equation (C.21)) is plotted along with the Monte Carlo solutions. The Monte Carlo distribution and the Gaussian solution are seen to match relatively well by the time $\hat{t} = 0.3$, which is in agreement with a prediction of Chatwin (1970) that the Gaussian limit is applicable beyond $\hat{t} = 0.25$.

The solution for the axial distribution from a point source at any initial radial position can also be calculated using the Monte Carlo technique. Figure C.4 shows the progression of the axial distribution from an instantaneous point source with $\eta_o = 0$. From Table C.1, it is seen that all the mean values have small error ($< 1\%$), while a fairly large error occurs in the variance of the first distribution. This more substantial error is a result of the highly skewed shape of the distribution, for which a small error in representing its long tail results in a large error in the variance. As the distribution becomes more symmetric and approaches a Gaussian shape, errors in the variance are reduced. This is consistent with theoretical requirements that errors in the mean go to zero as $1/\sqrt{N}$ for any distribution, while errors in the variance are guaranteed to go to zero as $\sqrt{2/N}$ only for a Gaussian distribution , N being the number of samples from the distribution (Hammersley and Handscomb 1979). The

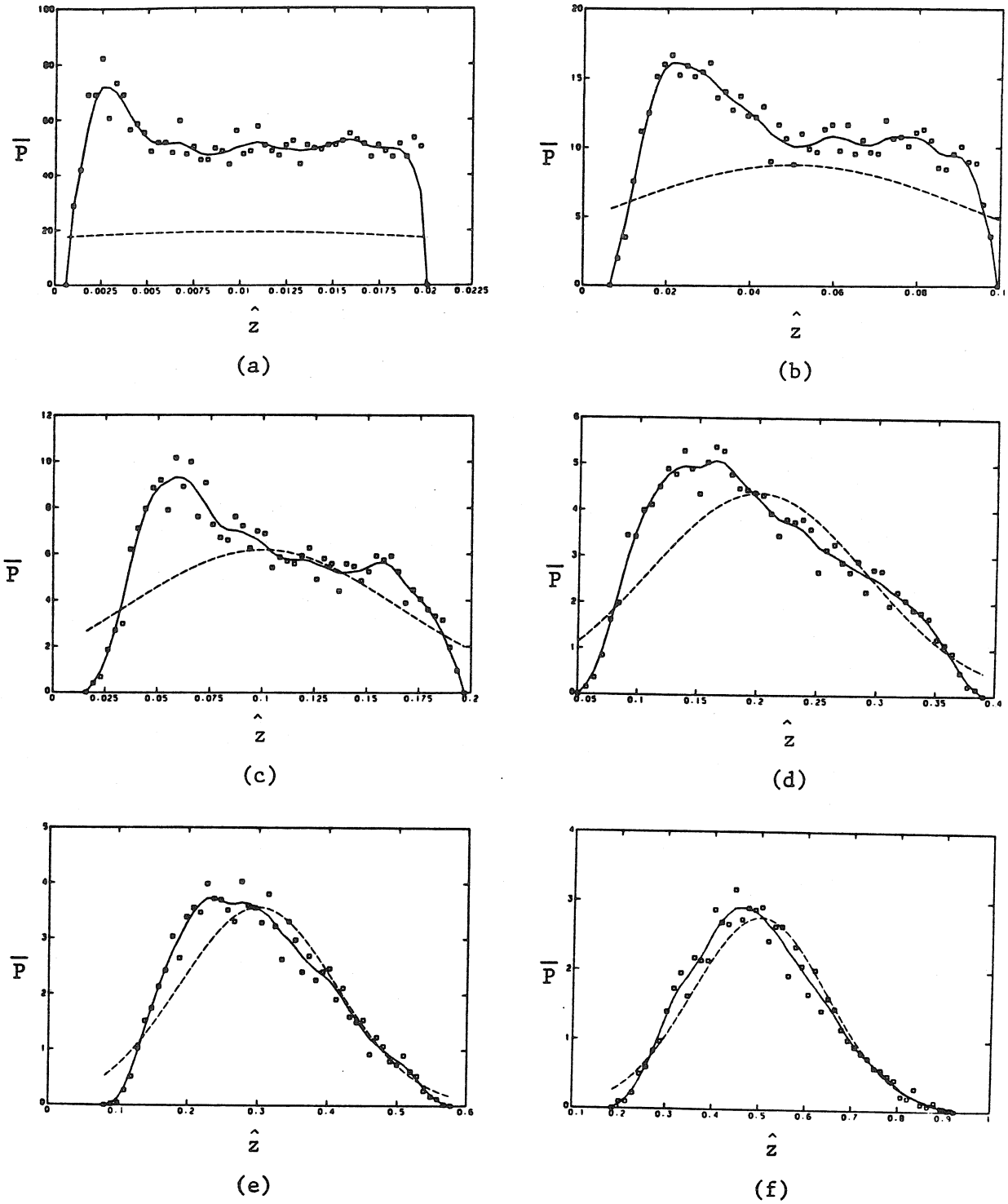

FIGURE C.3

Axial distributions, area source: probability density, $\overline{P}$, vs. axial distance, $\hat{z}$. □ , Monte Carlo (unfiltered), 5000 particles; ———, Monte Carlo (filtered); -----, equation (C.21). Times: (a) $\hat{t} = 0.01$, (b) $\hat{t} = 0.05$, (c) $\hat{t} = 0.10$, (d) $\hat{t} = 0.20$, (e) $\hat{t} = 0.30$, (f) $\hat{t} = 0.50$.

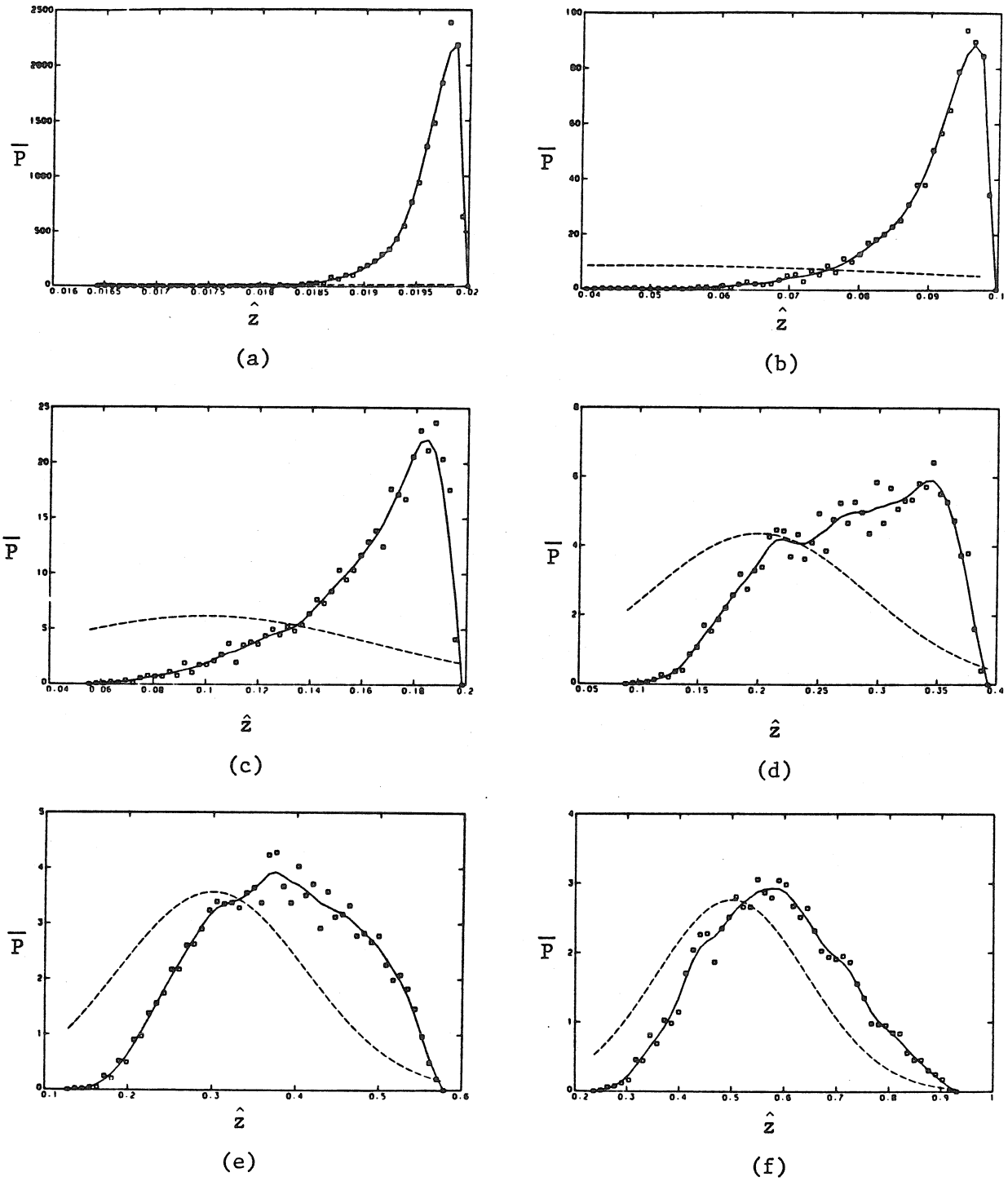

FIGURE C.4

Axial distributions, point source, $\eta_o = 0$: probability density, $\overline{P}$, vs. axial distance, $\hat{z}$. □, Monte Carlo (unfiltered), 5000 particles; ———, Monte Carlo (filtered); -----, equation (C.21). Times: (a) $\hat{t} = 0.01$, (b) $\hat{t} = 0.05$, (c) $\hat{t} = 0.10$, (d) $\hat{t} = 0.20$, (e) $\hat{t} = 0.30$, (f) $\hat{t} = 0.50$.

development of a "knee" in the distribution at $\hat{t} = 0.2$ is a result of interaction between the capillary wall and the radially diffusing tracer. At $\hat{t} = 0.1$, the capillary wall lies roughly 2.2 standard deviations from the source position, while at $\hat{t} = 0.2$, the wall is within 1.6 standard deviations. This means roughly 10% of the particles have diffused to the wall when $\hat{t} = 0.2$, compared to about 2% at $\hat{t} = 0.1$. Being unable to diffuse further out, the particles begin to migrate radially inward. The axial position of particles which have traversed the cross section should be roughly equal to the cross sectional mean velocity, V, times t, which in dimensionless terms means $\hat{z} = \hat{t}$. This corresponds closely to the location of the knee.

C.6 Results of Calculations: Residence Time Distributions

Residence time distributions provide the complement of axial distributions, being the distribution of the particle's probability density over time at a fixed location. This viewpoint is by far the most common in experimental work. Rather than introducing particles uniformly in the cross section as we did for axial distributions, a more interesting problem is to allow particles to enter in proportion to the flux along a given streamline. This will model a uniform flux of tracer particles along the tube, where we are interested in the residence time for the particles in a particular axial section. For example, a well-mixed solution pumped through a short tube under steady-state conditions would be represented by this initial condition, neglecting end effects. The probability that a particle will enter the

axial section at a given radius η within a differential range $d\eta$ is $(1-\eta^2)\eta\, d\eta$ (Saffman 1959). The cumulative distribution is

$$S(\eta_o) = 4\int_o^{\eta_o} (1-\eta^2)\eta d\eta \qquad (C.36)$$

therefore,

$$\eta_o^2 = 1 - \sqrt{1-S}$$

Now if S is a uniform random number, it has the same distribution as 1-S so

$$\eta_o = \sqrt{1-\sqrt{S}}$$

Figure C.5 shows the comparison of the pure advection solution with Monte Carlo. From equation (C.36) it is seen that $f(\eta) = 2(1-\eta^2)$. Substituting into equation (C.34), we find for pure advection,

$$\overline{P}(\hat{z},\hat{t}) = \hat{z}/2\hat{t}^2 \qquad 0 \leq \hat{z} \leq 2\hat{t}$$

$$\overline{P}(\hat{z},\hat{t}) = 0 \qquad \text{OTHERWISE} \qquad (C.37)$$

Advection is seen to be the prime phenomenon that initially shapes the residence time distribution. Figure C.6 shows the sequence of distributions starting at $\hat{z} = 0.01$ through $\hat{z} = 0.5$. Taylor's (1953) asymptotic solution (equation (C.32)) is again plotted along with the Monte Carlo solution. By $\hat{z} = 0.5$, the asymptotic solution is a reasonable approximation. Figure C.7 shows the sequence of

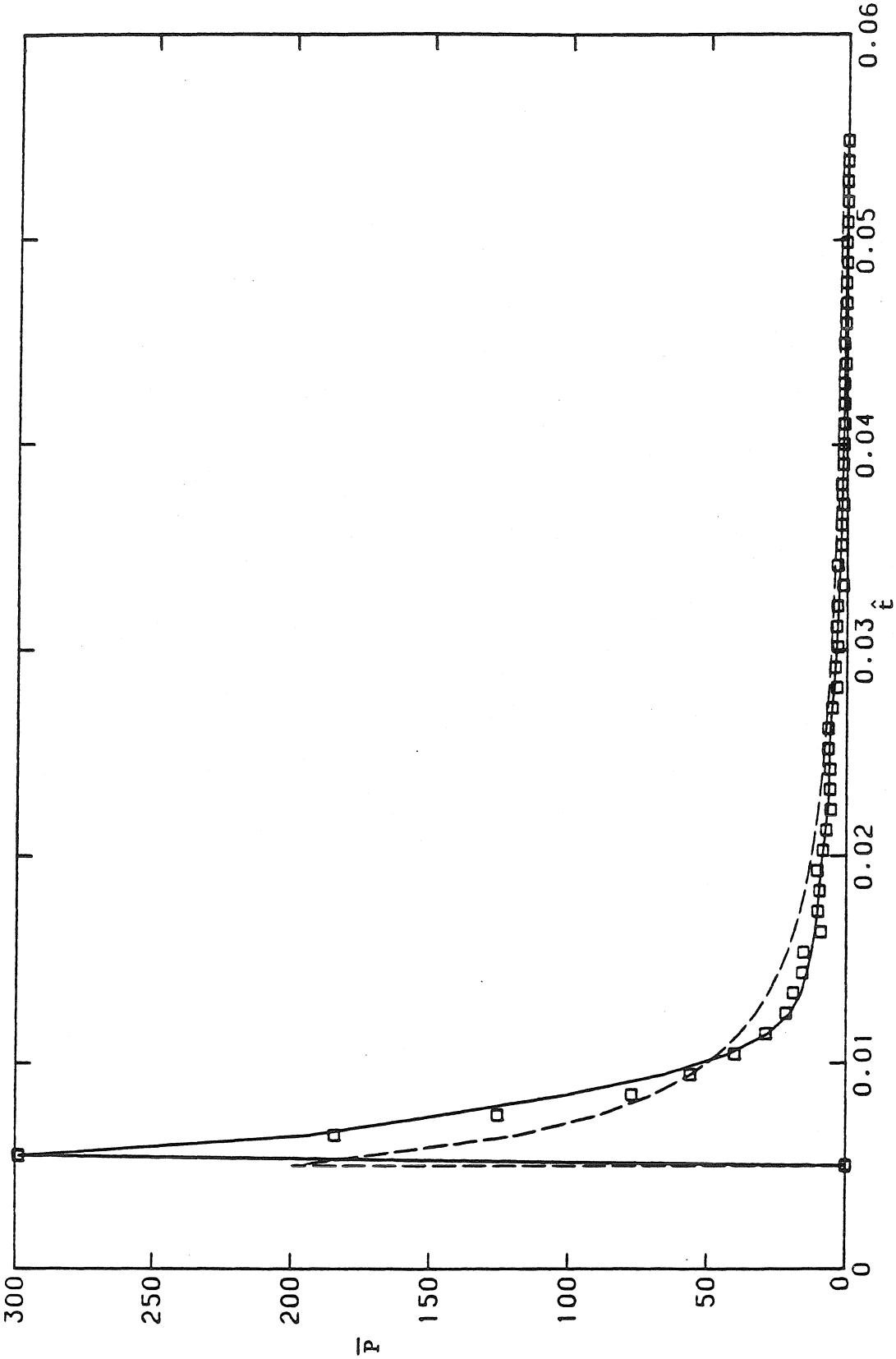

FIGURE C.5

Residence time distribution, flux source: probability density, $\bar{P}$, vs. residence time, $\hat{t}$. $\hat{}$, $\square$, Monte Carlo (unfiltered), 5000 particles; ——, Monte Carlo (filtered); - - - - -, equation (C.37). $z = 0.01$.

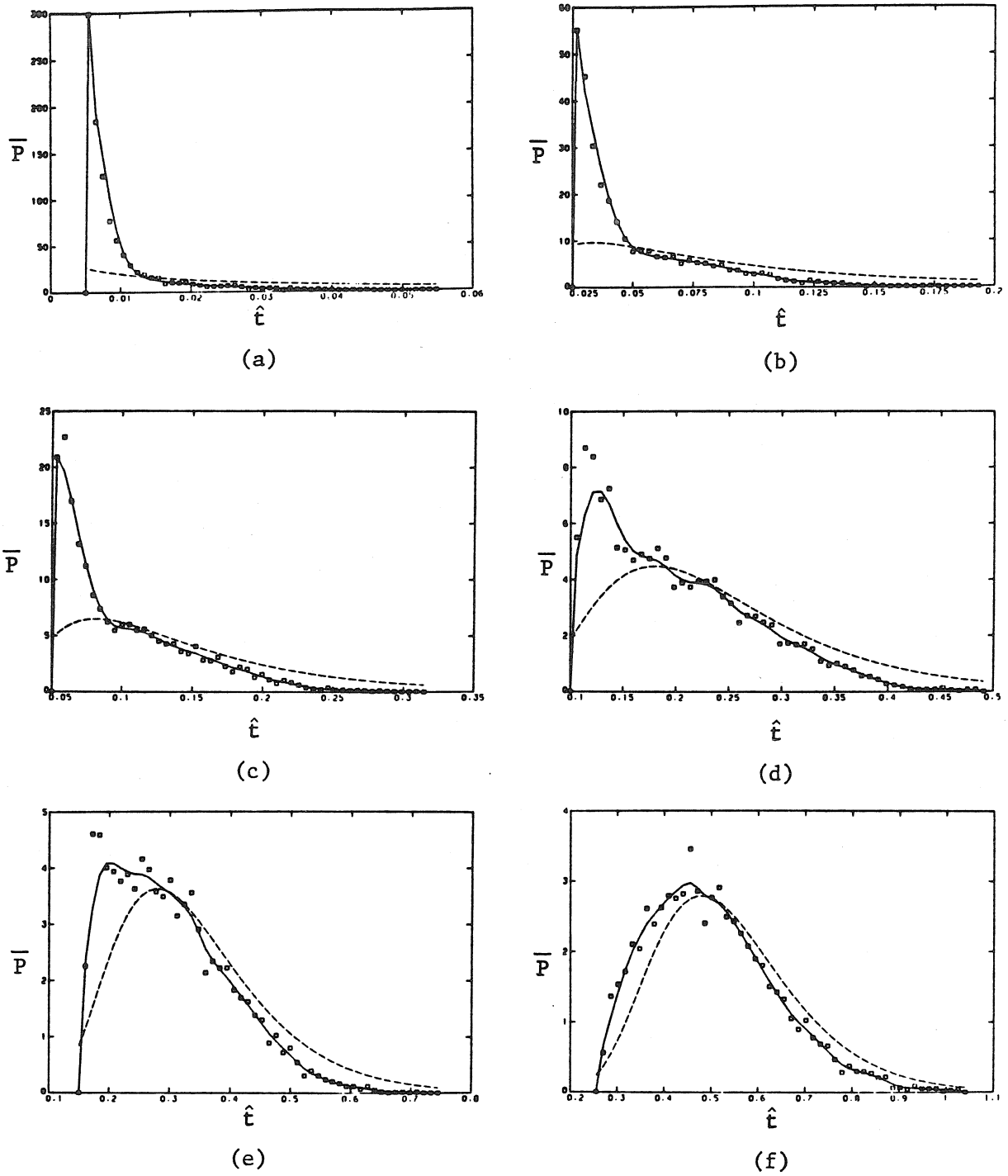

FIGURE C.6

Residence time distributions, flux source: probability density, $\overline{P}$, vs. residence time, $\hat{t}$. □, Monte Carlo (unfiltered), 5000 particles; ———, Monte Carlo (filtered); -----, equation (C.21). Locations: (a) $\hat{z}$ = 0.01, (b) $\hat{z}$ = 0.05, (c) $\hat{z}$ = 0.10, (d) $\hat{z}$ = 0.20, (e) $\hat{z}$ = 0.30, (f) $\hat{z}$ = 0.50.

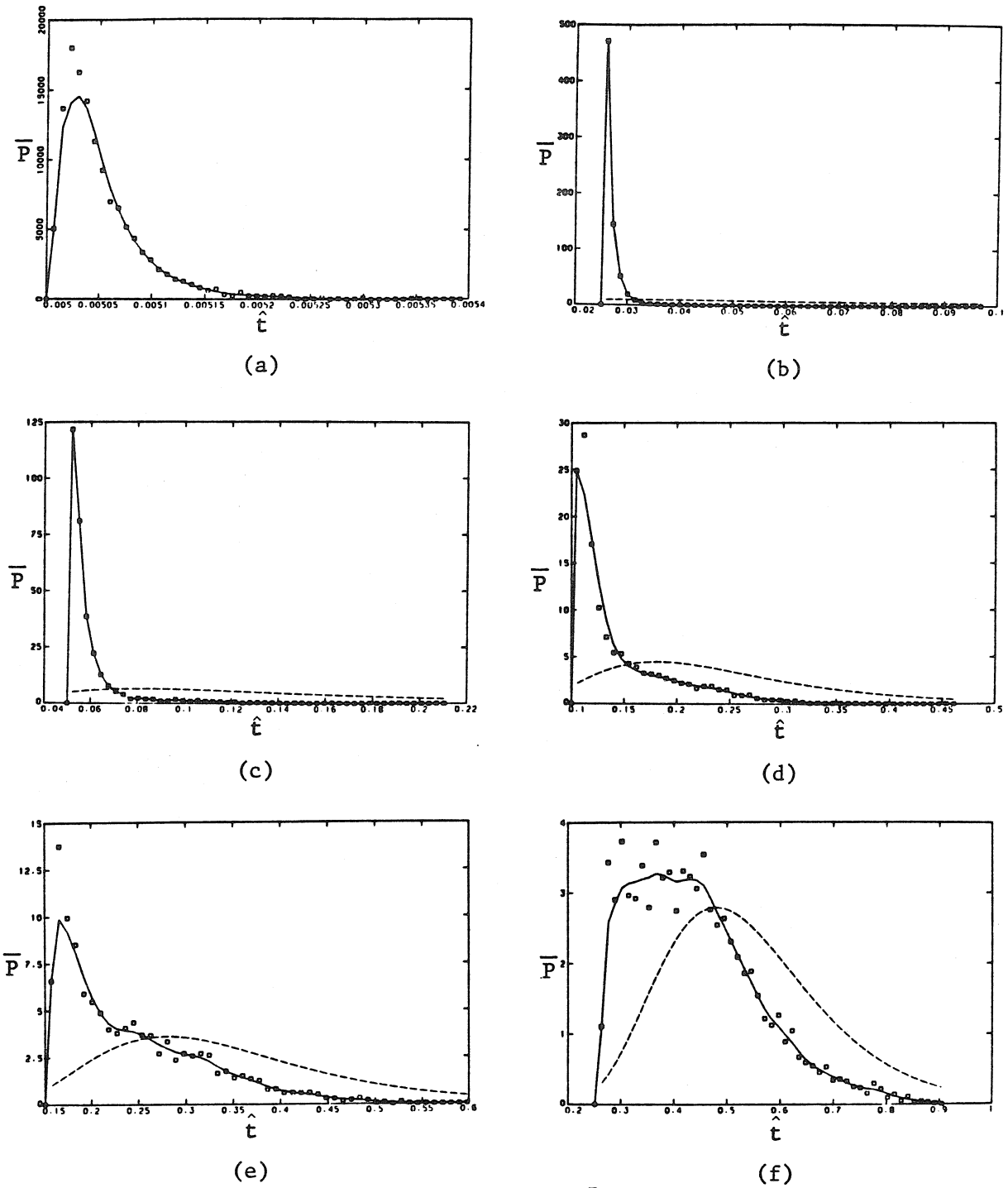

FIGURE C.7

Residence time distributions, point source, $\eta_o = 0$: probability density, $\overline{P}$, vs. residence time, $\hat{t}$. □, Monte Carlo (unfiltered), 5000 particles; ———, Monte Carlo (filtered); -----, equation (C.21). Locations (a) $\hat{z} = 0.01$, (b) $\hat{z} = 0.05$, (c) $\hat{z} = 0.10$, (d) $\hat{z} = 0.20$, (e) $\hat{z} = 0.30$, (f) $\hat{z} = 0.50$.

distributions from a point source at $\eta_o = 0$ to successively more distant axial stations. Note the sharpening of the peak between $\hat{z} = 0.01$ and $\hat{z} = 0.05$. As in the case with a flux source, the residence time distributions are skewed to the right, a feature found in all residence time distributions investigated. Table C.2 displays some statistical properties of the residence time distributions calculated with the Monte Carlo model. The median residence time, $\hat{t}_{50}(\hat{z})$ in Table C.1, is the time for 50% of the particles to pass the downstream position $\hat{z}$. For the uniform "flux" case at the nearest station ($\hat{z} = 0.01$), the residence time distribution is highly skewed, having 50% of the particles pass through the section in a time roughly 30% less than the mean residence time. As the distance to the downstream section increases, the median moves closer to the mean (in a relative sense) and the distribution becomes more symmetric.

The mean residence time as a function of axial distance for various source positions is shown in Figure C.8. The mean residence time here is nondimensionalized as $< \overline{t}(\hat{z}) > = < Vt(z)/z > = < \hat{t}(\hat{z}) >/\hat{z}$. The approximate theoretical solution obtained earlier (equation (3.19)) is shown with the Monte Carlo solution. The approximate solution is seen to maintain roughly 10% accuracy if $\hat{z} \leq 0.1(1 - \eta_o^2)(1 - \eta_o)^2$. Since the dimensionless mean residence time, $< \overline{t}(\hat{z}) >$, will always initially rise (except for a source at the wall), and since $< \overline{t}(\hat{z}) > \to 1$ as $\hat{z} \to \infty$, particles starting out on streamlines slower than the mean velocity must necessarily display a maximum at some intermediate $\hat{z}$. As it turns out, particles started on streamlines somewhat faster than the

Table C.2

Residence Time Distribution Data

Source Location	Dimensionless Distance $\hat{z}$	Monte Carlo Average $\langle\hat{t}(\hat{z})\rangle$	Monte Carlo Median $\hat{t}_{50}(\hat{z})$	Monte Carlo Variance $\langle\hat{t}^2(\hat{z})\rangle$
0.0	0.01	0.005052	0.005040	0.1700 (-8)
0.0	0.05	0.02661	0.02602	0.5200 (-5)
0.0	0.10	0.05919	0.05464	0.2061 (-3)
0.0	0.20	0.1437	0.1222	0.002274
0.0	0.30	0.2401	0.2180	0.005764
0.0	0.50	0.4375	0.4223	0.01401
0.67	0.01	0.01033	0.009178	0.1558 (-4)
0.67	0.05	0.05970	0.05021	0.7059 (-3)
0.67	0.10	0.1162	0.1071	0.002109
0.67	0.20	0.2215	0.2126	0.005130
0.67	0.30	0.3229	0.3123	0.009575
0.67	0.50	0.5245	0.5094	0.01829
1.0	0.01	0.02886	0.02737	0.1023 (-3)
1.0	0.05	0.09100	0.08736	0.8942 (-3)
1.0	0.10	0.1518	0.1477	0.002263
1.0	0.20	0.2598	0.2528	0.005764
1.0	0.30	0.3617	0.3546	0.009834
1.0	0.50	0.5641	0.5523	0.01850
FLUX*	0.01	0.009813	0.007144	0.4706 (-4)
FLUX	0.05	0.04920	0.03814	0.6995 (-3)
FLUX	0.10	0.09978	0.08323	0.002117
FLUX	0.20	0.1996	0.1846	0.005534
FLUX	0.30	0.2997	0.2850	0.009631
FLUX	0.50	0.5006	0.4833	0.01835

*Equivalent to a steady-state, uniformly mixed source of particles entering the capillary tube

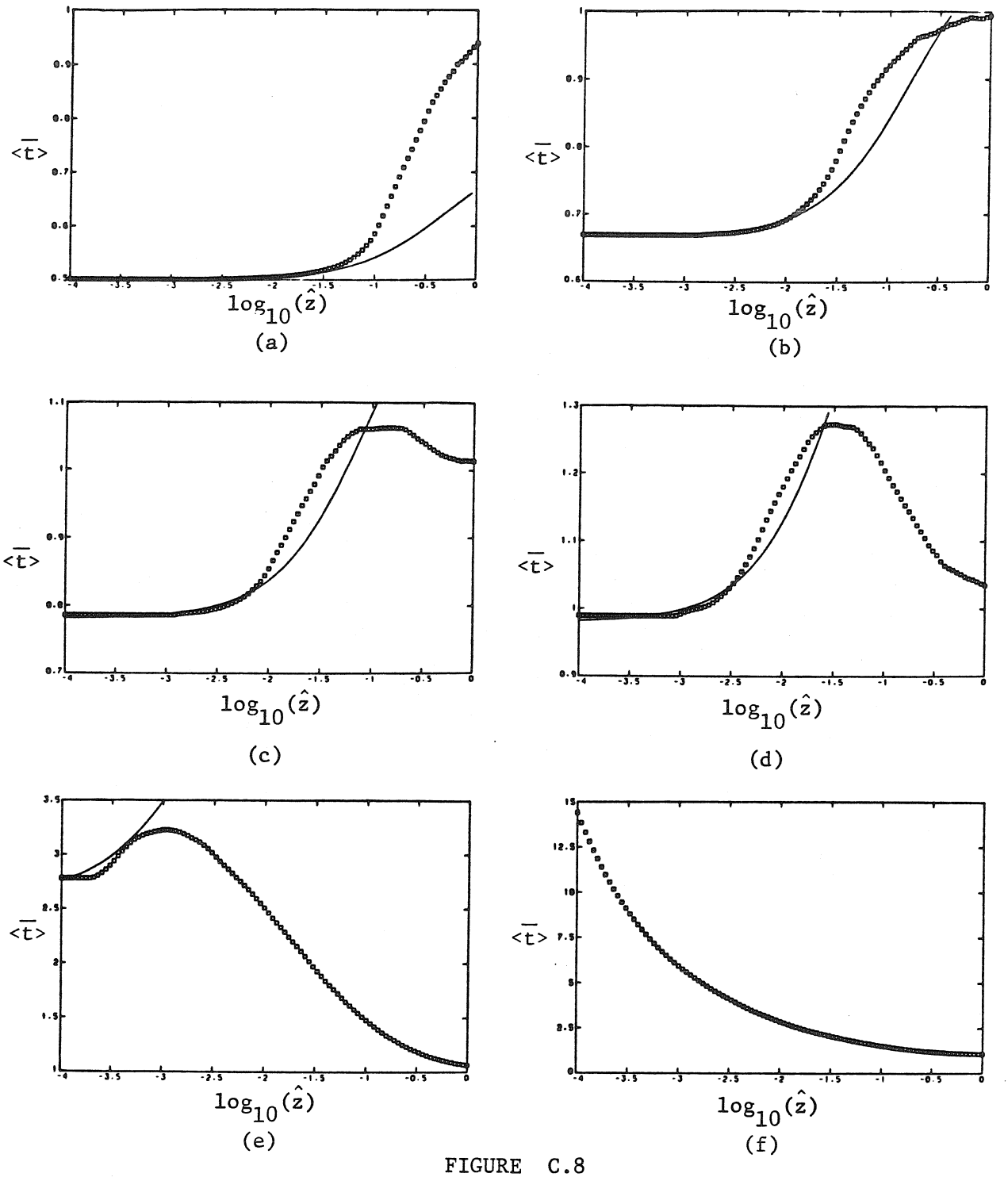

FIGURE C.8

Mean residence time, $\overline{<t(\hat{z})>}$, vs. $\log_{10}(\hat{z})$. □, Monte Carlo (unfiltered), 2000 particles; ———, equation (C.28). Locations (a) $\eta_o = 0$, (b) $\eta_o = 0.5$, (c) $\eta_o = 0.6$, (d) $\eta_o = 0.7$, (e) $\eta_o = 0.9$, (f) $\eta_o = 1.0$.

mean also display this maximum behavior since the initial rise in the mean residence time may exceed 1.

The initial rise in mean residence time is intuitively easy to understand. Consider a linear velocity profile with a continuous point source of tracer material being measured at a fixed downstream station. Particles diffusing into the lower velocity region will take longer to pass by the downstream station and hence will have more time to diffuse laterally, allowing some particles to sample even lower axial velocities. Particles diffusing into the higher velocity zone are more rapidly swept by the downstream station and do not have as much time to diffuse laterally. This asymmetry causes the initial rise in mean residence time, with the boundary preventing further increase.

C.7 Conclusions

Theoretical studies of near field advective diffusion have been successful in analyzing some of the features of the cross-sectionally averaged axial distribution. A Monte Carlo method is used here to investigate some of the important features of the residence time distribution for both point and uniform sources. The residence time distribution is shown to change from a highly skewed character to a more symmetric form with increasing axial distance for both point sources and a uniform flux of particles along the tube. All residence time distributions maintain the same sense to their skewness in that the median always lies at a smaller time than the mean, which in short sections can be quite pronounced. The dimensionless mean residence time $< \overline{t}(\hat{z}) >$ displays a maximum as a function of downstream distance for point sources located approximately between $\eta_o = 0.6$ and $\eta_o < 1$. Through integration of an approximate theoretical solution due to Chatwin (1976), the mean and variance of the residence time distribution are found for $\hat{z} << 1$. For a point source located at η_o, $0 < \eta_o < 1$, the variance $< \hat{t}^2(\hat{z}) >$ is found to initially increase in proportion to $\hat{z}^3$ before converging to an asymptotic growth rate proportional to $\hat{z}$. The dimensionless mean residence time $< \overline{t}(\hat{z}) >$ is found to initially rise with increasing downstream distance for any point source in the cross section, with the exception of a point source at the capillary wall. This phenomenon is in agreement with the Monte Carlo calculations and with intuitive reasoning.

REFERENCES

Aris, R. 1956 On the dispersion of a solute in a fluid flowing through a tube. Proc. Roy. Soc. A, 235, 67.

Barton, N. G. 1983 On the method of moments for solute dispersion. J. Fluid Mech. 126, 205.

Chatwin, P. C. 1970 The approach to normality of the concentration distribution of a solute in a solvent flowing along a straight pipe. J. Fluid Mech. 43, 321.

Chatwin, P. C. 1976 The initial dispersion of contaminant in Poiseuille flow and the smoothing of the snout. J. Fluid Mech. 77, 593.

Chatwin, P. C. 1977 The initial development of longitudinal dispersion in straight tubes. J. Fluid Mech. 80, 33.

Crank, J. 1956 The Mathematics of Diffusion. Oxford University Press.

Dewey, Raymond J. & Paul J. Sullivan, 1982 Longitudinal-dispersion calculations in laminar flows by statistical analysis of molecular motions. J. Fluid Mech. 125, 203.

Elder, J. W. 1959 The dispersion of marked fluid in turbulent shear flow. J. Fluid Mech. 5, 554.

Fischer, H. B. 1967 The mechanics of dispersion in natural waters. J. Hydraulics Div. ASCE. 93, 187.

Gill, W. N. & V. Ananthakrishnan, 1967 Laminar dispersion in capillaries: part 4. the slug stimulus. AIChE J. 13, 801.

Hammersley, J. M. & Handscomb, D. C. 1979 Monte Carlo Methods. Chapman and Hall.

Jayaraj, K. & R. Shankar Subramanian, 1978 On relaxation phenomena in field-flow fractionation. Sep. Sci. Tech. 13, 791.

Knuth, Donald E. 1969 Seminumerical Algorithms - The Art of Computer Programming. Vol. 2 Addison-Wesley.

Kraichnan, R. H. 1970 Diffusion by a random velocity field. Phys. Fluids. 13, 22.

Saffman, P. G. 1962 The effect of wind shear on horizontal spread from an instantaneous ground source. Quar. J. Roy. Met. Soc. 88, 382.

Saffman, P. G. 1960 On the effect of the molecular diffusivity in turbulent diffusion. J. Fluid Mech. 8, 273.

Saffman, P. G. 1959 A theory of dispersion in a porous medium. J. Fluid Mech. 6, 321.

Smith, R. 1982a Non-uniform discharges of contaminants in shear flows. J. Fluid Mech. 120, 71.

Smith, R. 1982b Gaussian approximation for contaminant dispersion. Quar. J. Mech. App. Math. 35, 345.

Sullivan, P. J. 1971 Longitudinal dispersion within a two-dimensional turbulent shear flow. J. Fluid Mech. 49, 551.

Taylor, G. I. 1954 The dispersion of matter in turbulent flow through a pipe. Proc. Roy. Soc. A 223, 446.

Taylor, G. I. 1953 Dispersion of soluble matter in solvent flowing slowly through a tube. Proc. Roy. Soc. A 219, 186.

Tsai, Yuh Hua & Edward R. Holley, 1978 Temporal moments for longitudinal dispersion. J. Hydraulics Div. ASCE. 12, 1617.